ÉCOLE DE TECHNOLOGIE SUPÉRIEURE
UNIVERSITÉ DU QUÉBEC

THESIS PRESENTED TO
ÉCOLE DE TECHNOLOGIE SUPÉRIEURE

IN PARTIAL FULFILLMENT OF THE REQUIREMENTS FOR
THE DEGREE OF DOCTOR OF PHILOSOPHY
Ph. D.

BY
Abbasali SABOKTAKIN RIZI

INTEGRITY ASSESSMENT OF PREFORMS AND THICK TEXTILE REINFORCED COMPOSITES FOR AEROSPACE APPLICATIONS

MONTRÉAL, DECEMBER 20, 2013

.

BOARD OF EXAMINERS (THESIS PH.D.)

THIS THESIS HAS BEEN EVALUATED

BY THE FOLLOWING BOARD OF EXAMINERS

Prof. Toan Vu-Khanh, Thesis adviser
Dept. of mechanical engineering, École de technologie supérieure

Prof. Simon Joncas, Committee President
Dept. of automated manufacturing engineering, École de technologie supérieure

Prof. François Robitaille, External Examiner
Dept. of mechanical engineering, University of Ottawa

Prof. Martin Viens, Examiner
Dept. of mechanical engineering, École de technologie supérieure

Prof. Minh-Tan Ton-That, Independent Examiner
Dept. Mechanical & Industrial Engineering, Concordia University

THIS THESIS WAS PRENSENTED AND DEFENDED

IN THE PRESENCE OF A BOARD OF EXAMINERS AND PUBLIC

ON NOVEMBER 01, 2013

AT ÉCOLE DE TECHNOLOGIE SUPÉRIEURE

FOREWORD

This thesis is dedicated to people who taught me how to live,

how to research.

To

My parents and grandfather-Mohammadmorad Saboktakin Rizi

and

Professor Toan Vu-Khanh
for his three decades of strong research activities

and

Professor Mahmoud Farzin (Isfahan University of Technology)

In the memory of

Hossein-ali Ghojehi-Rizi (July 7, 1958 – May 6, 1982),

Professor Mahmoud Hessaby (Feb 23, 1903 – Sep 3, 1992)

and

Mohammad-ali Shahmoradi (April 4, 1959 – Jan 6, 1987)

ACKNOWLEDGMENTS

First of all, I am tremendously thankful to my adviser Prof. Toan Vu-Khanh for his great supervision. Without his guidance and help this thesis would not have been possible. I am very grateful to my Co-adviser Dr. Nguyen Tri Phuong for his continuous support, guidance and encouragement during my research. I would like to thank my committee chair and members: Prof. Simon Joncas (ETS), Prof. Martin Viens (ETS), Prof. Minh-Tan Ton-That (Concordia Univ.) and Prof. François Robitaille (Ottawa Univ.). Furthermore, special thanks go to the following people: Faculty professors and industry experts including Jesse Garant (Jgarantmc), Fabio Visentin (Jgarantmc), Andrew J. Good (Jgarantmc), Yoann Bonnofen (Composite BHS), Léna Swennen (Composite BHS), J. Haines (Composite BHS), Prof. Stephen Tsai (Stanford Univ.), Dr. Hychem Boukehili, Prof. Nico Declercq (Gatech), Prof. Xavier Maldague (Laval Univ.), Dr. Steven M. Shepard (Thermalwave), Dr. Andre Cocquyt (Grpguru), Dr. Jonathan H. Gosse (Boeing), Prof. Mahmoud Farzin (IUT), Dr. Giuseppe Dell'Anno (Cranfield Univ.), Andreas Hänsch (Trans-Textil GmbH), Dr. Keith Sharp (3TEX), Prof. Peter Middendorf (Stuttgart Univ.), Prof. Roberto Palazzetti (Bologna Univ.), Prof. S. Arivalagan (Dr M.G.R. Univ.), Prof. Karlis Rocens (Riga Tech Univ.), Prof. Alberto Milazzo (Palermo Univ.), Prof. Zauner Gerald (Applied Science Univ.), Dr. P. Palanichamy (Igar), Prof. Jozef Bicerano (Polymerexpert), Prof. Carosena Meola (Bologna Univ.), Prof. Krutikova Lyudmila (Yandex), David.Stresing (Saint-gobain), Steven Kidd (themixplastics), Prof. Carl Zweben (AIAA), Dirk Dusharme (Qualitydigest), Prof. Alberto Milazzo (Palermo Univ.), Davide Micheli (Roma Univ.), Dr. Z. Naeimi (Iasbs), Gangadhara Prusty (NSW Univ.), Piaras Kelly (Auckland Univ.), Prof. Manfred Staat (Aachen Univ.), Christoph Greb (Aachen Univ.), Dr. Hossein Monajati (ETS), Prof. Mohd Rozi Ahmad (Teknologi MARA Univ.), Dr. Olivier Vermeersch (CCTG), Herb Armstrong (EEMS), Lary Etheringt (Eclipse), Prof. Antoine Tahan (ETS), Prof. Gerd Dobmann (Fraunhofer), Minder Christian (Tissa), Dr. Clemente Ibarra Castanedo (Laval Univ.), Aldjia Begriche (CCTG), Prof. Anh D. Ngo (ETS), Prof. Mohammad Jahazi (ETS), Dr. Patricia Dolez (CTTG), Dr. Aidin Delnavaz (ETS) and Heather Uva (TFP), Dr. Carlos Arrieta (ETS), Andre Goyette (ETS) and Technical Staff including Radu Romanesque, Jonathan Levesque, Serge

Plamondon, Mario Corbin, Jean-Guy Gagnon, Hugo Landry and Claude Legault. Last but not least, I am so grateful to my best friends: Saeid Hedaytresa, Mohammad Sleiman, Hamid Habibzadeh, Monzer Daoud, Daniel Fernández, Ali Niknam, Saad-amine Taki, Mahmoud Ghanbari, Mehdi Saboori, Laurent Cormier, Cesar Augusto, Amir ghazi Saeedi, Husain Dibajian, Ehsan Rezaie, Hamid Javani, Sergey Dubinskiy, Hamed Saghafi, Hani Bakhshai, Mohsen Adibi, Mohammad M. Safaei, Louis A. Généreux, Ennouri Triki, Ludwig Vinches, Rachid El Aidani, Marc Grenier, Matthieu Klein, Vahab Akbarzadeh, Pierre-luc Vachon, Adel Ziadi, Wael Ben Larbi, Masoud Jandaghian, Kaveh Azizian, Mohammadreza Motamedi, Behrang Majedi, Yousef Babazadeh, Vahid Sabri, Hani Vahedi, Ahmad Khani, Amèvi Tongne, Majid Rafiei, Nader Aghaesmaeili, Guillermo Quesada, Mojtaba Ghaderi, Esmaeil Arabzadeh, Saeid Jafari, Ali Moazzam, Hossein Safaei, Ehsan Arabnejad and Bouchaib Zazoum.

Finally, I would like to express my sincere appreciation to my family for their endless love and support.

INTEGRITY ASSESSMENT OF PREFORMS AND THICK TEXTILE REINFORCED COMPOSITES FOR AEROSPACE APPLICATIONS

Abbbasali SABOKTAKIN RIZI

ABSTRACT

Three-dimensional (3D) textile composites containing in-plane fibers and fibers oriented in the thickness direction offer some advantages over two-dimensional (2D) textile composites. These advantages include high delamination resistance and improved damage tolerance. Textile composites containing 3D textile preforms have mostly been developed by the aerospace industry for structural applications such as wing panels, landing gear, rocket nozzles, and the Orion capsule, and so forth.

This thesis is devoted to structural integrity assessment of textile composites including 2D and 3D tufted composites by combining destructive and non-destructive techniques. In the first part of the thesis, non-destructive techniques including X-ray computed tomography (CT) and ultrasound-based techniques (UT) were used to detect two significant process-induced defects called fiber breakage and fabric misalignment. The second part focuses on studying of the influence of manufacturing defects introduced during the tufting process on the mechanical properties.

Experimental results proved that X-ray CT facilitates the characterization of those two manufacturing defects as well as the architecture of the textile fabrics. Furthermore, meso-scale modeling of a 2D woven composite was successfully performed for the analysis of the fiber breakage defect influence and fiber architecture on wave propagation.

Experimental results prove that tufting the preform assists in locking and restricting the yarn's movement in the preform. The threads used for tufting have a major influence on tensile strength, as stronger threads may give higher resistance. Tufting increases the compaction force due locking of fiber bundles, therefore, a higher compaction force is needed to obtain a fiber volume of up to 50 percent in comparison to an untufted preform. The drape behaviour of a tufted preform is influenced by tufting so that high drapability is observed for a tufted preform along with local variation of fiber bundle occurred around tufting reinforcements. The variation of preform geometry was achieved by laser scanning.

Furthermore, the CT capability was investigated as a means for recognizing the shapes and locations of voids in composites.

Tufted composites with transverse tufting suffer less reduction in the tensile strength than those with longitudinal tufting. Tufted composites are found to have lower fatigue life ithan untufted composites, while an improved compressive strength and tensile strength at high strain rate are observed.

Tufting improves the mechanical properties of tufted honeycomb composites under local compression and bending loadings. Mostly, the damage initiates from resin-rich regions around the tufting reinforcements.

The acceptance of 3D tufted composites for use in primary aerospace structures is highly dependent on the accuracy and reliability of experimental data to recognize the degree to which tufting reinforcements improve or degrade the mechanical properties. In this thesis, the correlation between the tufted preforms and composite properties and the changes to mechanical properties is discussed for a specific tufting configuration. Experimental data are reported on both the low-rate and high-rate static and fatigue strengths at various stress levels. Microstructural examination is carried out by using the high resolution microscopy and CT techniques. The results of this thesis contribute to the investigation of the integrity and damage tolerance in 3D tufted composites toward certifying purposes for future transport aircraft. Since the certification of tufted composites for aerospace applications is still problematic due to the lack of dependable non-destructive evaluation techniques for their inspection and those manufacturing factors can considerably influence their performance, this is an important problem to tackle in the field of aerospace composite engineering.

.

Keywords: Textile preform, Textile composite, Non-destructive testing, Destructive testing, Preform characteristics, Composite performance, Failure mechanisms

INTEGRITY ASSESSMENT OF PREFORMS AND THICK TEXTILE REINFORCED COMPOSITES FOR AEROSPACE APPLICATIONS

ABBBASALI SABOKTAKIN RIZI

RÉSUMÉ

Les composites à renforts textiles 3D, contenant des fibres dans le plan et dans la direction de l'épaisseur, offrent certains avantages par rapport aux composites à renforts textiles 2D. Ces avantages comprennent une grande résistance à la délamination et une meilleure tolérance à l'endommagement. La plupart des textiles 3D ont été développés pour des pièces destinées à l'industrie aérospatiale telles que des panneaux d'ailes, des trains d'atterrissage, des tuyères de fusée et la capsule Orion. Cette thèse vise à évaluer l'intégrité structurelle des textiles composites en combinant des techniques d'inspection destructives et non destructives. Dans la première partie de la thèse, des techniques non destructives, y compris les rayons-X (CT) et des techniques basées sur les ultrasons (UT), ont été développées pour détecter les défauts importants comme la rupture des fibres et le désalignement des tissus. La deuxième partie porte sur l'étude de l'influence des défauts de fabrication qui se produisent dans les processus d' touffetage sur les performances mécaniques.

Des résultats expérimentaux ont montré que tomographie rayons-X facilite la détection et la caractérisation de ces deux défauts de fabrication, ainsi que de l'architecture des tissus.

En outre, la modélisation méso-échelle d'un composite tissé en 2D a été réalisée avec succès pour l'analyse de l'influence du défaut de rupture des fibres et de l'architecture des fibres de propagation de l'onde. Les résultats expérimentaux montrent que le touffetage des préforme limite ou élimine le mouvement de leurs fils. En plus, la touffetage par des fils de haute résistance à la traction peut améliorer celle de leurs préforme 3D. La touffe d'un préforme fait augmenter la force de compactage des fibres. À cet effet, cette méthode est nécessaire pour augmenter le volume des fibres de plus de 50 % en comparaison d'un préforme non touffeté. La résistance à la déformation d'une préforme est influencée par l'opération de touffetage. En effet, une préforme touffetée est plus résistance à la déformation qu'une préforme non touffetée. La variation de la géométrie de la préforme a été mesurée par balayage laser. En outre, la capacité CT a été étudiée en tant que moyen pour reconnaître les formes et les emplacements des vides dans les matériaux composites. La résistance à la

traction des composites avec un touffetage transversale a eu moins de réduction de que celle avec touffetage longitudinal. Les tests de fatigue à haute vitesse de déformation montrent que les composites touffetés ont une durée de vie inférieure à celle des composite non touffetés. L'opération de touffetage permet d'améliorer les propriétés mécaniques despanneaux sandwichs à noyau en nid d'abeilles sollicités en compression locale et en flexion trois points. Les dommages sont souvent initiés dans les régions riches en résine qui entourent le renfort de touffetage. L'acceptation primaire de l'utilisation des composites touffetés 3D dans les structures aérospatiales est très dépendantes de l'exactitude et de la fiabilité des données expérimentales pour identifier le degré auquel les renforts améliorent ou dégradent les propriétés mécaniques. Dans cette thèse, la corrélation entre les préformes touffues, les propriétés des composites et leurs modifications dues au touffetagesont traités pour une configuration spécifique. Les données expérimentales sont présentées à la fois sur un taux faible et à haut débit statique et des forces de fatigue à différents niveaux de contrainte. L'examen microstructural est effectué en utilisant la microscopie à haute résolution et les techniques de CT. Les résultats de cette thèse contribuent à l'enquête sur la tolérance d'intégrité et de dommage dans les matériaux composites tuftés 3D en vue d'unecertification pour l'utilisation dans les futurs avions de transport. Cependant, la certification des composites tuftés pour les applications aérospatiales est toujours problématique en raison de l'absence de techniques d'évaluation non destructive fiables pour leur inspection et les facteurs de fabrication peuvent influencer considérablement leur performance, il s'agit d'un problème important auquel on doit s'attaquer dans le domaine de composite pour l'aérospatial.

Mots-clés: Préformes textiles, composites à renforts textiles, Essais nonestructifs, Essais destructifs, Caractéristiques des préformes, Performance des composites, Mécanismes de défaillance

TABLE OF CONTENTS

LIST OF TABLES

Page

LIST OF FIGURES

Page

INTRODUCTION

Composite materials have been used for various structural applications due to their high specific strength and stiffness. The first generation of composites is two-dimensional (2D) laminates. Although, these types of composites are known by high in-plane strength and stiffness, they suffer from both the need to use a time-consuming lay-up step during the manufacturing process and poor out-of-plane properties. Over the last two decades, three-dimensional (3D) textile composite structures have been developed to overcome the disadvantages of 2D textile composites. The 3D textile composites have been developed to enhance the mechanical properties in the through-thickness direction, improve damage tolerance, and decrease fabrication costs. The development of 3D textile composites based on 3D preforms has been undertaken mostly by NASA (Dow M. and Benso H., 1997; (Poe C.C. and Dexter H.B., 1997).

Textile processes have reduced the cost for manufacturing many textile composite components and improved important aspects of mechanical performance such as impact damage tolerance. Manufacturing defects introduced during the manufacturing process can degrade the performance of a composite. The extent of performance degradation at which the severity of the defect becomes safety-critical depends on the application and can only be determined by structural integrity assessment.

Research objectives and methodology

This research thesis is devoted to structural integrity assessment of textile composites by the combination of inspection procedures and standard mechanical tests. Therefore, the objectives of the thesis are:

- To select the most suitable NDT techniques to detect major manufacturing defects in 2D textile composites, such as: ply misalignment defect and fibre breakage defect; and extract actual defects parameters such as type, size, shape and location;
- To determine the most convenient inspection method(s) for the inspection of 3D tufted preforms and composites with subsequent experimental validation;

- To measure the influence of defects during static and dynamic loadings.

This thesis explores these research objectives based on the information obtained through a comprehensive literature review and our experimental results. Since each non-destructive method has advantages and disadvantages that influence the choice of inspection method for the textile preform and composite, the success or failure of any technique to detect defects is determined by its limitations. I assess three techniques; namely, ultrasonic, optical methods, and X-ray, as feasible methods for inspecting preforms and textile composites. On the other hand, due to the inhomogeneous structures of textile composites, their inspection is quite different and more complex than those intended for common composite structures. Hence reaching our goals and answering all issues described in this thesis required using more than one non-destructive method.

The combination of the proposed methods is expected to improve the reliability of preforms and final composite structures that is in agreement with our goals.

Understanding the behaviour of defects under mechanical loads and examining of the resistance characteristics of composites to these defects is another goal. This goal is pursued by investigating the influence of defects on composite performance; including an assessment of the static and fatigue performance of composite samples in presence of defects such as fiber breakage, fiber misalignment, etc.

Our approach toward reaching our objectives is to progress systematically from the testing of 2D textile composite specimens to 3D composites, as well as from thin textile composites to thick ones. This systematic approach simplifies the understanding of practical aspects of each NDT technique, their capabilities and limitations, and enables the examination of the suitability of each method towards the structural integrity assessment of textile composites.

For all specimens, research is conducted in two phases: (a) inspection of composite specimen, and (b) investigation of the effect of defects on mechanical performance. Below we illustrate how the proposed phases in this thesis related to each other to form an appropriate strategy to achieve our objectives:

The first phase of this work consisted of:

- Identification of the types of defects in textile preform and composite;

- Identification of state-of-the-art non-destructive evaluation (NDE) technologies that can be used for detecting defects in textile composite;
- Development of the techniques to successfully inspect flat textile composite panels

The second phase of this work consisted of:

- Fabrication of composite specimens while controlling important parameters to minimize void formation during the manufacturing process;
- Inspection of specimens containing artificial defects as well as defect-free specimens;
- Determination of the influence of defects on the mechanical performance according to the results obtained from different mechanical tests and analysis of the behavior of defective samples under different loading conditions.

Thesis contribution

3D Textile preforms and composites have been used in a large number of aerospace applications such as pressure vessels, rotor blades, external fuel tanks for commercial aircraft and composite fuselages, etc. Because of these advanced applications, there is a high need to investigate the structural integrity in these types of composites. The objectives explained in this thesis are aimed at investigating the inspection of textile composites and finding a correlation between defects and the mechanical performance. Mechanical testing including static and fatigue tests for both textile preform and composites, and a fractographic method combined with NDT methods have been considered to survey the 3D tufted composite performance. Therefore, the contributions in this thesis can be divided into the following sections that are intended to fulfill the research objectives explained above:

- For the first time in this thesis, ultrasonic polar scanning is applied to detect manufacturing defects such as fiber breakage and fiber misalignment in 2D woven composites in addition to X-ray computed tomography for characterizing of 3D tufted composites. The results provide useful information concerning the capabilities of these testing methods to detect micro damage in textile composites.
- Implementation of a finite element method to analyze wave propagation in a woven textile composite at the meso-scale contributes to the detection of small fiber

breakage which opens a new research field on analysis of wave propagation in damaged textile composites in the presence of manufacturing defect.

- The use of laser scanning for measuring preform geometry deviation contributes to the subsequent research on the application of non-contact CMM scanning for 3D preforms.
- Evaluation of tufted preform formability promotes to the manufacturing of complex shaped composite parts.
- Fatigue performance characterization of 3D tufted composite at different stress levels for the present configuration contributes the abilities to predict the fatigue life and to perform comparisons with other tufting configurations.
- Damage growth and stiffness degradation for the 3D tufted textile composite discussed in this thesis help to analyse damage tolerance in 3D tufted composites, a challenge which still needs to be addressed.
- An invaluable collection of SEM fractographs for 3D tufted composite is allowing to correct interpretation and increase accuracy of failure analysis because it is mitigating the previous lack of information.
- Figure 1 displays different levels of mechanical test known as the test pyramid for aerospace structures. Research results achieved at the coupon level in this thesis can be developed for larger structural elements, components, and complete assemblies in the aerospace industry.

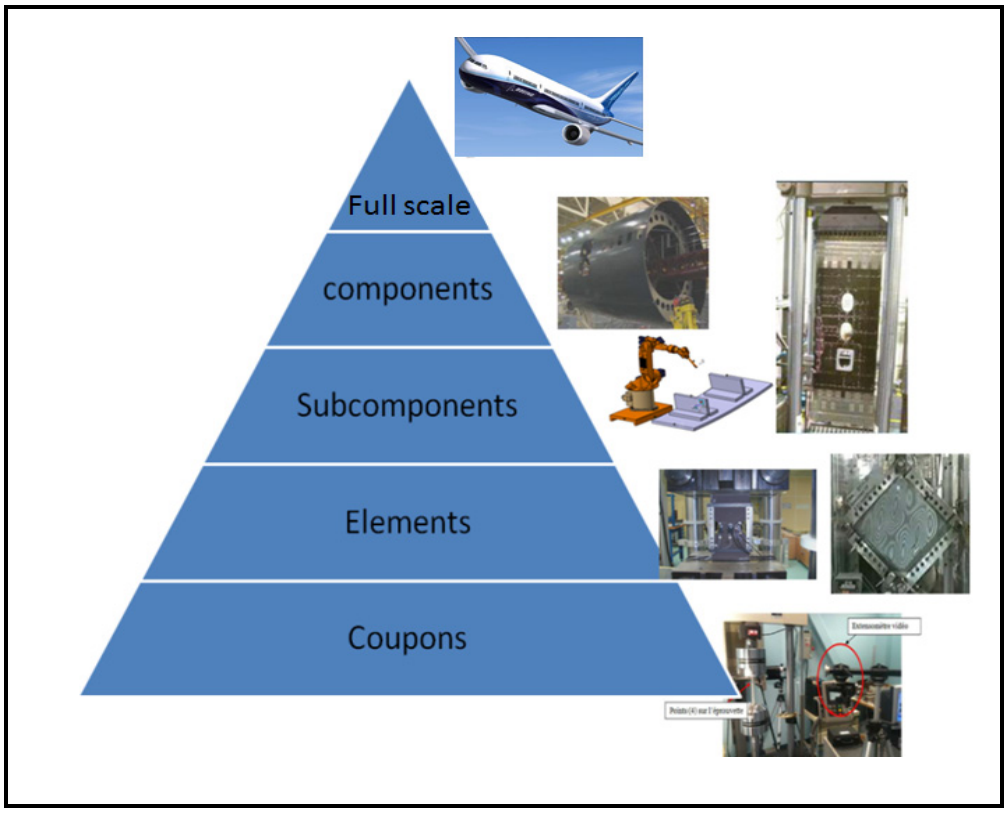

Figure 1. Test pyramid for aircraft composite structures.

Thesis outline

This thesis is divided into five major sections: Part I, introduction and literature review; and Parts II-V research results, conclusions, and potential applications of this thesis.

Composite defects, their inspection and influence on composite performance are illustrated in Chapter II. This chapter is intended to apply all research results to the integrity assessment of 3D reinforced composites elaborated in following chapters. In this part, at first, quality issues related to damage detection, manufacturing process and mechanical performance of textile composite are described in detail. These quality issues include microscopic assessment (SEM, optical microscopy) presented in several distinct sections. Moreover, the effect of textile structure complexity on their inspection using NDE techniques is illustrated as well as geometry inspection of composite using a coordinate measuring system. Chapters III and IV are focused on the 3D preforms and composite characteristics which are introduced as major research topics. These chapters assess the impact of initial defects containing fiber breakage

on the mechanical performance. The critical level of the samples containing these defects subjected to static and cyclic loading is examined. The location, size, shape, and distribution of porosity through the composite thickness are investigated using X-ray tomography as well as cross-sectioning analysis of the composite samples for the quality control purposes. Chapter V is devoted to the use of microscopic and X-ray techniques for the detection of a wide range of 3D composites defects as well as for the assessment of which damage modes occur during loading and if the initial damage develops during static and fatigue loading tests.

Finally, Chapter VI summarizes the thesis and provides recommendations for future research.

CHAPTER 1

LITERATURE REVIEW ON 3D TEXTILE COMPOSITES AND NONDESTRUCTIVE TECHNIQUES

1.1 Introduction

3D Composites materials are composed of two main constituents: matrix and fabric. The fabric, termed 3D preform, is an integrated textile architecture having in-plane fibers and fibers oriented through the thickness (Jinlian H., 2008). 3D preform in 3D textile composites may contribute to improve the strength and stiffness in the thickness direction, eliminate the interlaminar surfaces due to integrated structure and present possibilities of designing and manufacturing near-net-shape composite components. A variety of textile processes including 3D weaving, stitching, knitting, and braiding have been used to insert the through-thickness fibres (Richard H. A., 2000). A categorization of 3D fabrics based on the presence of reinforcing fibers oriented in the through-thickness direction is shown in Figure 1.1.

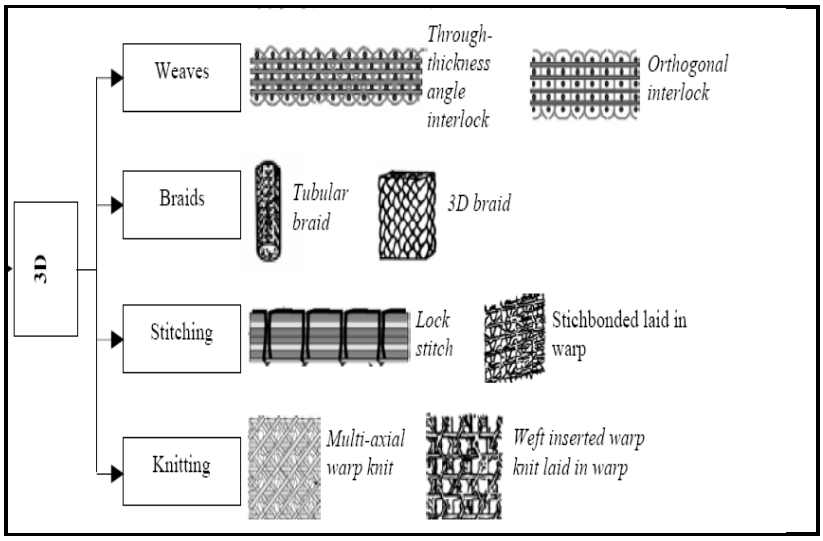

Figure 1.1. The main categories of 3D textile performs
(Richard H. A., 2000)

In textile composite structures, failures originate from manufacturing defects or service-induced damage. Manufacturing defects can degrade the performance of textile composites to a point where the composite cannot be used safely for an aircraft structure. The point at which the severity of the defect becomes safety-critical (denote those defects that significantly decrease damage tolerance of aircraft structures and leads to very low mechanical properties) depends on the application and can only be determined by structural integrity assessment. This chapter reviews all the processes used to produce 3D preforms, preform architectures, their specifications and deformation modes. Finally, the chapter discusses those inspection procedures that can be applied to structural integrity assessment of textile composite.

1.2 Textile techniques

1.2.1 Weaving

The weaving process includes the placing of weft yarns between warp yarns. The warp yarns are placed in the direction of the weaving process and weft yarns lie perpendicular to the warp yarns. In addition, the yarns in the through-thickness direction named Z- binders are used to bind several layers of interlaced warps and wefts. Figure 1.2 displays a schematic of weaving process and a weaving loom machine. Jacquard looms are the most popular due to their high degrees of automation and good control of the fiber structures. The benefits of this automation in weaving process are: reducing the manufacturing costs, in-process inspections, and increasing repeatability and quality control. The loom can be used to manufacture integrated and net-shape preforms such as blade stiffened panels (Mouritz A., 1997; (Rudov-C. S., 2007).

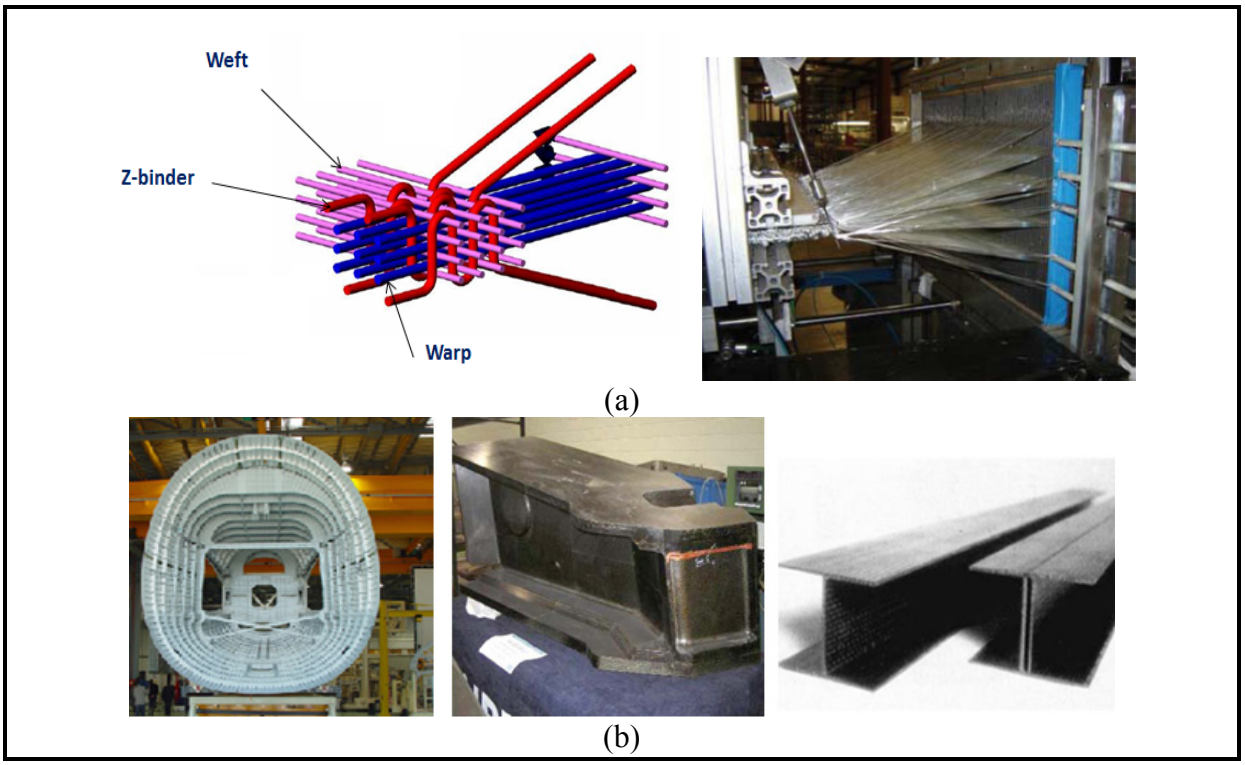

Figure 1.2. (a) 3D weaving process. From lef totight: Schematics of 3D weaving process, 3D Weaving machine (b) 3D woven composite applications. From left to right: Fuselage, Landing gear, 3D composite I beam (Bogdanovich A.E. and Mohamed M.H., 2009; (Buckley M., 2007; (Hybridmat, 2006; (Mouritz A., 1997)

1.2.2 Stitching

Over last two decades, a variety of stitching techniques has been used considerably to stitch textile fabric toward manufacturing reinforced composite structures with high damage resistance. The stitching process is carried out using industrial stitching machines. Stitching machines can stitch various kinds of preforms with high performance yarns as stitching threads. For the stitched composite structure, the extent of through-thickness fibers is between 1 to 5%, which is a same extent of through-thickness reinforcement for other type of 3D composites (Herszberg B., 1997; (Tong L., Mouritz A.P. and Bannister M.K., 2002). The stitching process may offer the following advantages: joining composite structures, provide high strength and resistance in through-thickness directions to peel loads, decreasing the manufacturing cost, improving interlaminar fracture toughness, impact resistance and

tolerance, construct 3D complex shapes by stitching several separate preforms together and consequently reduction the need for fasteners, and finally, weight reduction (Weimer C., 2003). Figure 1.3 displays the manufacturing stage of an aircraft composite panel stiffened by stitching process.

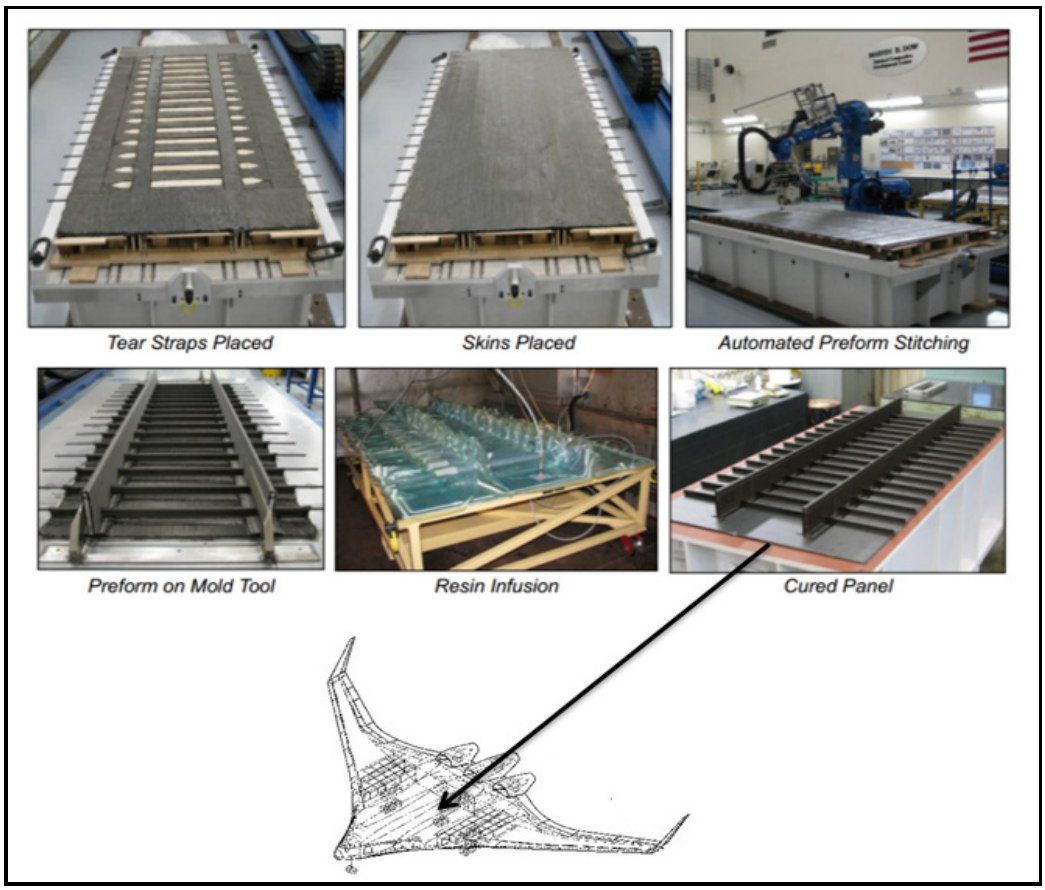

Figure 1.3. Manufacturing process of stiffened stitched panel using vacuum infusion process and its location on the BWB aircraft (http://www.aeronautics.nasa.gov)

Despite these advantages for stitched composites, the following disadvantages can be attributed to the stitching process: reduction in the in-plane properties of composite structures due to fiber breakage occurring in penetrating the needle into fabrics, the performance reduction due to the fabrics crimping. Stitching process causes distortions in the fabric, fiber breakage and resin rich regions in the composite which acting as potential sites for damage

initiation and decreasing the performance of composite. More details on the damage caused during stitching can be found in the next section (Tong L. M., 2002).

Stitching types

The type of stitching has significant effect on the mechanical performance of stitched composites (Karal M., 2005). Lock stitch is one of the most common types of stitching techniques. Mostly, this stitch has been applied in clothing industry and two thread loops is placing between the bobbin and the needle (see Figure 1.4a). The lock stitch requires access to both top and bottom of the stacked fabrics (Herszberg B., 1997; (Tong L. M., 2002). This type of stitching is not appropriate for composites because the thread intersection in the middle of the fabrics causes a stress concentration. Therefore, modified lock stitch shown in Figure 1.4b is typically used in composite industry that allows the needle thread to move on the composite surface instead of the middle of composite (Kimberley D., Caroline B. and Yiu-Wing M., 1994).

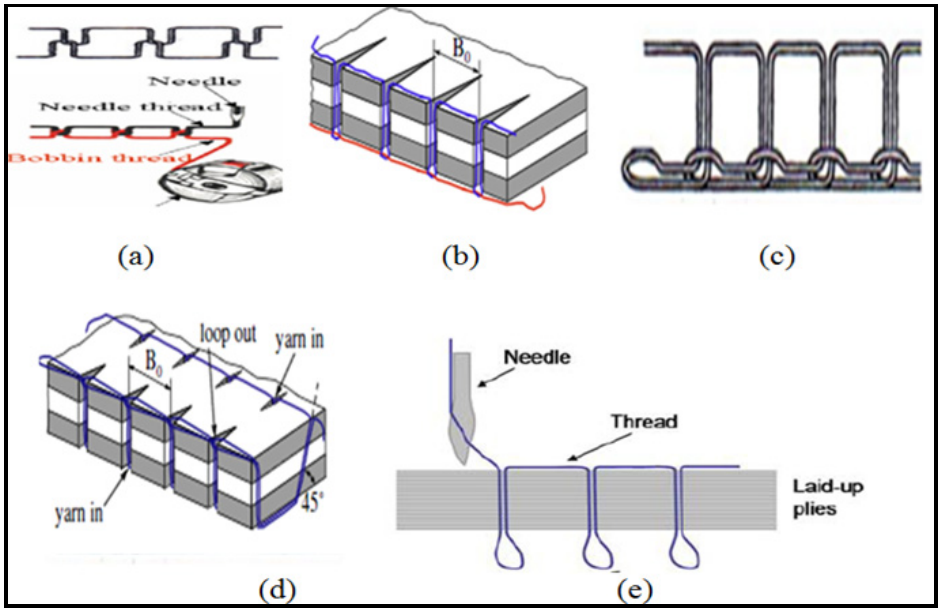

Figure 1.4. Stitching Types (Dell'Anno G. et al., 2007; (Koissin V. et al., 2008; (Tomek R., 2004) (a) Conventional lock stitch (b) Modified lock stitch (c) Chain stitch (d) Dual lock stitch (e) Tufting

Moreover, a chain stitch method shown in Figure 1.4c is used in composite industry. This method has similar mechanism to the lock stitch. Other sewing machines can generate two types of stitches; dual-needle stitching (see Figure 1.4d) and tufting (see Figure 1.4e). In addition to conventional stitching techniques which require access to both fabrics sides, there are other techniques that need only one side of fabrics (See Figure 1.5). In these techniques, curved needle or hooked needle has been used. The maximum thickness of preform to be stitched using these techniques is around 20mm.

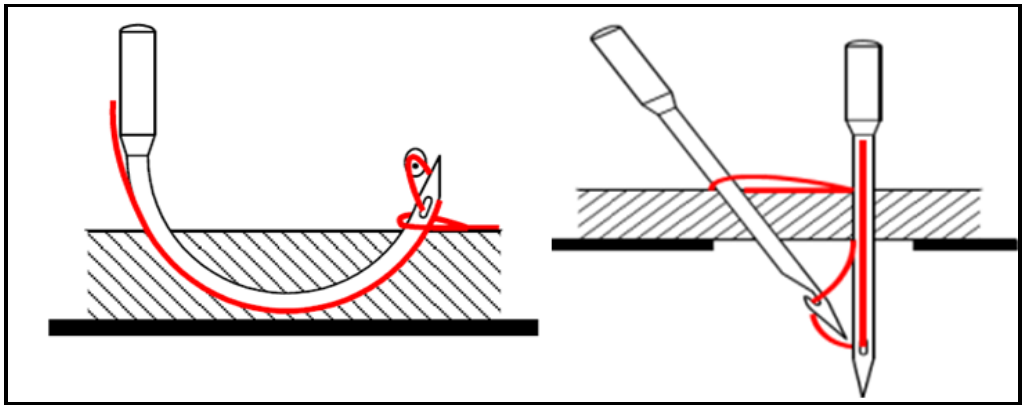

Figure 1.5. Different types of blind stitch technique developed for composite industry (http://www.qinetiq.com)

The significance of stitching parameters on mechanical performance, in particular ballistic performance and fracture toughness, becomes obvious during preform resin impregnation (Hosur M. V. et al., 2004; (Solaimurugan S. and Velmurugan R., 2008). Large number of variables in stitching techniques has been reported while there are many interactions among these variables. The major parameters of stitching process are as follows: stitching pattern, stitch density, and thread type and diameter as well as manufacturing variables including thread tension, foot pressure, needle type/size, textile fabric, and machine type. These parameters have significant effect on strain distribution and concentration in 3D composite structure (Mitschang P. and Ogale A., 2009; (Ogale A. and Mitschang P., 2004).

Needle diameter dominates the amount of the spreading of the fiber during the penetration process such that it can be said the expansion of needle holes is strongly function of needle

diameter. To reduce the extent of fibre damage, small needle diameter should be considered. Needle deflection depends on needle diameter and preform thickness. Various tests are required to evaluate these effects. Therefore, experimental design techniques play a major role for these types of reinforced preforms.

Tailored fiber placement

Technical embroidery or tailored fibre placement (TFP) mostly have been used to place the reinforcement fibers in directions according to the load requirements (Sickinger C. and Herrmann A., 2001). In this stitching technique shown in Figure 1.6, a reinforcement thread is fed into the stitching path and is stitched onto the preform surface in a zigzag pattern while the machine automatically moves the material corresponding to the pattern defined by software developed for TFP (LayStitch LTD.; (Stuttgart Uni.). Recently, CNC machines have been used to facilitate the placing the reinforcement thread in complex paths to meet the maximum stress distribution in desired directions. The high level of automation in CNC machine makes them able to produce complex shaped preforms with considerable cost saving.

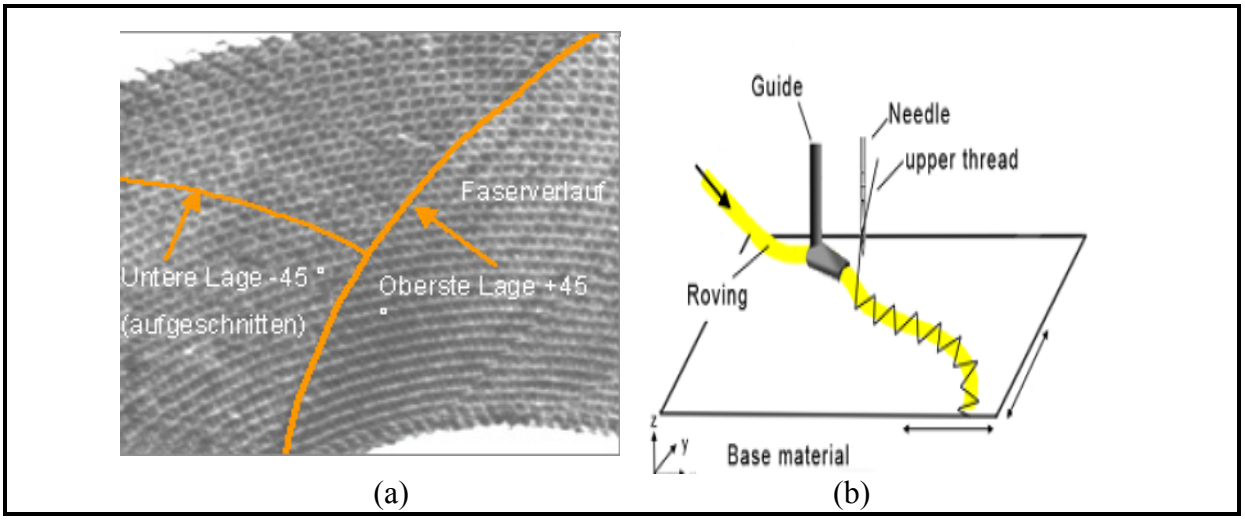

Figure 1.6. (a) Example preform produced by tailored fibre placement (b) Schematic of embroidery machine
(http://www.avantgardetechnologie.de/)

Tufting

As shown in Figure 1.7a, tufting is a one sided stitching technique in which the formation of loops is done by a tension-free stitching thread. Figure 1.7b shows top-side and underside of a tufted preform along with tufting machine. In this technique, the bonding between the matrix and stitching thread is created only after resin injection. However, significant fibre damage occurring in the tufting can reduce in-plane strength of final composite parts (Dell'Anno G. et al., 2007). Based on literature review the knitted fabrics are inappropriate for use with this technique whilst woven fabrics are somewhat easy to tuft due to their interlaced architectures. Furthermore, non-crimped-fibre (NCF) fabrics seem appropriate for tufting process.

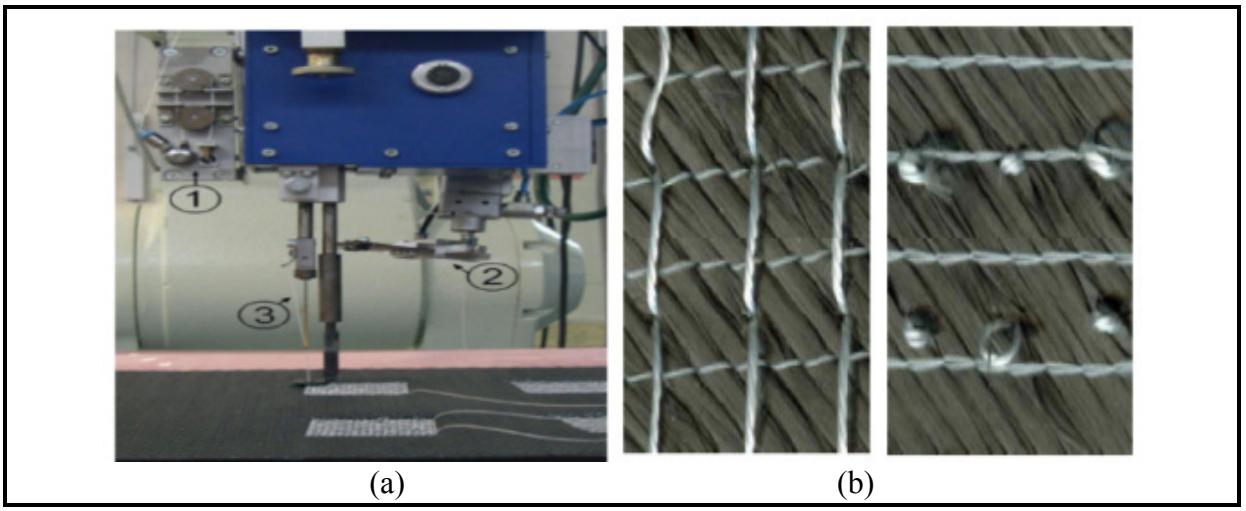

Figure 1.7. (a) Tufting machine (b) An example of tufted fabric
(Dell'Anno G. et al., 2007; (Friedrich K., Fakirov S. and Zhong Z., 2005)

Applications of stitched preforms

Many research projects have been carried out to evaluate the applicability of stitched textile preforms for aerospace structures. For instance, in order to fabricate large wing panels, the Boeing developed a specific machine for stitching process (James H. S., Benson H. and Norman J. J., 2003). That machine was intended to decrease the weight by 25% and 20% in costs compared with equivalent aluminum parts (see Figure 1.8). Other example for stitched

preform is shown in Figure 1.8a. Recently, Airbus and its collaborators have moved to stitching techniques for the manufacture of primary structure of aircraft such as passenger door of commercial aircrafts shown in Figure 1.9.

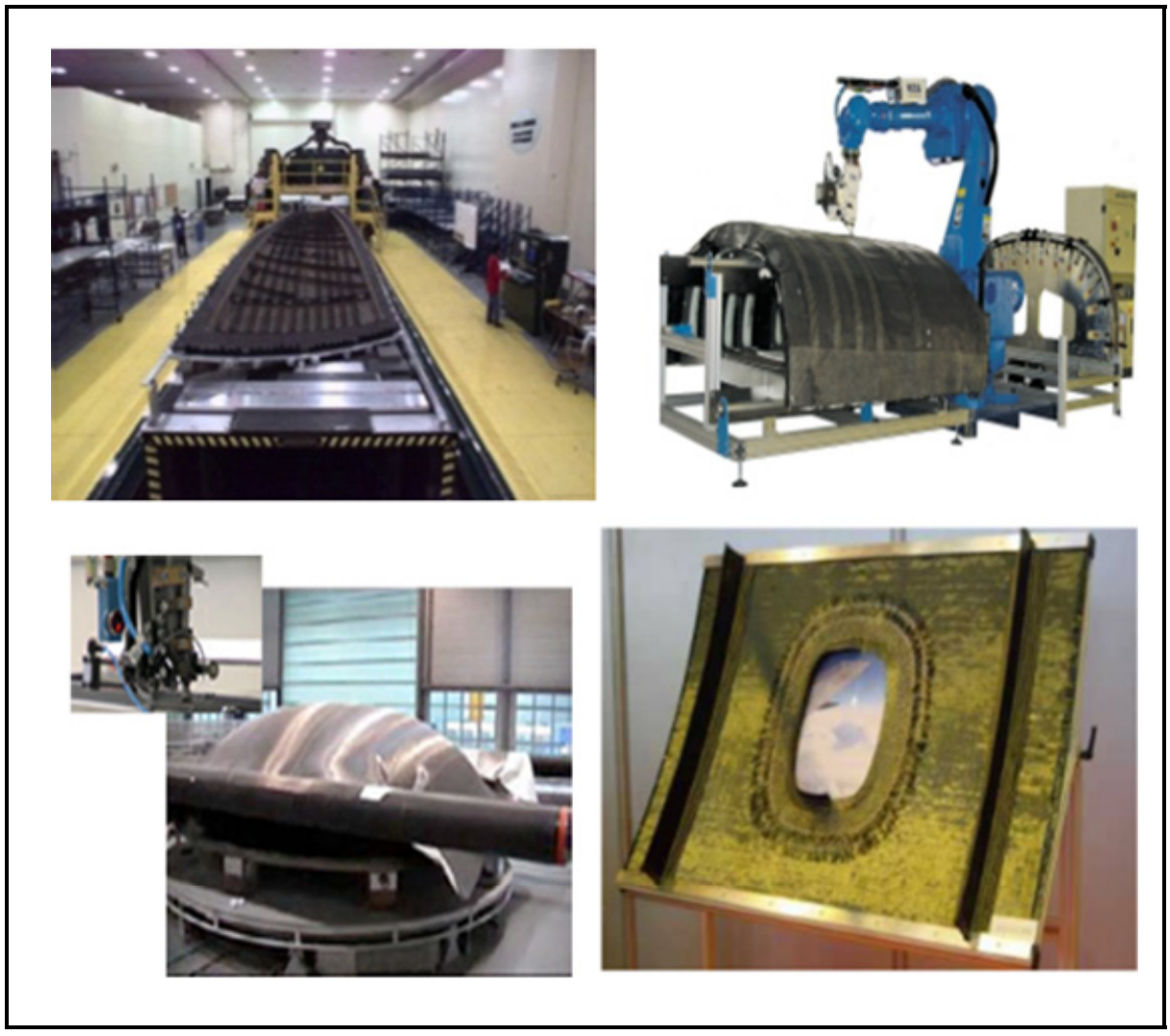

Figure 1.8. Production of complex shape preforms using stitching techniques. From left to right: wing panel, fuselage, pressure bulkhead, window (http://www.interempresas.net; (Michulitz C., 2007; (Potluri P., Sharif T. and Jetavat D., 2008; (www.compositesworld.com)

Furthermore, the stitching technique has been developed to produce a CFRP stator. These developments of stitching techniques seem promising for the automotive industry to benefit

of the tremendous weight reduction and specific mechanical properties in particular to increase crash performance (Claudia H., 2003).

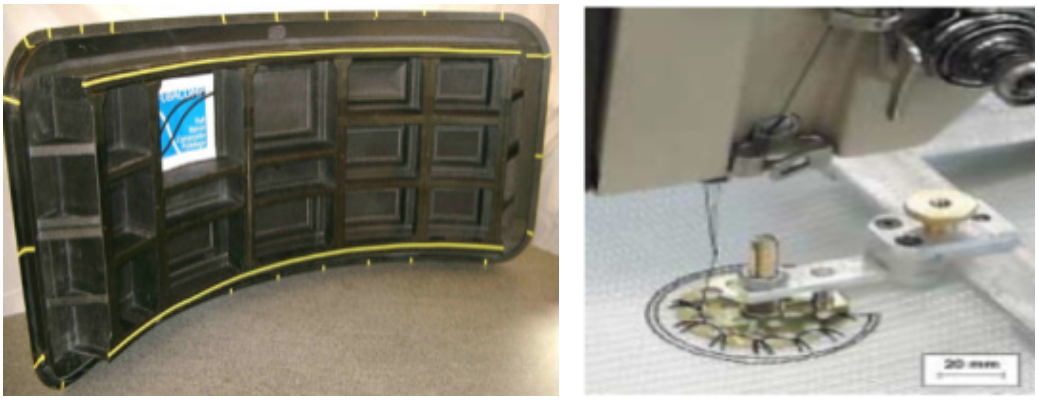

(a) (b)

Figure 1.9. (a) Production of aircraft door using stitching process (b) Replacing welding and jointing bolt with stitching process
(Neitzel M. and Mitschang P., 2004; (www.compositesworld.com)

Furthermore, stitching can be used to connect several composite parts without the need for mechanical fasteners such as bolts and screws, thus decreasing the manufacturing difficulties. This method distributes the stress received by composite over the joint area and also decreases. Lately, 3D stitching robots have been employed to make the textile preforms in the shape of a desired component (Tong L. M., 2002). The robot can stitch the net-shape preform to improve the strength and weight to meet the end application requirements and also decrease handling and lay-up times. Furthermore, the robotic stitching provides 3D dimensional motion to produce very complex shaped preforms (Michulitz C., 2007). Although the stitching technique using robots has been reliable in its performance, the development of appropriate fixation devices for the production of textile preforms using robots is the main challenge.

1.2.3 Braiding

Figure 1.10 shows typical 2D and 3D braided structures. 2D braided structures (Figure 1.10a) are composed of interweaved fibers oriented in 0°and $\pm\theta$ fibre orientations. 3D braiding preforms, shown in Fig. 1.10b, are the extension of 2D braided fabrics constructed by interlacing in-plane yarns with the through-thickness reinforcements (Jinlian H., 2008). 3D braiding process can be used for producing a near net-shape preforms, for instance, rib stiffened panels, airframe spars, rocket nose cones, fuselage barrels, tail shafts, and rocket engine nozzles (Poe C.C. and Dexter H.B., 1997).

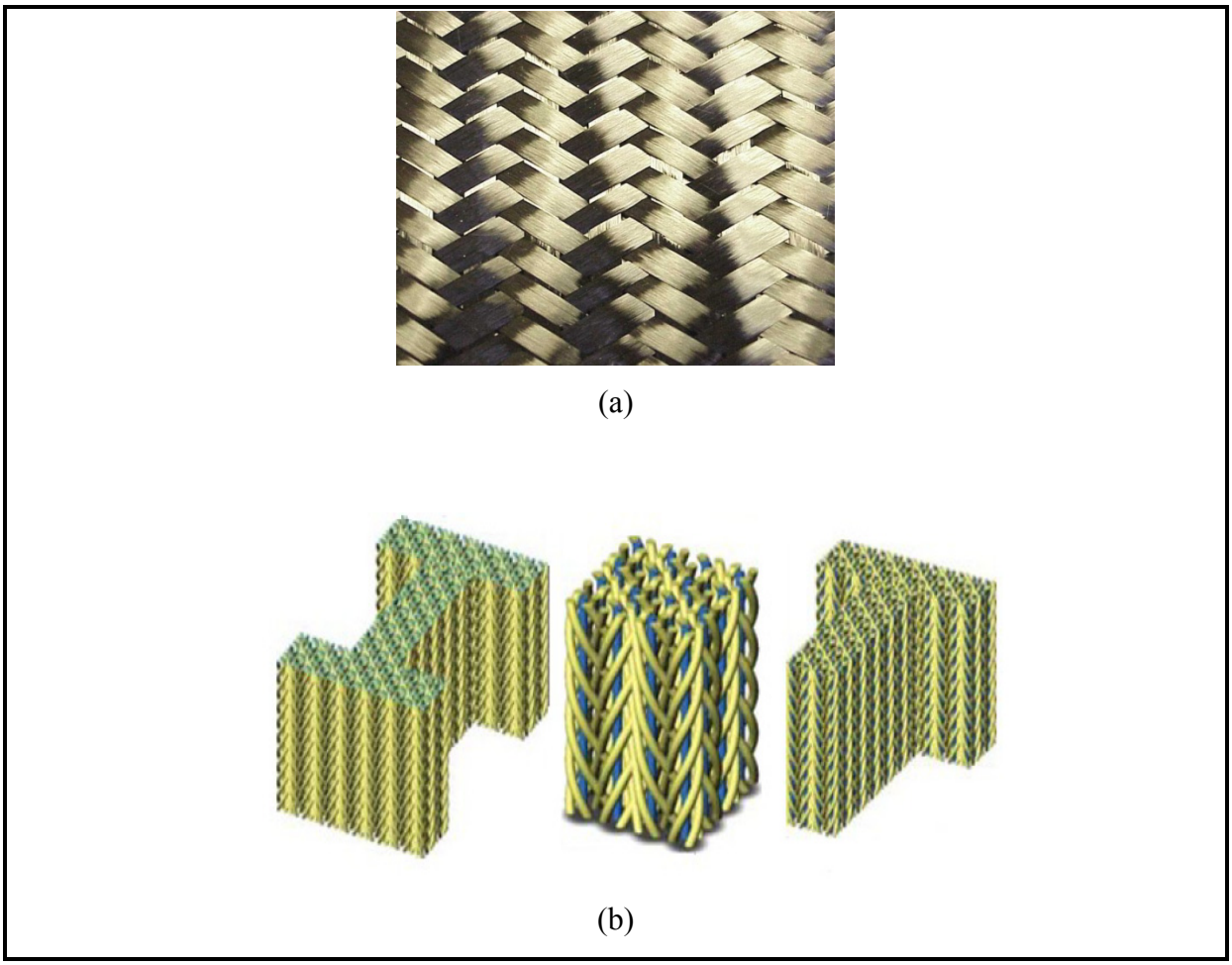

(a)

(b)

Figure 1.10. Braided fabric and preforms (a) 2D braided (Courtesy of A&P Tech) (b) 3D braided preforms (Hybridmat, 2006)

Generally, braided machines have been divided into two categories: rectangular and circular. Tubular braiding shown in Figure 1.11 is other braiding technique established in industry for producing 3-dimensionally shaped preforms of high-performance fibres such as I or T beams. In addition, the braiding yarns can be placed on cores which may be handled by a robot to ensure proper fibre orientation. If necessary, it is possible to remove the core and in a second step form the braiding to get stringer shaped preforms.

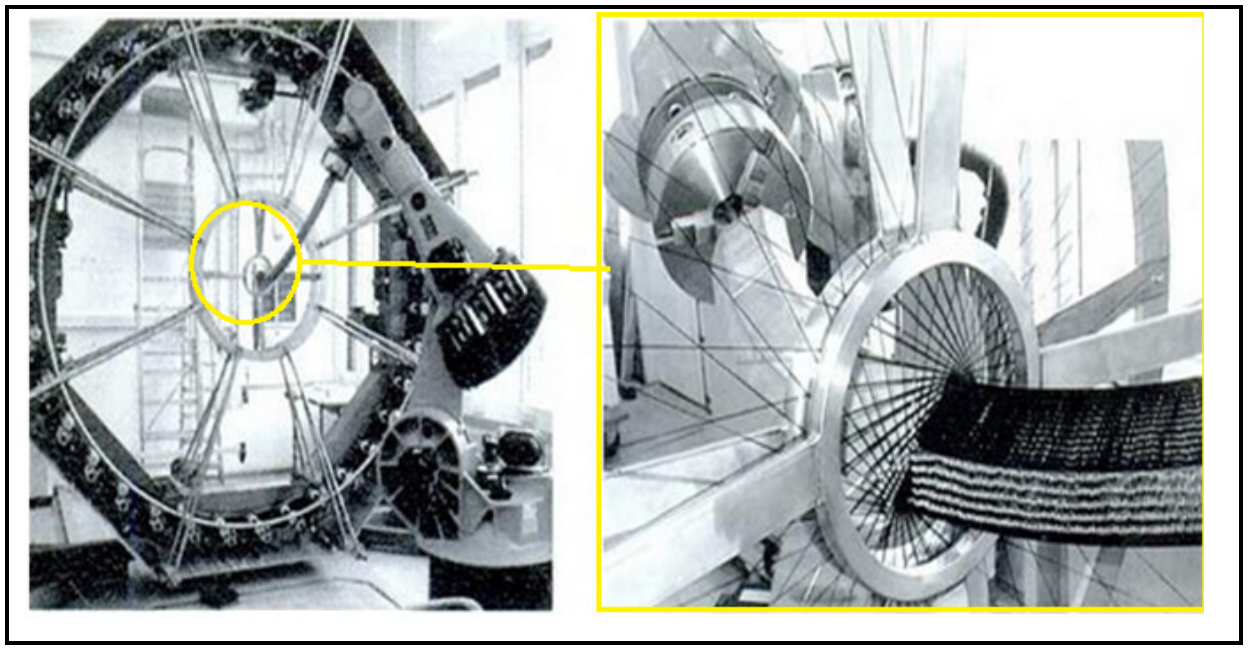

Figure 1.11. Robotic braiding of a J-stiffener (Neitzel M. and Mitschang P., 2004)

1.2.4 Kniting

Knitting is widely used for the production of garments. It has received attention from preform manufacturers for producing complex 3D structures. Figure 1.12 shows a 3D knitted structure. Due to the curved structure of yarns, the knitted preform has a very flexible structure. These characteristics permit the preform to be used to produce very complex structures. However the major disadvantage of this process is fiber breakage occurring during the manufacturing of preform in particular for carbon fibers. Other major problem around the knitted reinforcements is the loop structure makes local stress concentrations, so their mechanical properties are generally lower than alternative techniques.

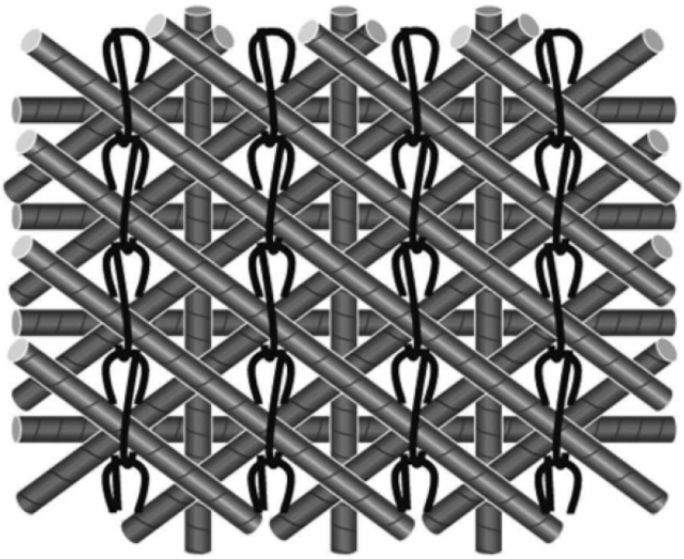

Figure 1.12. Multiaxial warp knitted fabric (Jinlian H., 2008)

1.3 Preform characteristics

The textile fabric structure influence the manufacturing properties such as deformability, porosity and permeability and mechanical properties of final composite parts. The characterisation of local fiber variation occurring during forming, fiber volume fraction and fiber thickness are significant parameters to describe the performance of textile fabrics. During the forming of textile fabrics, the following deformation mode occurs: shearing, straightening, wrinkling, stretching, interply slipping and intera-ply slippage (see Figure 1.12).

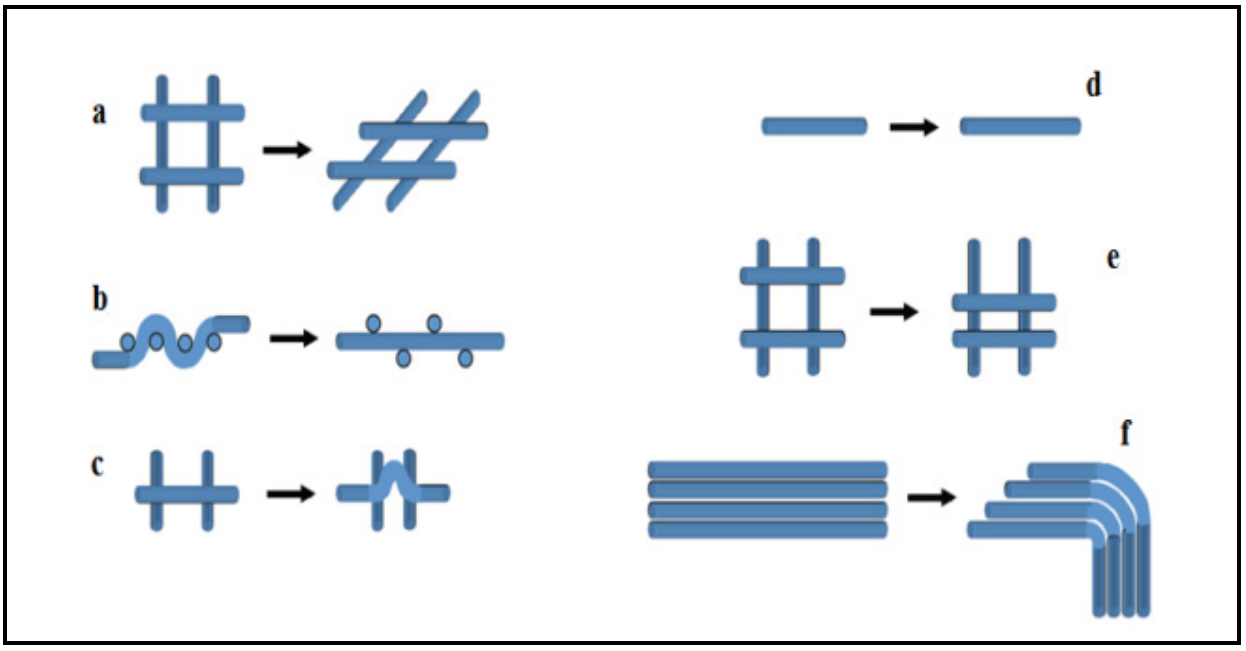

Figure 1.13. Deformation modes of textile fabric (Paolo E., 2009)
(a) shearing (b) straightening (c) wrinkling (d) stretching
(e) intra-ply slippage (f) interply slippage

If the directions of applied tensile load to textile fabric do not coincide with the fibre tow orientation, fabric shear mode occurs. This deformation mode is subject to high friction in the crossing points depicted in Figure 1.13a. Figure 1.13.b&c depict the shearing modes occurred in transverse or parallel to fiber tow. Fibre curvature changes under tensile and compressive load. The effect of fibre straightening is substantial for knitted fabrics. However, the effect is low for other fabrics with low-undulation structure. Elastic stretching of fiber has minor importance, because the reinforcement textiles used for advanced applications have high tensile moduli. Interply deformations allow the preform layers to slip with respect to each other when the fabric is bent by forming forces. Figure 1.14 displays the presence of high fiber slipping at the corner (Endruweit A. and Ermanni P., 2004).

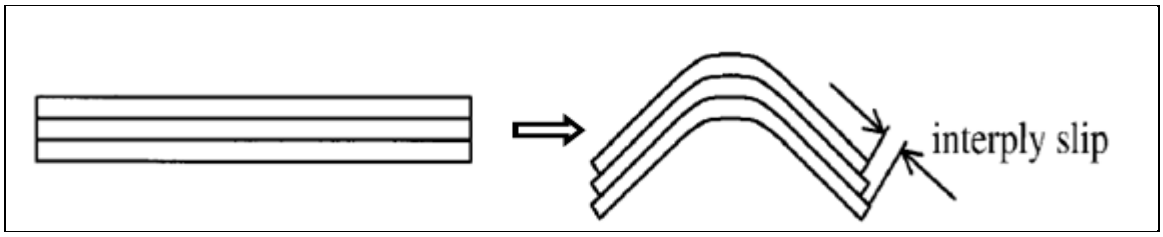

Figure 1.14. Schematic image of intera-ply slippage occurring in sharp corner (Antonio M., 1999)

Other deformation modes in textile fabrics, bending and torsion modes can be occurred due to friction between the fibre bundles and the compression resulted from forces in perpendicular to the fiber bundles axis. Figure 1.15 represents schematic images of these deformation modes.

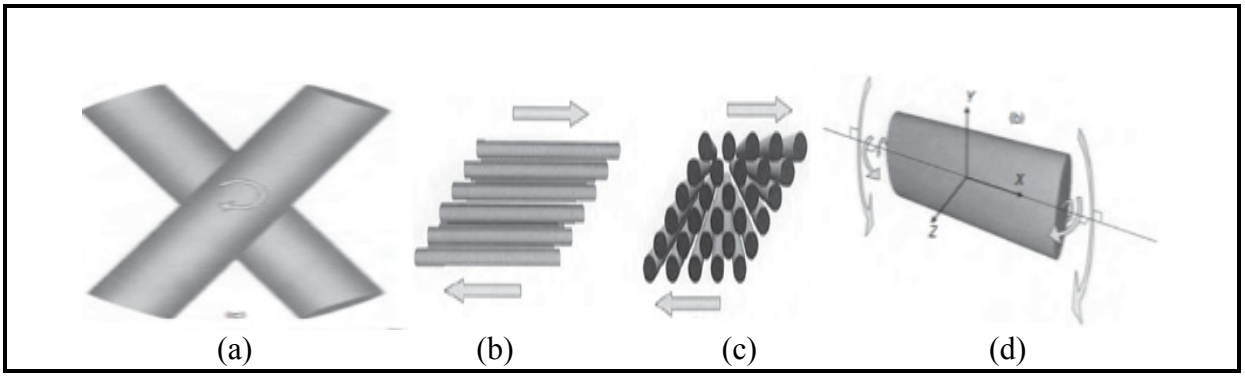

Figure 1.15. Deformations of fiber bundles: (a) Crossover shear (b) Inter fiber shearing in direction of fiber tow (c) Inter fiber shearing in transverse direction (D) Bending and twisting (Long A., 2006)

Based on the deformation modes demonstrated above, textile mechanics must include a description of their behaviour under combined biaxial tension (Lomov S. V., Boisse P. and Morestin E., 2008), shear and compression loading conditions (Chen B. and Chou T., 2000; (Sozer E.M. et al., 1999), bending and friction tests (Potluri P. and Atkinson J., 2003).

1.4 Textile forming

Complex shaped textile composite needs the formation of textile fabric in tools before resin injection. The draping of textile fabrics on double curved surfaces has received much attention both in 2D and 3D textile structure for description of the textile behaviour for forming (Yu J. Z., Cai Z. and Ko F. K., 1994). For instance, drapability of fabric for manufacturing an aircraft nose cone or blade geometries are the main characteristics that have been investigated for the adaptation of fabric on their tools (see Figure 1.16) (Safran Group Ltd., 2011).

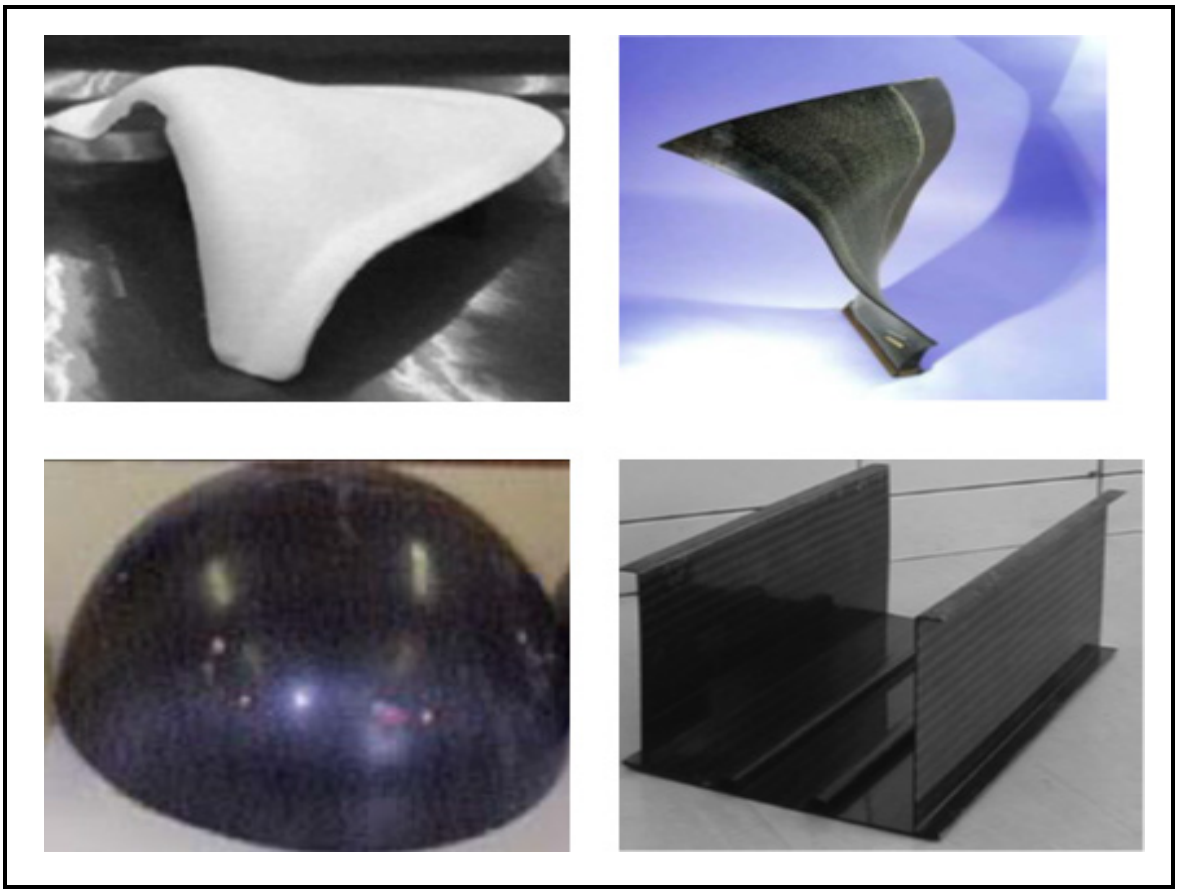

Figure 1.16. Typical complex shape parts composed of textile fabrics (Luycker E. et al., 2009; (Mouritz A., 1997; (Uozumi T., Kito A. and Yamamoto T., 2005)

The drape of textile fabrics can be expressed in terms of shear deformation, local shear angle, and yarn slippage. The wrinkling defect occurs due to compression loading appearing during shear deformation of fabric tows beyond the locking angle (maximum shear angle). This defect results in buckling deformation through the fabric thickness (Long A., 2006). To be clearer, drape test of four different types of textile fabric including a basket, plain, twill and satin weave are depicted in Figure 1.17.

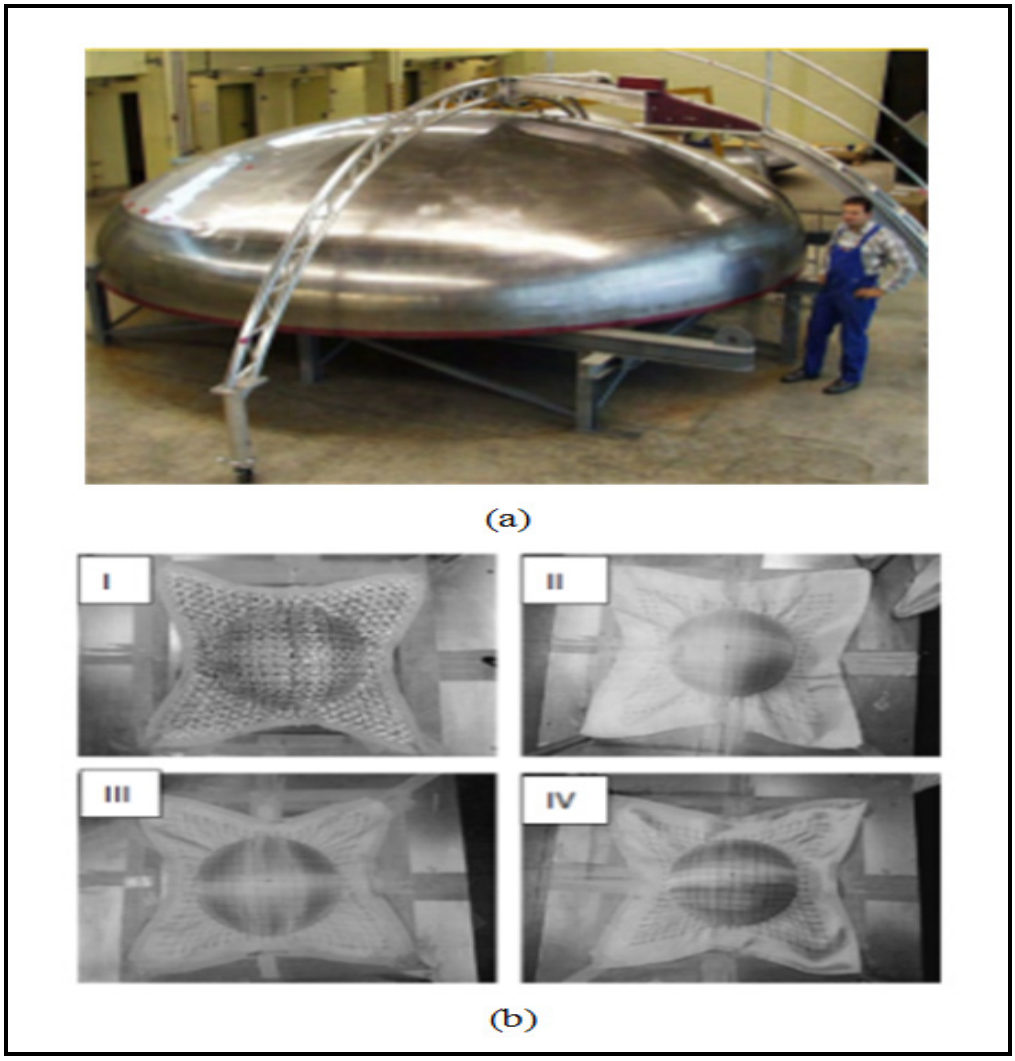

Figure 1.17. (a) Curved surface used for manufacturing pressure bulkhead (Chen B. and Chou T., 2000; (Hybridmat, 2006)
(b) Textile fabrics draped on hemispherical die I) Basket II) Plain III) Twill IV) 5-harness Satin

Plain weave exhibits low shear deformation and the worst drapability due to high level of fiber undulation in compared with other fabrics. It is worth noting that these low shear deformations can result local change of fiber volume fraction.

Shearing of aligned reinforcement results in two effects in the architecture of fabric: changes in fibre orientations and decrease in tow spacing. The decrease of tow spacing causes the density increase and consequently a local change in fibre volume fraction occurs.

Figure 1.18 represents a comparison between several textile woven fabrics based on the deformability and stiffness.

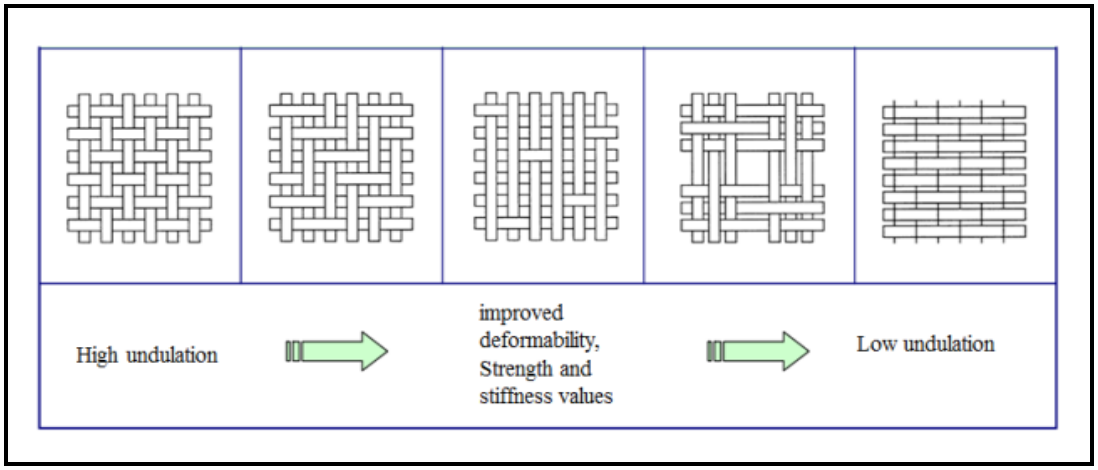

Figure 1.18. Comparison of different types of woven fabrics and their characteristics (Chen B. and Chou T., 2000)

1.5 Classification of fiber structure

Characterisation of the textile fabric based on shear stiffness and drapability is needed for accurate prediction of the fabric forming for 3D-complex shaped composite structure. Figure 1.19 depicts relation between shear stiffness and drapability for different fabrics. It is clearly seen that unidirectional (UD) tape has low drapability and shear stiffness. Since, UD tapes indicate high fixation of the yarns permitting no large shear angles during forming, and the fabric cannot be distorted easily. Knitted preforms have high conformability, however lower in shear stiffness due to curved fibers.

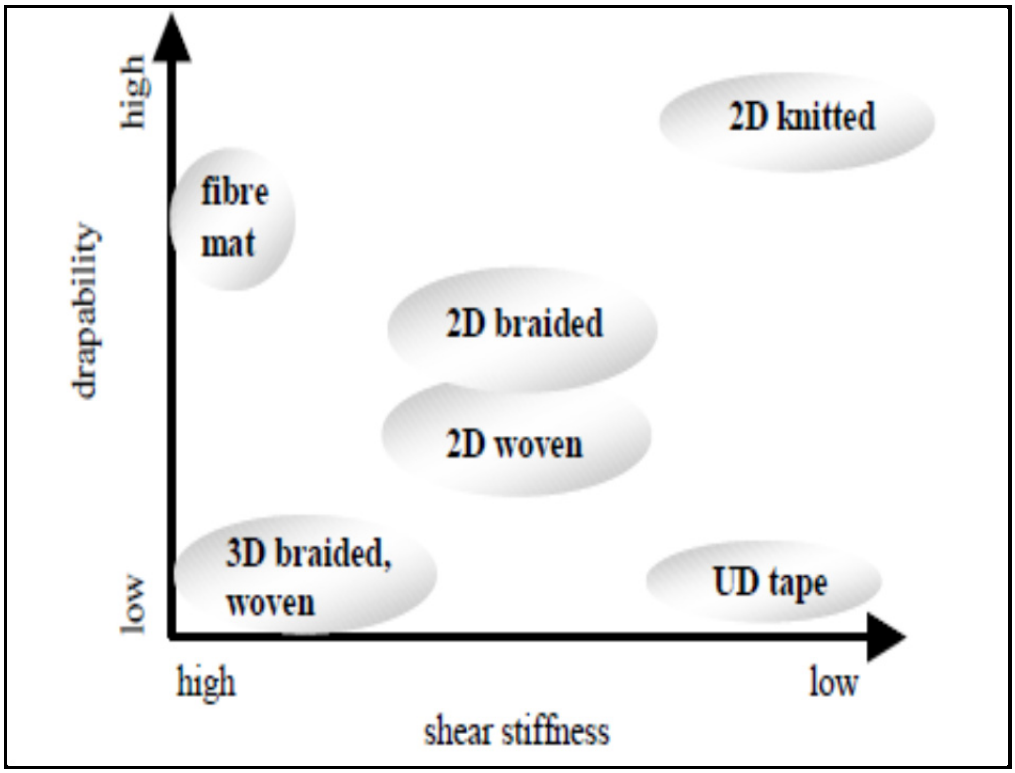

Figure 1.19. Textile fabric characteristic based on drapability and shear stiffness (Paolo E., 2009)

3D woven has high stability and shear stiffness due to reinforcing fiber in the through thickness direction. Braided fiber in compared with other fabrics has low shear resistance, but relatively high drapability. Based on Figure 1.19, it can be conclude that braided preform are more appropriate for complex shapes with varying cross-section such as nozzles and cones (Hybridmat, 2006).

1.6 Textile composite manufacturing process

A wide range of manufacturing processes are available for the textile composite (Baoxing C. and Tsu-Wei C., 1999; (Long A., 2006). The most commonly used process is Resin Transfer Molding (RTM) which enables industry to manufacture net shape parts in closed tooling a shown in Figure 1.20. The main feature of RTM is the injection of the liquid polymer through a dry preform laid in a closed mold. Figure 1.21 depicts an example RTM molding to

produce a complex shaped aerospace structure. The impregnation quality depends on the combination of pressure at which the resin is injected, temperature, resin viscosity, mold cavity shape and preform properties.

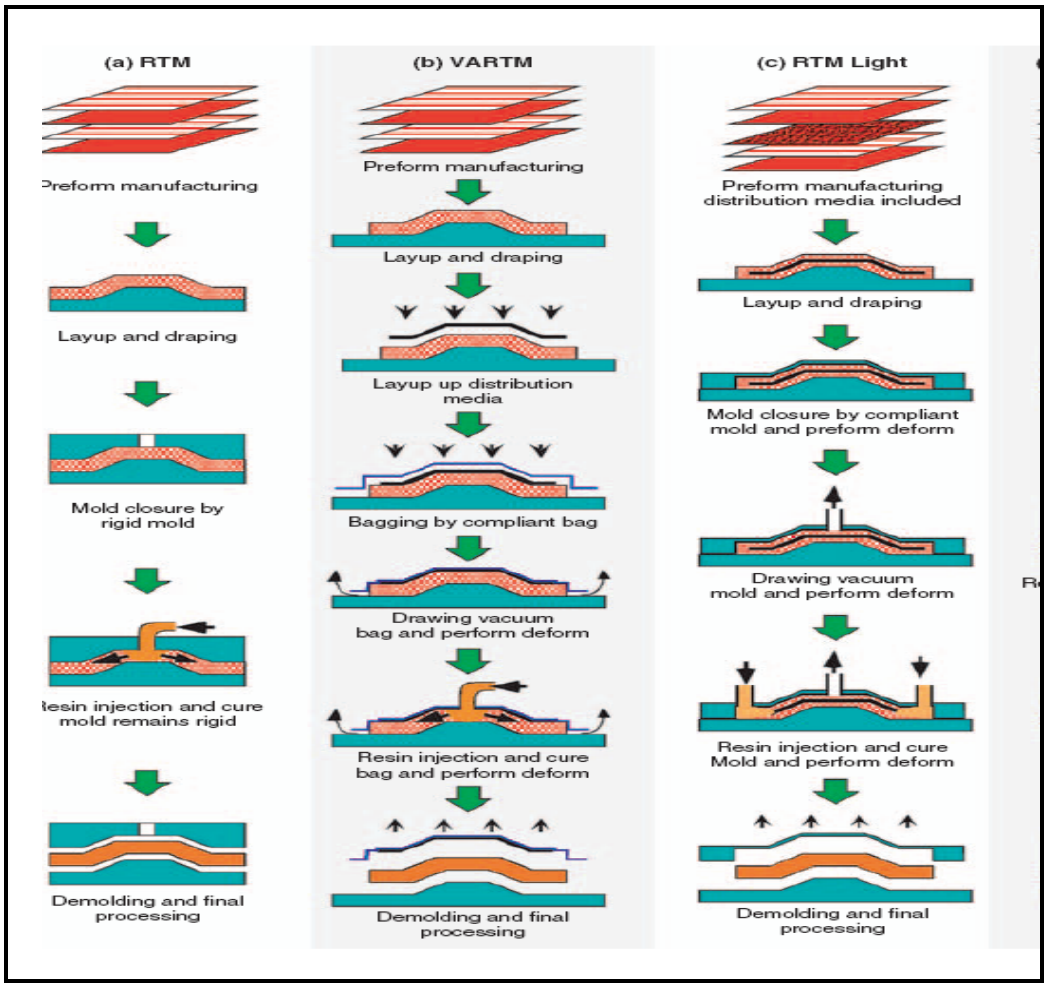

Figure 1.20. Typical composite manufacturing process
(Simacek P., Advani S.G. and Iobst S.A., 2008)

Many other techniques are derived from this manufacturing method, such as the resin infusion process or Vacuum Assisted Resin Transfer Molding (VARTM) in which resin flows through the mold and impregnates the fibers due to vacuum applied in the outlet. This technique allows the possibility to fabricate various composite components with high performance. As shown in Fig. 1.22, highly complex structures can be produced by using of

VARTM that reducing part-count and off-setting costs with the intermediate assembly stage (Mazumdar S. K., 2002).

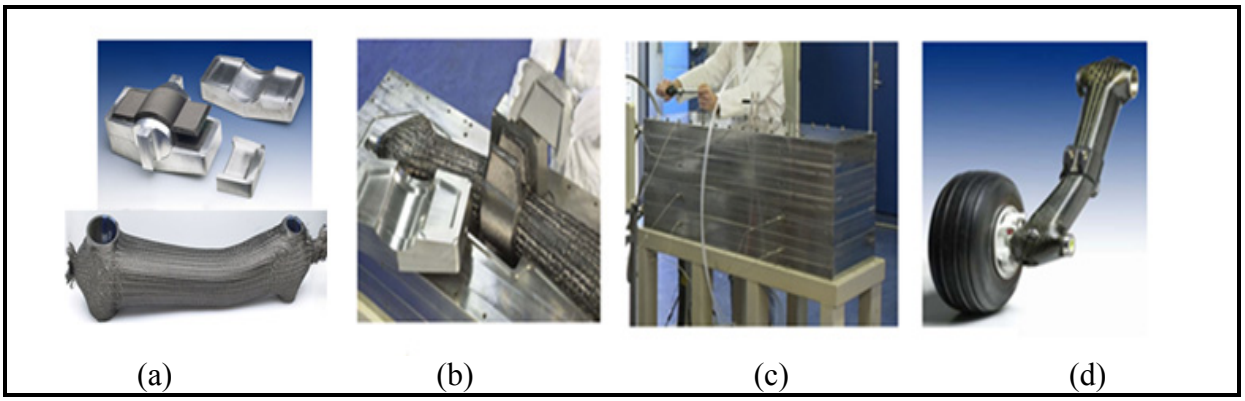

Figure 1.21. Manufacturing process of a landing arm for helicopter NH-90 (Thuis H., 2004)
(a) Braided preform (b) assembling of the preform into the mould
(c) RTM setup to inject resin to the mould (d) final product

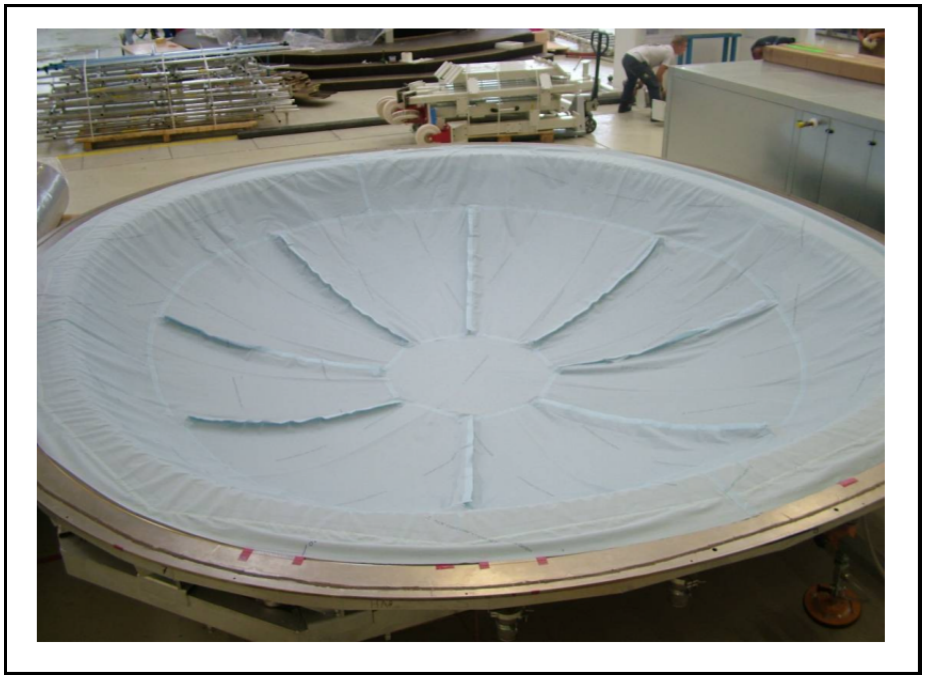

Figure 1.22. Fabrication of pressure bulkhead using vacuum infusion process (courtesy of Trans-Textil GmbH)

1.6.1 Dependency of resin flow to fabric structure

Prediction of resin flow to produce high quality composite using RTM and VARTM process requires detailed knowledge of preform permeability and the impregnation behavior of the fiber preform materials under compaction.

On the other hand, permeability and flow pattern highly depend on preform structure. Below gives a summary of preform characterisation in terms of thickness, porosity and permeability and their effect on flow pattern.

1.6.2 Effect of preform thickness on flow patterns

During forming process, the fiber volume fraction and the compression applied into the preform are influenced by the preform thickness. Figure 1.23 depicts examples 3D preform with different thickness. Preform thickness has high influence on flow fronts and lag formation (Bekir Y., Murat S. and Murat S., 2009; (Merotte J., Simacek P. and Advani S. G., 2010).

As shown in Figure 1.24, the lag formed in the resin flow front is due to the presence of high permeability on the top surface of the preform. The lag increases with increasing specimen thickness because of the increased volume of resin needed to flow through the thickness and fill greater volume of pores in the preform.

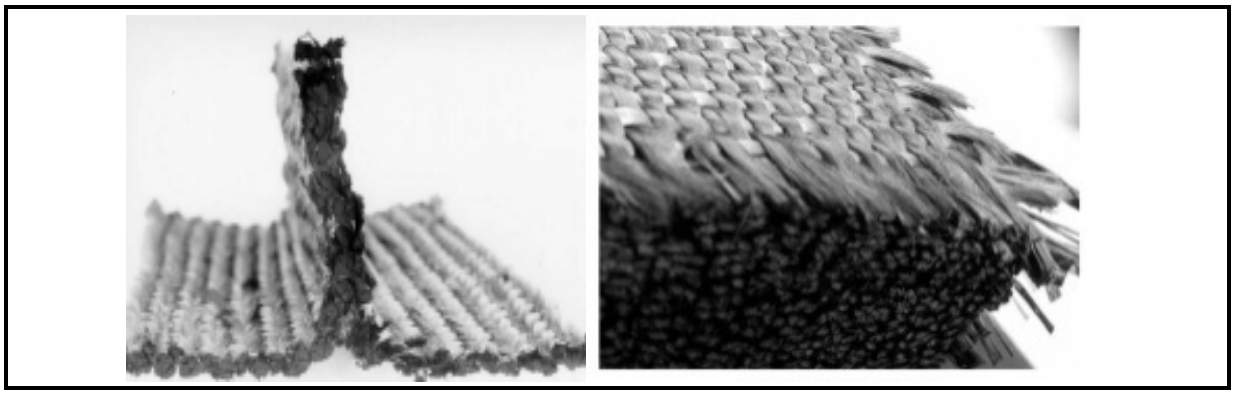

Figure 1.23. Typical example of thin braided and thick woven (100mm)
(Luycker E. et al., 2009; (Tong L., Mouritz A.P. and Bannister M.K., 2002)

In order to eliminate the lag phenomena, the infusion process needs to continue until the lagging region is completely impregnated with resin. It should be noted that the flexible vacuum bag in VARTM process and varying pressure inside the mold cavity causes the preform thickness variation and, therefore, the fiber volume fraction of the preform alter during infusion. To produce high quality composite, the permeability of the preform should be examined at varying fiber volume for different case of the variation of compaction pressure.

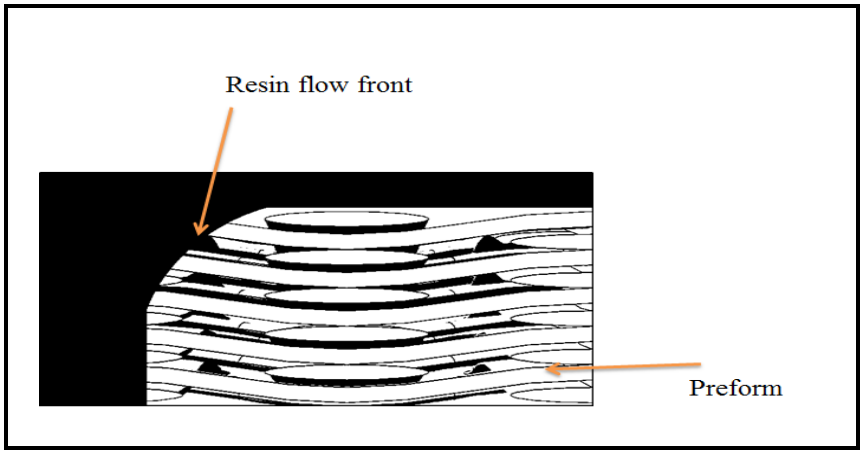

Figure 1.24. Flow front and formation of resin lag due to high permeability on the preform surface

In the resin transfer molding (RTM) process, the preform architectures, thickness and layup sequence of textile fabrics influence the injection pressure. Occasionally, a small variation in preform thickness can severely influence out of plane permeability and the injection pressure. A reduction in local mold thickness results in local fiber volume fraction increase, which decreases preform permeability, and increasing molding pressure. For instance, a local reduced thickness in a corner of the mold may lead to preform permeability decrease, and consequently, molding pressure increase.

1.6.3 Compressibility of textile fabric

Two phenomena are observed during the preform compaction to achieve high fiber volume and lower porosity. First, the response of dry preform under the compaction loading is not

elastic, and the hysteresis occurs during unloading process. The hysteresis mainly is because of the preform relaxation behavior happened during compression and decompression experiment (Francois R. and Raymond G., 1998). Second, the wet fiber impregnated with resin is compacted more than the dry preform under the identical compression loading due to the effect of resin lubricant.

Before resin impregnation, the dry preform is under vacuum compression. The compression strain highly depends on fibers elastic properties and their slippage at fiber crossover points. After the resin injection, the local pressure applied to the preform drops.

Figure 1.25 represents the typical pressure vs. porosity curve recorded for textile fabric. For dry fabric, there is homogeneous porosity because fabrics are homogeneously compressed. On the contrary, for wet fabric, an inhomogeneous distribution of porosity occurs because of the injection pressure inside the fabric.

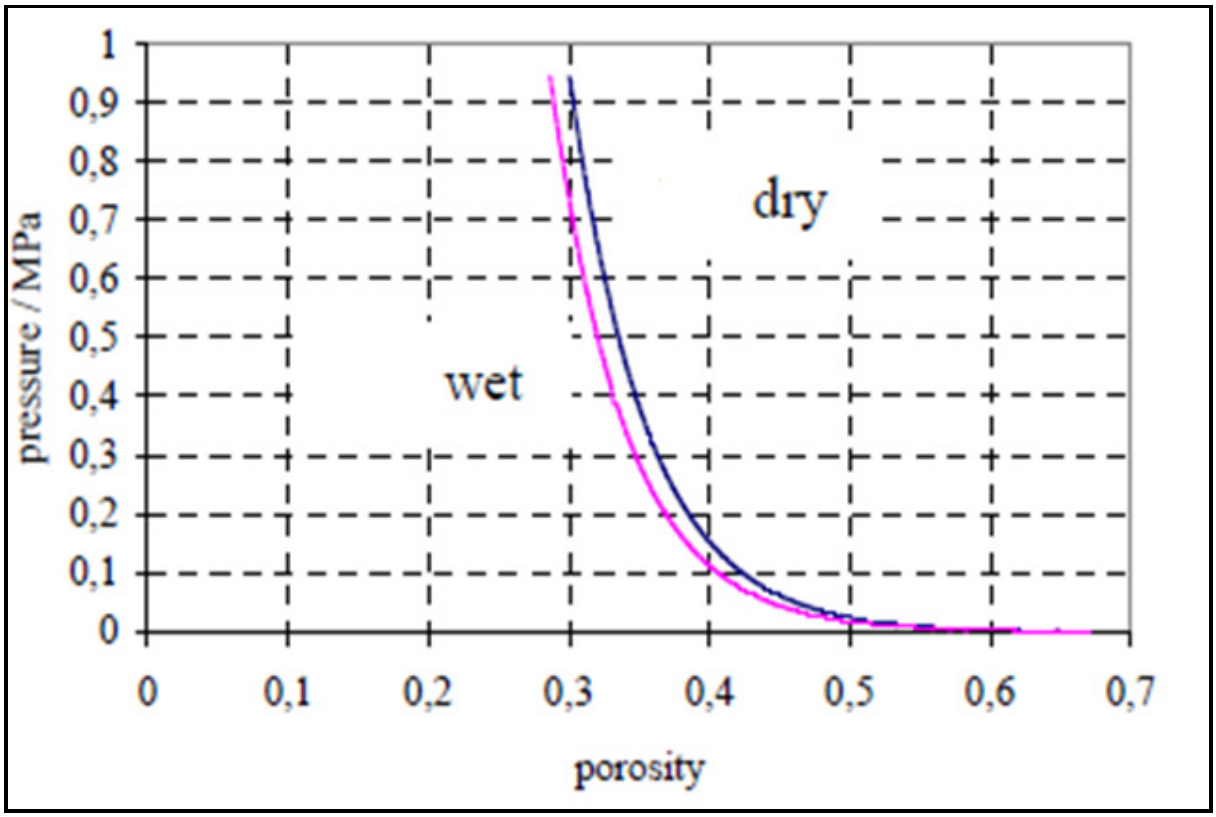

Figure 1.25. Compression pressure relationship of biaxial (BD) dry and wet fabric. (Andreas E., 2003)

1.6.4 Dependence of permeability in textile fabric

The quality (reduction of manufacturing defects) of the composite parts extremely depend preform permeability that affects the injection process. In-homogeneities in porosity and fabric geometry occurring during deformation and preform compression severely influence the textile permeability. Fabric drape is composed of different deformation modes such as the shearing, straightening, stretching, and yarn slippage. These deformation modes could result in local change of fiber orientation and permeability. Figure 1.26 depicts two elliptical flow front related to a satin weave fabric before drape (perfect) and after drape (sheared). Drape process results inhomogeneous permeability distribution such that the shape of flow front deviates from initial shape (perfect) to sheared shape because of sheared fabric.

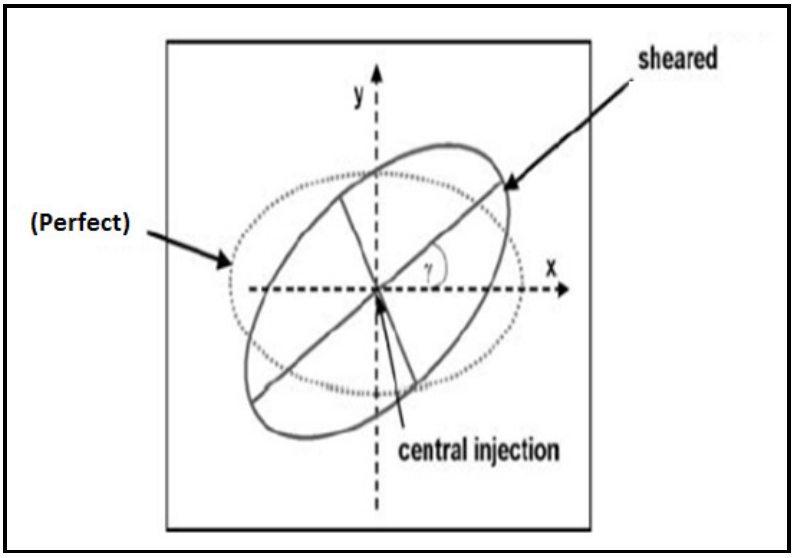

Figure 1.26. Deviation of flow front due to fabric shearing
(Louis M. and Huber U., 2003)

1.6.5 Mechanical properties

Several structural 3D reinforcement techniques have been developed to improve the delamination toughness of polymer composites. These include 3D weaving, stitching and Z-pinning. Stitching process can improve the interlaminar properties, fracture toughness and impact damage resistance (Tomek R., 2004). Figure 1.27 shows a comparison of open-hole stitched composites subjected to tensile loading based on the trough thickness reinforcement

(TTR). It is worth noting that composite laminate tensile strength is highly dependent on the angle between fiber direction and loading direction. Hence, TFP could be used to optimize the fiber orientation.

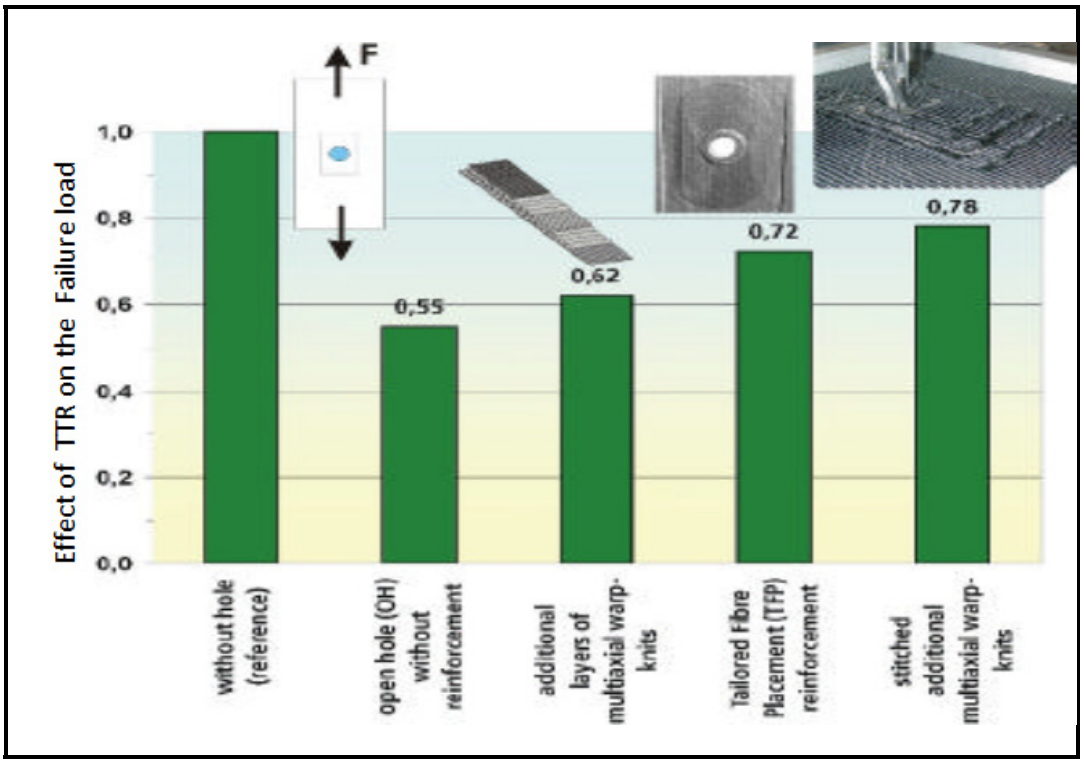

Figure 1.27. Comparison of strength of laminated and stitched composite (Sickinger C., Wilmes H. and Herbeck L., 2000)

Some experimental results display that stitching process diminishes the stiffness, and fatigue strength of 3D composites around 10-20%. Based on literature and technical documents numerous experimental tests have been conducted to realize the amount of the loss in the stiffness and strength in different tensile and compression condition, fatigue life and other mechanical properties (Jin L. et al., 2013; (Mouritz A. P. and Cox B. N., 2000; (Sickinger C., Wilmes H. and Herbeck L., 2000; (Sickinger C. and Herrmann A., 2001). Based on literature, stitching technique cannot be fitted to prepreg laminates due to considerable fine damage occurring during stitching process. Regarding dry fabrics, fibre breakages may become source of stress concentration which facilitates the macro damage formation in

particular in fatigue loading. To summarize, damage in stitched preforms and subsequent composite failures due to static or dynamic loading are a major concern to their aerospace applications (Carvelli V. et al., 2010; (Mouritz A.P. and Cox B. N., 2000). Therefore, understanding the behaviour of a stitched composite structure subjected to mechanical loadings in particular impacts and hole-edge delaminations due to static or fatigue loads is vital task.

1.7 Quality issues for the manufacturing of textile composite

The RTM process can be used to fabricate high performance textile composite structures. Nevertheless, to enhance product quality in RTM process, resin curing process and accurate control of relevant processing parameters must be improved. If processing parameters are not controlled, the void formation can result the reduction in the mechanical properties (Hamidi Y.K., Aktas L. and Altan M. C. , 2009). The main reasons leading to form void in RTM technique can be classified as follows:

Evaporation of mold: Evaporation of mold in the formation of bubbles in the preform surface leads to macro-voids.

Resin outgassing: Voids can form from the gaseous components coming out of the resin during the vacuum process. Therefore, the resin has to be degassed to reduce the resin outgassing.

Preform permeability: permeability which includes the characteristics of fiber dimensions and arrangement is significant parameters in resin infusion. This parameter allows controlling the fiber impregnation, complete fiber wetting and ensuring high quality textile composite structure. Non-uniform permeability because of preform inhomogeneity causes the resin velocity to change from point to point at micro scale. Differences in permeability result in either bubbles inside fibre bundles, or in the space between fibre bundles (see Fig.1.28).

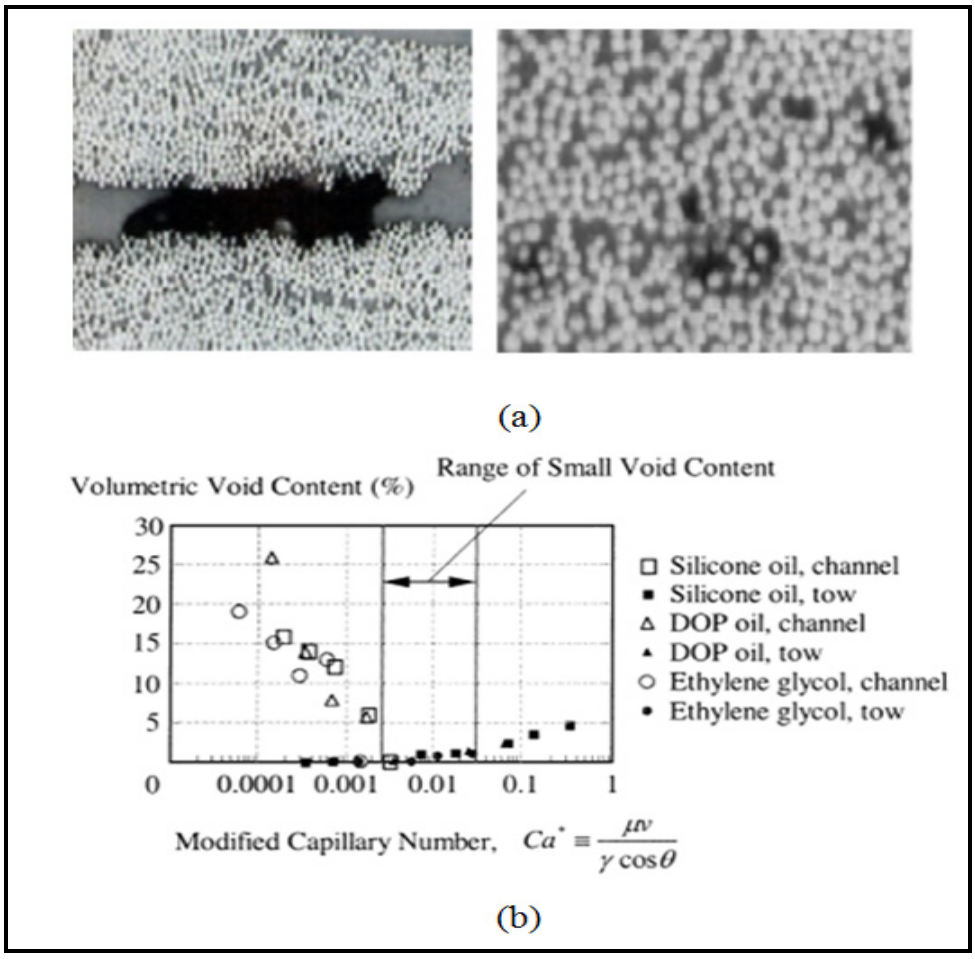

Figure 1.28. (a) Example images of void in textile composite: marcovoid (left) and microvoid (right) (b) Void content vs. capillary number. (Hamidi Y.K., Aktas L. and Altan M. C. , 2009)

Permeability variations can result in macrovoids and microvoids. Also, void locations highly depend on resin velocity in such a way that the resin with high velocity will lead the formation of void within preform tows because the flow in the tow is slower than in the channel. However, low resin velocity will form the voids in channels between fibers bundles. Effect of fiber content: Increasing the fiber content of composite cause reasonably the decreasing the permeability and voids number. For instance, 85% reduction in void content in composite can be occurred by increasing the fiber volume fraction from 10% to 40% (Varada R. A. and Blouin A.).

Race tracking: Race tracking occurs when the resin races around the edges of the mold. Large voids and porosities could originate from this event in the mold center. Race tracking can be avoided by placing the resin vent in appropriate location and applying sealing tape along the mould edges. Furthermore, high viscosity resin could be helpful to decrease the occurrence of this defect (Lawrence J., Fried P. and Advani S., 2005).

Thickness deviation: During the infusion process, the preform is submitted to a non-uniform pressure distribution at the inlet and vacuum port. When the preform is impregnated by resin whose pressure is changing during the flow, consequently, the thickness of preform continuously varies (Jing L., 2003). To understand the relationship between resin flow rate inside preform and vacuum pressure, the Darcy's law is applied to describe the flow inside a porous matter. Darcy's law can be expressed to flow the resin through a preform as

$$\mathbf{v} = -\frac{\mathbf{K}}{\mu}\Delta P \tag{1}$$

Where **v** is the volume-averaged Darcy velocity of resin in preform, μ is the resin viscosity, and K the permeability tensor of the preform, and ΔP is the pressure gradient. The permeability tensor describes the resistance of the flow of the preform. By inserting equation (1) into continuity equation and applying appropriate boundary conditions, the resin pressure during impregnation can be obtained (Simacek P., Advani S.G. and Iobst S.A., 2008).

1.8 Defects in textile composite and preforms

Inspection of textile preforms needs to have sufficient knowledge about the various types of defects in textile preforms and textile composites. This section provides a description of possible defects in textile preforms and composites and then state of the art non-destructive testing techniques to detect damage in preforms and composite will be discussed later.

Defects in composites

Most common defects appearing in textile composite structures are: delamination, ply misalignment, disbands, voids, impact damage, porosity, inclusions, erosion (environmental

effect such as the damage caused by the liquid drop impact), matrix cracking, inaccurate fibre volume fraction, fiber breakage, kissing bonds, and incorrect cure. Figure 1.29 exhibits example microscopic images of these defects.

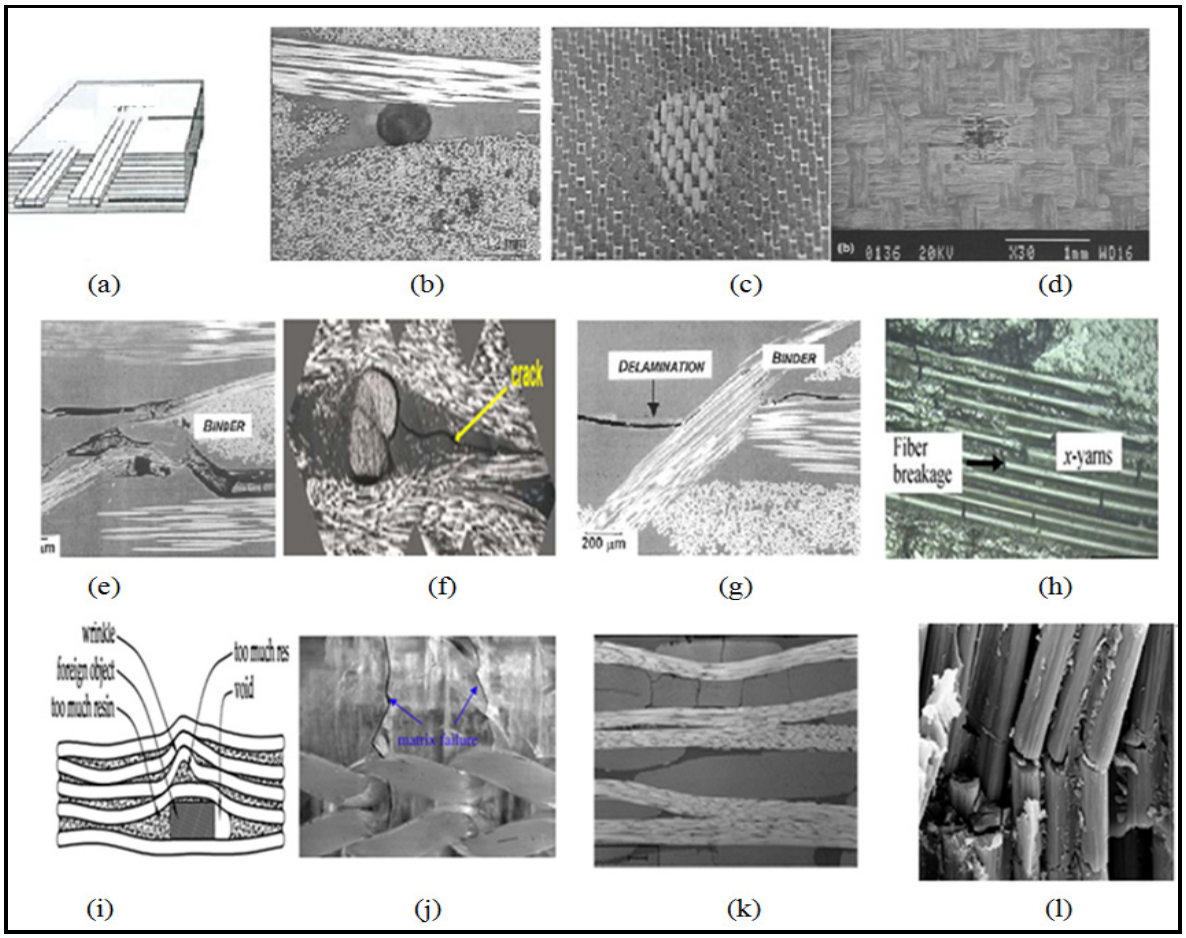

Figure 1.29. Example image of major defects in textile composite (Tong L. M., 2002; (Unnþórsson R., 2004) (a) Edge damage occurring in machining process (b) void between fiber bundle (c) Dry path (d) Micrometroid damage (e) Brocken Z-binder (f) Micro-crack in the stitched composite (g) Delamination in woven composite (h) fiber breakage (i) Inclusion (j) Matrix crack (k) Matrix crack (l) fiber breakage

In all textile composite manufacturing processes, these defects can be observed in composite parts, however the process cycle has high effect on the size, shape and the occurrence frequency of each defect. To have a better understanding of manufacturing defects, a description for each defect is provided as follows:

Porosity is introduced to samples if air and volatile resin are not controlled correctly. Any local change in the shape of ideal fiber could results fiber misalignment. Ply misalignment is created as a result of any mistake made during the layup stacking (Kang K., Lee H. and Hahn T., 2000; (Tong L. M., 2002). Fiber breakage in fibers is created during fiber manufacturing and could result sites that damage progression is initiated from them (Mouritz A. P. and Cox B. N., 2010). Delamination defect is produced by machining or contamination placed between fabric layers. To obtain composite with less damage, water jet machine, laser cutting or a thin mill tool on CNC machine with careful feed and speed have to be used to cut composite structures to prevent edge damage (see Fig. 1.30).

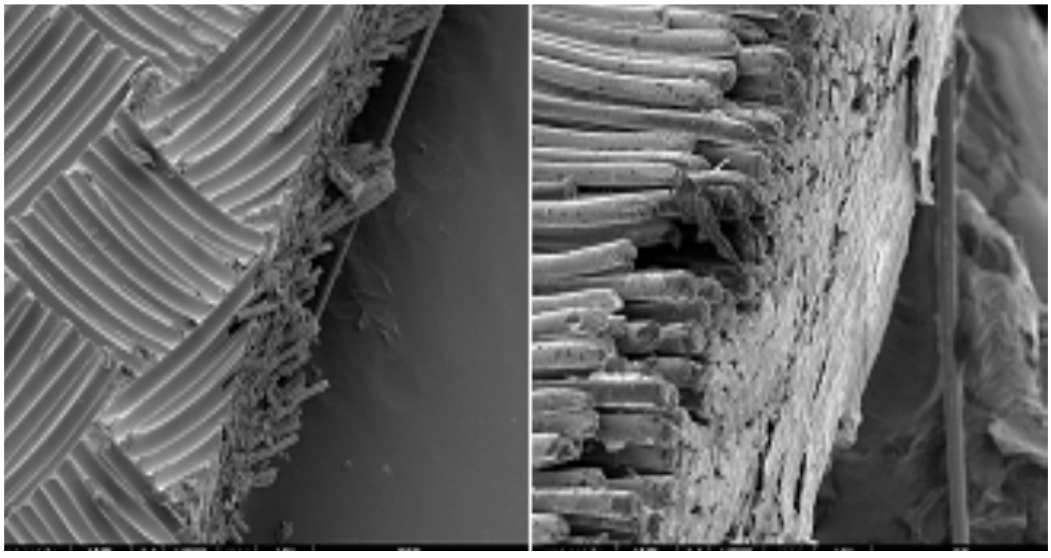

Figure 1.30. Comparison of cutting by laser (a) and mechanical machining (b) (http://www.industrial-lasers.com)

Damage in 3D textile preforms

The quality of textile preform has considerable effect on the mechanical properties of the textile composite. During manufacturing process, various defects can be introduced into textile preform and decrease the composite performance. The different types of defects in

textile preforms (2D and 3D) shown in Figure 1.31 are illustrated below, and then the state of the art non-destructive testing to detect these damage found in the literature will be discussed in the next section.

Fiber misalignment: The exact position and orientation of the textile layers have a great effect on composite mechanical characteristics and it can considerably change the performance of the final composite (Tong L. M., 2002). Stitching cause fiber bundle misalignment around stitch reinforcements which degrades in-plane mechanical properties of composite.

Fiber crimping: Crimping appears by the high shear stress and strain due to the local bending effect of the fibers on the surface of the preform resulting loss of properties (Tong L. M., 2002). This defect schematically is shown in Figure 1.31d. The amount of fiber crimping depends on the tension applied on stitching yarn. Also, the amount of crimping in 3D preforms varies due to differences in weave architecture and manufacturing process.

Fiber breakage: This defect occurs because of some problem in the preforms manufacturing process (Mouritz A. P. and Cox B. N., 2010). For example, in the stitching process, the needle penetration into fabrics causes localized in plane fiber breakage and fabric misalignment, which reduces the composite performance. The extent of fiber breakages in stitched preforms depend on the stitch thread diameter and stitching tension and fabric density.

Resin-rich pocket: The fiber crimping and misalignment occurring in stitching results in small elliptical forms around the stitching thread where low fiber content (see Figure 1.31e) (Tong L., Mouritz A.P. and Bannister M.K., 2002).

Compaction: This defect occurs when the stitching tread is applying high tensile load to the preform. Consequently, the excessive loading leads the preform to have higher fiber volume fractions more than it is expected.

Stitch distortions: Distorted stitching patterns and threads can be occurred due to high compaction loading applied on the preform.

Fiber pull out: The stitching thread may be damaged during stitching process due to twisting, bending, looping action and sliding as the thread passes through the stitching machine.

Inclusions: Any impurities in the preform can harm the strength of the fibers. For instance small objects inside preform lead the void formation or debonding defect. Sharp-edged inclusions may damage the fibers during infiltration process (Tong L., Mouritz A.P. and Bannister M.K., 2002).

Moisture entrapment: Moisture can be accumulated by the preform, if it is exposed to humidity for a long time. Therefore, it is necessary to keep preforms under controlled moisture environment and temperatures.

Stitched preforms composed of several 2D fabrics stacked together using stitching should be inspected before stacking. The most common defects in the textile layers are as follows: kinked or wavy bundles, broken fibers, inclusions/Impurity, fabric wrinkles, sheared fabric, free edges damage, loosed fibers, Fiber gaps, moisture entrapment, knots and slubs, mispick and kinky filling (Warren J., 1994).

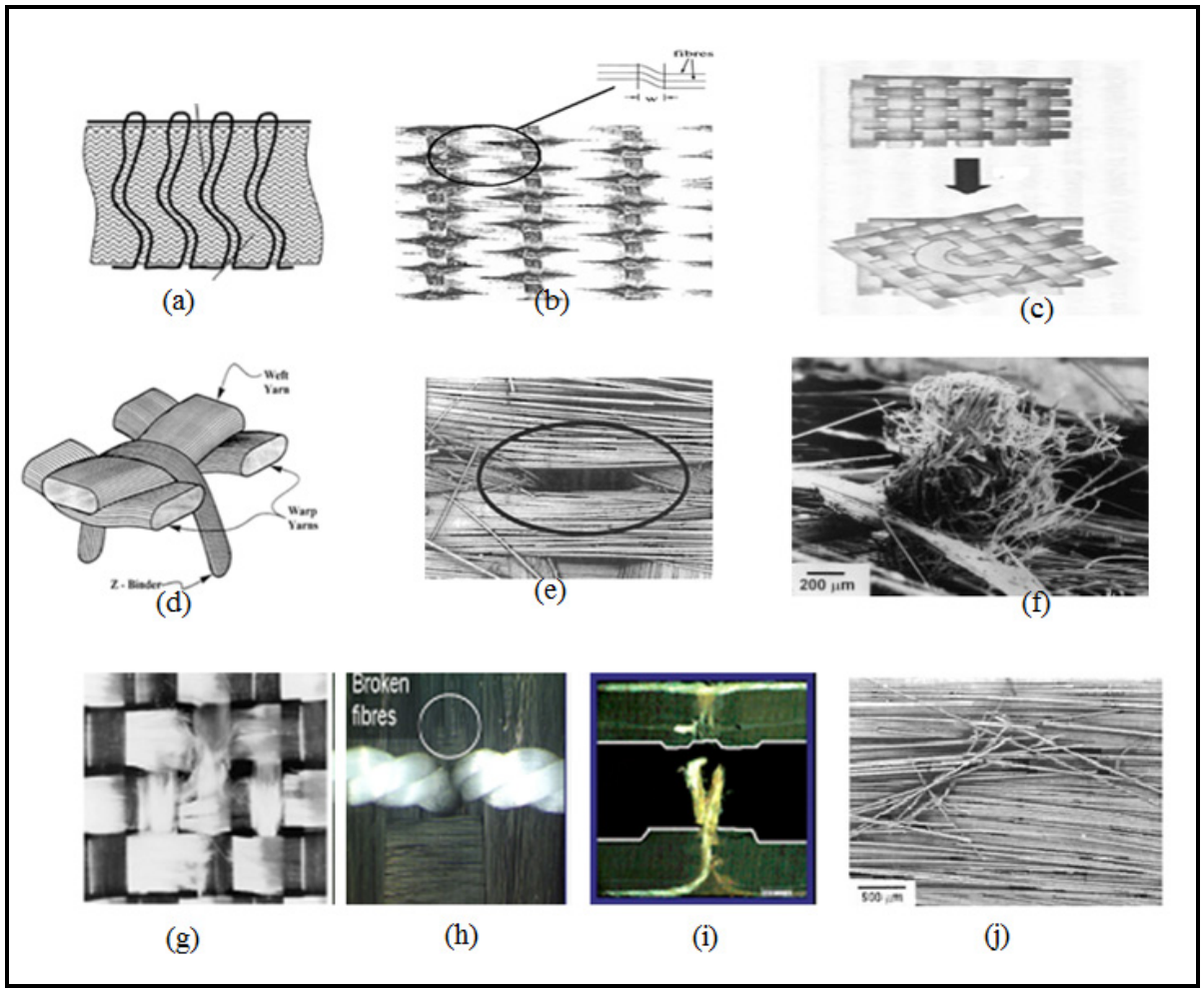

Figure 1.31. Different types of preform defects (Tong L. M., 2002)
(a) Misaligned through the thickness yarn (b) Misalignment of fiber bundle due to stitching (c) Textile fabric misalignment (d) Fiber crimping (e) Resin rich region (f) Fiber pullout (g-j)fiber breakage

1.9 Non-destructive testing of 3D textile composite

Because of advanced applications of 3D textile composite, these composites should be inspected using non-destructive evaluation (NDE) techniques. Non-destructive testing process for textile composite can be divided into two parts: inspection of preform and final composite.

1.9.1 Preform inspection

According to literature, all techniques to inspect textile preforms can be classified as visual testing and radioscopic testing techniques. Visual inspection techniques are the most common NDT methods used to inspect preforms. These techniques are used to inspect visually for the surface defects such as surface breaking, fiber pull out, etc.

In recent years, laser scanning methods have been used for inspection of preform surfaces on the basis of triangulation principle. The technique is a combination of a camera for image processing and an integrated laser light section sensor (Andrea M., 2009; (Schmitt R., 2007). The technique could be beneficial to improve the quality of the final product and measure and evaluate deviations in the fiber orientation. Furthermore, it can recognize the textile architecture and measure the amount of deformations occurring in fabrics (see Fig. 1.32).

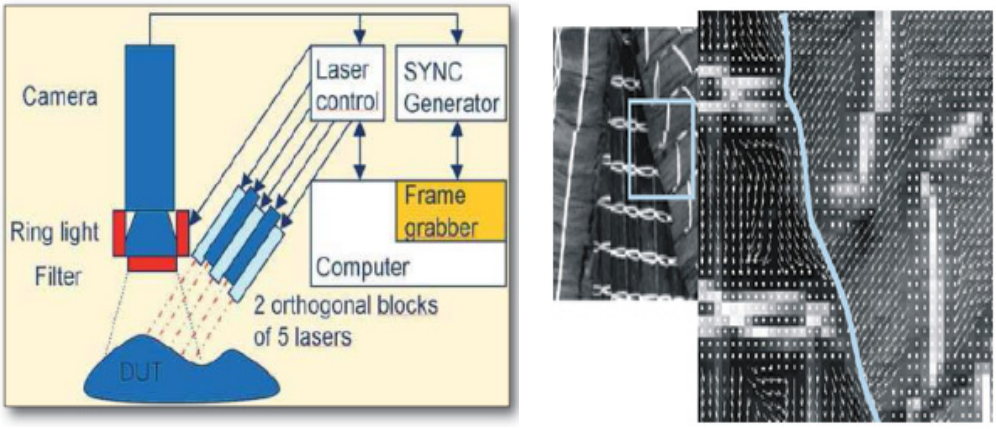

Figure 1.32. (a) Schematic of the principle of laser sectioning system (Andrea M., 2009)
(b) Example image of fiber orientation detection using laser sectioning system

Geometrical measurement of preform can be performed using laser scanning technique which allows reaching higher quality for the preform prior to install it in the mould to be injected by resin. The dimensional measurement of textile preform involves the 3D image

acquisition of preform using appropriate sensor. The type of sensor depends on depending on the preform shape and dimension.
Laser scanning method may be able to conduct distortion analysis for large area preform and complex shape and also monitor the surface conditions before and after the stitching. To sum up, visual inspection cannot detect internal damage in preforms, therefore other methods such as X-ray radiographic have been employed.

1.9.2 Textile composite inspection

Developments in non-destructive testing of 3D textile composite inspection may be built on the experience gained with common composite, but of the most methods frequently used with common composite, only X-ray and ultrasonic techniques are more sensitive to textile composite defects due to high thickness and complexity of textile fiber architectures (Hybridmat, 2006; (Stein J., 2008). The following represents our recent literature review on the non-destructive testing techniques used for the inspection of preform and textile composite and also techniques that have good potential for this purpose. Emphasis has been on NDE techniques that can detect two significant manufacturing defects, namely ply misalignment and fiber breakage.

Ultrasonic techniques

The fundamental principle of ultrasonic detection relies on pulses of high-frequency ultrasonic waves transmitted into the composite. These pulses are either transmitted through a specimen or reflected to the transducer by internal damage. The ultrasonic results are in the form of a C-scan, B-scan, or A-scan. By using ultrasonic C-scanning it is possible to detect delaminations and disbonds as well as volumetric defects including voids within the composite structure. Figure 1.33 displays an example application of pulse echo ultrasonic to inspect the pressure bulkhead of aircraft.

Figure 1.33. Example of ultrasonic C-scan of aircraft pressure bulkhead (http://www.airbus.com)

The ultrasonic waves propagating in the composite are one longitudinal and two transverse to the direction of propagation. For longitudinal waves, the particles of the material vibrate along the wave propagation, while for transverse waves; the particles of the solid vibrate in a perpendicular to the direction of wave propagation. The ultrasonic wave velocity is highly dependent on the specimen density and the stiffness. However, in the case of composite materials, due to anisotropy and inhomogeneity, in micro-scale the stiffness and density vary at different points in different directions. However by assuming an equivalent homogeneous media in macro-scale, the velocity is only direction dependent. To be clear, a brief introduction to ultrasonic wave propagation in composite materials and proportion of wave reflection and transmission in composite immersed in liquid are demonstrated below and more details can be found in many excellent books about the elastic waves propagation in layered media (Nayfeh A.H., 1995; (Stanislav R., Dale C. and Peter N., 2011).

Waves propagation in composites

In the case of composite plate immersed in fluid, the percentages of transmitted energy (T) and reflected energy (R) are computed from the wave potentials in upper and lower half spaces and displacement/stress-potential relations defined as (Maslova K., 1997):

$$R = \frac{M_{32} - i\omega Z_L M_{33} + i\omega Z_U (M_{22} - i\omega Z_L M_{23})}{M_{32} - i\omega Z_L M_{33} - i\omega Z_U (M_{22} - i\omega Z_L M_{23})} \quad (2)$$

$$T = \frac{-2i\omega Z_L \, \rho_U / \rho_L}{M_{32} - i\omega Z_L M_{33} - i\omega Z_U (M_{22} - i\omega Z_L M_{23})} \quad (3)$$

Where

$$Z_L = \rho_L \alpha_L / \cos\theta_L \text{ and } Z_U = \rho_U \alpha_U / \cos\theta_U \quad (4)$$

M_{ij} is defined as a 4×4 matrix obtained by multiplying stiffness matrices of composite layers, Z_L is the acoustic impedances of the lower fluid half spaces, Z_U is the acoustic impedances of the upper fluid half spaces, θ_U is the wave incidence angle, θ_L is the existence angle ,α_U is the velocity of wave in water, α_L is the velocity of wave in sample, and ω is signal frequency. ρ_L and ρ_U signify the density of lower and upper fluid and $i = \sqrt{-1}$. For an anisotropic material, the equation of motion has the form (Stanislav R., Dale C. and Peter N., 2011):

$$C_{ijkl} \frac{\partial^2 u_i}{\partial x_j \partial x_i} = \rho \frac{\partial^2 u_i}{\partial t^2} \quad (I, j, k, l=1, 2, 3) \quad (5)$$

Where C_{ijkl} is the elastic constant and ρ is the mass density and u_i are the displacements induced in the material by the ultrasonic wave. A plane wave propagating in composite can be represented as:

$$u_i = U_i \exp[ik_{ijkl}(n_j x_j - Vt)] \tag{6}$$

Where U_i is the amplitude, k the wave number, n_j the wave vector, $x_j = (x_1, x_2, x_3)$ the coordinate system, and V the phase velocity. If Eq. (6) is substituted into Eq. (5) then results

$$C_{ijkl} n_j n_l u_k - \rho v^2 u_i = 0 \tag{7}$$

The Eq. (7) called Christoffel equation that its solution gives the phase velocity in terms of the elastic constants for any propagation direction. Composites are heterogeneous and anisotropic materials; therefore theoretical modeling of wave propagation in such materials needs several simplifying assumptions. For perfectly bonded constituents, transversely isotropic layers with homogenized macromechanical properties are assumed in which the independent elastic constants are reduced from nine (for the case of orthotropic materials)to five constants. Considering the x_1-axis as symmetry axis along the fiber direction, and the x_2-x_3 plane as the isotropic plane, and then elastic constants are:

$$[C_{ij}] = \begin{bmatrix} C_{11} & C_{12} & C_{12} & 0 & 0 & 0 \\ C_{12} & C_{33} & C_{23} & 0 & 0 & 0 \\ C_{12} & C_{23} & C_{33} & 0 & 0 & 0 \\ 0 & 0 & 0 & C_{44} & 0 & 0 \\ 0 & 0 & 0 & 0 & C_{55} & 0 \\ 0 & 0 & 0 & 0 & 0 & C_{55} \end{bmatrix} \tag{8}$$

Where $C_{44}=(C_{33}-C_{23})/2$. For instance, for wave propagation along the x_3-direction, the relations between the phase velocities and the elastic constants can be obtained by the following equations:

$$V_{33} = \sqrt{\frac{C_{33}}{\rho}}, V_{31} = \sqrt{\frac{C_{55}}{\rho}}, V_{32} = \sqrt{\frac{C_{44}}{\rho}} \tag{9}$$

where V_{33} is the longitudinal wave speed, V_{31} and V_{32} are shear wave speeds with polarization along the x_1- and x_2-directions, respectively.

To solve the wave propagation inside multi-layer composite, the composite layers should be linked together using the imposing of the equilibrium and compatibility conditions at each interface by well know numerical approaches including the global matrix approach and the transfer matrix approach (Stanislav R., Dale C. and Peter N., 2011). For instance, in the global matrix approach, the wave components are simultaneously solved in all of the composite layers and the matrix order is a function of the composite layers numbers.

Wave attenuation phenomenon in composites is an essential subject which has absorbed considerable attention in past decades. This phenomenon is mainly due to energy dissipation via inherent material damping (viscoelasticity), wave scattering and reflection at boundaries, material interfaces, imperfections and micro cracks and also friction between poorly bonded constituents. Effects of these parameters can be modeled by assuming stiffness constants, C_{ij}, in the form (Mal A.K., Bar-C. and Lih S. Y., 1992):

$$C_{11} = \frac{c_{11}}{1 + ip\sqrt{c_{55}/c_{11}}}, C_{22} = \frac{c_{22}}{1 + ip\sqrt{c_{55}/c_{11}}}, C_{12} + C_{55} = \frac{c_{12}+c_{55}}{1 + ip\sqrt{c_{55}/(c_{12} + c_{55})}}, \quad (10)$$

$$C_{44} = \frac{C_{22} - C_{23}}{2} = \frac{c_{44}}{1 + ip\sqrt{c_{55}/c_{44}}}, C_{55} = \frac{c_{55}}{1 + ip} \quad (11)$$

Using standard notation, C_{ij} are components of the elastic stiffness tensor and p is defined as the damping factor. The composite damping is a function of resin properties (viscoelastic behaviour), fiber volume fraction, and fiber orientation (Chandra R., Singh S. P. and Gupta K., 1999; (Yim J. and Gillespie J., 2000). For composite materials, damping properties, which are anistotropic, can be changed by variation in fiber orientation, fiber volume fraction, etc. Figure 1.34 displays the effect of ply orientation on the damping loss factor. Mostly, damping in the fiber direction is less than transverse and shear directions.

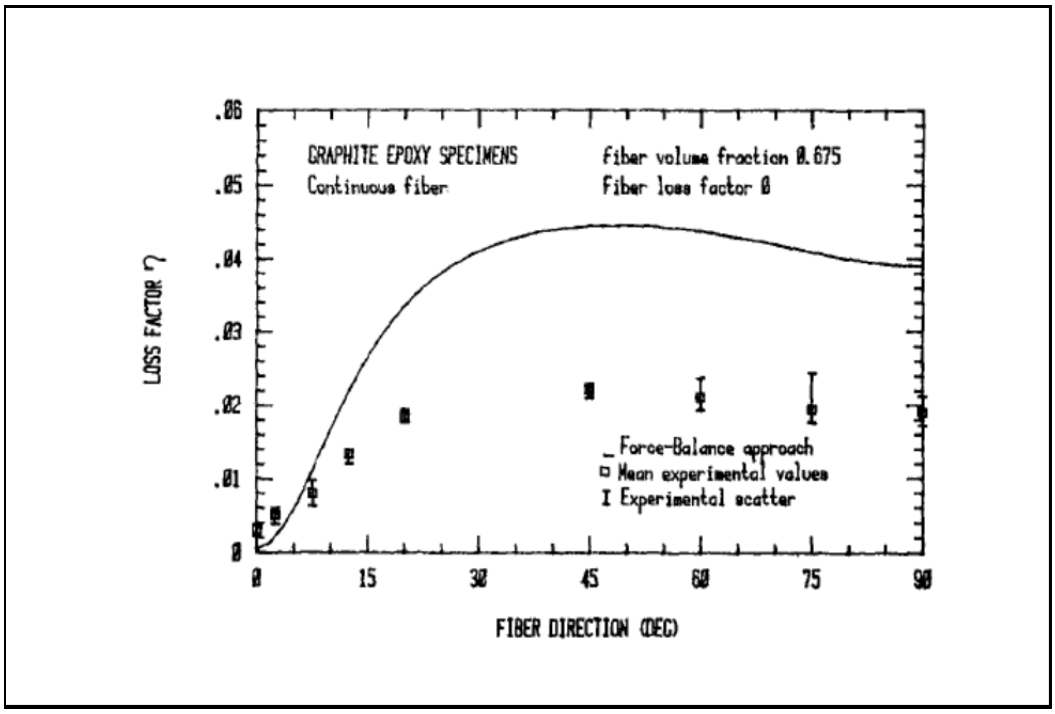

Figure 1.34. Damping factor versus direction for graphic/epoxy composite (Suarez S. A. et al., 1986)

Over the last decades, many researches have concentrated on non-destructive testing using Lamb waves. Lamb waves are sensitive to interior damage of composite, and testing results is in the form of dispersion curves. For a given frequency in composite, infinite wave numbers can be obtained by a root-finding method such as Newton-Raphson (Nayfeh A.H., 1995). The derivation of dispersion curves of Lamb waves in composite plates can be obtained by different methods such as Transfer matrix, Global matrix, and Stiffness matrix.

Wave modes propagation in a traction-free plate with the polarization in a plane perpendicular to the plate surface is called Lamb waves. Whereas, the leaky Lamb wave is identified the propagation of Lamb wave inside the plate immersed in the fluid in pitch-catch ultrasonic setup. The existence of a fluid in contact with the plate causes the waves damping and leakage a part of wave into fluid and the perturbation in the wave spectrum (Kundu T., 2004; (Yoseph B.-C. and Shyh-Sh. L., 2001).

Leaky Lamb wave technique have been used for the composite inspection based on the Lamb waves and pitch-catch mode (Yoseph B.-C. and Shyh-Sh. L., 2001). Previous researches at

using ultrasonic waves to detect small defects using Lamb wave were carried out by Nayfeh (Nayfeh A.H., 1995), Nagy (Stanislav R., Dale C. and Peter N., 2011), Bar-Cohen (Yoseph B.-C. and Shyh-Sh. L., 2001), and Kundu (Kundu T., 1999; (Maslova K., 1997). Most of these works include flaws such as delamination, porosity, fiber breakage change the characteristics of Lamb wave propagation, the dispersion curves. Therefore, this type of ultrasonic waves seems to be able to detect small damage in composites. Figure 1.35a exhibit a schematic of experimental setup for leaky Lamb wave technique and Figure 1.35b depicts the dispersion curve for a carbon/epoxy. The solid and broken lines signify dry and immersed specimens respectively. It is clearly seen that A_0 and S_0 has been altered due to the presence of fluid in addition to occurrence of a surface wave named Scholte moving on interface of fluid and composite plate.

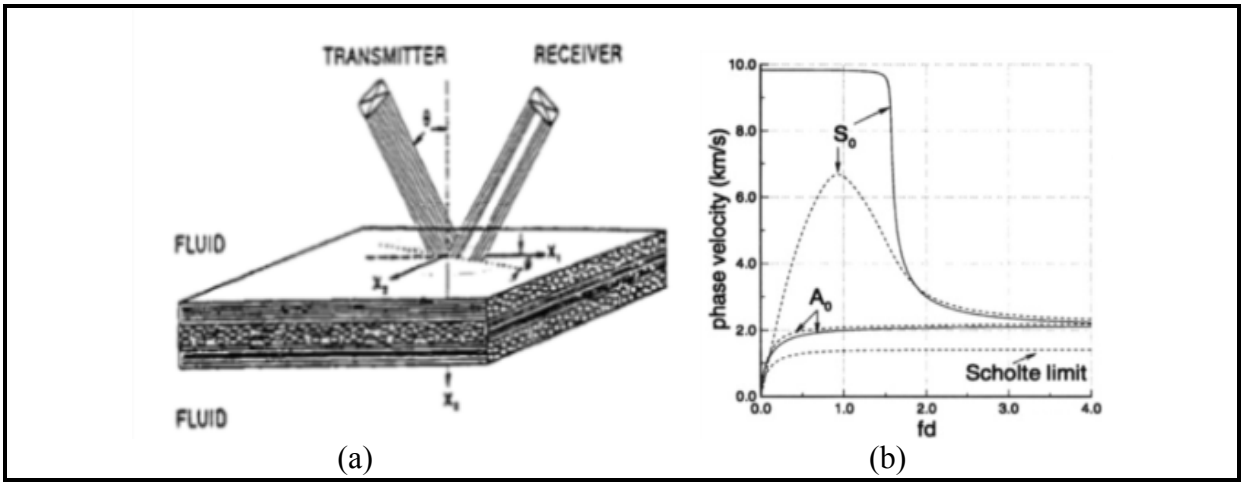

Figure 1.35. (a) Schematic image of leaky Lamb wave inspection applied to composite (Yoseph B.-C. and Shyh-Sh. L., 2001)
(b) Wave modes for dry (solid lines) and immersed (dashed lines) graphite epoxy (Nayfeh A.H., 1995)

Ultrasonic polar scan

In polar scan technique, the transducer is inclined at an acute angle perpendicular to the specimen surface and reflected wave is monitored by another transducer in pulse echo mode. The transducer is revolved about the axis perpendicular to the specimen surface. Van

Dreumel (Van D. and Speijer W., 1981) developed polar scan ultrasonic to detect the fiber orientation in composite materials, and more research work about this field has been carried out by Declercq (Declercq N. F., Degrieck J. and Leroy O., 2006). Declercq (Declercq N. F., Teklu A. and Breazeale M., 2005) used schlieren ultrasonic polar scanning for the inspection of carbon fiber composites. The method was a combination of ultrasonic and optical technique. Bar-Cohen (Bar-C. Y., 1993) developed polar backscatter ultrasonic to determine fiber misalignments and ply gaps in unidirectional composites. The technique can be applied with a variable angle and separate transducers located on opposite or same sides of the specimen. Fiber breakage and fiber orientations can be determined by ultrasonic polar scan. Furthermore, this technique can detect local fiber wrinkling or waviness, ply-end discontinuities and matrix cracks. In this technique, angle α should be selected precisely; otherwise the intended wave mode will not be propagated in composite. The technique is very surface-orientation sensitive and a suitable set-up is required to maintain correct alignment.

As mentioned above, the main technical difficulties associated with composite inspection are the attenuation, absorption, multiple scattering due to inclusions, and interphase layers. Those difficulties make it more challenging to test specimens which are thick or of complex shape. Although the effect of attenuation and scattering can be reduced by using appropriate probe and adjusting pulse parameters, the method is time consuming and the need for coupling medium such as water or gel is a disadvantage. Other ways of transmitting of ultrasonic into the composites can be using roller probes and air-coupled transducers. The major problem with air-coupled transducers is high acoustic mismatch between air and the composite transmit sound.

Laser ultrasonic (LU) is another ultrasonic NDT technique that uses lasers to induce and detect ultrasonic waves in a composite structure. LU is an efficient non-contact technique, has facilitated inspection of thick and complex-shaped composite such as the fuselage stringer sections in aircraft industry. LU system has been scheduled for on-line monitoring of composite manufacturing processes at Airbus Company (Esmeralda C., Miquel L. and Mónica G., 2012; (Mark O. and David K., 2008). The Lockheed Martin (LM) has developed Laser Ultrasonic for the inspection of various composite structures used in aircraft. LU does

not need specific tooling fixtures and most composite parts can be inspected on a table (Osterkamp M., 2006). In this technique the laser pulses heat the specimen and cause the thermoelastic regime acting a source of elastics waves inside the sample (Hussain M. A. Q. and Subhendu K. D., 2008).

To study analytically, at first, by the Fourier transform is applied to transfer the governing the governing equations and boundary conditions from time domain into frequency domain. After solving the governing equations, the numerical integration methods are used to find the response in time domain for further analysis (Datta S. K. and Shah A. H., 2009). Figure 1.36 depicts the dispersion curves of guided waves excitation in a CFRF cross ply plate. It is clearly seen that the symmetric Lamb mode (S_0) is faster than antisymmetric (A_0) modes and there are two wave modes below cut off frequency of A_1. The analytical research results on laser ultrasound illustrated that mostly, lowest Lamb wave mode is generated during excitation (Datta S. K. and Shah A. H., 2009; (Hussain M. A. Q. and Subhendu K. D., 2008).

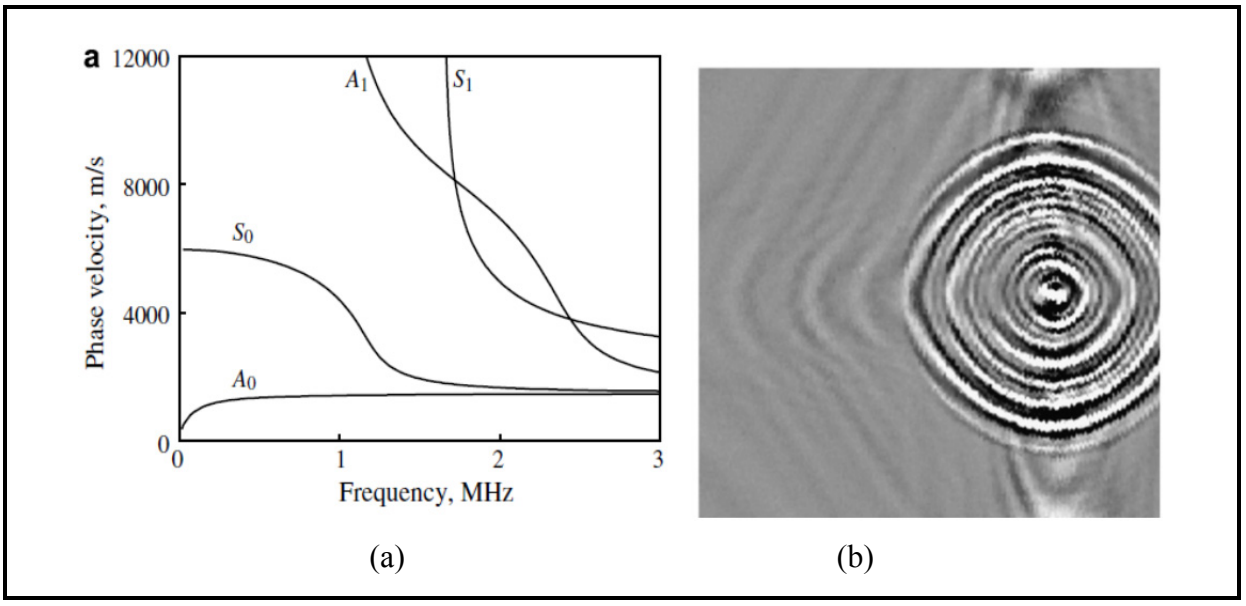

Figure 1.36. (a) Dispersion curve of Lamb wave modes (Yashiro S. and Takatsubo J., 2007) (b) CFRP cross-ply and its visualized wave propagation

Ultrasonic beam and Schlieren photography

This technique is a combination of Schlieren photography and an ultrasonic beam of 10 MHz shown in Fig. 1.37. The ultrasonic waves are generated by a conventional probe and camera is employed to provide real-time ultrasonic images (Declercq N. F., Teklu A. and Breazeale M., 2005). This approach is able to detect the fiber orientation in unidirectional composite using analyzing of the reflected waves close to the surface by comparing the reflected waves and their density and pattern. In addition, the technique can be used to detect voids, delaminations and small surface cracks. This system needs special equipment while the resolution of images obtained by this technique is not clearer than conventional ultrasonic C scans and much time is required to understand the details of the reflected wave pattern.

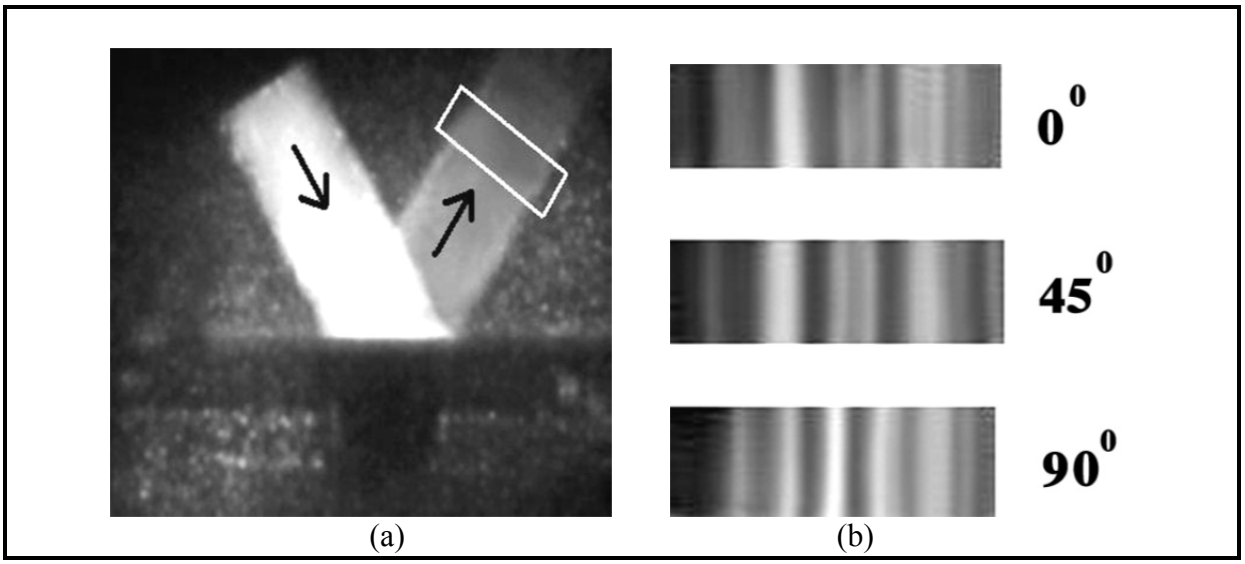

Figure 1.37. Some results of ultrasonic imaging using Schlieren photography (Declercq N. F., Teklu A. and Breazeale M., 2005) (a) Ultrasonic beam incident and reflected on an aluminum block (b) Example images of reflected beam pattern to detect fiber orientation

X-ray techniques

X-radiography is a promising technique to detect damage in preforms and composite by creating a two or three dimensional X-ray image of the specimen (Aroush D., 2006; (Randolf H., Theobald F. and Norman U., 2008; (Ulf H., 2008). X-rays for the non-destructive

applications are generated during acceleration of electrons in a vacuum while interact with tungsten. The interaction of electron with tungsten release photons which can penetrate solid materials. The penetration of photon in solid materials is directly related to the X-ray photon wavelength (10^{-6} to 10^{-10} cm). Figure 1.38a shows views of x-ray images of most conventional x-ray unit for non-destructive applications. X-radiography can be applied to the detection of voids in composites, but it is very difficult to detect the fiber volume fraction variations in CFRP composites using conventional radiography is difficult, because the matrix and the reinforcement fibres have high content of carbon and similar radiation absorption.

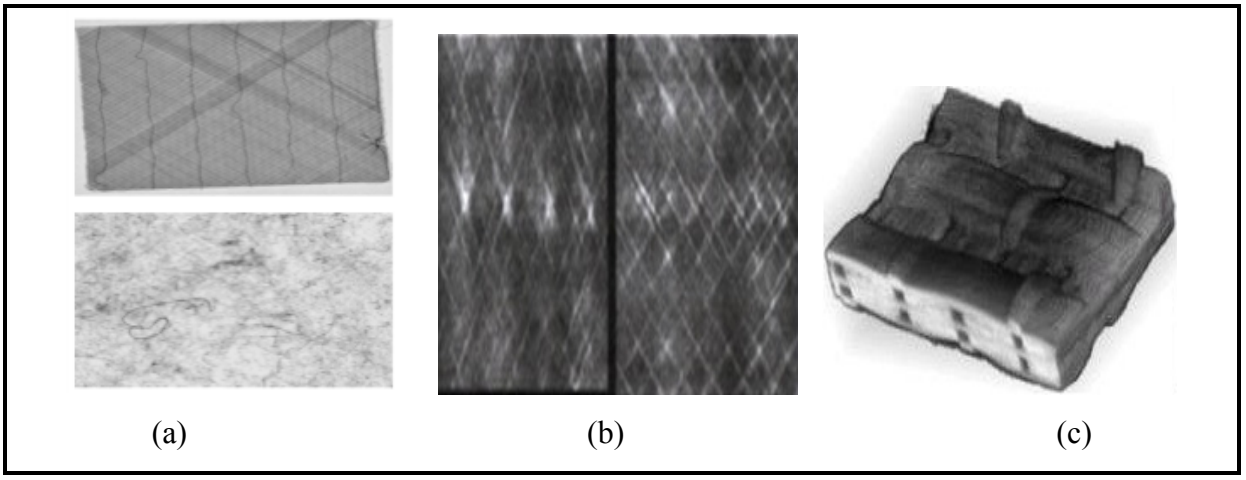

Figure 1.38. Example X-ray images
(a) Conventional X-ray (b) X-ray tomosynthesis (c) Micro tomography (Randolf H., Theobald F. and Norman U., 2008; (Ulf H., Stephan S. and Randolf H., 2007)

Digital x-ray tomosynthesis is other X-ray technique used towards the determination of the fiber distribution in the stitching process and also for the identification of the orientation of the fabrics inside a preform (Ulf H., 2008). In this method, the X-ray tube and the detector move in a circular way to generate several slice images at different depths of sample. The low contrast and low image quality is the main drawback of this technique (Ajay K., 2008).
X-ray computed tomography as promising NDT techniques focuses the X-ray beam to 10-micron spot sizes and a series of typically 360 to 720 radiographs. This radiograph images

are taken by rotating the object about one axis (see Figure 1.38c). The resulting data is reconstructed in software to produce a 3D image of the component that can be viewed through any image plane. Micro tomography could create cross-sections of a 3D preforms that can be used to observe the internal geometry of preform and textile composites. In this thesis, the characterization of 3D tufted composites will be performed using X-ray tomography. Therefore, more details about this technique are presented below.

Construction of radiographic image in CT technique represents a quantitative map of the linear X-ray attenuation caused due to absorption and scattering as X-ray beam propagates in the specimen. By ignoring the scattering, attenuation is expressed by Lambert's law as below (E1441-00, 2002):

$$I = I_0 e^{-\mu x} \tag{12}$$

where I represents the intensity of transmitted x-ray beam through specimen thickness x, I_0 is the intensity of the incident beam, and μ is the linear absorption coefficient. If x-rays penetrate a non-homogeneous material, the Eq. (12) should be expressed

$$I = I_0 e^{-\int \mu(s) ds} \tag{13}$$

where μ (s) is the absorption coefficient. Rearranging Eq. (13) results

$$-\ln\left(I/I_0\right) = \int \mu(s) ds \tag{14}$$

The CT reconstruction process mostly comprises two kinds of transform methods: the convolution backprojection and straight backprojection algorithms. In convolution-backprojection method the results of Eq. (14) can be expressed as:

$$P(\theta, \rho) = -\ln[I(\theta, \rho)/I_0] = \int \mu(x, y) ds \tag{15}$$

where I as single ideal measurement of the intensity is the function of detector orientation at angle θ and position, ρ, μ is the linear attenuation coefficient, and d_s is the distance along the x-ray path through the specimen at an angle θ and position ρ. Based on this notation, the convolution backprojection can be written as follows:

$$\mu(x,y) = \int_0^x \int_{-\infty}^{+\infty} P(\theta,\rho)g(\rho-\eta)d\eta d\theta \tag{16}$$

where g is the convolution function of the shape-theoretical form and

$$g(r) = \frac{\pi^2}{2}\left(\frac{\delta(r)}{r} - \frac{1}{r^2}\right) \tag{17}$$

where$\delta(r)$ and r are the Dirac delta function, and the radius of reconstruction area, respectively.

Shearography

Shearographic inspection is a full-field and non-contacting non-destructive technique that has been applied to detect surface and internal damage in composite materials. The damage detection is based on analysing of fringe pattern and any anomaly appeared on it. In this technique, the sample should be loaded for recoding the displacement derivatives as shown in example Fig. 1.39 (Francis D., Tatam R. P. and Groves R. M., 2010; (Hung Y.Y., 2009; (Hunga Y. and Hob P., 2005). Therefore, those damage could lead stress concentrations in the sample will be detected using shearography technique.

As shown in Figure 1.40a, the principal fundamental in this technique is that the two light waves reflected from specimen surface interface to each other producing a speckle pattern. Speckle patterns before and after deformation occurring due to excitation are compared producing a fringe pattern. In this technique, mostly a shearing device is applied to bring reflected light from specimens on a CCD camera. The first derivative (strain data) of the fringe pattern is corresponding to image shown in Fig. 1.40b.

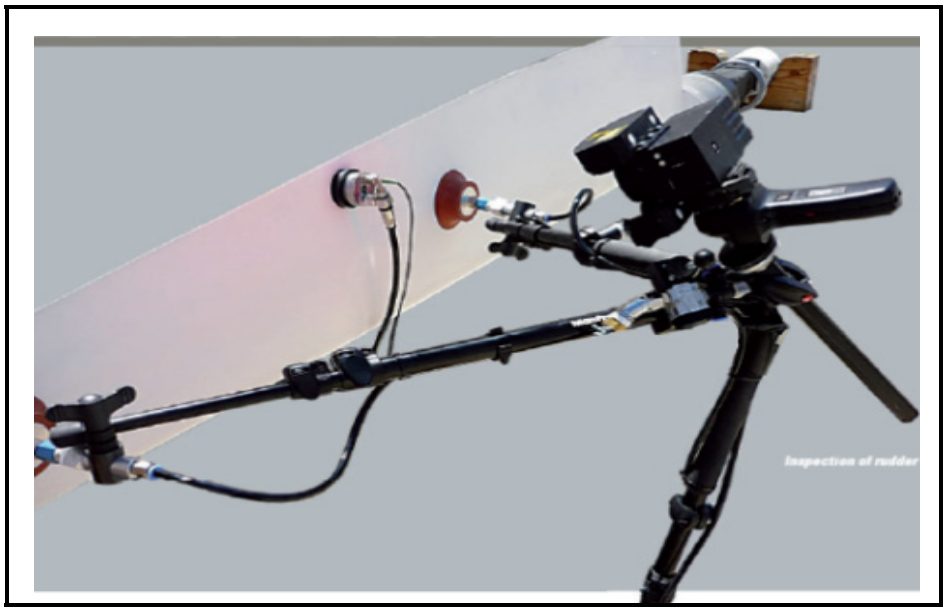

Figure 1.39. The blade inspection using shearography technique (courtesy of Edevis Company)

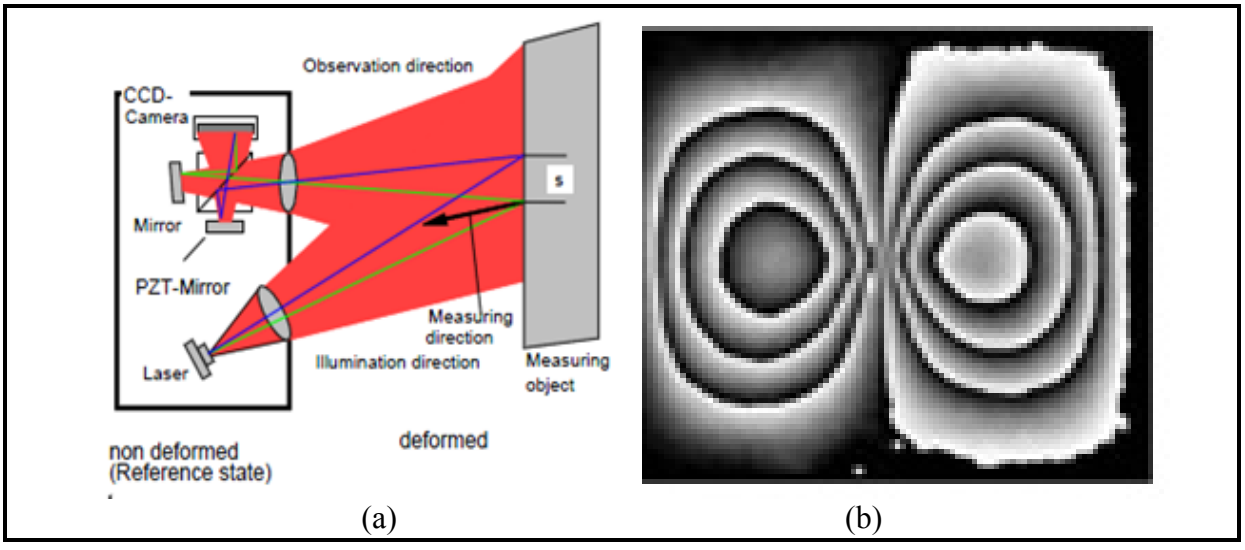

Figure 1.40. (a) Principle of shearography inspection technique (b) Example of fringe pattern (Francis D., Tatam R. P. and Groves R. M., 2010; (Hunga Y. and Hob P., 2005)

The identification of fringe orders is vital in traditional fringe analysis, but, identification of phase change in the computerized shearography is done using a phase determination technique.

Vibration based method

For damage detection using vibration methods, the composite structure is excited by an external source and then the dynamic responses are analyzed. There are numerous researches on analysis of dynamic response of composite materials for damage identification (Adams D. and Cawley P., 1988; (Hong H. and Yong X., 2002; (Kyriazoglou C., 2004; (Yam C., 2005). The majority of NDT techniques discussed in literature have been focused on unidirectional composites to detect internal damage. Based on the literature, radiography, ultrasonic testing, infrared thermography and vibration based damage detection are promising techniques in aerospace industry. There are numerous researches on analysis of dynamic response of composite materials for damage identification. For instance the damage could be identified in a cross ply carbon fiber composite structure by assessing the natural frequencies (Cawley P. and Adams R., 1979) and the relation between them (Yam C., 2005). Based on the literature, with increasing the delamination size, the natural frequency decreases (Arkadiusz J. Ż., 2005). This research declared that results considerably depend on excitation and vibration response is sensitive to delamination size and location. Frequency response functions were analysed to detect delamination. Extensive research on damage identification using vibration methods have been carried out by (Adams R.D. and P., 1988; (Kyriazoglou C., 2004). The fundamental concept behind vibration-based damage detection is that there is relarion between composite properties and its modal characteristics including natural frequencies, mode shapes, etc.

Electromagnetic techniques

This section reviews eddy current technique for the detection of the stacking sequences in composite materials. Eddy current inspection includes the generation of electrical currents in conductive objects with an alternating magnetic field (Bachnak R. and Scott K., 2007). In

eddy current, test probe does not need to contact the part and it can easily inspect complex shapes conductive materials. The Eddy current technique can be used to detect surface and near surface defects (Mook G. and Koeser R., 2001). Fiber misalignment defect can be detected with observing any discontinuity occurring in the flow of eddy currents (Mook G. and Koeser R., 2001). For instance, a newly developed eddy current probes with high directivity shown in Fig. 1.41a could detect the fiber orientation in unidirectional composite. Figure 1.41b shows the example plot obtained by the eddy current system.

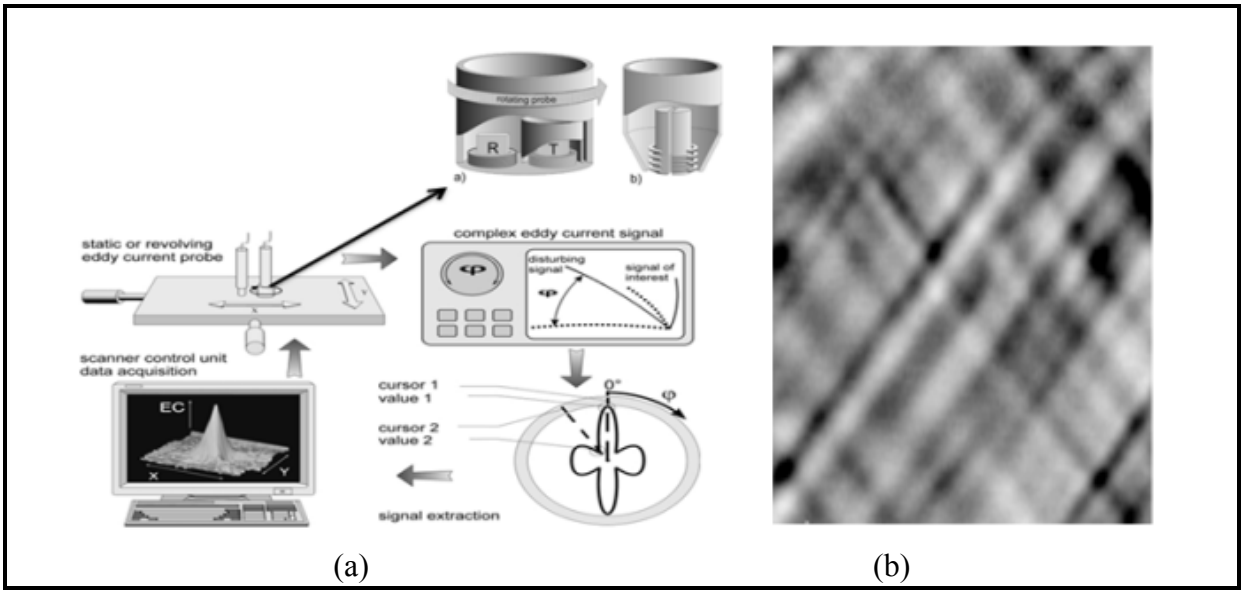

Figure 1.41. Eddy current inspection (Mook G. and Koeser R., 2001) (a) Eddy current measurement equipment (b) Eddy current images of CFRP showing the fiber orientation

Some of the disadvantages of eddy current inspection include the limitation to conductive materials and the accessibility of the surface, surface roughness. In this technique, the depth of penetration is limited and cracks parallel to the probe coil winding and probe scan direction cannot be detected.

Thermography

In recent decades, thermographic NDT techniques have been used to detect various internal damage in composites in particular impact induced delamination. These techniques can be used where ultrasonic and radiographic results are difficult to interpret (Maldague X.P.V., 2001).

Infrared thermography is a measure of thermal energy emitted by matter in the infrared band, and then creates a mapping surface temperature (Carosena M. and Giovanni C., 2004). Infrared may be referred to any invisible electromagnetic spectrum with wavelengths shorter than the microwave band and above the visible band. The near-infrared band (NIR) is placed between the visible and infrared medium wave (about 3-5 um). In through the transmission on the basis of the NIR thermography, transmission through a sample is a function of two factors whose absorption and dispersion which are both a function of wavelength.

Infrared thermography is mapping the temperature of sample surface by measuring the thermal energy which is radiated by composite in the infrared band of the electromagnetic spectrum.

There are two approaches for the thermography inspection: passive and active (Meola C. and Carlomagno G., 2009; (Swiderski W., Szabra D. and Szudrowicz M., 2008). In active methods, thermal gradient is maintained by the application of cyclic stress while passive methods include the measuring of object temperature using the object emissivity and no heat source is needed.

Pulsed thermography is one of the most commonly used thermal methods in active thermography for composite inspection. Lock-in thermography known as active inspection technique, the composite is excited with a periodic energy (Vorgelegt V., 2007; (Wael B. L., Ibarra-C. C. and Xavier M., 2009). Internal defects alter the phase delay and amplitude of the signal received at the composite surface. Figure 1.40a&b depict example thermal images revealed impact damaged regions in armour and fiber waviness defect in a preform, respectively.

Eddy current thermography known as latest active thermography includes inductive excitation to generate eddy currents at a particular depth to heating up the composite and the subsequent internal defects detection (Mook G. and Koeser R., 2001). Damage can cause

variations on the eddy current patterns resulting the distribution of temperature on the composite surface. As excitation forms mentioned above, the temperature variations appeared on the composite surface is sensed using an infrared camera (Maldague X.P.V., 2001). Figure 1.42c displays the fiber orientation of CFRC perpendicular to the direction of the magnetic field detected in lock-in frequency of 0.3 Hz.

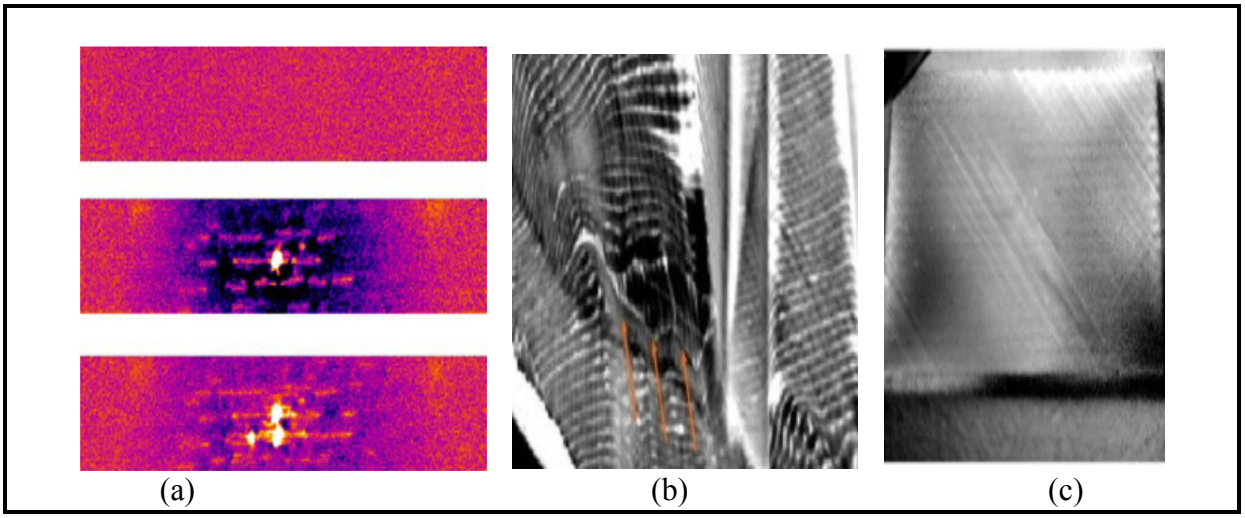

Figure 1.42. Non-destructive testing of composite by using IR thermographic methods
(a) Pulse themography (b & c) Inductive thermography
(Swiderski W., Szabra D. and Szudrowicz M., 2008; (Vorgelegt V., 2007)
(courtesy of Edeviscompony)

Other techniques

Vibrothermography is a non-destructive testing method in which damage in a composite is made visible through thermal waves resulted from high frequency ultrasonic excitation. In fact, mechanical energy dissipation at the damage surface due to thermoplastic and hysteresis generates the heat generation (Mabrouki F. et al., 2009; (Renshaw J. et al., 2011).

1.10 Geometry inspection

Ccoordinate measuring machines (CMMs) are used in the composite manufacturing industry to provide high measuring accuracy and stability. This technique has opened some interesting

possibilities for structural integrity assessment of composite parts (Ali R., 2008; (Dong C., 2003). CMM scanning can be useful technique to detect surface damage or foreign objects in composite which appear as any abnormality in the surface (Dennis R., Kirk R. and Randy D., 2010). Measurement data obtaining systems for CMM scanning are divided into two main categories: contact measurement and non-contact measurement. In traditional CMM scanning, measurement data is obtained by physically probing the parts. CMM obtains geometric information by moving a probe point by point along mechanical part and recording touched points coordinates. However, there is limitation in probing parts with very small sizes because of access problem for probe. Another disadvantage of CMM is its lower speed for obtaining coordinates of points and many factors that affect the digitizing uncertainty of CMMs, such as the scanning speed, pitch values, probe angles, probe sizes, and sample sizes should be considered during scanning.

Non-contact measuring methods called laser scanning have eliminated disadvantages mentioned for CMM technique. A non-contact sensor usually has a view field all points inside which can be simultaneously measured (Chao Z. X., Ong S. S. and Tan S. L., 2011; (Leopold J., Günther H. and Leopold R.m., 2003). This characteristic increases measurement speed significantly. In addition, unlike CMM, there is no need for positioning and fixtures by using non-contact methods. Therefore, the only approach for fixtureless inspection of non-rigid parts is application of non-contact measurement methods. Accuracy of non-contact methods is generally lower than CMM touch scanning (Alten F. and Grandt J., 2004).

1.11 Mechanical performance

Aerospace industries are always looking for the composite materials that can provide high damage tolerance. 3D composites containing through-thickness reinforcements are promising materials because they improve the damage resistance. However, few 3D composites are currently used in aerospace industry due to lack of crucial information about their mechanical performance in the presence of defects. Manufacturing defects including, fiber misalignment, broken fibres, and resin-rich regions occurring in stitched preforms can significantly affect mechanical properties. For instance, the stitching improves damage tolerance and can

considerably reduce delamination area, but it decreases tensile strength compared with unstitched composites. In addition, stitching can increase Mode I interlaminar fracture toughness and decrease the effect of in-plane fibre distortion occurred during stitching. However, some research results have shown that stitching does not improve the the damage resistance (Mitschang P. and Ogale A., 2009; (Mouritz A., 1997; (Mouritz A.P. and Cox B. N., 2000). This contradictory data does not assist designers to apply these materials in the aerospace industry. Thus, over the last decade, analyses of damage mechanisms in textile composites have been challenging researchers.

Understanding the behaviour of a damaged textile composite structure subjected to mechanical loadings is the basis for damage-tolerant design. Based on literature, the research on damage development in textile composites have been categorized as either experimental or numerical (Hufenbach W. et al., 2004).

The researchers have developed numerical models to predict the behavior of damage in textile which are still under development due to the complex 3-D nature of these kinds of composites. The complex structure of textile composites can cause intricate and different failure modes. Failures process cause non-linear stress-strain behaviour on the structural level (macro scale). These investigations towards determining the damage mechanisms and the composite degradation behavior have resulted in various models based on the principles of continuum damage mechanics (CDM).

Theoretical models based on CDM developed by Matzenmiller (Matzenmiller A., Lubliner J. and R., 1995), Hashin (Hashin Z., 1980) have been used to analyse progressive damage in composites. The major difference among these models is related to damage modes. The model developed by Matzenmiller includes formulations for the fiber rupture, fiber kinking, matrix cracking and matrix crushing. In this model, because the area of load carrying is decreased due to damage, the stresses σ in the failure criteria is introduced as effective stresses $\hat{\sigma}$ as follow (Lapczyk I. and Hurtado J., 2007):

$$\hat{\sigma} = \frac{\sigma}{1 - d} \tag{18}$$

where σ is the nominal stress, and the quantity d is a damage variable that ranges from 0 (undamaged) to 1 (damaged). From this, an effective stress tensor is represented as:

$$\{\hat{\sigma}\} = [M]\{\sigma\} \tag{19}$$

Where $\{\sigma\}$ is the usual stress, and [M] is a represents the damage operator that describes the reduction of the elastic modulus as follows:

$$[M] = diag\left(\frac{1}{1-d_f}, \frac{1}{1-d_m}, \frac{1}{1-d_s}\right) \tag{20}$$

Where d_f, d_m, and d_s are fiber, matrix and shear damage variable, respectively. The effect of damage on constitutive relation is represented by:

$$\{\hat{\sigma}\} = [M]\begin{bmatrix} \frac{E_1}{1-\nu_{12}\nu_{21}} & \frac{\nu_{12}E_1}{1-\nu_{12}\nu_{21}} & 0 \\ \frac{\nu_{21}E_1}{1-\nu_{12}\nu_{21}} & \frac{E_2}{1-\nu_{12}\nu_{21}} & 0 \\ 0 & 0 & G_{12} \end{bmatrix}\{\varepsilon\} = [C_d]\{\varepsilon\} \tag{21}$$

where {ε} is the usual strain in column matrix form and results in strain softening response. C_d is effective elasticity matrix is defined:

$$[C_d] = \frac{1}{D}\begin{bmatrix} (1-d_f)E_1 & (1-d_f)(1-d_m)\nu_{21}E_1 & 0 \\ (1-d_f)(1-d_m)\nu_{12}E_2 & (1-d_f)E_1 & 0 \\ 0 & 0 & (1-d_s)G_{12} \end{bmatrix} \tag{22}$$

where $D = 1-(1-d_f)(1-d_m)\nu_{12}\nu_{21}$, and E_1, E_2, G_{12}, υ_{12} and υ_{21} are the elastic constants.

The progressive damage failures in composites occur in six modes (Choi S.W., Hahn H. T. and Shyprykevich P. , 2002): fiber compression, fiber tension, matrix tension and matrix compression, shearing and delamination. Therefore, composite degradation is realized

through a set of factors, dependent on these failure modes and is applied to the composite stiffness.

1.12 Comparisons and future challenges

According to the literature review, 3D textile preform and composite inspection have been in research and application stage in developed countries for many years. It seems that no alternative to current X-ray techniques in particular micro CT for preform inspection has been seen. X-ray techniques, C-scan ultrasonic and laser ultrasound are existing techniques to inspect 3D textile composite. Ultrasonic technique benefits from further improvement and will find increasing application due to its low cost in compared to other technique and its expected advancement in ultrasonic probe in coming years. Future challenges with thick complex preform and composite inspection will be highlighted by focusing on the need to achieve high repeatability and probability. Furthermore, the research will continue to detect very small damage in 3D composites, further decrease the complexity associated with inspection processes and reduce the role of the NDT operators to make critical decision. The author speculates a large number of research and development about 3D preform and composites will be reported in near future. Most of this type of information developed by industry for 3D composites will remain proprietary, but sufficient data for future researchers will be provided.

1.13 Conclusion

The review has covered an introduction into 3D textile preforms and composite, various types of damage found in textile preforms and composite. The state-of-the art non-destructive testing (NDT) techniques developed for detecting defects in preforms was presented. In addition, advantages and disadvantages of each method were presented. It has been found, there are significant factors that influence the choice of inspection method for the textile composite. Promising ND methods developed for other composite can be used to detect small damage in textile composite was described. At the moment, it can be claimed that X-ray imaging method especially micro CT technique and C-scan ultrasonic are the most useful

methods to detect damage in textile preform and composite. Advantages of micro-CT over C-scan and conventional X-ray method include the ability to detect accurately fiber damage and monitor of the internal defects as well as the external surface damage. The ultrasonic C-scan has useful sensitivity to detect various types of damage such as porosity, delamination, and disbond. Other methods to detect damage in preforms can be used to inspect textile preforms, however further research is required to be able for accurately detecting damage.

CHAPTER 2

CHARACTERIZATION OF 2D TEXTILE COMPOSITES

2.1 Introduction

During the past 20 years, applications of woven textile composites have grown rapidly. Woven composites have been primarily used in aerospace structures in which weight efficiency is critical. However, advances in manufacturing processes and essential need to decrease the costs of raw materials have resulted to their extensive use in other applications such as the automotive, the infrastructure market, and sporting goods industries. One of the major challenges in textile composites is the verification of their manufacturing quality which has large influence on the mechanical properties. Because of the complexity of these materials, conventional NDE techniques are often incapable of characterizing the materials adequately. The objective of this chapter is to develop effective NDE techniques for detecting and characterizing those manufacturing defects known to affect strength in woven fiber-reinforced composites. Manufacturing defects studied in this research are the fiber breakage and fiber misalignment. Emphasis is given on the ability of the NDE techniques to provide a detailed and accurate description of these defects. Accordingly, our methodology is organized as follows:

Section 2.2 concerns the manufacturing process of composite panels containing known defects. These composite specimens will be used to realize which NDT technique has high sensitivity to defects. Furthermore, destructive inspection methods that can serve to verify the composite quality are discussed.

NDE Techniques including ultrasound, vibrational and X-ray-computed tomography are then described in section 2.3, and damage types and features detectable through these methods are investigated.

Section 2.4 contains the experimental results and discussion and the relative merits of these three NDE approaches. Then Finite element modeling (FEM) of textile composite in macro and meso-scale is discussed in section 2.5.

Finally section 2.6 summarizes the findings of these investigations.

2.2 Materials and experimental equipment

2.2.1 Composite sample manufacturing with known defects

Five fiber glass/epoxy composite panels with controlled defects in the textile fabrics were prepared by VARTM. Each plate contained five layers of twill weave e-glass fabric (306 g/m^2, JB Martin, St-Jean-sur-le Richelieu, QC) as shown in table 2.1.

Table 2.1. Woven layer properties

Data	Comment
Material: Textile	Manufactured by J.B Martin Co. # TG09T60B
Thickness of textile layers = 0.4	
Unit cell size: 1.7x1.7 mm	
Construction: Plain weave	
Yarn width: 1.5mm	
Kozeny Constant= 0.0018	
Yarn cross section: Ellipse	
Areal Density = 306 g/m^2	

The woven layers are stacked one by one on top of another layer. Weft and the warp fibers are perpendicular to each other and parallel or oriented to the corresponding weft and warp fibers of the other preform layer. Figures 2.1 shows the required stacking sequence of fabric for the manufacture of perfect sample.

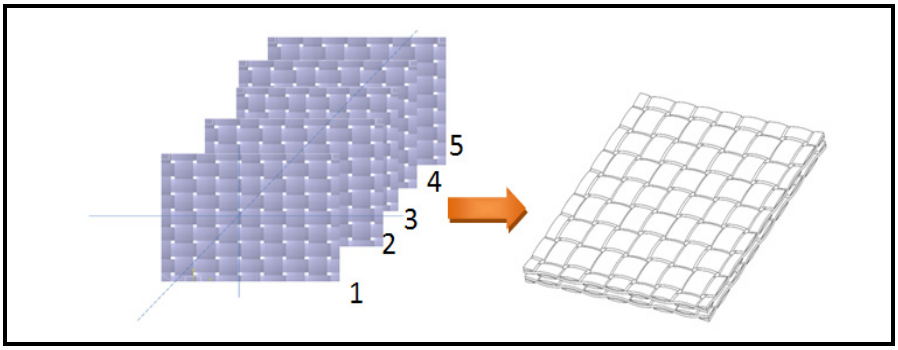

Figure 2.1. Layup sequences for perfect woven composite

One specimen (plate I in table 2.1) was produced as a reference without any defect. Plate II included three types of fiber breakage defects. One type of defect corresponds to the removal of a full unit cell, the second defect consists in a yarn-width long cut made on the side of a unit cell, and the last fiber breakage defect is similar to the second one but covers only the half yarn width. Details of these defects are illustrated in Figure 2.2.

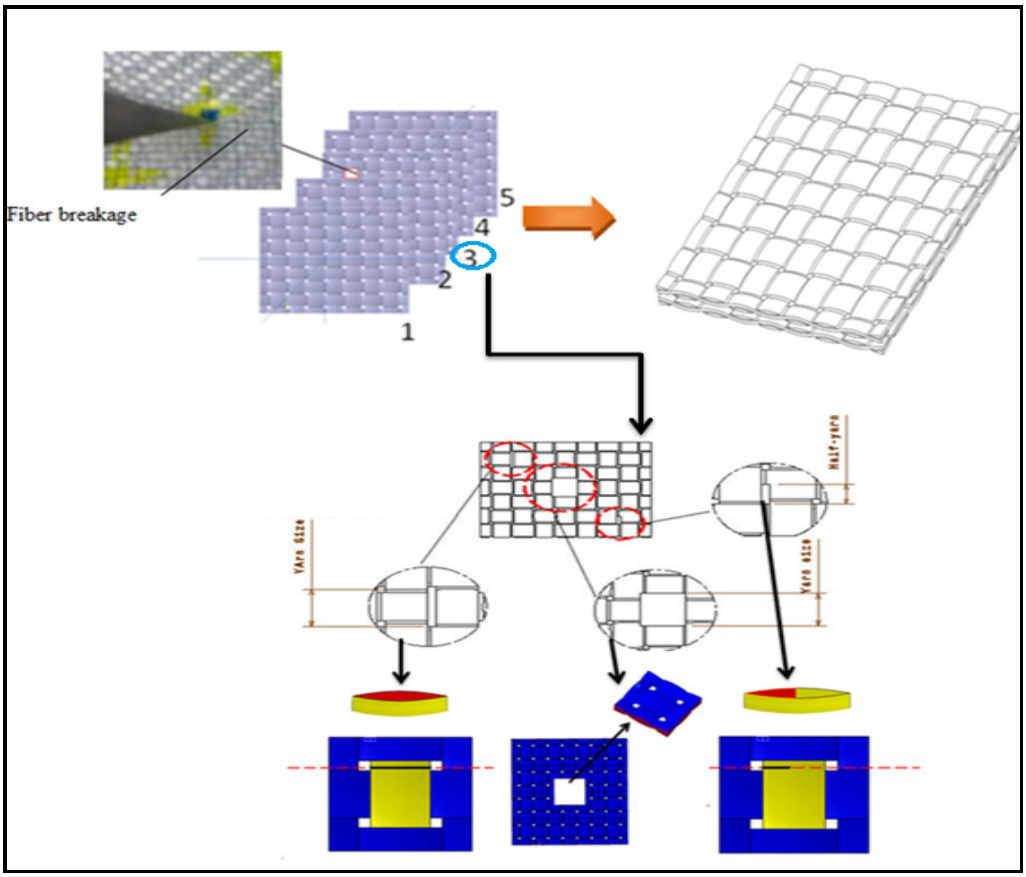

Figure 2.2. Fabric layup sequence for defective woven composite sample containing several fiber breakages on 3rd preform layer

Three other composite panels were produced with a controlled misalignment of the middle layer. Misalignment angle values of 5, 10 and 20º were selected as indicated in Figure 2.3.

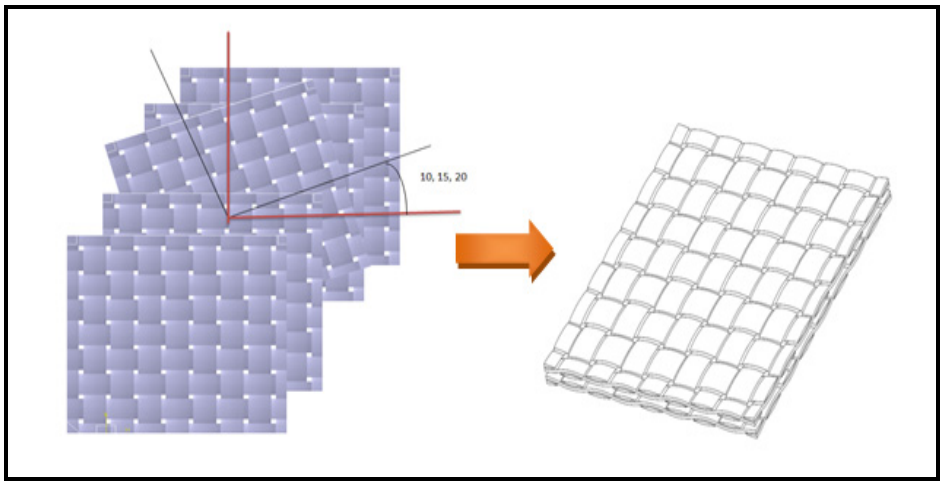

Figure 2.3. Fabric layup sequence of defective woven composite samples with angle increments 5^{o}, 10^{o}, 20^{o} of the 3^{rd} preform layer

After stacking the fabrics and placing the nylon fabrics and natlex mesh on top of the top nylon fabrics, the mould was tested for any leaks by creating a vacuum. When all leaks have been eliminated and the vacuum bag completely sealed, the mould became ready to be impregnated with the resin. The resin was mixed with hardener according to the proportions suggested by Adtech Company (see table 2.2). The mixture was placed in a vacuum chamber to be degassed.

Table 2.2. Epoxy resin properties

Type	820 epoxy resin manufactured by Adtech company
Mix ratio by weight	100/18 (resin to hardener)
Mixed density	1107 kg/m^3
Viscosity	350 cPas
Cure sycle:	25 Hours at 25^{o}
Work life:	30 min

After injection stage, the mould was kept at room temperature for a few hours in order to assure that the woven composites panel reaches to required mechanical properties. After

curing, the laminate panels were cut to the dimensions as illustrated in Table 2.3. Five plates had a nominal thickness of 1.5 mm. Three samples from each composite panel were cut with diamond saw and polished for microscopy assessment as described next section.

Table 2.3. Characteristics of composite plates

Plate Id	**Dimension (mm^2)**	**Layup**	**Defect**
I	200*110	$[0]_5$	-
II	200*110	$[0]_5$	Fiber Breakage
III	200*110	[0,0,5,0,0]	Misalignment
IV	200*110	[0,0,10,0,0]	Misalignment
V	200*110	[0,0,20,0,0]	Misalignment

2.2.2 Quality control

As stated before, the objective is to fabricate several composite samples should be inspected by nondestructive testing techniques. Therefore, controlling the manufacturing process is essential for the samples to ensure their low void content.

All woven fabrics were inspected one by one before stacking. All fibers were carefully adjusted in order to the desired directions. The stacked fabrics qualities again were checked.

To decrease the void content, the quality of the impregnation process was determined by the resin flow, and the viscosity of the resin. For this purpose, a series of experiments were designed to determine the proper location of the resin line and the vacuum line. Void content was limited by the resin degassing to eliminate air bubbles entrapped in the resin. Figure 2.4 verify the effect of eliminating the voids to fabricate acceptable composite samples.

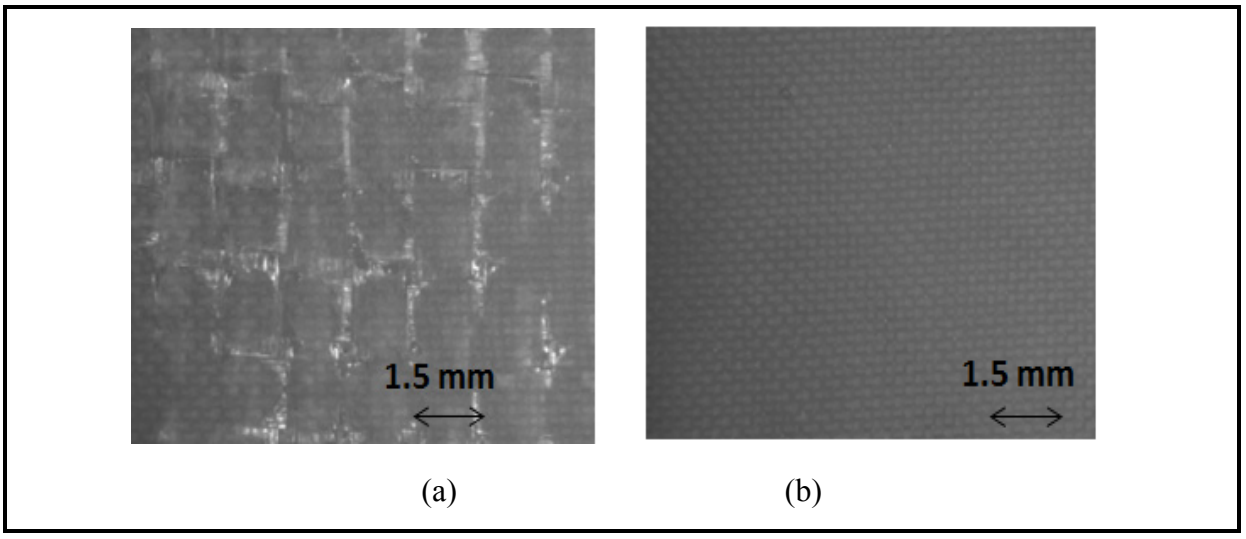

Figure 2.4. Micrographic images of samples surface (a) Voids at the tow intersection because of lack degassing process (b) Textile preform injected by degassed resin

Microscopy

After the resin injection into stacked fabrics, all composite specimens were sectioned parallel to the warp and weft axis. The samples were then polished using progressively finer particles. The polished specimens were sputter-coated with gold to enhance viewing with a scanning electron microscope (SEM). Scanning electron micrography produced images with sufficient contrast between the resin and glass fibers. Based on SEM images of three different cross sectional regions, no significant void or other impregnation-related defect was observed (see Figure 2.5).

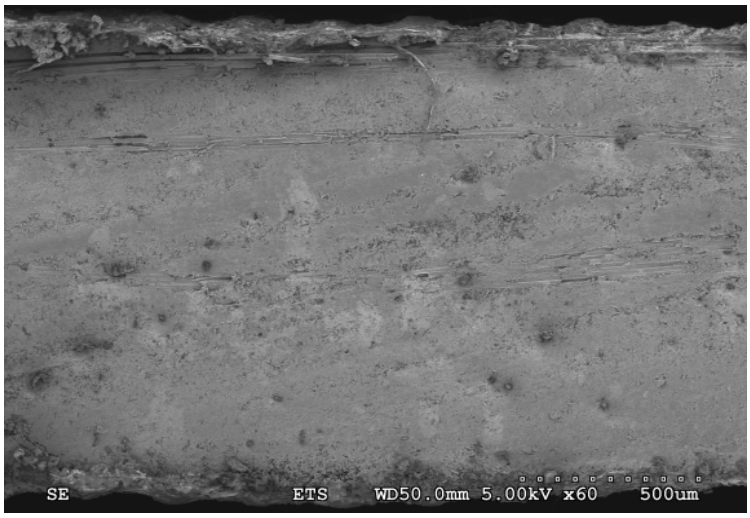

(a)

(b)

Figure 2.5. Micrographic images of perfect sample cross-section

Dimensional variation

CMM scanning was carried out to perform an analysis of the spatial distortion of the composite plates to identify thickness deviations that could be caused by defects and pressure difference in the textile reinforcement (see Fig. 2.6). Furthermore, the CMM scanning results

could ensure the ultrasonic result, because ultrasonic technique is sensitive to variation of sample thickness. Each composite sample was scanned with an accuracy of ± 0.01 mm at 4500 points and a pitch of 2mm. The scan area was 195 mm x 105 mm, which covered the whole sample surface. In addition, a small area of the sample plate was measured in some instances with a very small pitch of around 0.7mm and the profile of the desired area was obtained.

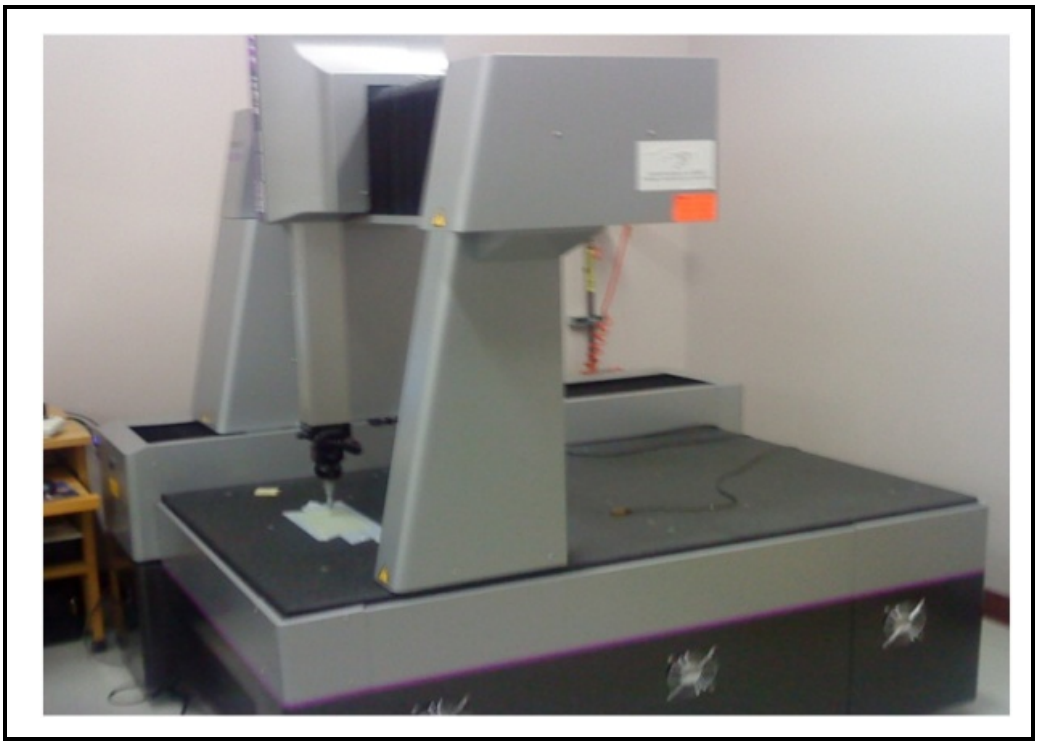

Figure 2.6. Experimental setup for CMM scanning of composite sample

Fig. 2.7 displays some examples of what was measured for Plate I. Some variations in thickness with a minimum located at the center and near resin outlet regions were observed. These differences of up to about 5% might be due to variations in fiber volume fraction as well as to some inhomogeneous resin distribution during infusion process.

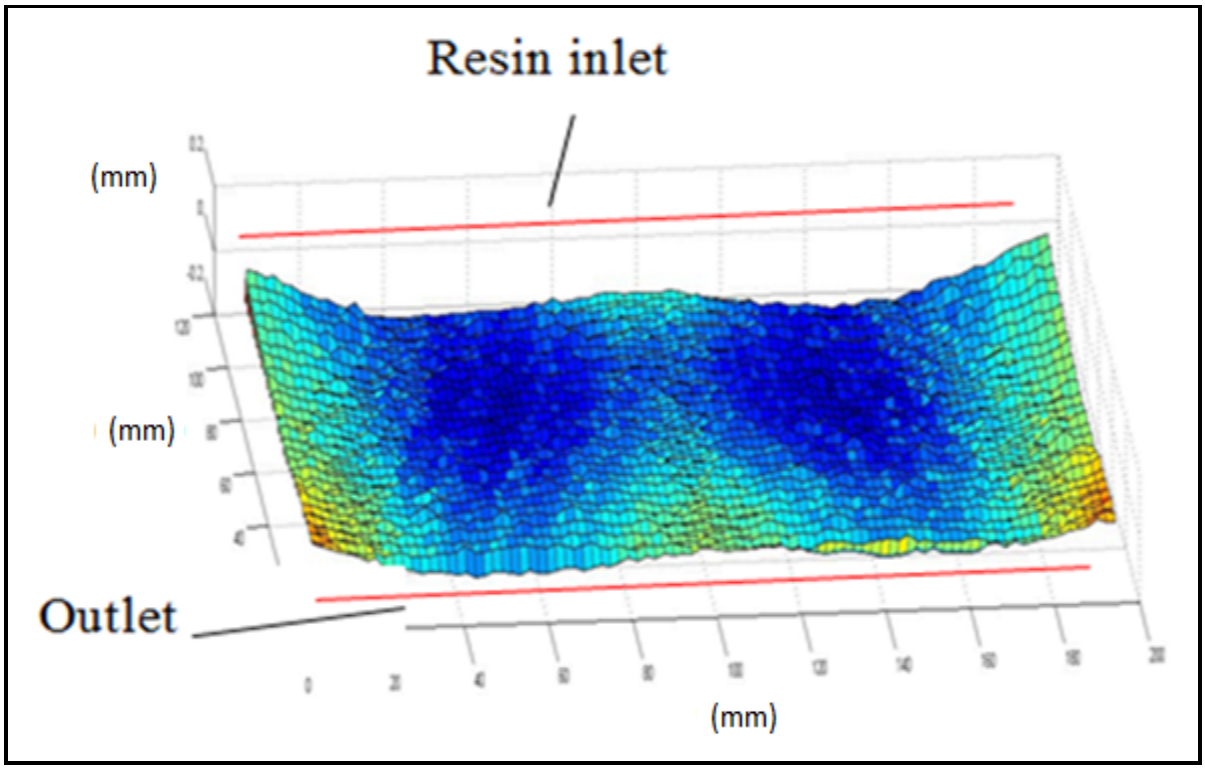

Figure 2.7. Graphical image of deviations values for sample I

Fig. 2.8 compares the results obtained for all composite plates. The variation measured for the reference sample appears to be much larger than what is obtained for the samples with textile defects.

In addition, a closer look was taken to investigate the effect of artificially induced fiber breakage and also natural waviness on the plate surface. For that purpose, the corresponding area was scanned at very small pitch around 0.7mm (see II-B in Figure 2.8). However, the improved accuracy of the measurement did not allow better evidencing the waviness due to small fiber bundle size and no abnormality due to fiber breakages.

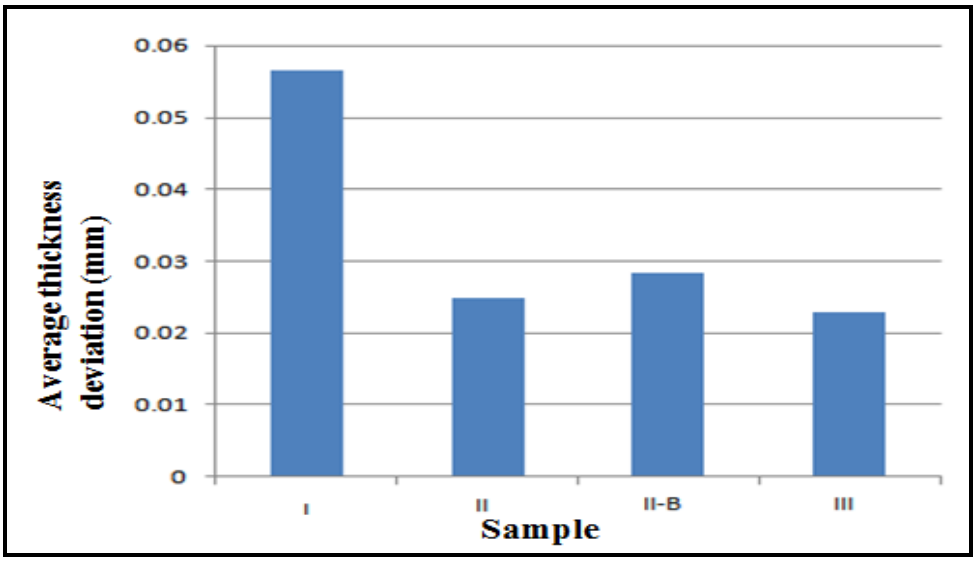

Figure 2.8. Average thickness deviation for plate I (reference), plate II and plate III

2.3 Experimental setup for NDT

The goal of this section is to investigate the capability of ultrasounds, vibrations and X-ray-computed tomography to detect artificial defects such as fiber breakage and fiber misalignment defects.

2.3.1 Ultrasonic

The experimental setup for C-scan pulse echo testing shown in Figure 2.9, contains a water tank, an ultrasonic probe installed on vertical arm, and a motor control prepared for polar scan mode. In this experiment, the transducer acts as an ultrasonic wave transmitter and also as the receiver. In this research, two ultrasonic scanning methods were applied to inspect five samples: conventional pulse echo scanning, and polar scanning.

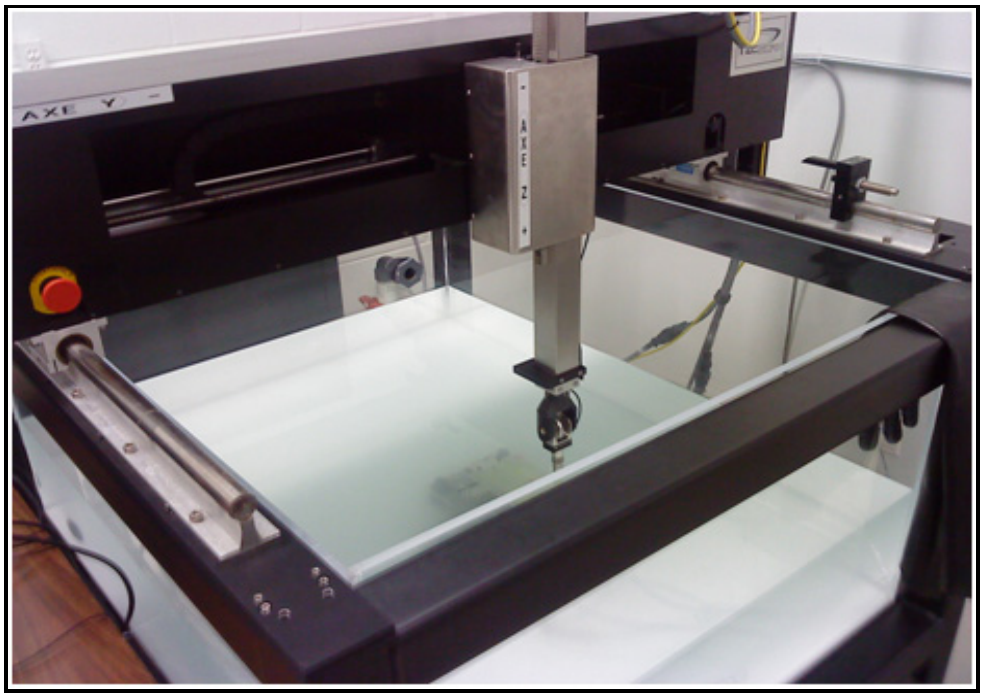

Figure 2.9. Experimental C-scan setup (Courtesy of NRC)

1) Conventional scanning

Pulse echo ultrasonic was used for scanning composite samples. In this technique the transducer acted as an ultrasonic wave transmitter and also the receiver of reflected waves from sample. Figure 2.10 display a schematic image of the ultrasonic transducer and composite sample. In this experiment, the ultrasonic signals are transmitted through the thickness of the composite specimen.

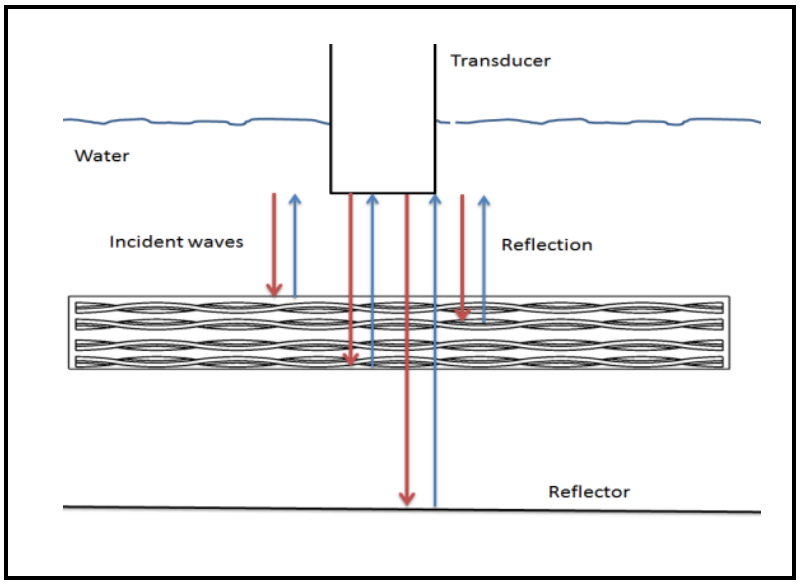

Figure 2.10. Schematic of pulse echo ultrasonic scanning

At the beginning of testing, a 10-MHz flat transducer was applied for testing, but the attenuation was high for this transducer. Consequently, a 5-MHz flat transducer was selected for testing all composite samples. The C-scan images of all samples were generated by moving the ultrasonic transducer in a pattern that covered the whole specimen surface shown in Figure 2.11.

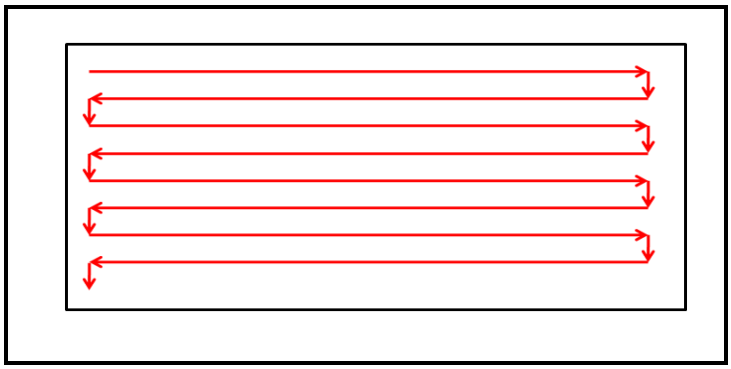

Figure 2.11. C-scanning pattern applied to a composite sample

2) Polar scanning

In addition to conventional pulse echo ultrasonic imaging technique, polar scan ultrasonic were performed using a 5 MHz flat transducer in a pulse-echo mode to inspect misaligned samples. In this experiment, the transducer was oriented at an angle of 30^{o} while rotating around Z axis ranging from 0^{o} to 90^{o} at the angle increment 2^{o} as shown in Figure 2.12. The transducer transmits the high frequency ultrasound into the composite sample and subsequently receives the ultrasonic signal backscattered from the sample. It should be noted that a try and error procedure was used to determine this incidence angle for generating waves inside sample. The idea was to generate acceptable reflected wave from the specimen to detect the ordinations of fabrics.

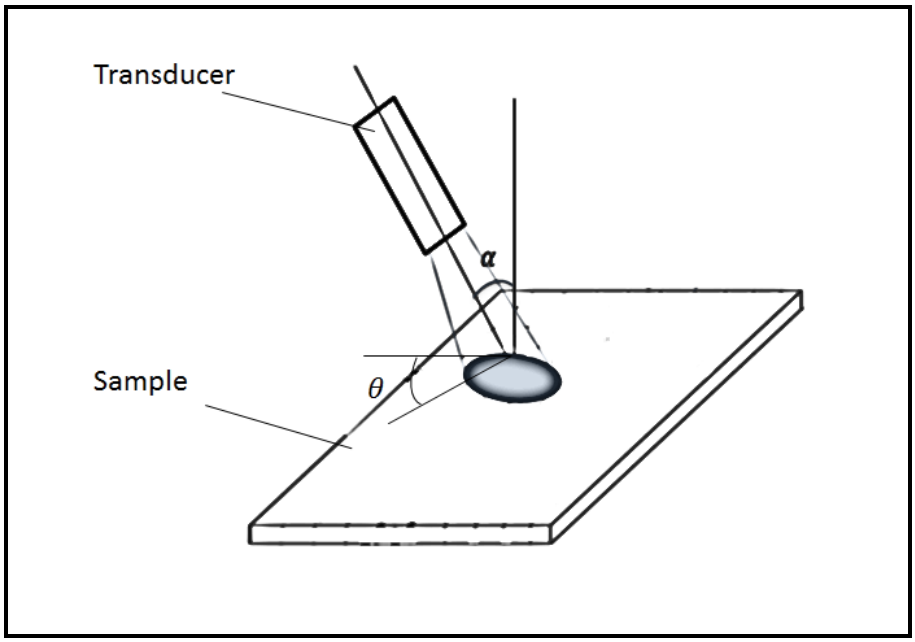

Figure 2.12. Image of transducer position for polar C-scanning

2.3.2 Vibration

Vibration technique in this research was based on analysing the dynamic response of samples using LMS system analyser. LMS system is an integrated solution for reproducing vibration environments including acoustics vibration control and structural testing. The system is equipped with software for measurement and analysis of vibration parameters and includes

different modules. LMS TEST.Lab Impact testing module includes a modal testing solution from measuring frequency responses to modal analysis. This module could be combined with other module such as LMS Test.Lab Geometry to generate a 3D visualization of test results.

In this research, impact hammer testing was conducted to investigate the effect of mid layer orientation on dynamic responses of composite plates. The experimental setup and the procedure are shown in Figure 2.13. As shown in Figure 2.14, one end of specimen was clamped and its free end was excited. Signals received from the vibration accelerometer were digitized and transformed to the frequency domain.

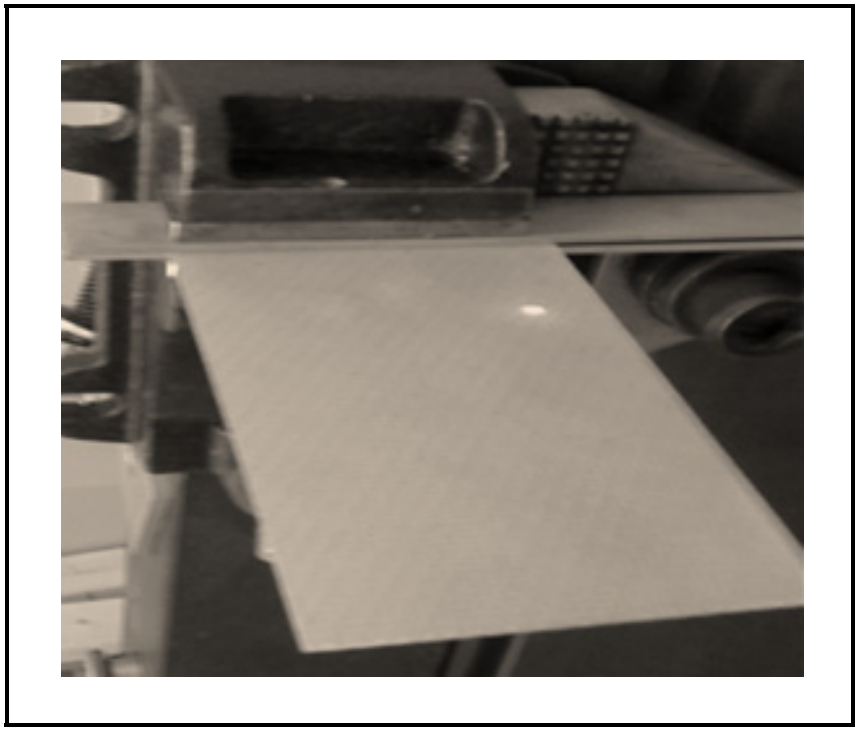

Figure 2.13. Experimental setup for vibration based testing

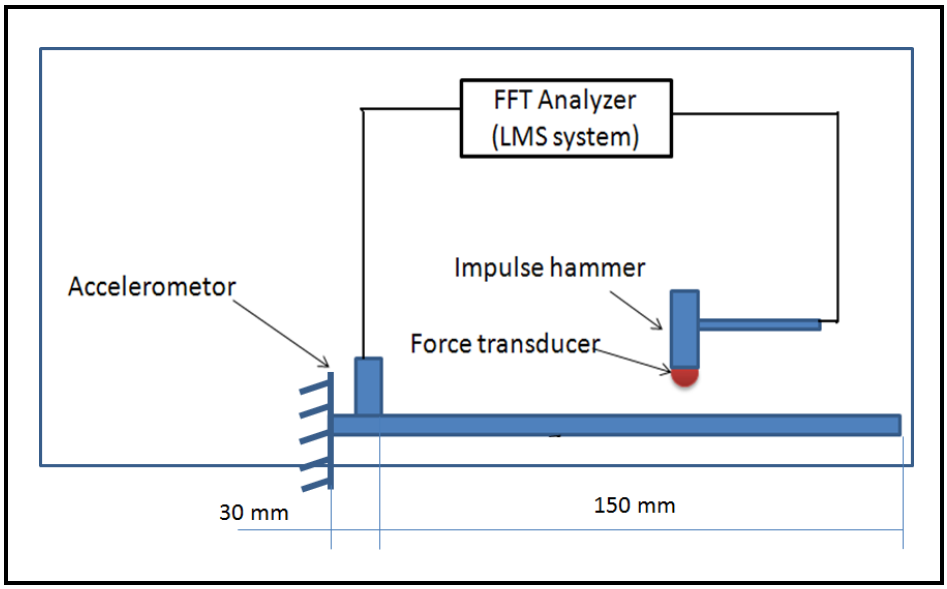

Figure 2.14. Schematic image of impact testing setup

The steel tip used in the impact hammer to strike the composite sample is shown in table 2.4. PCB Model 352C22 accelerometers (table 2.5) were used to measure the displacement on the composite plate. The accelerometer was glued to the composite sample using wax adhesive. The impact hammer and the accelerometer were connected to the LMS system as shown in Figure 2.14.

Table 2.4. Impact hammer characteristics

PCB 086C04 Impulse Hammer	
Model	086C04
Sensitivity	1.1 mV/N
Measurement range	4448 N pk
Frequency range	22 kHz
Mass	0.16 Kg
Hammer diameter	1.57 cm

Table 2.5. PCB accelerometer characteristics

PCB 352C65 Piezoelectric Accelerometer	
Model	352C65
Sensitivity @ 100.0 Hz	100.8 mV/N
Discharge time constant	1.3 s
Resonant frequency	53.1 kHz
Output Bias	10.9 VDC
Transverse sensitivity	2.3 %

The amplitude of the out-of-plan vibration at the location of the accelerometer was recorded for each composite sample under impulse excitations generated by the impact hammer. The frequency response functions (FRFs) for each sample were stored for post processing calculations. FRFs were analysed to determine the modal properties of the composite samples and obtain the natural frequencies.

2.3.3 X-ray

X-ray computed tomography (CT) scanning was conducted using a commercial scanner at Jesse Garant & Associates Company in Canada consisting of a micro focus x-ray tube at 36KV within spot size of 0.005 mm and 2376 projections. For this research, the sample size of 20mmX20mm was prepared from each composite plate to provide high resolution scanning around 0.045mm. The scanner created two dimensional images of composite sample, and a software program constructed 3D map from these 2D X-ray images. The 3D reconstructed CT data were analysed using the Volume graphic software (myVGL 2.2) toward determining of defects.

2.3.4 Mechanical characterization

Taking into account the mechanical properties of composites is highly dependent on layup sequence, a part of research was focused on the study of the influence of the misalignment defect on the tensile strength using experimental characterization. The tensile test specimens

were 15 mm wide by 130 mm length. MTS tensile machine equipped with a 100 KN load cell was considered for tension test. Tensile tests were carried out at a speed of 2 mm/min for a 70mm gauge length. Lastly, the cross sectional images of failed samples were analysed using SEM to deduce more information about damage and their shape after loading.

2.4 Results and discussion

2.4.1 Ultrasonic Results

Conventional scanning

Before scanning each panel with a 5-MHz flat transducer, the surface of each sample as fully immersed in the water tank was scrubbed to remove any air bubbles that could affect the quality of the signal. The inspection parameters included: scanning increment of 0.5mm, 1024 point per signal and sampling frequency of 125 MHz. The C-scan result for the reference plate is shown in Figure 2.15. The red color designates a high reflected signal, the blue signifies a weaker return, and the green (darker area) represents a very low return. Analysis of the C-scan data through sections perpendicular to the Z axis did not reveal any large difference in the return signal at the location corresponding to the red area.

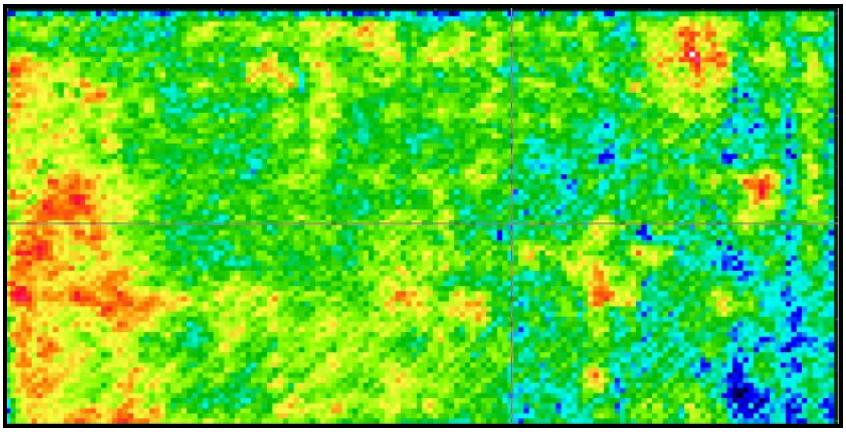

Figure 2.15. C-scan image of reference sample using a 5 MHz flat transducer and 0.5 mm scanning increment

To inspect those areas (contained fiber breakage) where C-scan inspection was not able to detect, A-scan was used to analyse the reflections from those regions. According to pulse echo A-Scan results (see Fig. 2.16), when ultrasonic waves traveling through one first layer of composite, a high portion of the incident acoustic energy is reflected back because of the fiber shape, while the remaining energy is transmitted into the next layer. As seen in this Figure 2.16, the pulse reflected from sample surface is observed, but the remaining pulses have very low amplitude, indicating a very high attenuation in the sample. The strength of the signal decreases considerably after first reflections (surface echo) at the specimen surface, therefore it is not possible to recognize the wave reflected from the back side. Hence no velocity was determined experimentaly.

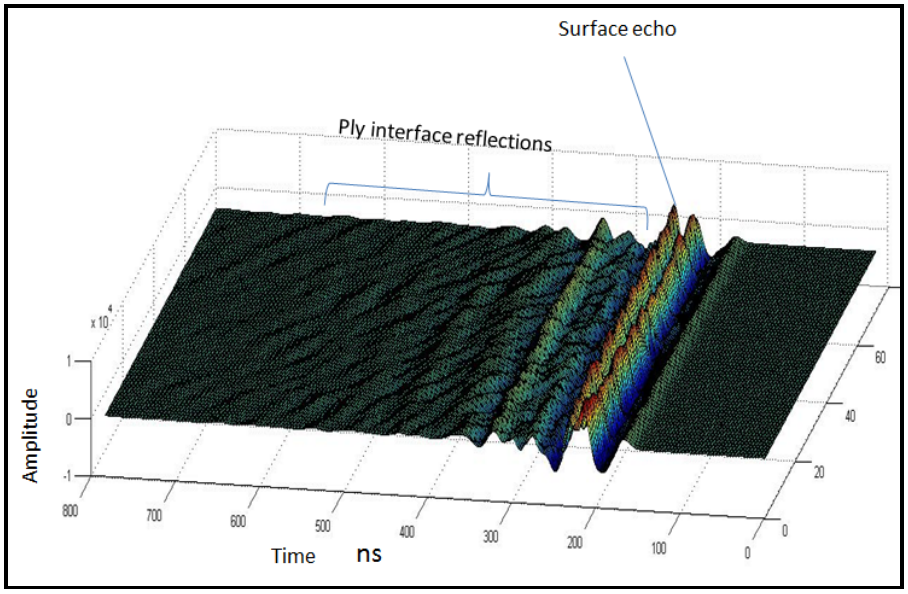

Figure 2.16. A-scan result of reference sample

Based on the A-scan results of plate II, it was not easy to distinguish between reflected waves caused by fibers and waves reflected by a localized defect. It was seen that the amplitude of the subsequent pulse is reduced by a larger amount, because the attenuation of the signal in these composites is comparatively high due to scattering and absorption by the fibers.

It should be noted that, using a 2 MHz flat transducer, the reflected wave amplitude is appeared to decrease considerably as the wave, which goes through the composite thickness.

A C-scan of the sample containing the fiber breakages is shown in Figure 2.17. The point shown inside this Figure indicates the region that small pieces of the fabrics were removed to artificially induce such defect. No return signal was observed within the gated area for this region. Thus, the C-scan ultrasonic did not detect the area where the fiber breakage was created.

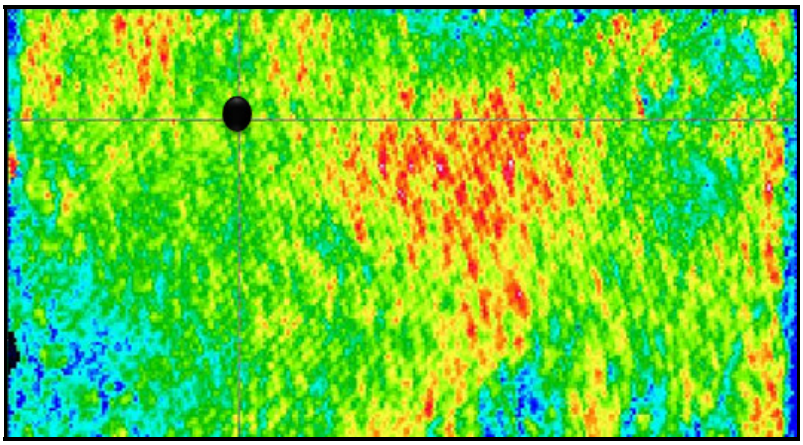

Figure 2.17. C-scan of sample II

The same effect was obtained for plates IV and V, corresponding to mid-layer misalignment angle of 10º and 20º. A comparison was also made based on A-scan images showing no difference as well.

For further analysis, B-scan images of all samples were investigated. The B-scan was considered to possibly determine the depth location of fiber breakages on a line across the specimen thickness. No significant indication of defects was observed but a strong gradient in the signal pattern was observable in the area identified by a circle in Fig. 2.18. The composite plate was cut through this location to define the defect signifying this abnormality, however, no damage was recognized in this location.

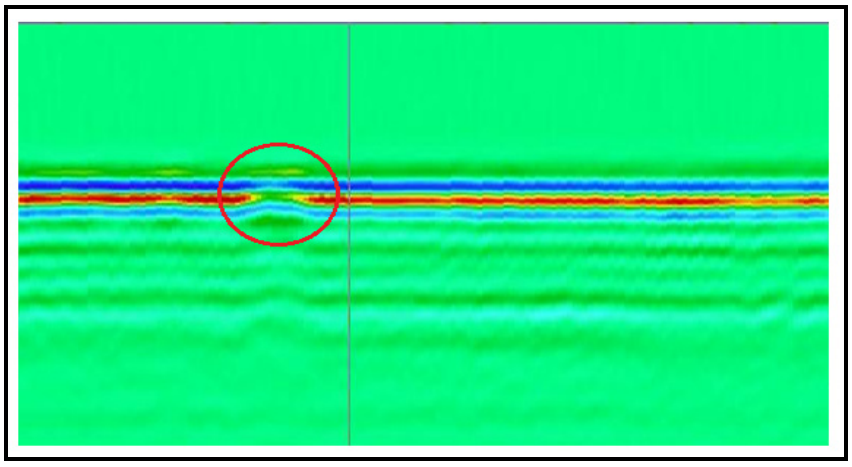

Figure 2.18. B-scan image of sample I (reference plate)

Polar scanning

The ultrasonic polar scans were performed using a 5MHz flat transducer. In the experiment the received amplitude was measured for each azimuthal angle (rotation around normal to sample surface). The results for the polar scanning approach are shown in Figure 2.19. In this plot signifying the signal intensity versus the rotation angle, the reflected signal reaches a maximum when the wave transmission is perpendicular to the fibre of the first layer as indicated by the red dots. The regions, which identified with a circle corresponds to maximum intensity and a signal amplitude received from the sample. It is seen that the two regions, displayed in the Figure 2.19, correspond to warp and weft oriented in 0^o and 90^o directions, respectively. Hence, polar scanning enables us to detect the first fabric orientation. No sign of the other 4 layers can be observed in the graph. This is attributed to the high scattering and absorption of the ultrasonic waves by the fabric layers.

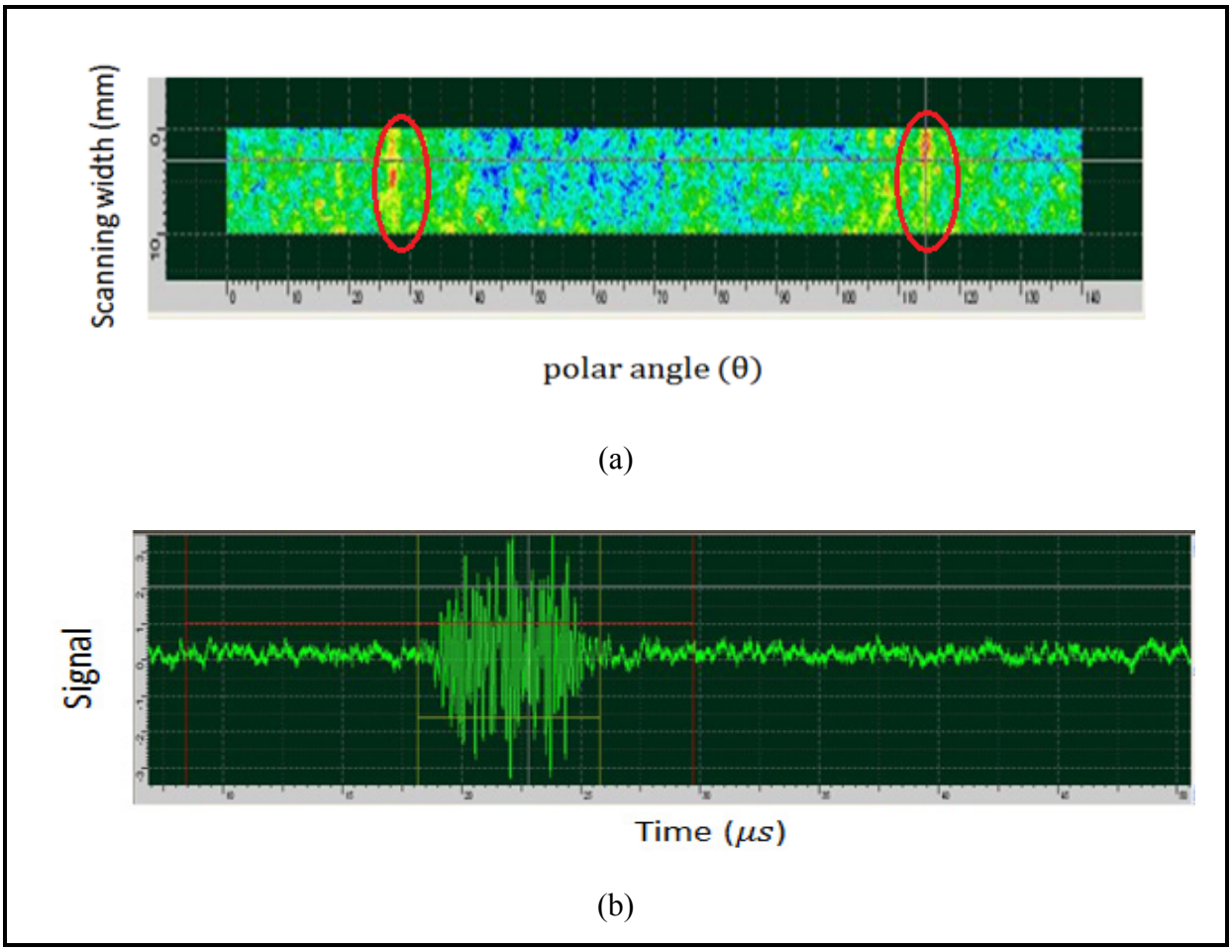

Figure 2.19. Polar C-scan of sample I using 5 MHz flat transducer (a) and corresponding A- Scan (b)

To investigate this problem, a composite sample containing 16 unidirectional fabrics was scanned using polar scanning approach. In this case, the effect of more number of layers on the incident ultrasonic waves was observed (see Fig. 2.20). Five regions observed in Figure 2.20 are corresponding to five unidirectional layer of composite shown in Figure 2.21. A quantitative estimate of fabric orientations is also made by comparing the amplitude of received signals with the sample plot described in Figure 2.19b. An increase in the amplitude of the received signal is observed for these regions.

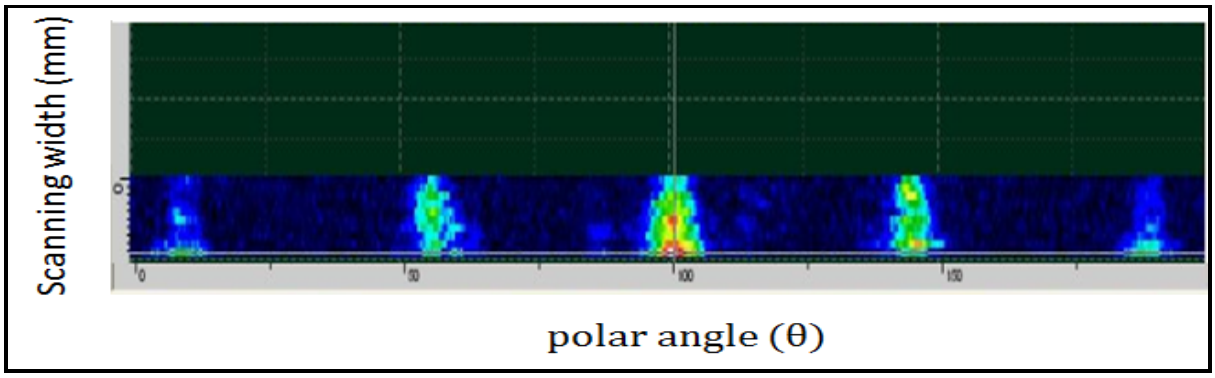

Figure 2.20. Polar scan ultrasonic of an unidirectional composite

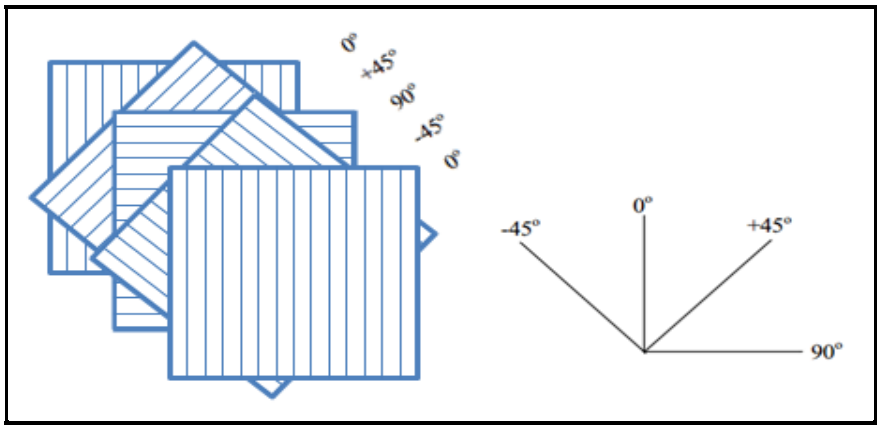

Figure 2.21. Stacking sequence of unidirectional composite sample

Signal processing in frequency domain

In this section, the possibility of detecting fiber breakage damage using the analysis of received signal in frequency domain was investigated by changing the angle of incidence. The curves shown in Fig. 2.22 represent the reflected amplitude versus frequency from 5 to 50 kHz for the sample II over non damaged region for 30^{o} angle of incidence. The signal received over the damaged region for sample II was compared with this curve, but no variation in the amplitude vs. frequency curve was observed.

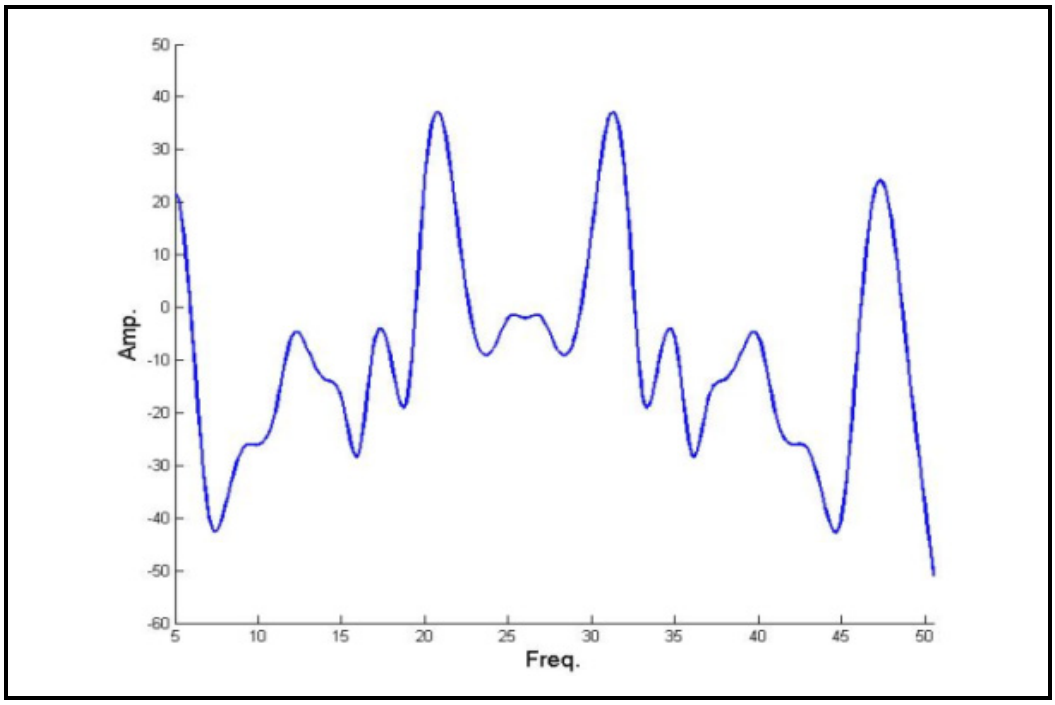

Figure 2.22. Amplitude vs. frequency curve for sample II obtained by a flat transducer with a central frequency of 5 MHz and 30^{o} incidence

2.4.2 Vibration Results

Fig. 2.23 displays the frequency response function obtained for the 5, 10 and 20º misaligned composite samples as well as that of the reference sample (no-misalignment). It should be noted, all samples were cut from same composite panel to remove any error in the test results. Differences in the spectra can be observed for the different samples. There are changes in the FRFs due to defects such a way that the FRFs were shifted to lower frequencies.

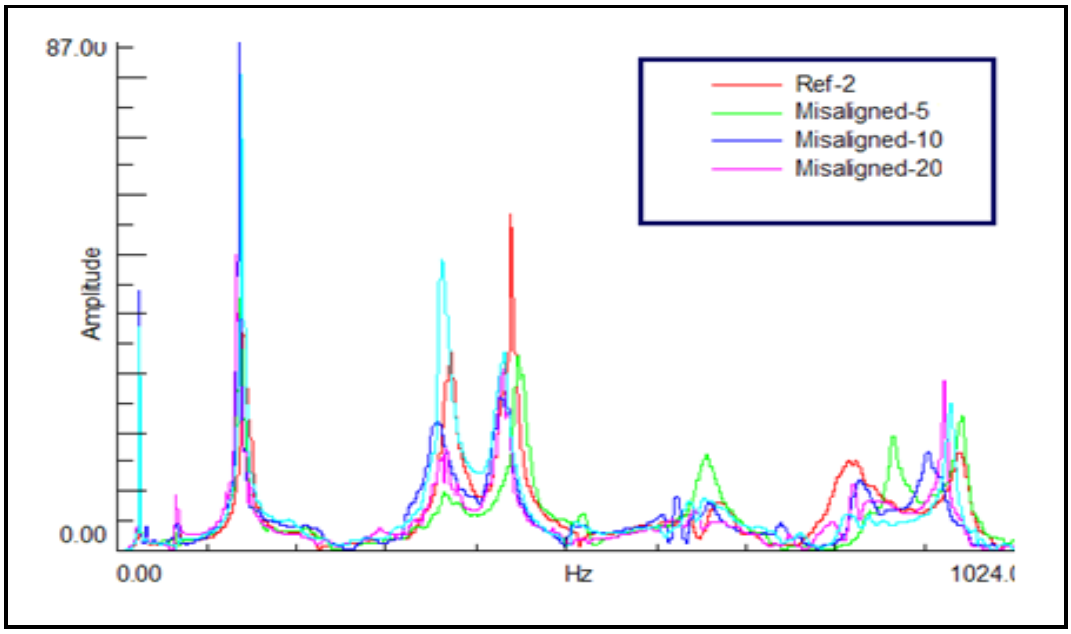

Figure 2.23. FRFs of misaligned and reference samples

A typical vibration measurement for four composite samples shown in Figure 2.24 represents the vibration amplitude for each sample versus frequency. The plot shows the decrease in natural frequency, with increasing mid layer orientation. Furthermore, the natural frequency decreases with increasing mid layer orientation, while the width of the resonance peak decreases. Note that sample II containing fiber breakage was not considered for this test.

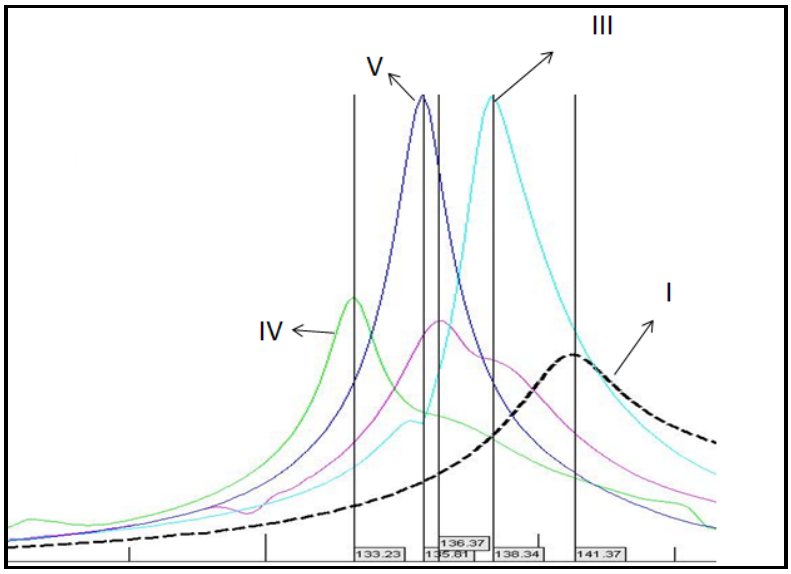

Figure 2.24. Natural frequency of composite samples at second vibration mode

The values for the 1st, 2nd and 3rd natural frequencies were extracted for all samples. The experimental modal analysis results are shown in Table 2.6. They are displayed in Fig. 2.25 as a function of the value of the misalignment angle. It can be observed that, as the mid-layer misorientation angle increases, the natural frequencies of the composite plate decreases. This effect is seen to increase for higher natural frequencies.

Table 2.6. Natural frequency of composite samples

Mode	**Average natural frequency of composite samples**			
	Sample I	**Sample III**	**Sample IV**	**Sample V**
1	26	25	25	24
2	144	138	136	133
3	372	363	354	348

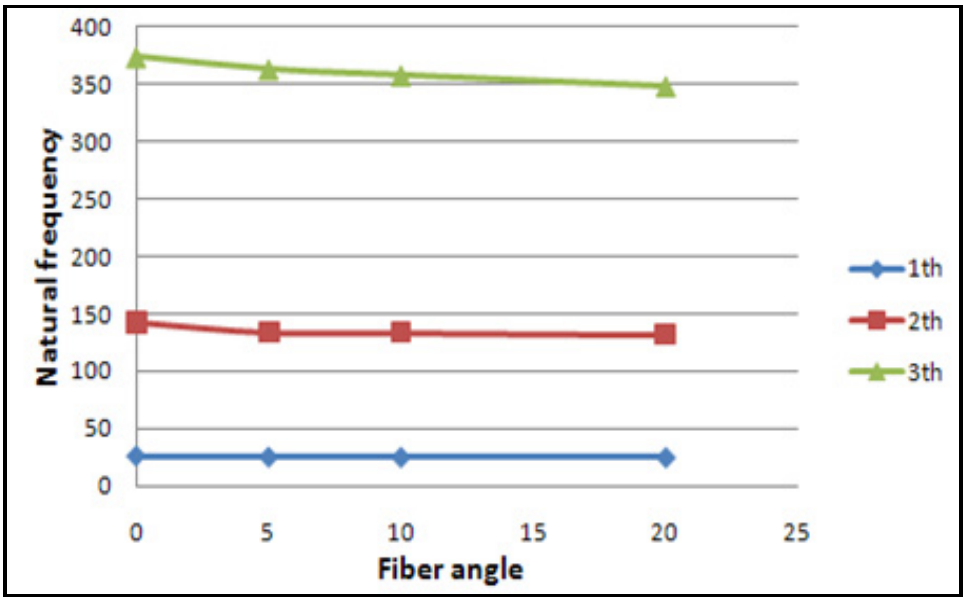

Figure 2.25. Variation of the natural frequencies of the samples as a function of the mid layer angle

2.4.3 X-ray result

X-ray computed tomography scanning process and its resolution was adjusted such a way that composite layers could be detected. Scanning data then was imported in volume graphics software to construct 3D reconstruction of composite samples. The 2D images of the sample I and II are shown in Fig. 2.26. The dark grey regions demonstrate resin and light grey regions represents twill woven glass fabric. Figure 2.26a clearly reveals the warp and weft yarns of mid layer at 0 and 90 directions while the Fig. 2.26b demonstrates the misalignment of mid-layer in the amount of 5 degree. The current research was carried out to examine the capabilities of micro-CT to observe mid layer orientation and the sample view was considerably decreased to observe all details in composite with high scanning resolution.

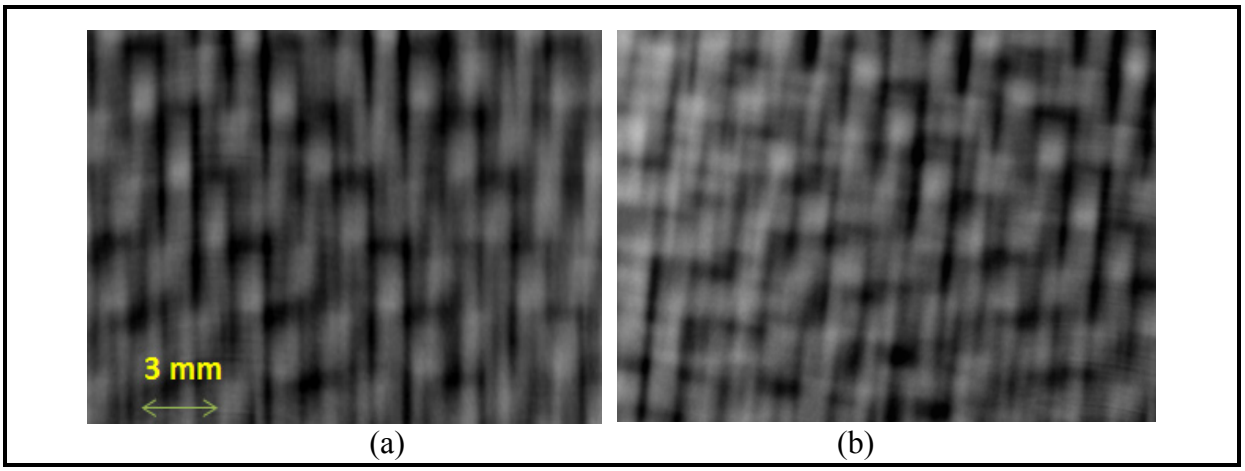

Figure 2.26. X-ray CT images of composite plates sectioned in thickness direction to observe mid layer orienataion (a) Sample I (b) Sample III

2.4.4 Tension test results

Static tension tests were carried out using MTS machine. Hydraulic jaws, which are capable of preventing the specimen slippage during the test, were used to clamp the samples. Appropriate hydraulic pressure was applied to the sample ends to reduce local stress concentrations and also to prevent the failure of the test specimen next to the hydraulic jaw grip. That was the main criteria which ensure the accuracy of our results. The experimental results are reported in Tables 2.7. Typical stress strain curves and the influence of mid-layer orientation on tensile strength are shown in Fig. 2.27. The stress–strain curve of reference sample is approximately linear until failure and the tensile strength is superior for reference sample compared to other misaligned samples. Sample I including all woven fabrics aligned in loading direction absorb tensile loading and equally distribute the load throughout the composite. Therefore, the sample could tolerate more tensile loading. However for misaligned samples, the tensile strength was relatively reduced, because the mid layer fabrics begin to slip when sample experienced the tensile loading.

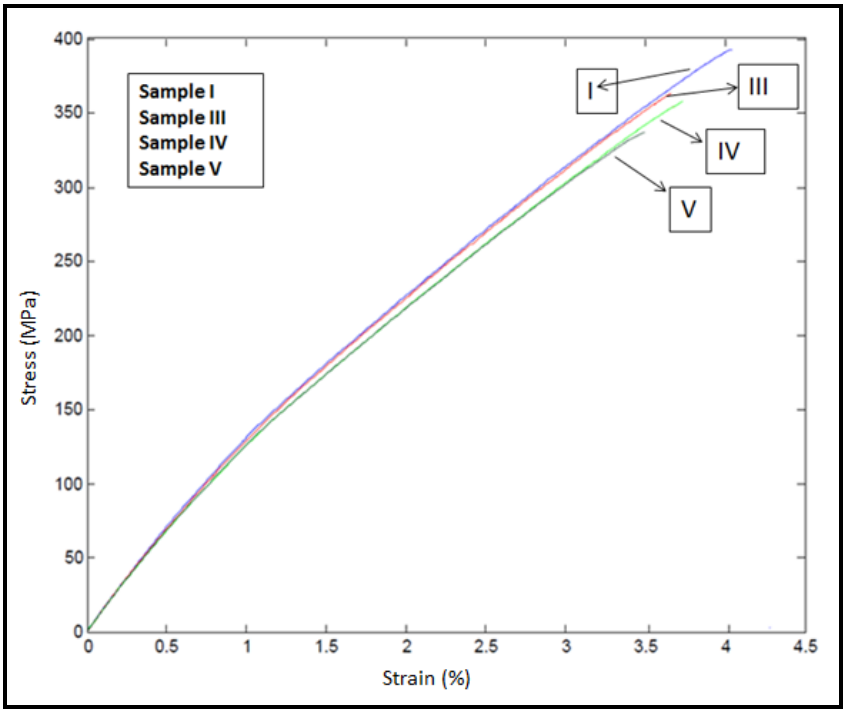

Figure 2.27. In-plan tensile strength of sample with different mid-layer orientation

Table 2.7. Tension test results of composite sample with known misalignment defect

specimens	1) Number of test	2) Average Strength (MPa)
3) Perfect sample	2	397.5
5^{o} Misalignment	2	368.75
10^{o} Misalignment	3	357.5
20^{o} Misalignment	2	340

For sample I, the rupture surface was nearly normal to the direction of loading. For other samples, the rupture occurred along the mid layer fabric oriented at an angle with the loading direction. Figure 2.28 depicts SEM images of sample III fractured in tensile mode. The fracture surface of sample indicates the pullout of fibers in the vicinity of rupture surface. In addition, delimitation was observed in the rupture region.

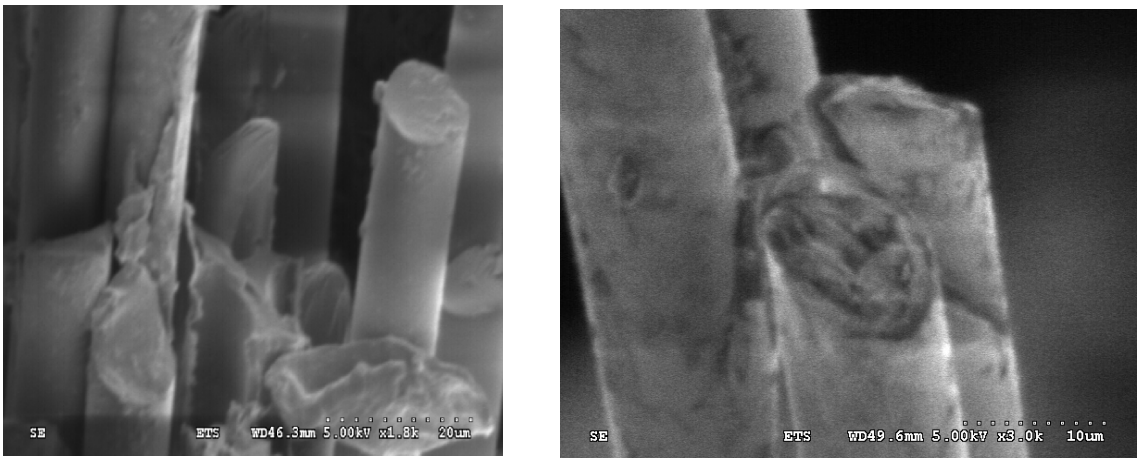

Figure 2.28. SEM images of samples ruptured in tension test
(a) Fiber pull out (b) Fibers ruptured in shear mode

2.5 Finite element modeling

2.5.1 Wave propagation at meso-scale level

Wave propagation in the composite materials is a complex process that results the challenge for the interpretation to detect damage. Wave propagation modeling is a useful approach to understand this phenomenon by solving the governing differential equations with consideration of boundary conditions. Three main numerical methods have been used to solve these equations including the finite difference method, the finite element method (FEM) or the boundary element method (BEM). There are commercial finite element codes to simulate the wave propagation in the composite materials (Moser F., Jacobs L. J. and Qu J., 1999).

The objective of this research is to apply finite element modeling technique to detect a localized damage in the woven textile composite. The modeling procedure was used to investigate the possibility of using of laser ultrasonic shown in Fig. 2.29 for our inspection purposes. The finite element model was constructed from a 3-D solid according to woven composite structures composed of five woven fabric layers.

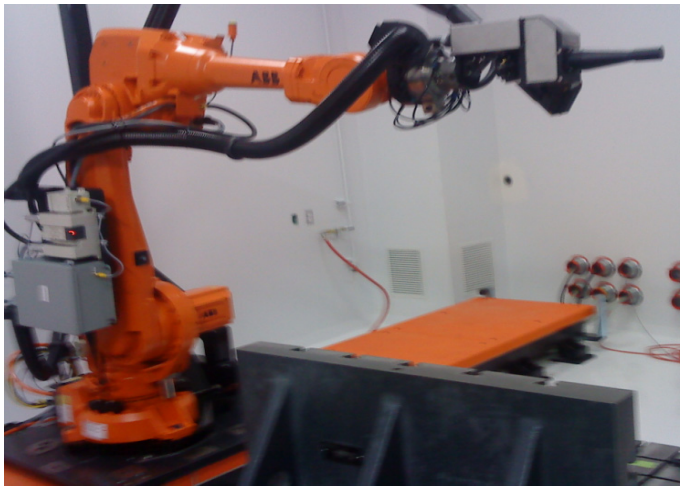

Figure 2.29. Experimental setup for the laser ultrasonic scanning (Courtesy of CTA)

In this model, a unit cell shown in Figure 2.30 was defined as the smallest repeating unit for the woven textile composite. CATIA software was used to construct these 3-D structures, and then the CAD files were imported into FEM software and assembled together.

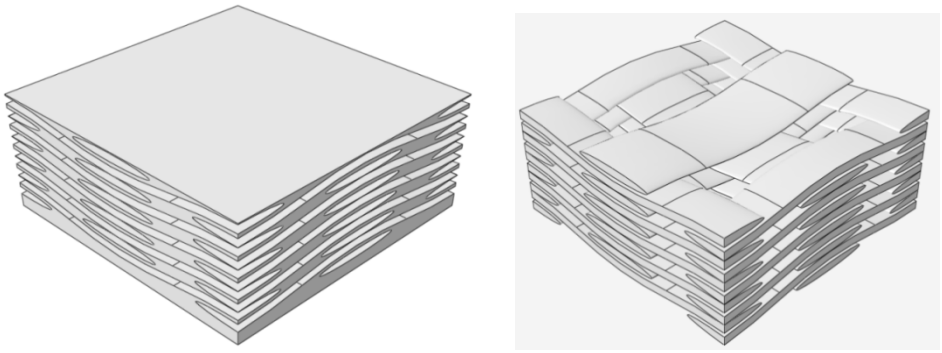

Figure 2.30. Model for finite element analysis (a) Fiber (b) Matrix

In this modeling, in order to achieve a stable solution along with sufficient accuracy the best effort made to use appropriate element size and time step. The element size was smaller than one tenth of wavelength in stiff material phase (fiber) for excitation frequency of 30 KHz

(see Fig.2.31). Around 900 hexahedral elements were therefore employed for FEM modelling of this five layer unit cell. The maximum size of time step was constrained by the time required for the high speed longitudinal elastic wave (in fibers) to travel this evaluated nominal element size. However, the time step determined by FEM software was much lower than this limit. The matrix was an isotropic polymer resin and fiber bundles were transversely isotropic. The objective of this part of study was to investigate the through-thickness propagation of a transversally induced wave and its interaction with textile layers. As the unit cell width is double of its height, the wave reflection from vertical boundaries does not affect the wave transmission from top to the bottom of unit cell. Hence, no absorbing boundary and periodic boundary condition is required for this purpose. Accordingly, the unit cell was simply supported vertically at 4 corners of bottom surface and natural free boundary was considered for the remaining boundary. Although supporting 4 corners does not affect the results obtained for desired time frame, it was however considered for having a more practical simulation, preventing rigid body motion in the model at further time steps. Excitation load was a sinusoidal wave in through-thickness direction.

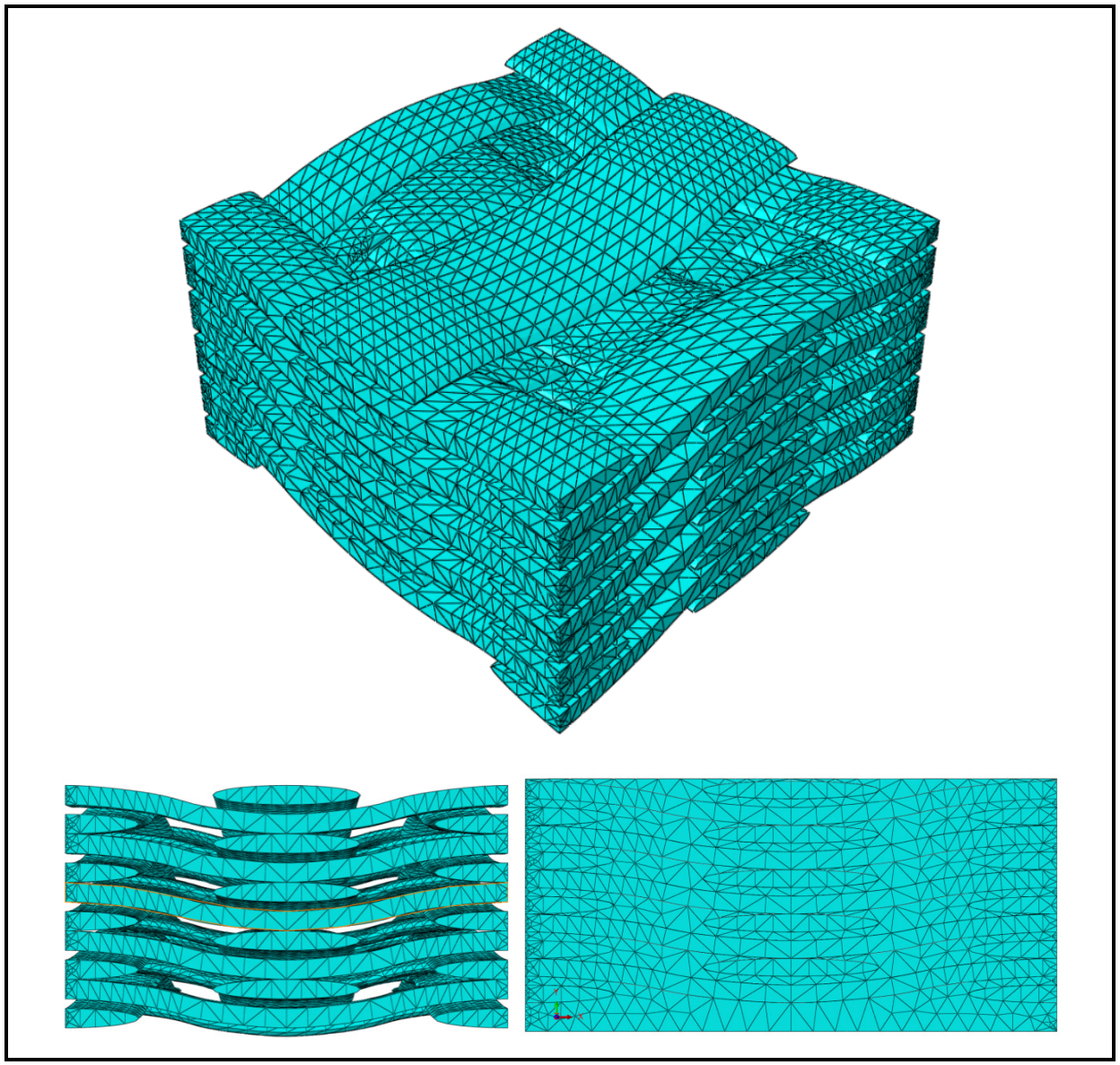

Figure 2.31. A complete mesh of woven composite at different view

Figure 2.32 depicts normal displacement of a woven composite damaged with fiber breakage at meso-scale excited by ultrasonic waves and its response signal captured at the back side of this 3-D solid model. The fiber breakage was not quantified using amplitude change and no information of the breakage location appeared. The main reason could be because the attenuation of the signal in this model was comparatively high due to scattering caused by the fibers. However, this modeling result confirms that the finite element modeling at meso-scale

could be suitable for modeling elastic wave propagation through textile composite part at meso scale level toward inspection purposes.

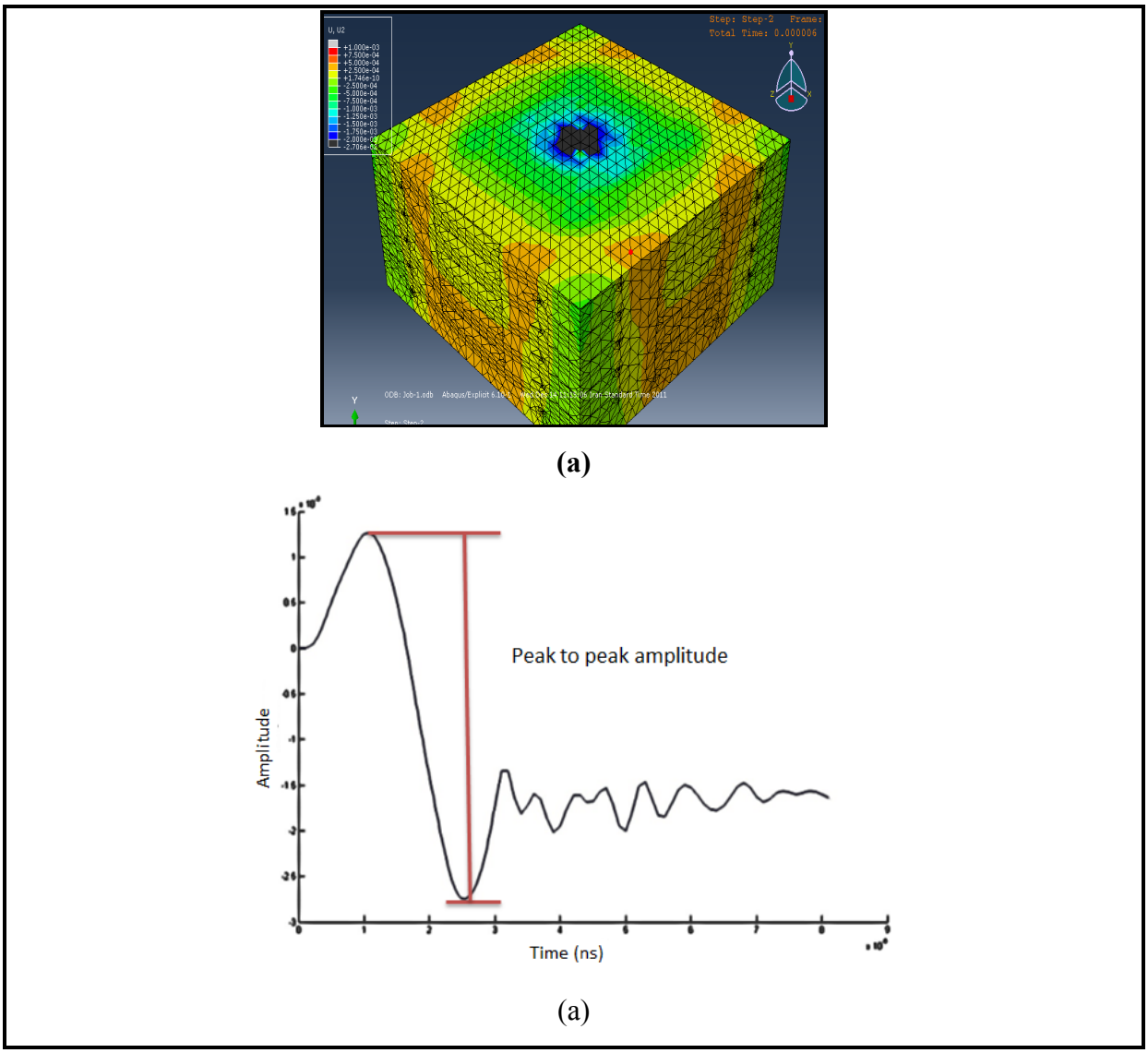

Figure 2.32. (a) Displacement contour of woven composite at meso scale level
(b) Received response in back side of composite model

2.5.2 Vibration modeling

In addition to experiments, an effort was made to best understand the influences of fiber orientation on the frequency response function of the composite samples using modeling procedure. It was concentrated on modeling textile composites composed of five layers at macro scale at free fix boundary conditions. A macro-mechanical FEM simulation was undertaken using ABAQUS software and modelling composite as homogeneous stacked solid layers.

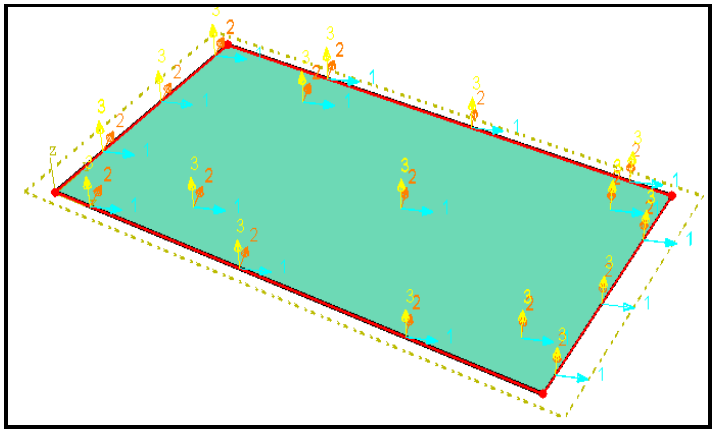

Figure 2.33. Modeling of fiber misorienation in 3rd layer of composite model

The effective mechanical properties of the homogenised composite laminate including Young's modules, Poisson's ratios, in-plane shear modulus and transverse shear module were extracted from literature (Huiwen H. and Jieming H., 2009) for a woven glass composite laminate with dimensions 150 x 50 x 2.5 mm.

It should be emphasized that this modeling was carried out only to investigate the effect of mid layer fabric orientation on the frequency response. The model properties were not same as those samples experimentally tested in this chapter. Hence, it is not possible to apply our modeling results for the composite plates fabricated from JB Martine fabrics.

The modeling procedure contained the following steps: first model called perfect plate was created as three dimensional deformable solid consist of five fabric layers, and its properties were defined, and assigned to the model. Second model as misoriented sample was generated

same as first model, but, the third layer of this model was rotated 20^{o} in Z- direction (perpendicular to the composite surface). FE model was created using linear solid elements with one element per model thickness as shown in Figure 2.34.

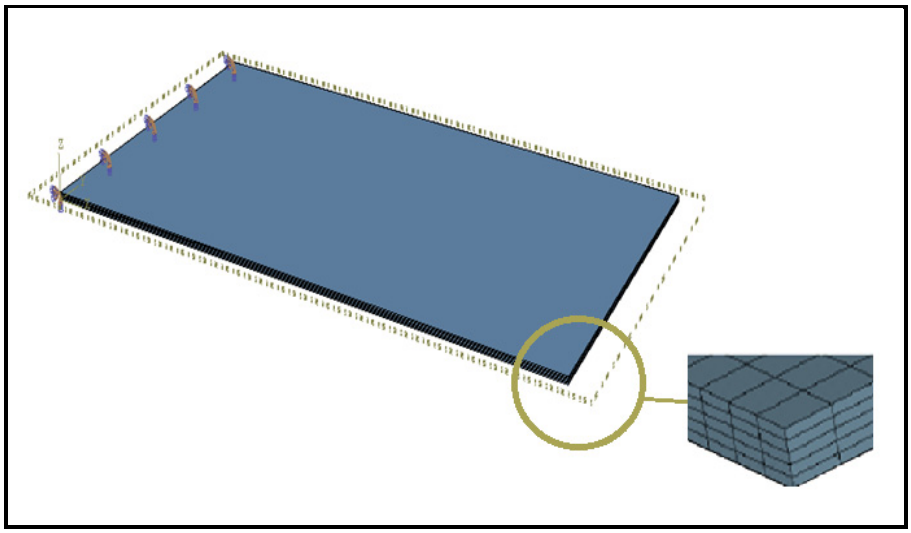

Figure 2.34. Boundary condition applied to the composite model
and solid element FE model of composite plate

After running, the output file including the modeling results was created. Finally the post-processing module was used to extract the natural frequencies of each plate from these output files. For broad band excitation of model one free end was subjected to a step load with alternate amplitude of 3N. Then the FRF response of the sample at a node 5 cm away from the loading point at the edge of the plate was extracted. A difference in FRF between the reference and the 5, 10 and 20º mid-layer orientation of samples was observed. Figure 2.35 shows difference between FRF of sample I and sample included with 20^{o} mid layer orientation. According to modeling results, the maximum difference was observed in the case of the effect of fiber orientation at $\theta = 0$ and $\theta = 20$.

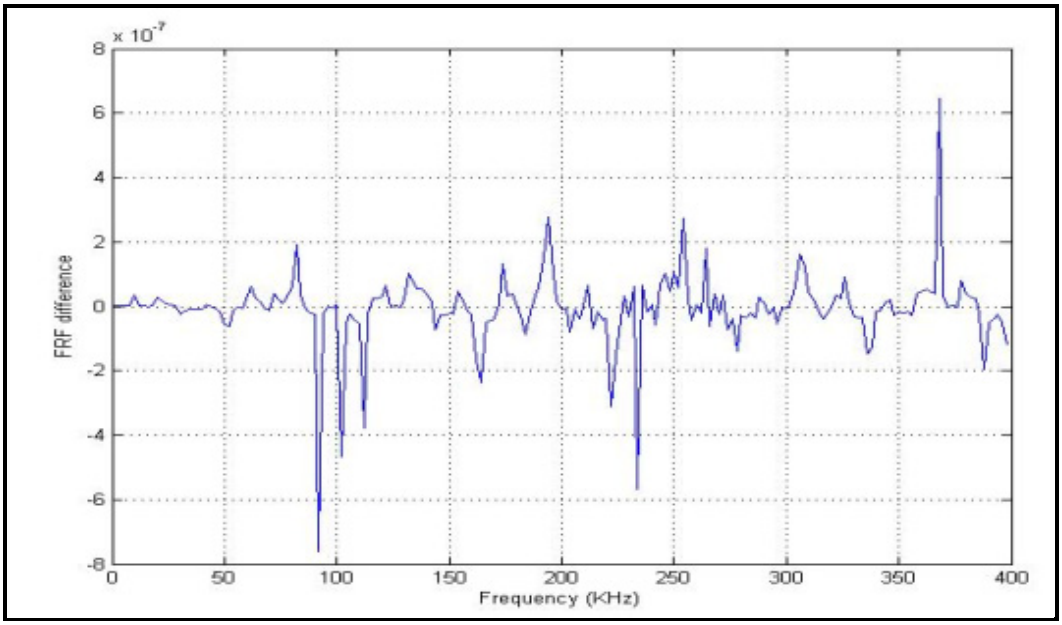

Figure 2.35. Difference between FRF of intact and defective samples

2.6 Conclusion

The applicability of several inspection methods based on ultrasounds, X-ray, vibrations for detecting two types of artificial defects in composites has been examined. Conventional and polar pulse echo C-scanning of the samples suffered from a high attenuation of the ultrasonic wave by the fabric layers, which prevented detecting the presence of the defects.

In this research, the scanning parameters were not fully optimized. Hence, for future research, ultrasonic parameters such transducer frequency, wave incidence angle need to be optimized depending on the fiber architecture.

From the vibration testing results, it was concluded that natural frequencies decrease, as the mid layer angle increases; and the maximum natural frequency occurred at $\theta = 0^o$ and mid layer $\theta = 20^o$ has a smaller natural frequency for that sample. From the results, it could be possible to investigate the stacking sequence of the textile composite based on their natural frequencies.

X-ray computed tomography was the best NDE technique for studying layers orientations in textile. The fiber orientation was appeared in X-ray images, however the small size of sample was limited us to scan whole sample.

Defects and fiber undulations in the textile did not translate into thickness variations in the composite plate large enough to be detected by CMM, however the thickness variation of composite sample was examined.

ABAQUS software was used for modeling of textile composites at different scales due to its capability for dynamic modeling and including a comprehensive library of material properties and elements types. The fiber breakage was not recognized using amplitude change due to high attenuation of the signal caused by the fiber bundles. Modeling results showed that the frequency response functions are sensitive to fiber orientation due to their direct relationship to stiffness.

The value of FEM application to simulate the propagation of ultrasonic waves in textile composite at meso-scale level was investigated. Influence of most significant parameters such as the length of element and the time step was investigated. This research could provide a basis for modeling the propagation of waves in other textile composite with different fiber configuration.

CHAPTER 3

3D TEXTILE PREFORM PERFORMANCE

3.1 Introduction

The use of tufted textile fabrics for aerospace composites can give the possibility to improve the delamination resistance and damage tolerance. Tufted preform structure could affect the processing properties such as porosity, permeability and mechanical performance of final composite. Therefore, the characterization of tufted preforms is a significant parameter to evaluate the performance of these materials for composite applications. In this chapter, the behavior of tufted preforms was examined under different loading conditions. The preform was tested under tensile and compressive loading in different directions. Its draping capability was also evaluated. The loading curves were investigated based on the behaviour of preforms under loading. The mechanical characterization results presented in this chapter may be useful for recognizing the formability of tufted preforms to produce complex shaped textile composites.

3.2 Materials and experimental equipment

3.2.1 Preform manufacturing

The two preforms were composed of eleven layers of twill woven glass fabrics with a lay-up of [0/45/90/45/90/45/90/45/90/45/0] such a way each preform has a total thickness of 5 mm. The 3k twill 2X2 woven fabrics have the areal weight of 305 g/m^2. The size of each preform was 500 mm X 500 mm. One preform was tufted with a twisted 240 Tex polyester thread using a KUKA 6-axis robot equipped with a commercial tufting head at CTT group, Canada. The tufting row was oriented at 0° direction with a tufting spacing of 8 mm and pitch of 8 mm. Figures 3.1 and 3.2 are the sketch of the tufted preforms which presents a tufted structure with polyester thread.

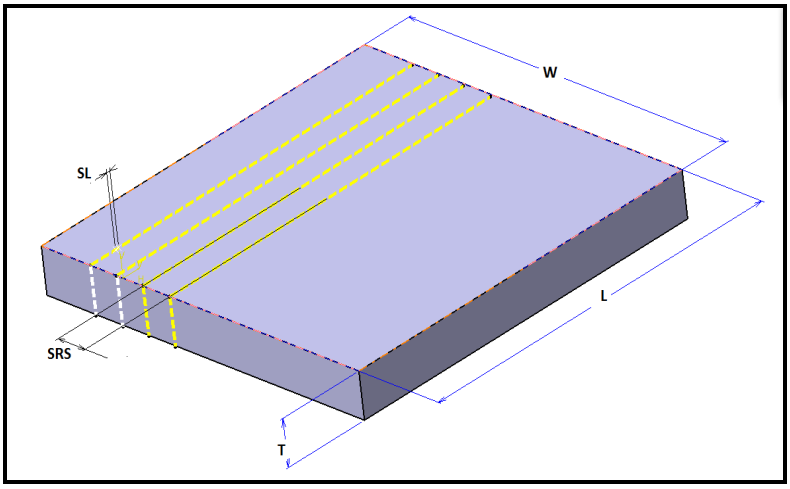

Figure 3.1. Schematic images of tufting thread arrangement

Table 3.1. Main tufting parameters of preform samples

Preform	**Fabric layup**	**Thread**	**Stitch type**	**fabric**	**SL (mm)**	**SRS (mm)**	**T (mm)**	**(L x W) (mm)**	**Qua.**
Tufted	Quasi-isotropic	Polyester 240 Tex	tufting	GF	8	8	5	500 x 500	1
Untufted	Quasi-isotropic	-	-	GF	-	-	-	500 x 500	1

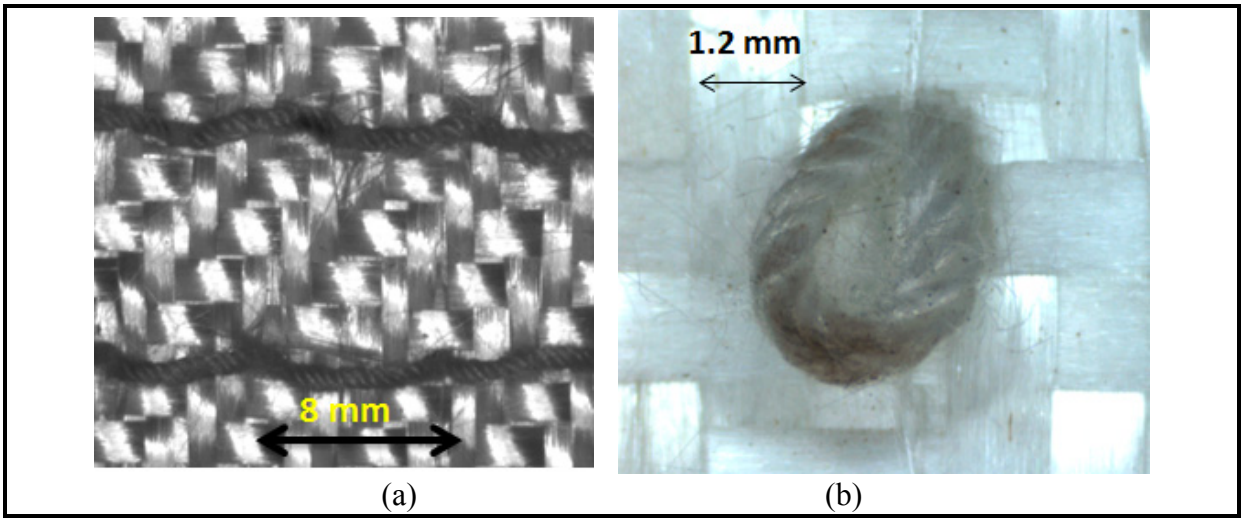

Figure 3.2. Architecture of tufted preform (a) Front-side (b) Back-side

3.2.2 Quality control

Preforms were inspected visually to detect any possible discontinuity to the tufting threads and fabrics. Then, microscopic characteristics of the preform using an optical and SEM technique were performed to see the effect of tufting process. The pictures obtained from the SEM and optical microscope are shown in Figure 3.3 reveals the localized damage including fiber breakage and fiber misalignment that occur in the woven fabrics because of the needle penetration.

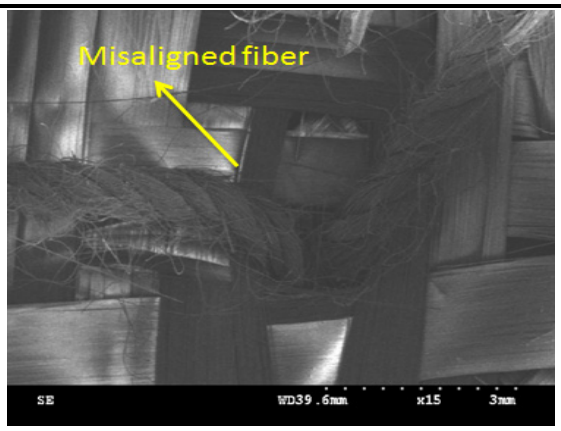

(a)

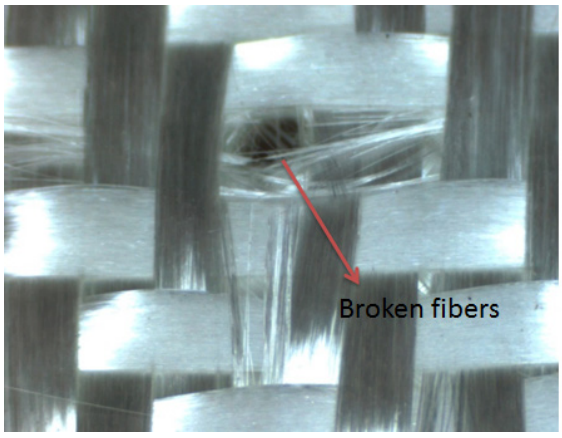

(b)

Figure 3.3. Micrographic images of the tufted region using (a) SEM (b) Optical microscopes

3.2.3 Specimens and mechanical test procedures

Specimens

Descriptions of specimens and the test procedures are contained in this section. Table 3.2 provides a matrix of tests performed in this study. Specimens were loaded along the tufting direction (0°) and perpendicular to the tufting direction (90°) to investigate the mechanical performance as noted at the beginning of chapter.

Table 3.2. List of specimens and tests for the preform characterization

Test type	Tufting orientation	W (mm)	L (mm)	No. of tufting lines	No of test	Symbol
Static tension	0^o	45	140	5	5	TL
	90^o	45	140	16	5	TT
	0^o-Untufted	45	140	-	4	TN
Static compression	0^o	60	60	6	2	CT
	0^o-Untufted	60	60	-	2	CN
Drape	0^o	140	140	16	2	DT
	Untufted	140	140	-	2	DN

Mechanical test

Tension

Tensile test of specimens was performed out by an MTS machine with a load cell capacity of 100 kN. Each specimen had an initial length of 140 mm, and an initial width of 45 mm (Table 3.2). At each end of the specimen, a length of 30 mm was clamped into the hydraulic grippers. To decrease the stress concentration in the clamping sections, thin aluminum sheets were bonded on the ends of each preform specimen. Each transverse (90°) tufted specimen included 16 lines of tufting within the length, yielding on average three stitches within the gauge section, and each longitudinal (0°) tufted specimen included 5 lines of tufting within the width.

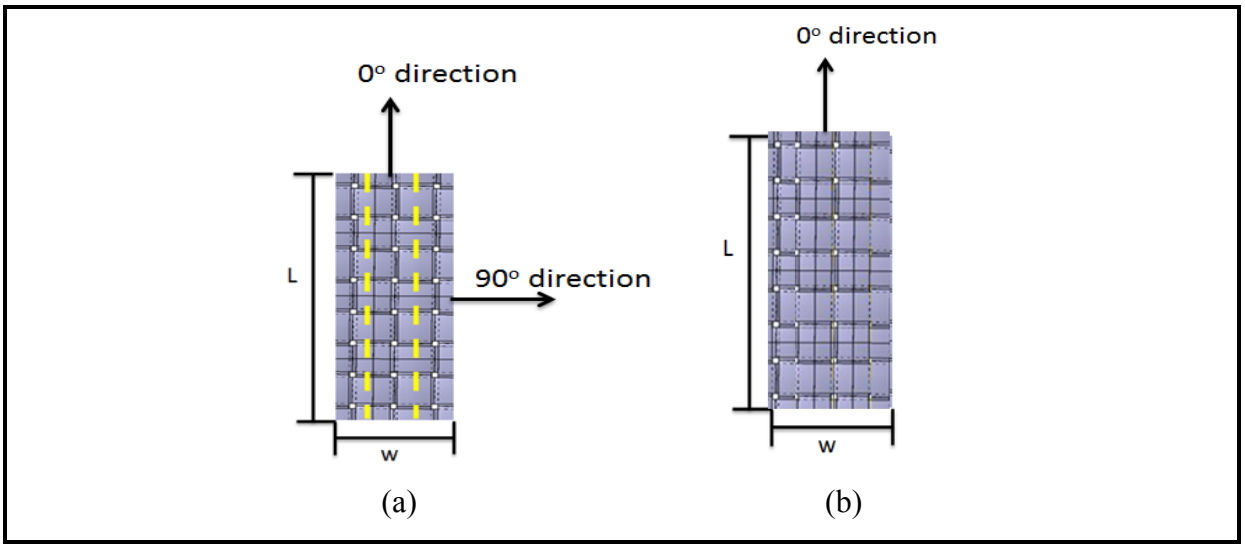

Figure 3.4. Schematic images of sample for tensile tests (a) Tufted (b) Untufted

The tensile tests were carried out with speed of 100 mm/min for all specimens up to complete failure. Figure 3.5 illustrates the tensile test set-up for the preform loaded perpendicularly to tufting direction.

Figure 3.5. A tufted sample clamped for in-plan tension test

Ten specimens were cut from the same tufted preform such that five preform specimens cut in parallel and five specimens cut in perpendicular of tufting direction. These are test

TL1-TL5 and TT1-TT5 respectively. Four specimens were cut from untufted preform in weft direction for comparison purposes. These are donated TN1-TN4.

Drapability

For drapability testing, a hemispherical plunger in the diameter of 32 mm with a 150 N load cell was mounted on the Instron machine to study the formability of tufted preforms. Figure 3.6 displays the drape test set-up consisting of a hemispherical plunger, preform holder and flat tufted preform. The fixture consisted of two plates, each having a hole around 90 mm at its center.

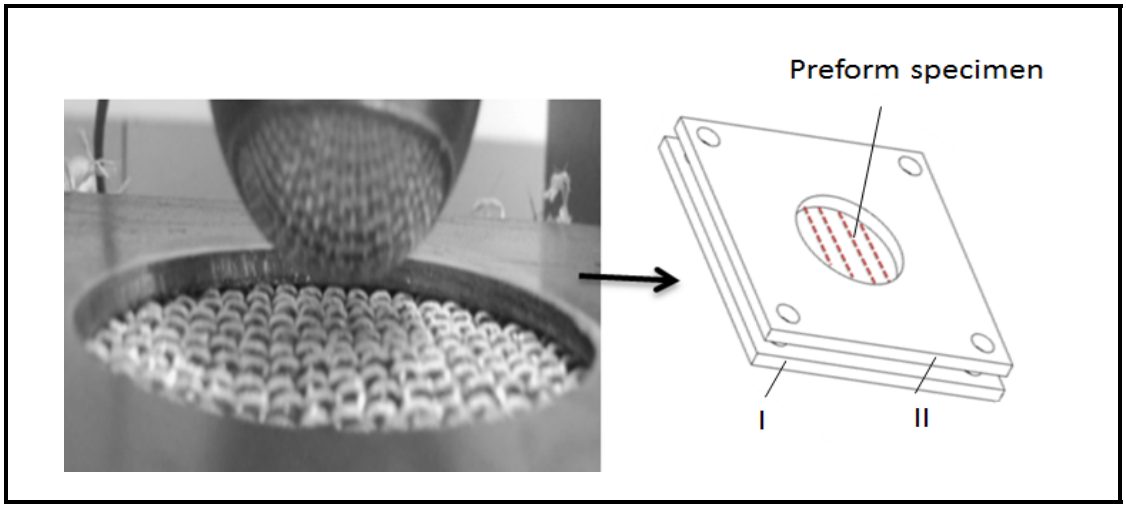

Figure 3.6. Experimental setup for the drape testing

Two specimens were cut from the tufted preform and two specimen cut from untufted preform for comparison purposes. Each preform samples size was 140 mm (L) by 140 mm (W). The sample was mounted between plate I and II shown in the Figure 3.6, and four screws were tighten with equal force using a torque wrench such a way that the sample could move freely during forming. The hemispherical plunger was moved down at a velocity of 5 mm/min. The touch point of plunger and preform was set as first position. The stop position of plunger was at 20 mm from the first position (Due to the low capacity of available load cell, the plunger movement exceeding 20mm was not possible). Preform was slowly

deformed by plunger and the load and displacement between these two points were recorded and integration of drape loading and plunger displacement were defined as forming energy.

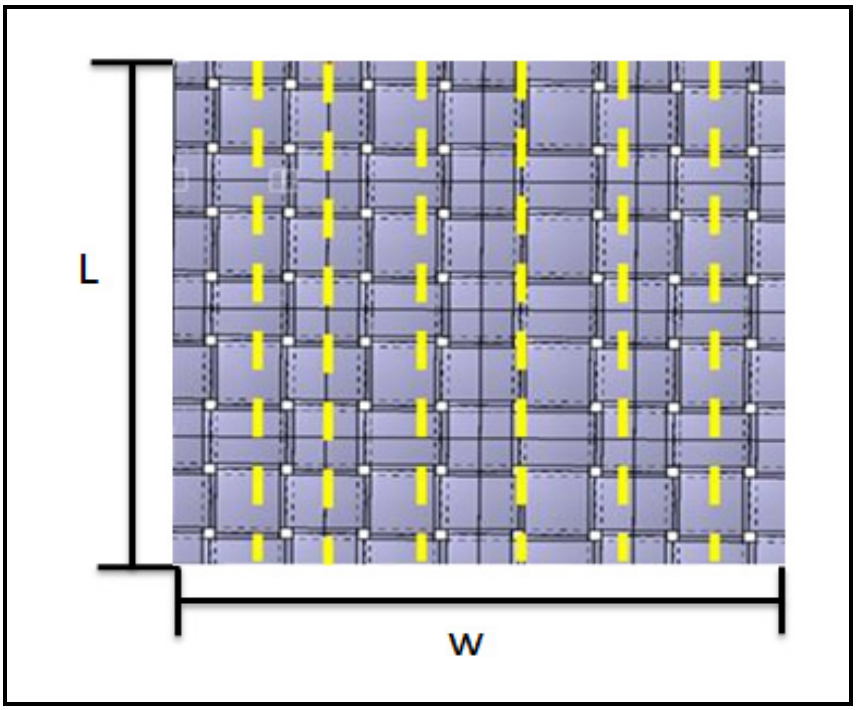

Figure 3.7. Schematic image of tufted preform for drape test

Compression test

Figure 3.8 represents a schematic illustration of the compression test carried out by an MTS machine with a load cell capacity of 100 kN. At first, the system was calibrated to ensure the accuracy of compression results. An upper circular punch moved down and compressed the tufted preform. The punch movement speed was 1 mm/min. The upper limit of the load was set at 20 kN. The displacement at which the compressive force reached 20 kN has been used as the final displacement and a load-deflection response was recorded for analysis purposes. Two specimens were cut from the tufted preform and two specimen cut from untufted preform for comparison purposes. Each specimen had an initial length of 60 mm, and an initial width of 60 mm (Table 3.2). The force and displacement were measured for each specimen during the compaction test.

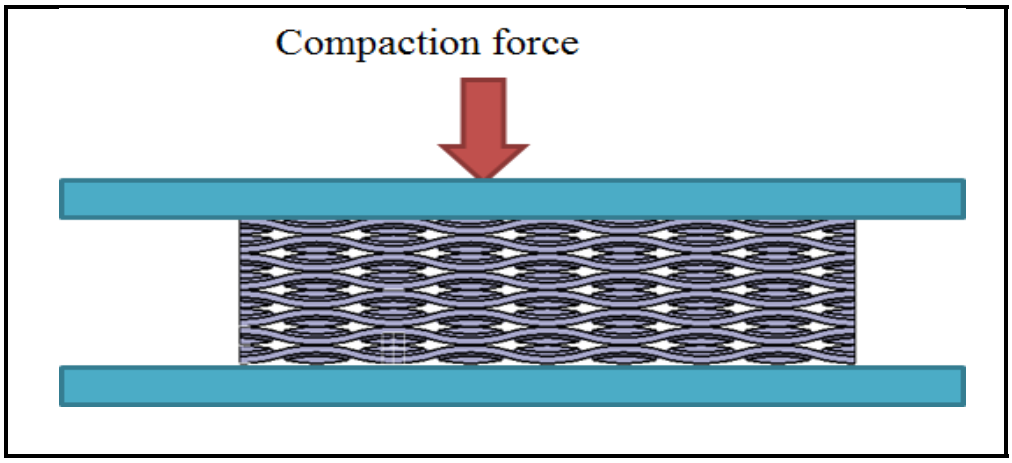

Figure 3.8. Testing setup for the preform compression

3.3 Results and discussion

3.3.1 Tension

The tension results of untufted preforms (TN1-TN4) with a gauge length of 70 mm are shown in Fig.3.9 and Table 3.3. The failure strength for the untufted preform load in warp direction is 6.6 kN, the average displacement at peak force is 1.6 mm, and the toughness is 5 kNmm. The variation among the test results is small.

Tension results of tufted preform (TL1-TL5) with a gauge length of 70mm loaded in tufting directing is shown in Fig. 3.10. The failure strength for the tufted preform load in tufting direction is 11.01 kN, the average displacement at peak force is 1.92mm, and the toughness (area under force-displacement curve until failure point) is 11.3 kNmm. Test result variation is high. This could be because of formation of damage in tufting thread and fiber bundles.

Results from samples (TT1-TT5) with a gauge length of 70 mm loaded perpendicular to the tufting directing are presented in Fig. 3.11 and Table 3.5. The failure strength for these preforms is 9.9 kN, the average displacement at peak force is 1.45 mm, and the toughness is 7.2 kNmm. The variation among the test results is lower than for the preform loaded in the tufting direction. This is because of uniform deformation of transverse preform under tension loading.

Tufted preforms (TT and TL) exhibited greater tensile strength values than untufted preforms (TN). Of the extracted results, those that had transverse tufting (TT) exhibited generally smaller mean strengths than those that had been loaded in the tufting direction (TL), although there was some overlap.

Research results indicate that, the effects of fiber misalignment and fiber breakage that occurring during tufting are compensated for by increased tension along tufting direction, and consequently the tension strength is not decreased. The uniaxial tensile strength of specimens tufted with polyester of 240 Tex is 40% higher than that of untufted specimens.

The specimens loaded along the tufting direction consistently exhibited greater strength and larger failure displacements than those specimens loaded perpendicular to the tufting direction.

Specimens tufted with polyester thread have toughnesses of 11.3 kNmm, 7.2 kNmm respectively. The toughness results represent difference between longitudinal and transverse tufting, although transverse tufted specimens required more work to fail than did any of the six longitudinal tufted specimens. A typical toughness- displacement of three different preform is shown in Figure 3.12.

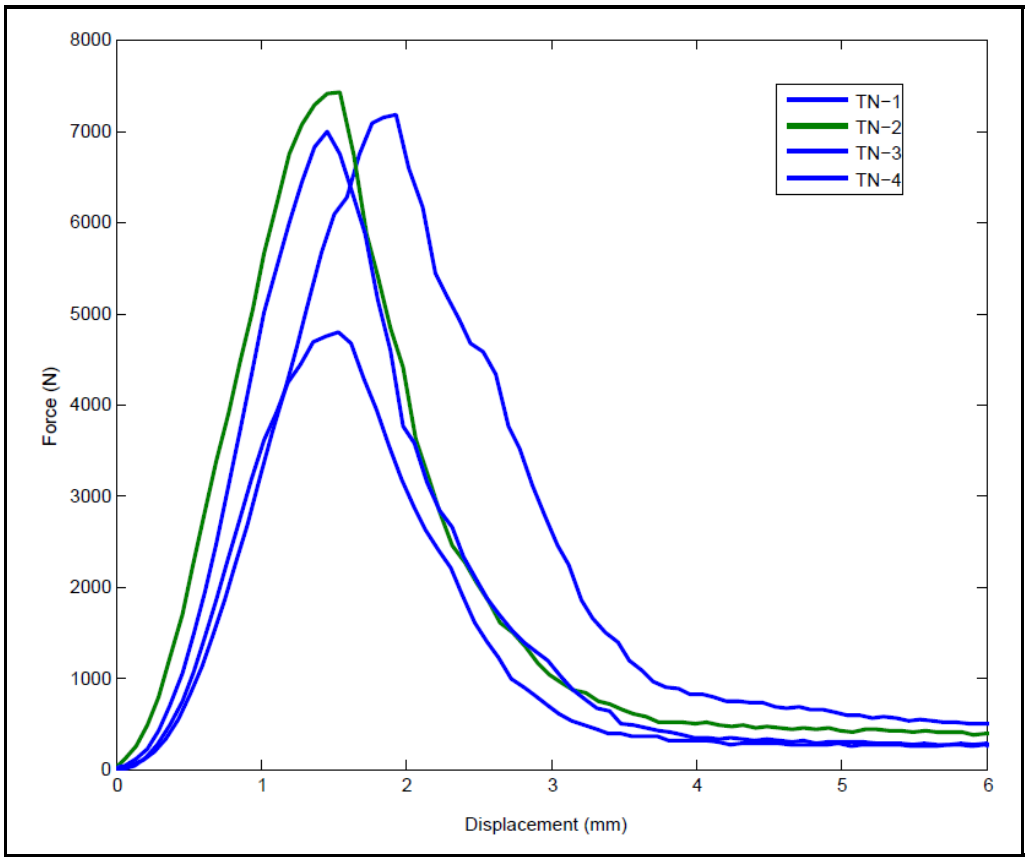

Figure 3.9. Untufted force-displacement results from four specimens loaded in uniaxial tension along the warp (0^o) direction

Table 3.3. Tension test results of untufted preform

Test	Force to failure (kN)	Failure displacement (mm)	Toughness (Nmm)
TN-1	6.99	1.45	5094
TN-2	7.16	1.93	6926
TN-3	4.79	1.53	3680
TN-4	7.42	1.54	5739
Mean	6.59	1.61	5003
Standard deviation	1.21	0.21	1984
Coefficient of variation	0.19	0.13	0.39

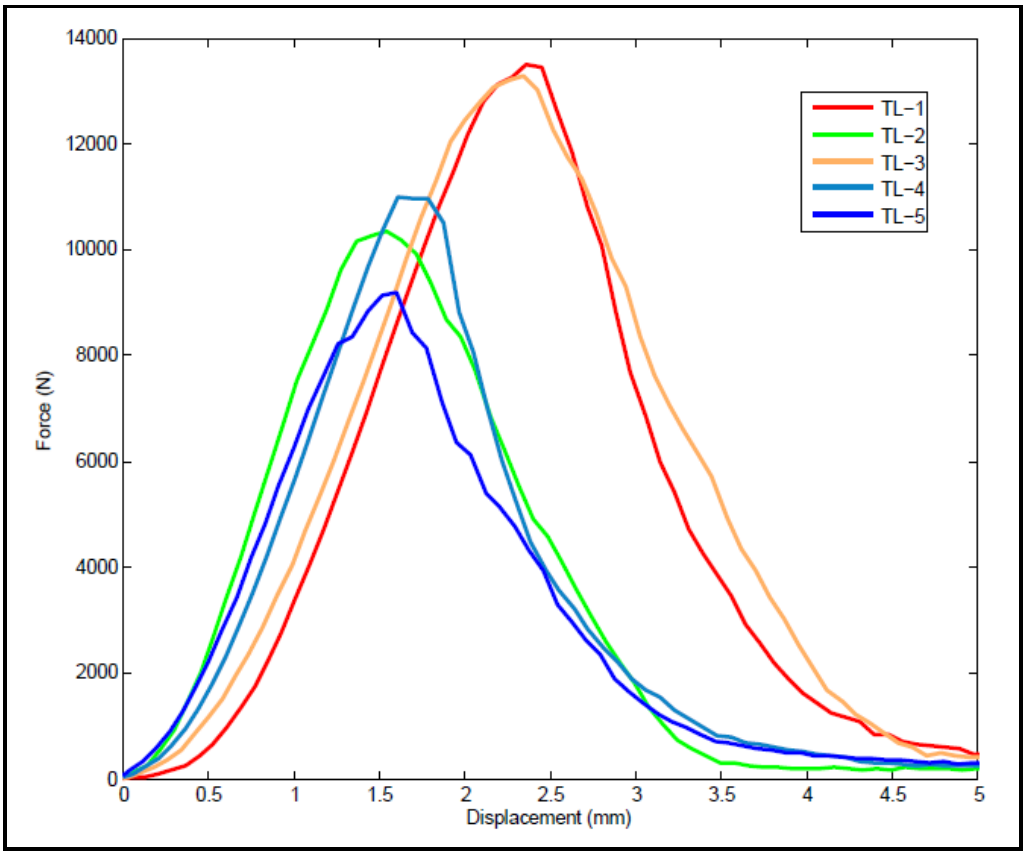

Figure 3.10. Tufted preform force-displacement results from five specimens loaded in uniaxial tension along tufting direction

Table 3.4. Tension test results of tufted preform loaded in tufting direction

Test	**Force to failure (kN)**	**Failure displacement (mm)**	**Toughness (Nmm)**
TL-1	13.50	2.36	15980
TL-2	10.35	1.54	8016
TL-3	13.28	2.34	15980
TL-4	10.99	1.60	7392
TL-5	8.80	2.09	9249
Mean	11.01	1.92	11323
Standard deviation	1.99	0.38	4303
Coefficient of variation	0.18	0.19	0.38

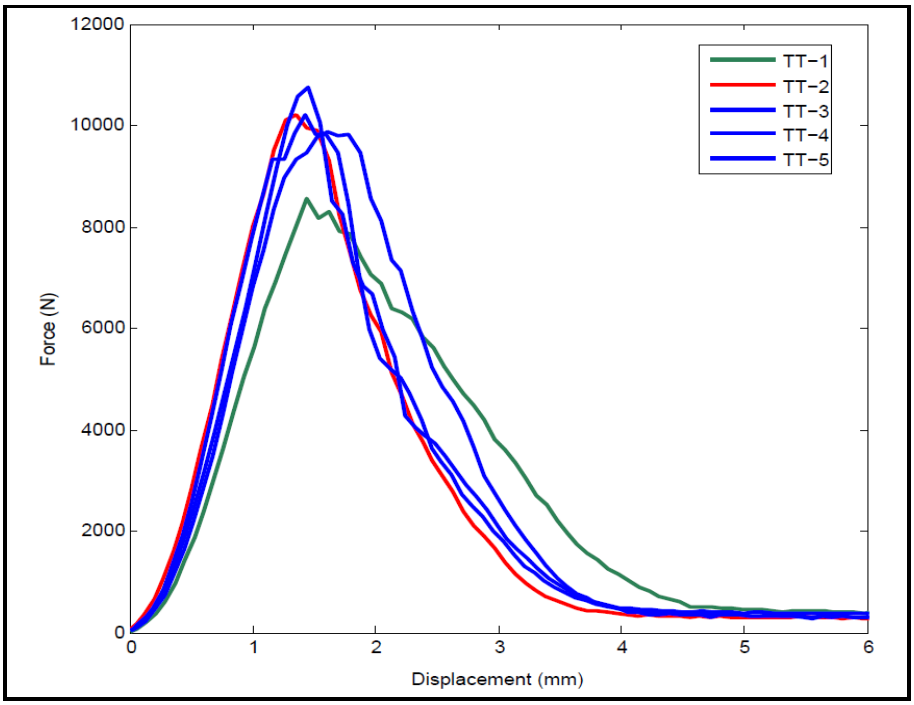

Figure 3.11. Tufted preform force-displacement results from five specimens loaded in uniaxial tension in perpendicular to tufting direction

Table 3.5. Tension3 test results of tufted preform loaded in tufting direction

Test	Force to failure (kN)	Failure Displacement (mm)	Toughness (Nmm)
TT-1	9.86	1.61	7940
TT-2	8.54	1.44	6162
TT-3	10.19	1.42	7283
TT-4	10.75	1.45	7838
TT-5	10.20	1.35	6905
Mean	9.9	1.45	7225
Standard deviation	0.8	0.09	0.1
Coefficient of variation	0.08	0.06	728

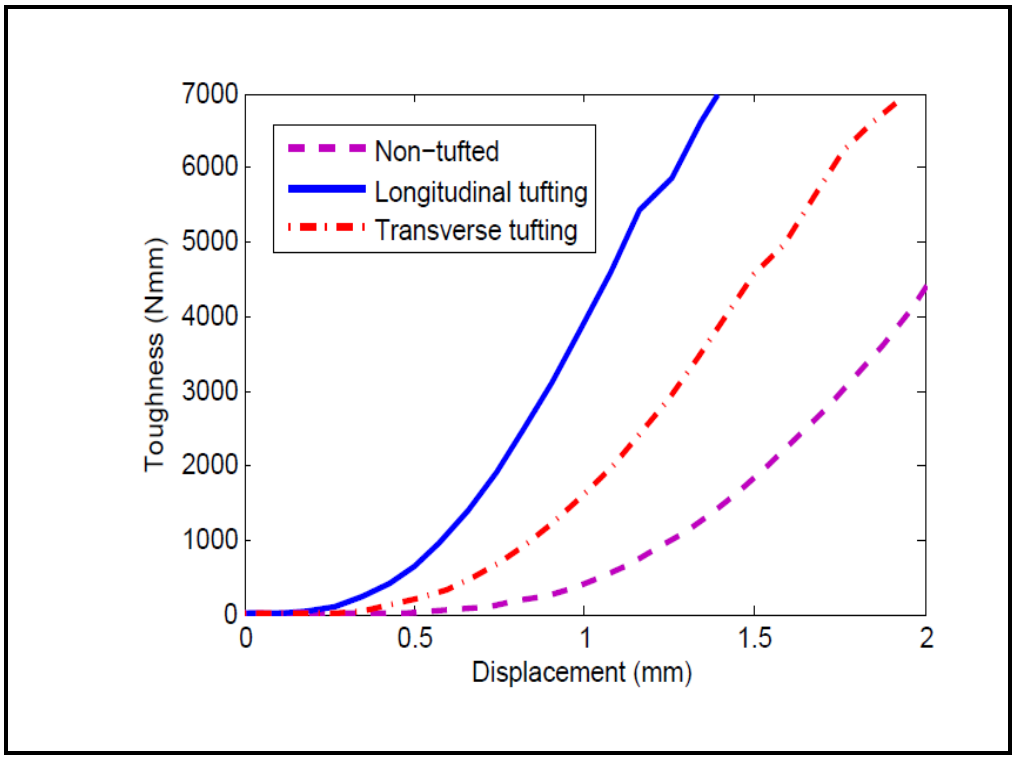

Figure 3.12. Typical toughness-displacement results from three specimens loaded in tension along the tufting direction, transverse direction and the warp direction.

Figure. 3.13 displays a typical load-displacement response of a tufted preform specimen. The behavior of the tufted fabric has four distinct regions during loading: a crimp region, a linear elastic region, a nonlinear pre-failure region, and a post-failure region.

In the crimp region, the curve displays an increase in displacement as the load increases. In this section, the load straightens the fiber bundles by removing the undulation. (In untufted preform, the loading rise was low in compare to the tufted preform, whereas in the tufted preform, the tufting threads prevented easy movement of fibers in the tufted preform, and a linear region appeared immediately). As the displacement increases, the fibers in the loading direction are highly stretched, and a linear response in behaviour of preforms appears, and the graph shows an increased slope. The loading behaviour of preforms exhibited a nonlinear region between first elastic region and ultimate strength point. The behavior in this region could be because of the failure in tufting threads and the fiber bundles. After the peak point,

the load is reduced to zero in a nonlinear behaviour as the displacement is increased. In this case, the tufted thread separates from preform and the failed threads slip away from tufted fabrics.

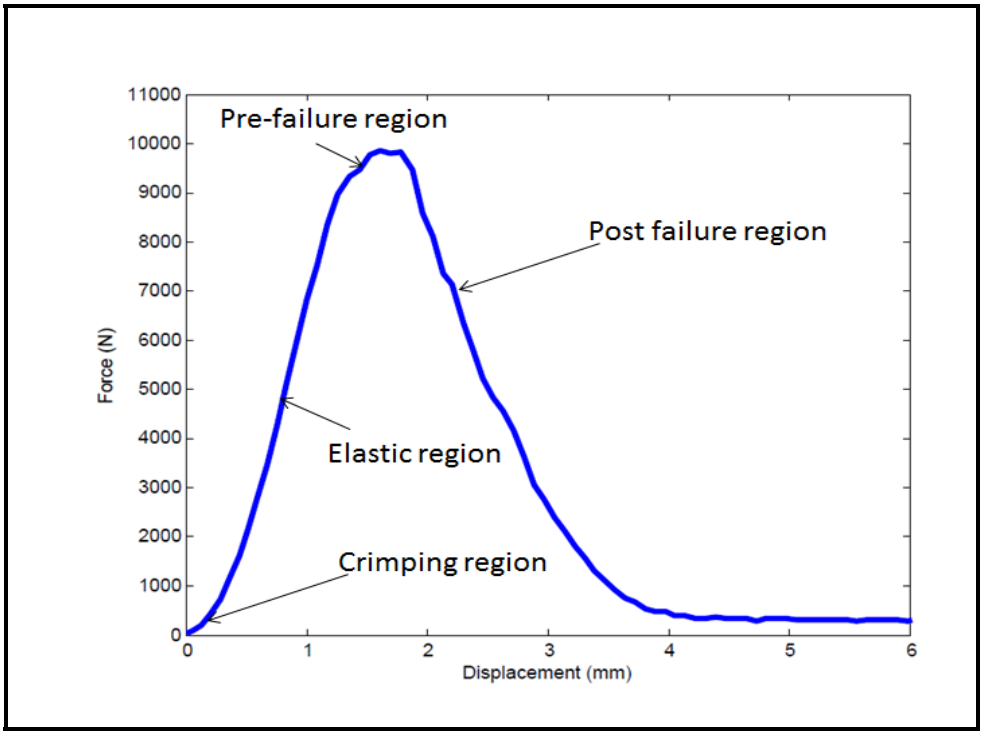

Figure 3.13. Typical force-displacement curve of tufted preform and four distinct regions

The tufted specimen obtained larger elongation values and reached the highest value of load at failure points. The research results indicate that the tufting process improved tension strength in spite of fiber breakage and fiber misalignment as shown in section 3.2. An explanation needs to be presented for this matter:

The phenomenon can be attributed to restriction of fibre movement by crossing of the tufting reinforcements and off-axis fabrics. The tufted preform is composed of eleven layers, with six oriented at ±45° and the five oriented in 0^o and 90^o directions. When tufted preforms are loaded in the tufting direction, the tow undulation is decreased in the loading direction and the tow undulation in the transverse direction increased for fabrics oriented in 0^o and 90^o

directions. However, the fabrics oriented in the 45^{o} direction, experience a shear deformation. As shown in Figure 3.14, the tufted preform (TL) displays a specific region (II) where yarns are not clamped from ends. The shearing deformation modes occur in this region.

In fact, in zone I, the warp and weft yarns are clamped at one end and low deformation is observed. In zone II located in the middle of the preform, the fibre bundles in off-axis fabrics alter until the fibre axes coincide with the directions of applied load.

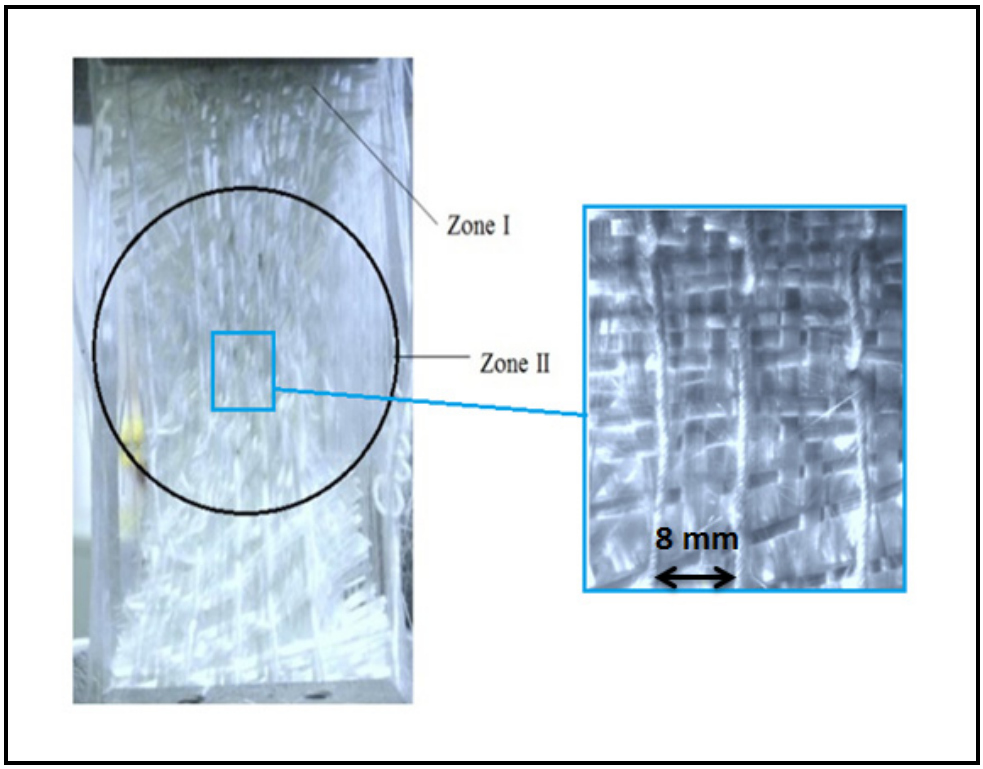

Figure 3.14. Tufted preforms loaded in tension in tufting direction

Tufting the preform assists in locking and restricting the yarn's movement in the preform. The threads used for tufting have a significant influence as stronger threads gives higher resistance. The number of tufting lines also has some influence. The higher the line, the higher is the resistance to failure. Glass yarns and fibres are normally brittle and may experience breakages due to the tufting process. These will affect the results as well.

3.3.2 Drapability

Typical load/deflection curves of drapability test when the displacement reached a level of 20 mm are shown in Figure 3.15 and the results of the tested specimens are given in Table 3.6. The variation among the test results is small, which ensures repeatability. Loading curve in Figure 3.15 indicate the force increase is not linear. The displacement of puncher increases and the slope of the load/deflection curve increases significantly. The highest values of loading at the same displacement were observed for preforms with tufting in comparison to preforms without tufting reinforcement. It should be noted that, because of limitation of the preform size, the maximum vertical displacement of the plunger along the z-axis for the plunger was set at 20 mm, but tufted preform could undergo a further displacement without breaking in the middle of preform.

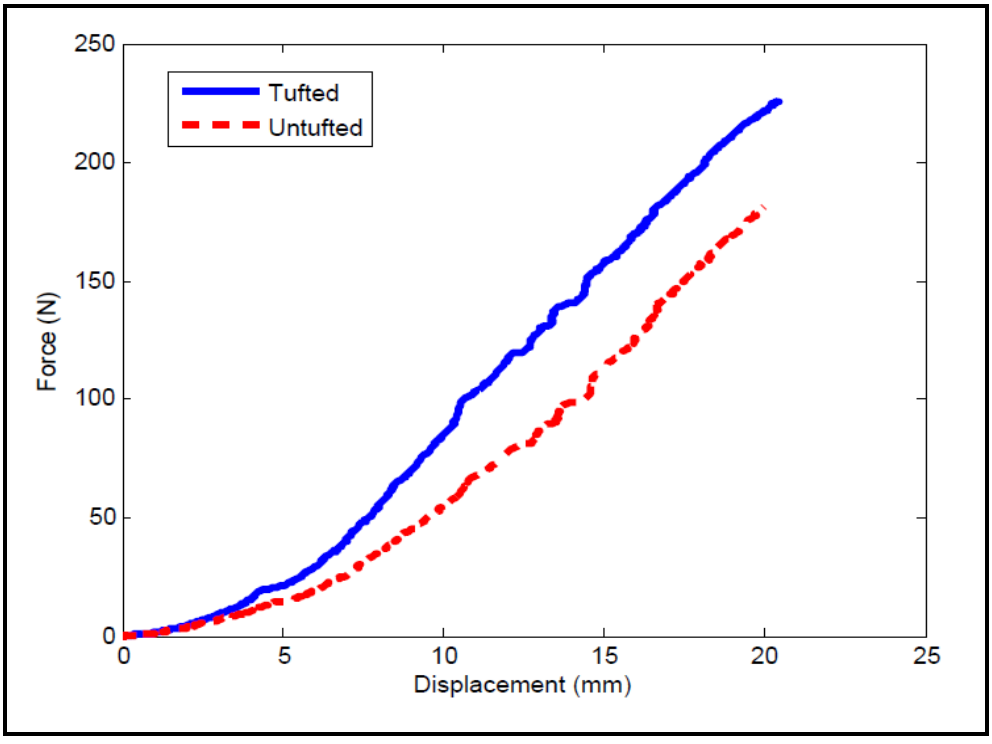

Figure 3.15. Load vs. deflection curve of tufted and untufted preforms

Table 3.6. Test results of preform drapability

Specimen	**Load (N)**		**Forming energy (Nmm)*10^3**	
	DT	DN	DT	DN
DT-1	226		2.67	
DT-2	222		2.53	
DN-1	-	181		2.28
DN-2	-	179		2.24
Mean	224	180	2.6	2.26
Standard deviation	2.82	1.41	0.09	0.02
Coefficient of variation	0.01	0.00	0.03	0.01

Effect of tufting process on the force is prominent. During a drape test, the tufted preform experiences different mode deformation including tensile, bending, transverse compression and shear. Considering these deformation modes, to define the deformability of preforms in drapability test, it is more appropriate to introduce the forming energy. Table 3.6 represents the amount of forming energy. The forming forces at 20 mm displacement of plunger for the tufted and untufted preform are 224 N and 180 N, respectively. The high forming energies were observed for the 3D tufted preform.

Tufted fabrics did not show any wrinkle onset on their surface when they were deformed except few localized misaligned fabric shown in Fig. 3.16. This is referred in-plane misalignment and rotation of the fibre during draping. The fiber misalignment damage could result a difficulty called high fiber buckling when composite sample is subjected to compressive loads.

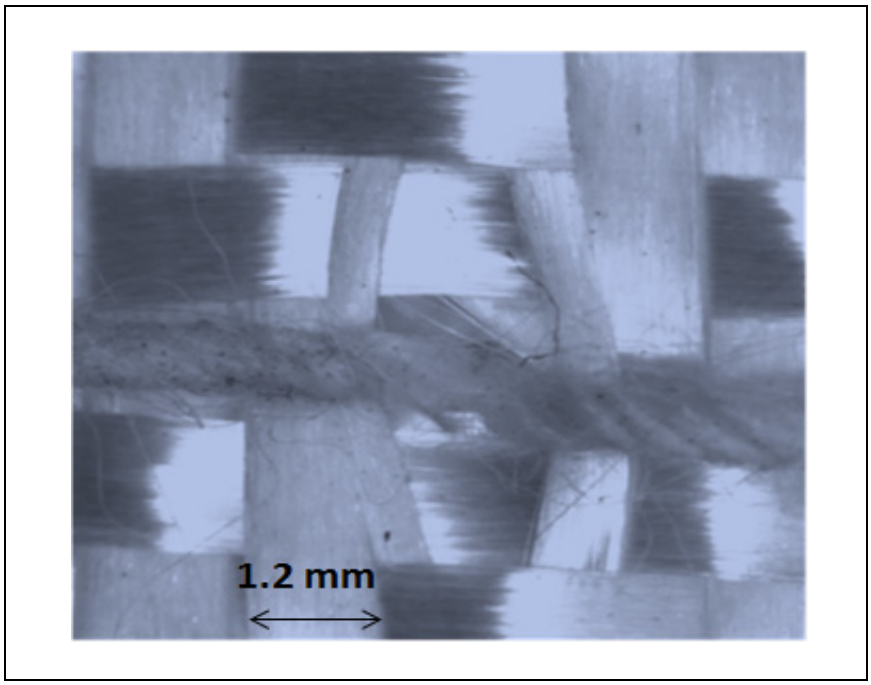

Figure 3.16. Microscopic image of localized fiber misalignment occurred in drape test

3.3.3 Compression

Figure 3.17 depicts the force-fiber volume fraction curves of tufted and un-tufted fabrics. It can be noted that samples did not follow the same loading path, however, the curves of both fabrics have same forming regions. Each curve consists of three parts: two linear parts and an exponential part. First linear part could be related to the decrease of porosity and gaps among the filaments and fiber bundles, whereas the exponential part may be related to the bending of woven fibers and tufting threads. The third linear region is where the preform has completely compressed and all the fibers cannot move further.

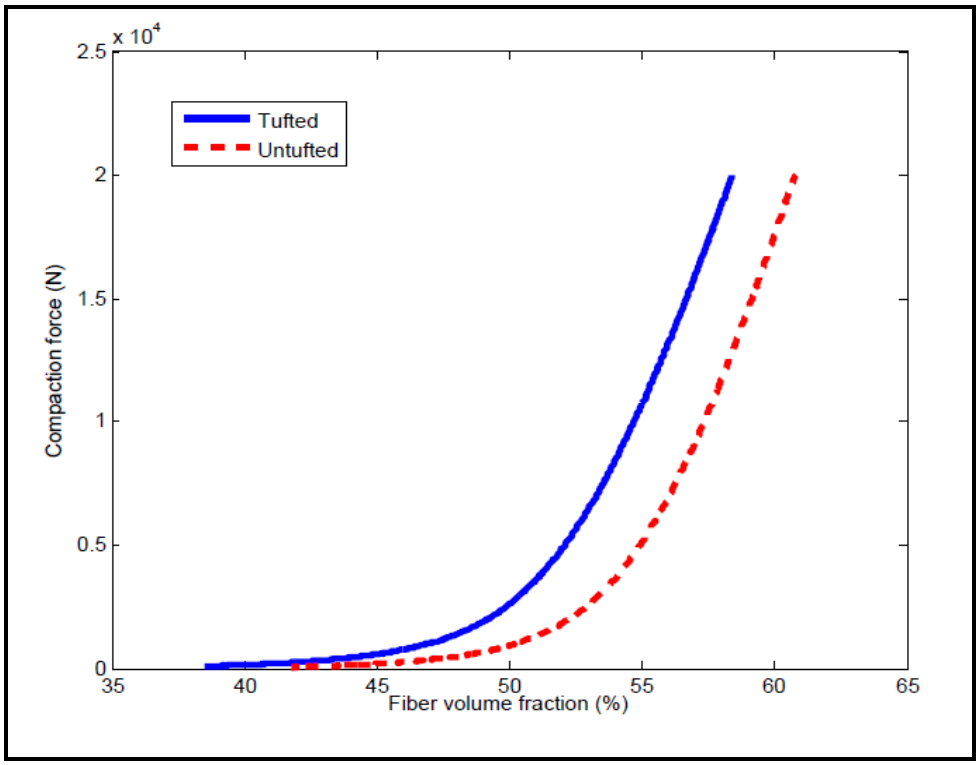

Figure 3.17. Load vs. displacement of specimens loaded in compression

Table 3.7. Test results of preform compaction

Specimen	**Displacement (mm)**		**Forming energy (Nmm)*10^3**	
	CT	CN	CT	CN
CT-1	1.81		8.18	
CT-2	2.01		8.14	
CN-1		1.72		7.6
CN-2		1.76		7.5
Mean	1.9	1.74	8.16	7.55
Standard deviation	0.14	.02	.02	0.07
Coefficient of variation	0.07	0.01	.003	0.00

Compression load applied to preforms results an increase in fibre volume fractions by tow flattening and decrease in tow crimp as shown in Figure 3.18 while all preforms are compressed by one type of plunger.

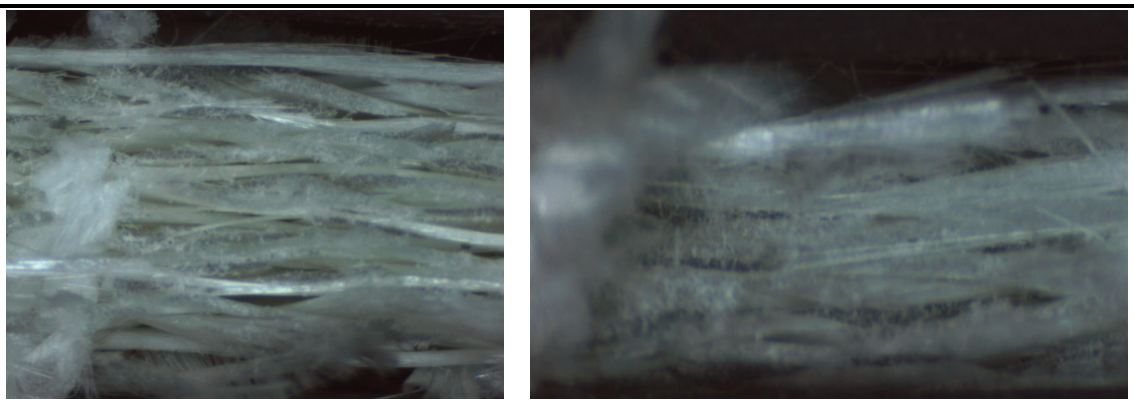

Figure 3.18. Cross-section of uncompacted and compacted tufted preform

The untufted preform is composed of eleven textile fabrics with a woven structure, and thus the nesting (shown in Figure 3.19) plays significant role on the compaction behavior. Nesting implies when the textile fabrics is compacted and fiber bundles from one layer penetrate into the adjacent fabric layers. The influence of nesting can be noted in Figure 3.17 for vf = 0.52, which shows that the compression loading increased much more quickly with an increase in fibre volume fraction.

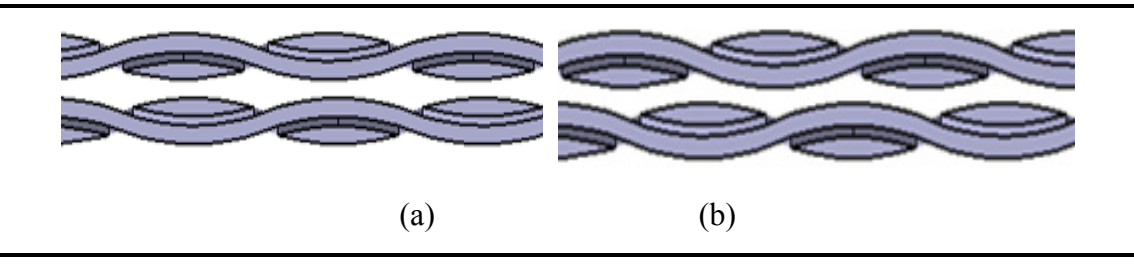

Figure 3.19. Woven fabric stacking (a) bundle to bundle (b) bundle to gap

Tufted preforms need greater force to be compressed than the untufted preforms, since the tufting threads placed in the textile fabrics result the fixation of fibers and restrict the fabric movements. As shown in Figure 3.20, tuft reinforcements in through-thickness directions caused less movement of the fibers and locking of fibers. For tufted preforms, to obtain a

fiber volume of 55%, a 15KN compaction force is needed, whereas the untufted preforms require low compaction loads to obtain this amount of fiber volume.

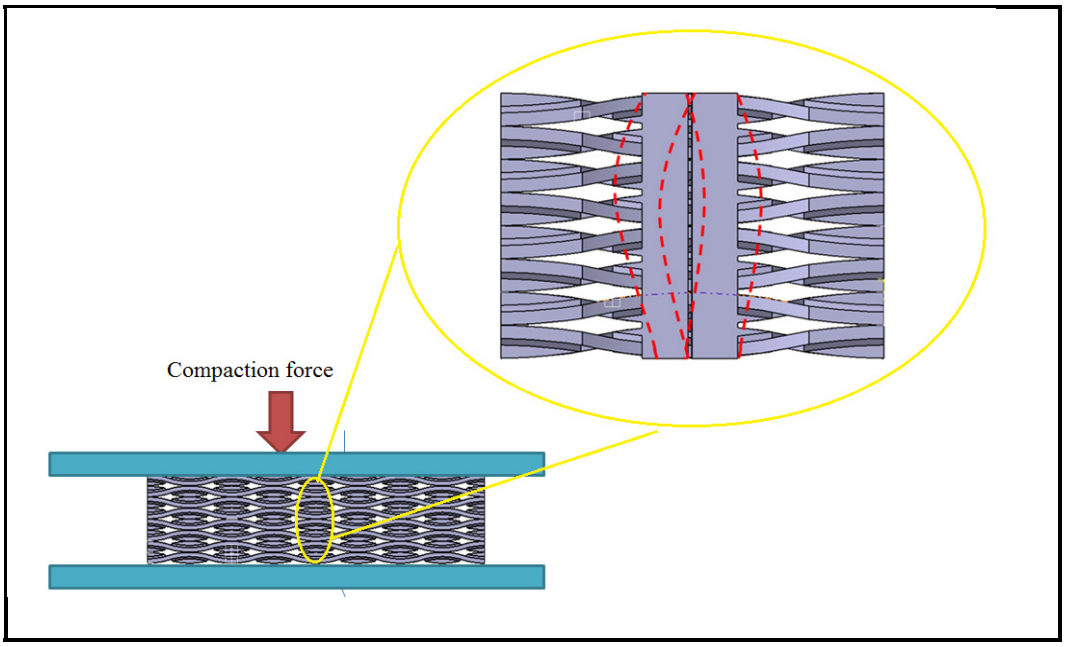

Figure 3.20. Deformation of tufting thread during compaction loading

3.4 Conclusion

Experimental characterizations including in-plane tensile tests, transverse compression tests and drapability tests of tufted preforms have been conducted. The force-displacement curves were analyzed to measure the tensile strength, maximum displacement, and toughness for all the specimens. Based on the research results, the following conclusions may be made:

- The analysis of tufting effect upon fabrics deformation behaviour has shown that preforms with tufting are stronger than untufted specimens. The preform load-extension curves reveal that, generally, a loading curve can be divided to four specific regions.
- Draping involved the drawing of a fabric over a hole placed in a drape fixture without wrinkling. Due to high drapability and stability observed for the tufted specimen, tufted

preforms can be considered as appropriate textile reinforcement for production of complex shape specimens.

- The compaction behaviour of the tufted preform was influenced by the tufting thread. The required load to achieve a specific fiber volume fraction was identified.

Microscopic evaluation of tufted preforms provided valuable information about the behavior of preforms during the forming process. Microscopic examinations at different magnifications were utilized to investigate the intrinsic damage in preforms and tufted composites before and after loading.

CHAPTER 4

MECHANICAL PERFORMANCE OF 3D TUFTED COMPOSITES

4.1 Introduction

This chapter evaluates the tufted composites from the aspect of the influence of tufting on the tensile, compression and fatigue behavior. Special attention is given to the influence of tufting related manufacturing damage; damage initiation and its propagation on samples. Furthermore, an investigation is conducted to recognize the influence of the open hole on the mechanical performance of tufted composites. Degradation under fatigue loading resulting from damage occurring during tufting is discussed. The S–N curve, stiffness degradation and variation of in-plane displacement occurring in the loading direction are investigated. Damage progression of the tufted composite subjected to fatigue loading is characterized.
Sandwich structures have been used widely in aerospace industry due to their lightweight and specific mechanical properties. A part of our research in this chapter is concentrated to fabricate thick sandwich panels and their characterization. The sandwich samples are consisted of tufted composite skins and aluminum honeycomb core. The main objective is to analyze the mechanical behaviour of these sandwich materials under Quasi-static local compression, and bending loadings and the evaluation of their damage progression.

4.2 Materials and experimental equipment

4.2.1 Composite panels manufacturing

Preparation of 3D tufted preforms

The three preforms were composed of eleven layers of twill woven glass fabrics with a lay-up of [0/45/90/45/90/45/90/45/90/45/0]. Each preform has a total thickness of 4.5 mm. The 3k twill 2X2 woven fabrics have the areal weight of 305 g/m^2. The size of each preform was 500 mm x 500 mm. The two preform was tufted in square pattern with a twisted 240 Tex

polyester thread using a KUKA 6-axis robot equipped with a commercial tufting head at CTT group, Canada. The tufting row was oriented at 0° direction with a tufting spacing of 8 mm and pitch of 8 mm. These preforms were as same as the preforms discussed in previous chapter. The third preform was the untufted woven preform which was the base materials for tufted preforms were mentioned above.

Fabrication of composite panels

The tufted and untufted preforms were impregnated with polyester resin using the vacuum process at Composites BHS Inc. in Sherbrooke, Qc, Canada. The tufted preform was placed into a flat mold. The polyester resin was used for the preform impregnation. The resin was injected into the mould using vacuum as shown in Figure 4.1. After demoulding, the composite plate was cured at room temperature. The tufted composite panels were 3.5 mm thick. The fiber volume fraction of the tufted composite was approximately 60%. This quantity was determined from three samples using the weight measurements. Table 4.1 lists the raw materials used to manufacture the specimens for this study.

Table 4.1. List of composite panels.

Panel / **Constituents**	**K (tufted)**	**M (tufted)**	**N (untufted)**
Matrix	Polyester resin TRL1520L-4195	Polyester resin TRL1520L-4195	Polyester resin TRL1520L-4195
Fabric pattern	2x2 Twill weave	2x2 Twill weave	2x2 Twill weave
Tufting thread	240 Tex polyester	240 Tex polyester	-

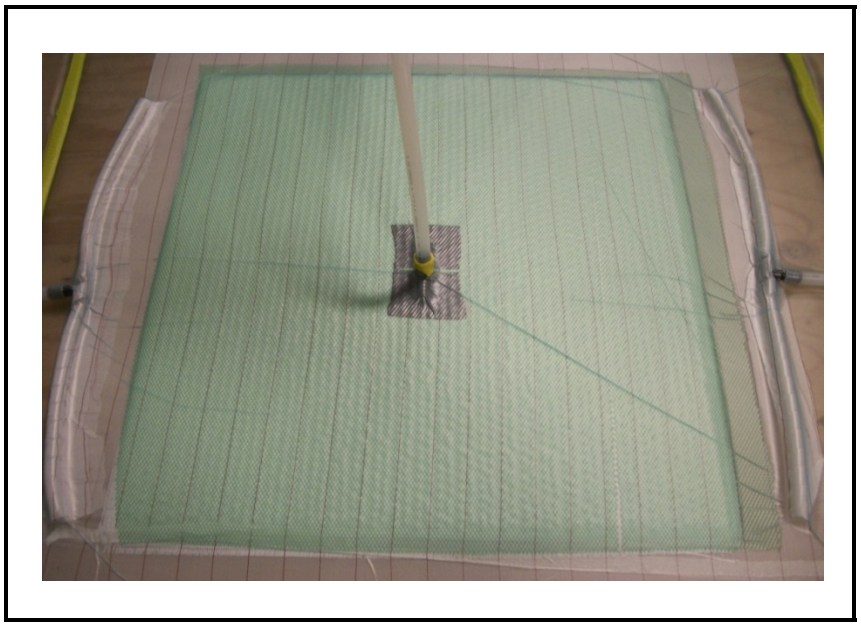

Figure 4.1. Resin impregnation of tufted preform

To fabricate sandwich composite, an aluminum honeycomb core shown in Figure 4.2 with 5 mm cell size (h), 20 mm thickness (t) and 50 kg/m^3 density was placed between two flat composite and all were bonded together with methacrylate glue.

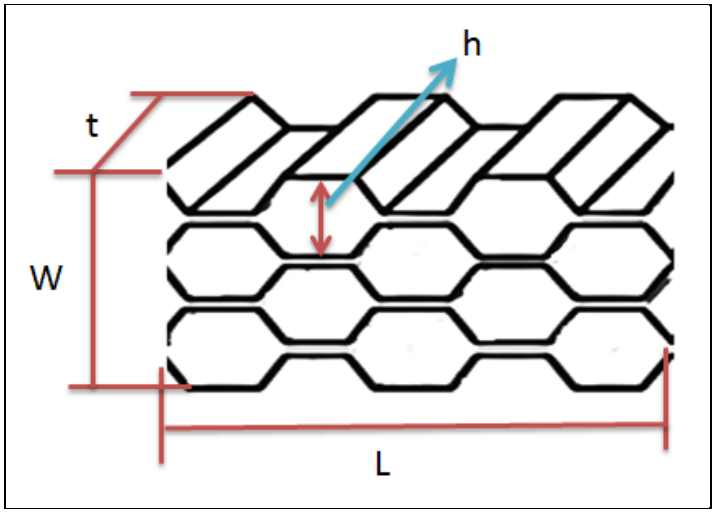

Figure 4.2. Honeycomb core size parameters

4.2.2 Quality control

Several techniques were used to inspect the fiber preforms before the rein infusion process to ensure consistent and acceptable quality. These techniques included visual inspection of the preforms before injection and composite panel inspections.

Preform inspection

At first, preforms were inspected visually to detect any discontinuity to tufting threads and fabric surface defects.

The tufting process results in considerable variability in the preform geometry in such a way that the micro and meso-structure of a tufted preform differ much from that of the untufted preform. The preform geometry has high influence on the fiber-volume-fraction and the compression behaviour of the preform, therefore, the preform geometry was inspected to determine the average thickness and respective fiber volume.

A possible technique to investigate the preform geometry is a CMM scanning equipped with a laser scanner. In the current research, a laser scanning approach was considered only for a stitched preform geometry measurement, but technique can be applied to other types of stitching techniques. The laser scanner was installed on the CMM machine equipped with a motorized head and five degrees of freedom and was calibrated. Fig. 4.3 shows a 3D laser sensor calibration using a ball artifact. A preform was placed on the machine and the point acquisition was done with the scanning resolution of 0.5 mm and 8420 points per scan.

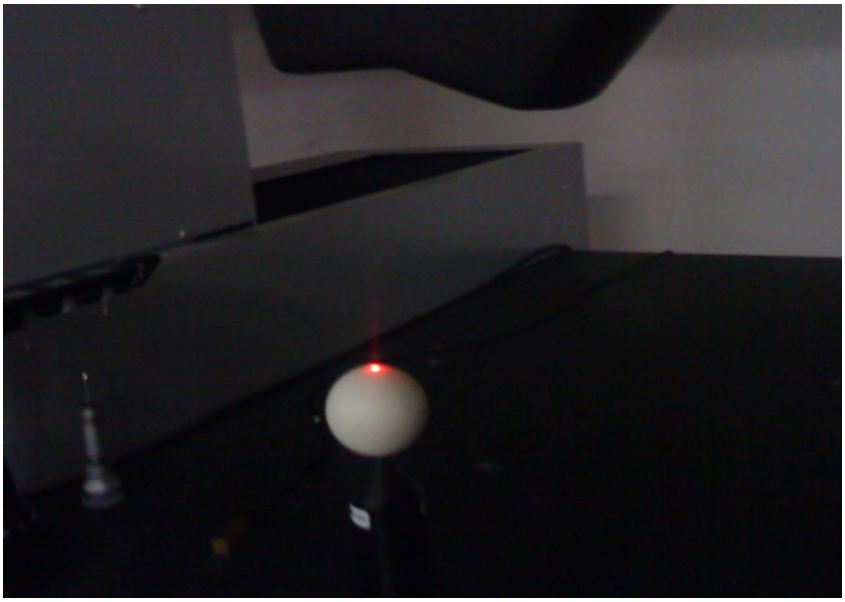

Figure 4.3. Calibration of the laser scanner for the preform scanning

Point clouds extracted from CMM were imported into Polyworks software to create a surface in IGES format shown in Figure 4.4. Next, the IGES file was imported into the Catia software to calculate the dimensional deviation. Based on CMM results, the thickness variation values were around 0.8 mm.

In this research we realized that the surface properties such as color and shininess had significant influences on the laser line scanning results. Therefore optimized scanning parameters were considered to get reliable results.

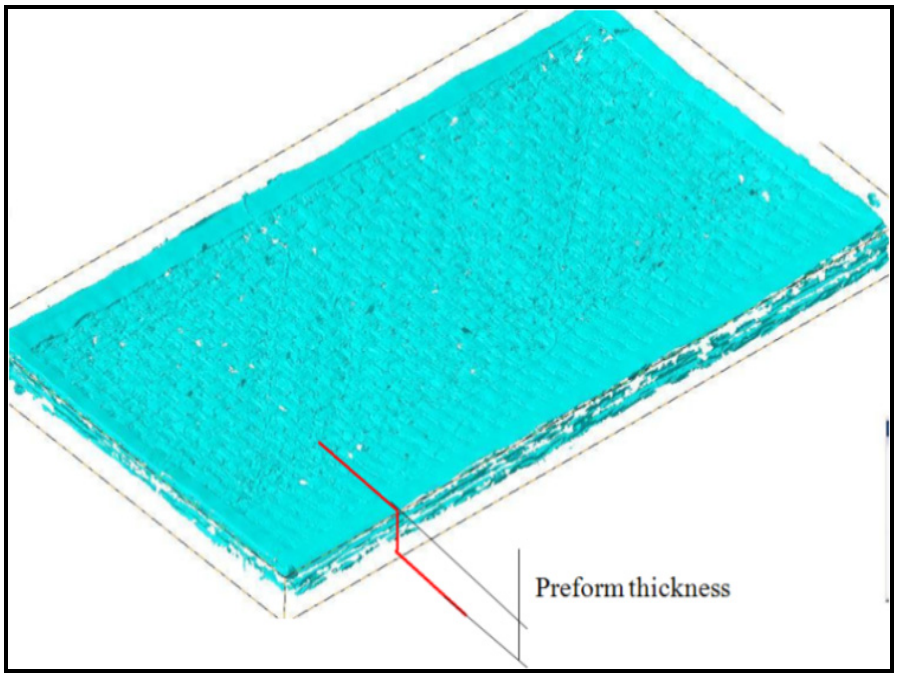

Figure 4.4. Integrated surface constructed from points cloud

Composite inspection

Each composite panel was inspected after resin injection using microscopy and X-ray computed tomography techniques to ensure full resin impregnation. Sectioning showed that the woven fabrics and tufting reinforcements were impregnated perfectly. Fig. 4.5 and 4.6 show the cross sections of the sample cut along a tufting thread.

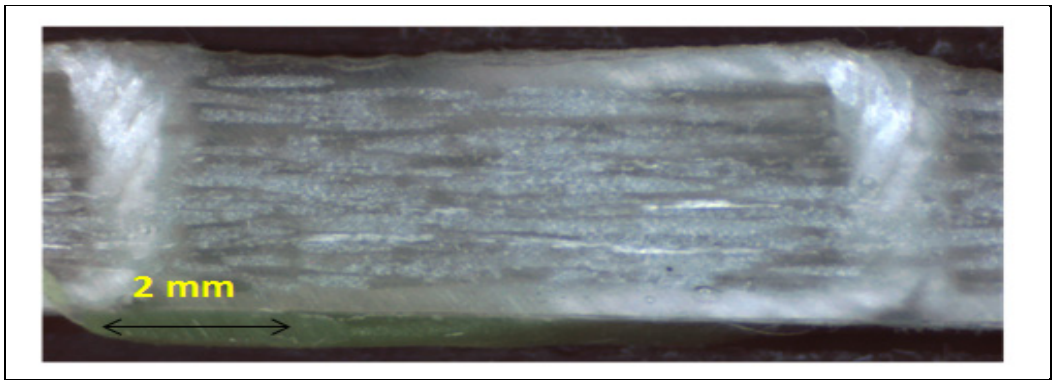

Figure 4.5. Optical microscopic image of the tufted composite

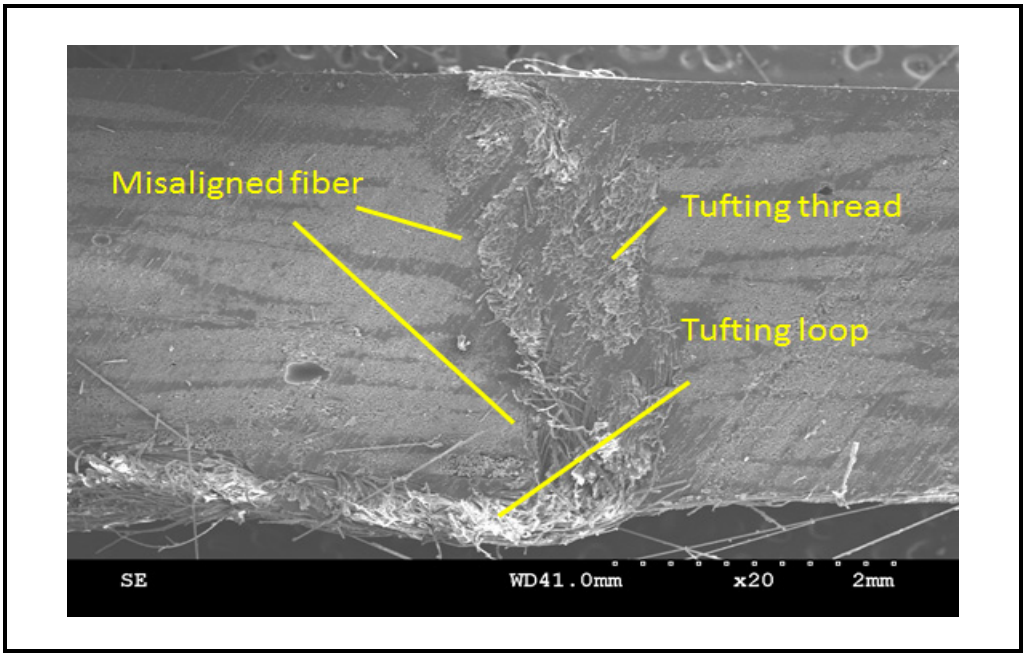

Figure 4.6. SEM micrograph of the tufted sample cut through a tufting site

In addition, X-ray computed tomography was employed to check the resin impregnation and the extent of void content. This technique produced clear images of interior regions of the composite samples. Figure 4.7 display example 3D X-ray images. By sectioning 3D image, its cross-sections shown in Fig. 4.8 were obtained. The change in the density through the section (grayscale images) allowed observing a clear view of the void size and locations

inside impregnated preforms. In this figure, the preform appears grey and matrix appears dark and porosity appears with white circular shapes.

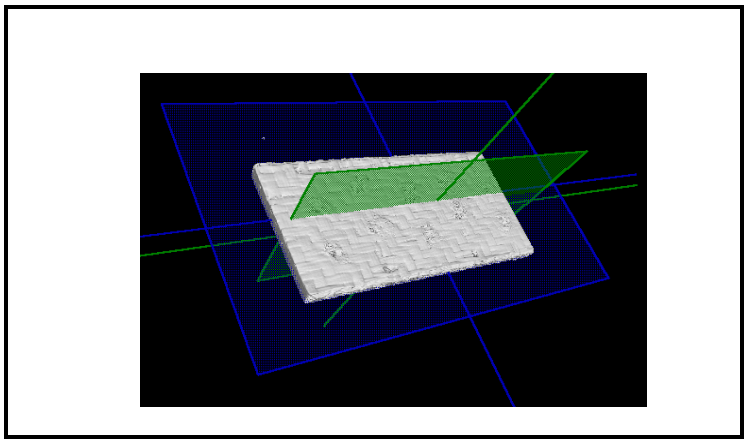

Figure 4.7. Three-dimensional volumetric model of tufted composite sample with dimensions of 25 mm x 20 mm (Note: the tufting threads are rendered invisible)

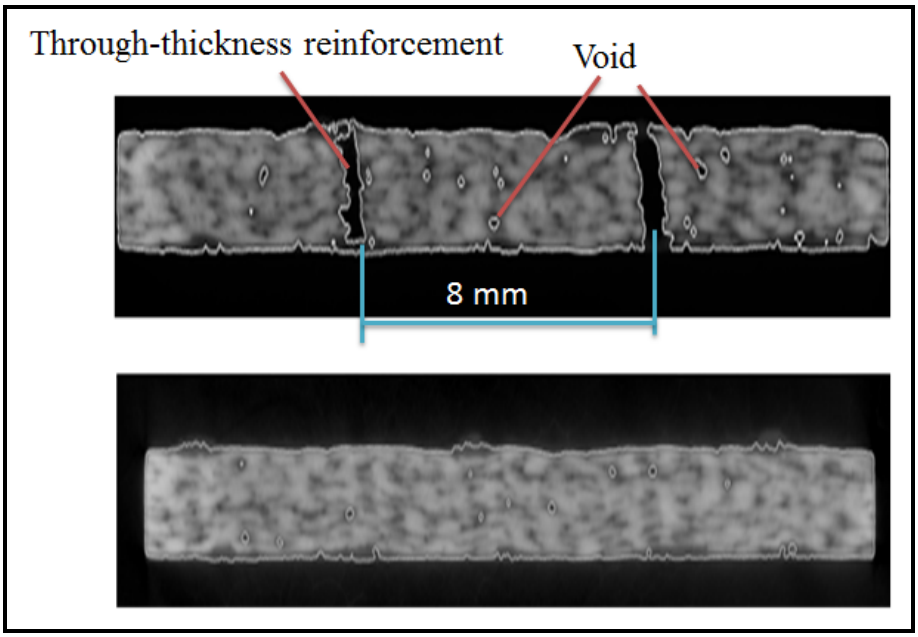

Figure 4.8. Cross-sectional X-ray images of tufted sample with dimension of 20 mm x 25 mm

The microstructure of twill fabric and tufting thread locations was clearly appeared in top images of sample as shown in Figure 4.9. In this figure the threads cannot be observed because those may contain low density areas. The porosity appearing in this image had nearly spherical and ellipse shapes. The spherical voids had a diameter of around 0.25 -.0.3 mm.

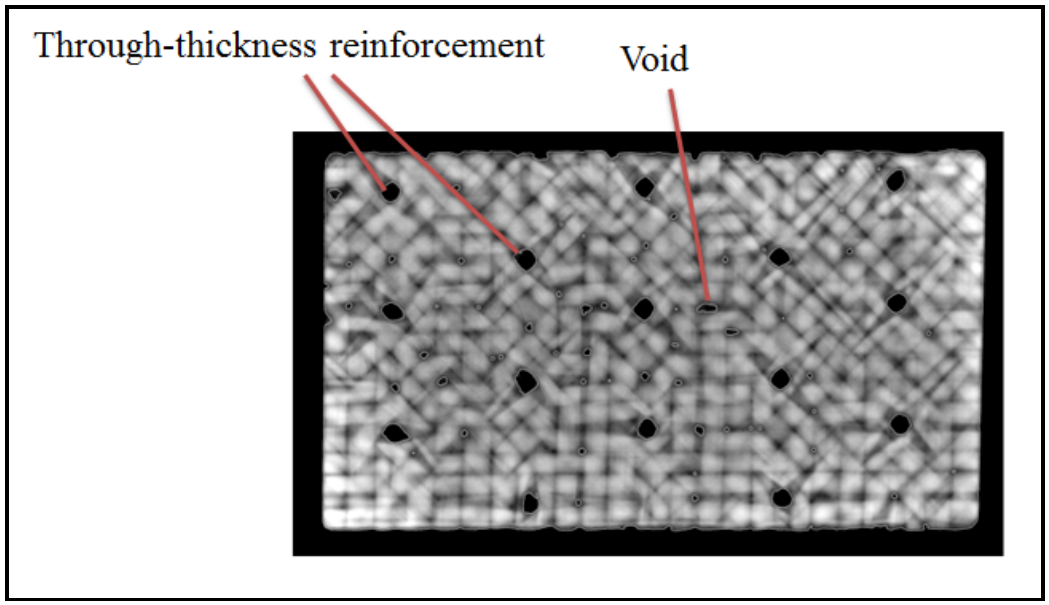

Figure 4.9. Planar X-ray image of tufted composite with dimensions of 25 mm x 20 mm

The cross-sectional computed tomography image displayed that the tufting process lead the displacing of the fiber bundles from their original alignment. Fiber misalignment around $\pm 20^{o}$ in the tufting region could be seen in Figure 4.10. This fiber distortion could highly influence the mechanical performance such that it causes micro buckling during compressive loading and act a potential region for the damage initiation during fatigue test.

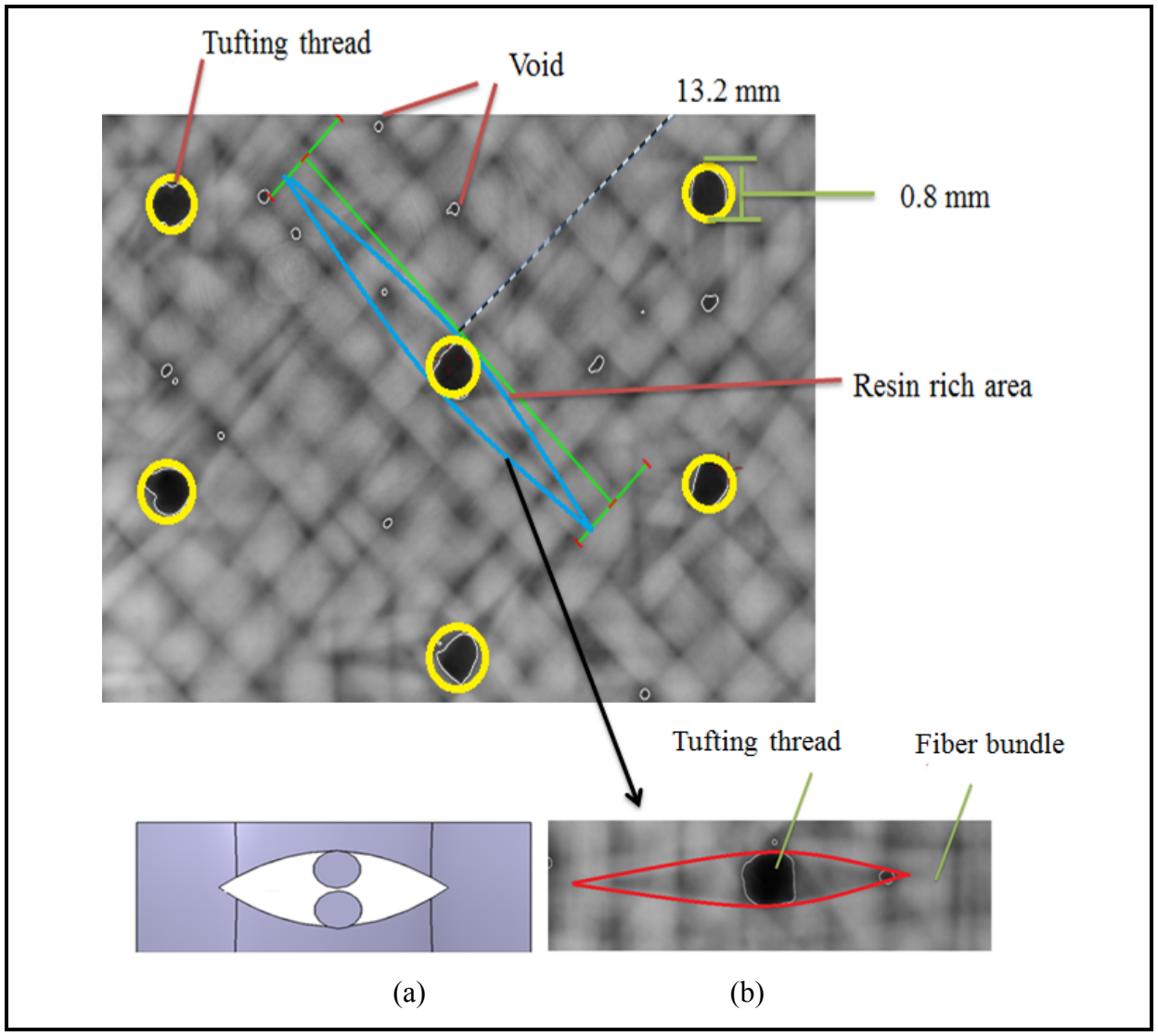

Figure 4.10. Fiber distortion due to tufting (a) Schematic image (b) X-ray image

4.2.3 Specimens and test procedures

Descriptions of the specimens and the test procedures are contained in this section. Table 4.2 provides a matrix of tests performed in this study. As the table indicates, both static tension, compression and tension-tension fatigue tests were conducted. Specimens were loaded along the tufting direction (0°) and perpendicular to the tufting direction (90°). In addition, a variety of destructive and non-destructive evaluations were made to monitor damage initiation and development (see chapter five).

Table 4.2. List of tests and composite specimens

Test type		**Tufting orientation**	**Number of tufting line**	**Number of test**	**Symbol**
Static tension	Static	0^o	3	3	KL
		90^o	30	3	KT
		0^o-open hole	3	2	KLH
		No tufting		3	NT
	High strain	0^o	3	1	KL
		90^o	30	1	KT
		0^o-open hole		1	KLH
		No tufting		1	NT
Static compression		0^o	4	3	MC
		No tufting	-	3	NC
Tension-tension fatigue		0^o	3	13	MFL
		Non tufted	-	2	NF
Residual strength		0^o	3	1	KRL
		90^o	30	1	KRT
		0^o-open hole	3	1	KRLH
		No tufting	-	1	NR
Honeycomb compression		0^o		2	HC
Honeycomb bending		0^o		2	HB

Tufted composite

Static tensile test

Tensile test of composite specimens in accordance with ASTM D3939 was performed by an MTS machine with a 100 kN load cell. The tensile tests were performed on nine specimens (see table 4.2) cut in perpendicular and parallel of tufting direction as shown in Figure 4.11. Size of each sample for the tensile test was 25 mm × 250 mm, and the test speed was 2 mm/min for all samples.

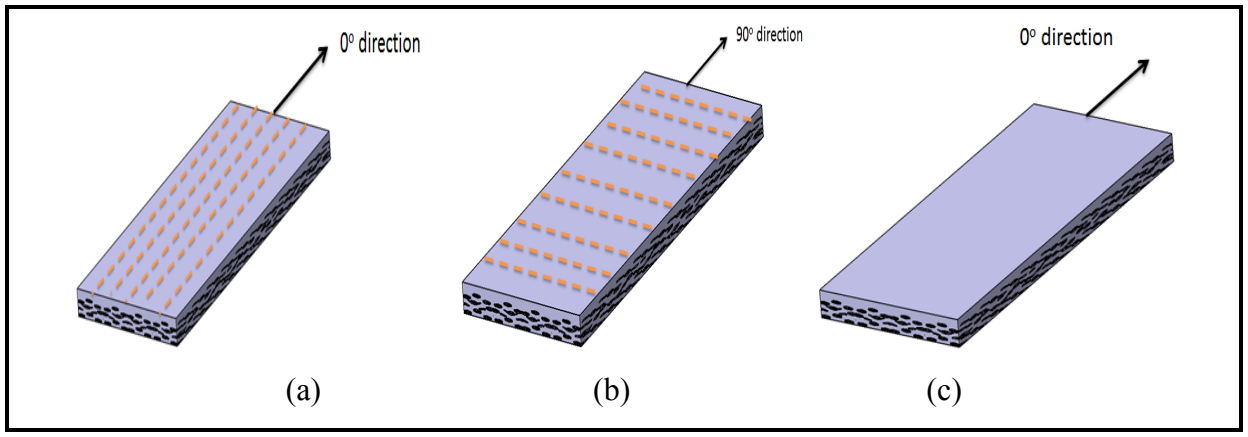

Figure 4.11. Schematic of tension samples and their loading directions
(a) Longitudinal tufted (b) Transverse tufted (c) Untufted

Furthermore, static tension test was conducted on two open hole tufted composites and one open hole untufted sample to determine the strength reduction of strength due to 6mm hole at the center of the coupon. Furthermore, an insight in the mechanical properties of composite samples at high strain rate was done to study effect of strain rate to those samples at low velocity tensile testing.

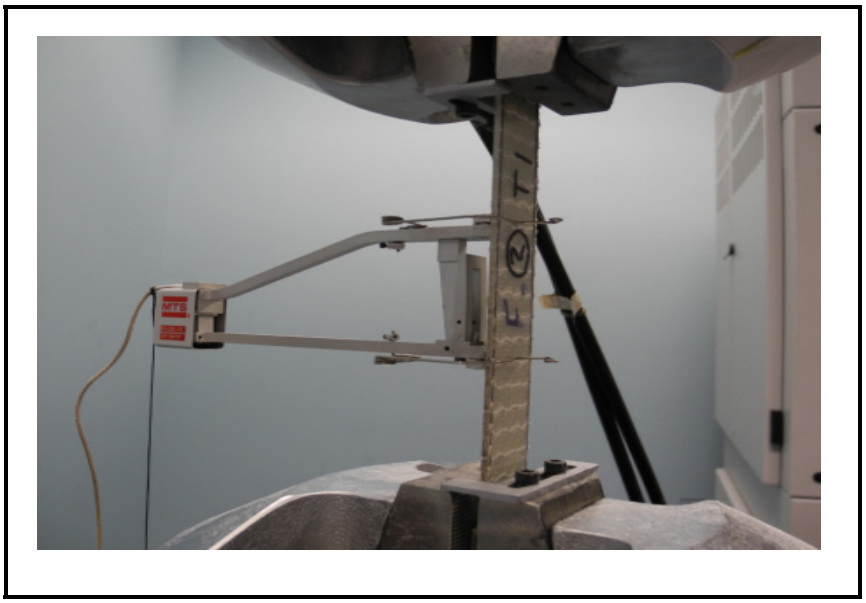

Figure 4.12. Tension test specimen and extensometer for fatigue test.

The testing machine for the tension- tension fatigue tests were similar to those used for static tensile test. The fatigue testing was performed according to ASTM D-3497 under the sinusoidal fatigue loading with the stress ratio R of 0.1, and the frequency of 5 Hz.

Compression test

Compression tests were carried out to determine the composite strength in accordance with ASTM D3410. Tabbed samples used in the compression tests measured in 40 mm wide and 100 mm long (see Figure 4.13). When sample mounted in the testing machine the length of unsupported section was 38mm. The sample was not supported along its length to prevent buckling. Furthermore, no strain gage was used to monitor any bending occurring in the compression test. Compression tests were conducted on MTS machine at a crosshead speed of 1 mm/min.

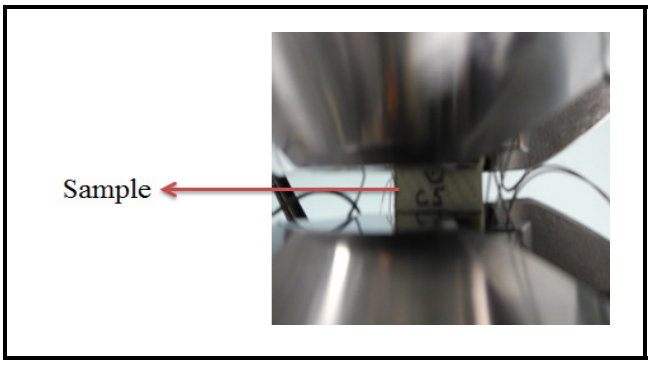

Figure 4.13. Compression testing setup

Honeycomb test

Local compression

The sample geometry for local compression was 100 mm x 100 mm. In order to simulate low velocity impact and observe damage, quasi-static compression using spherical plunger in diameter of 32 mm was conducted to the center of sample at a the speed of 0.5 mm/min, and then the response and behaviour of sample was carefully investigated (Hexcel Composites

Ltd., 2000). Figure 4.14 displays experimental setup for testing sandwich composite specimens under compression loading.

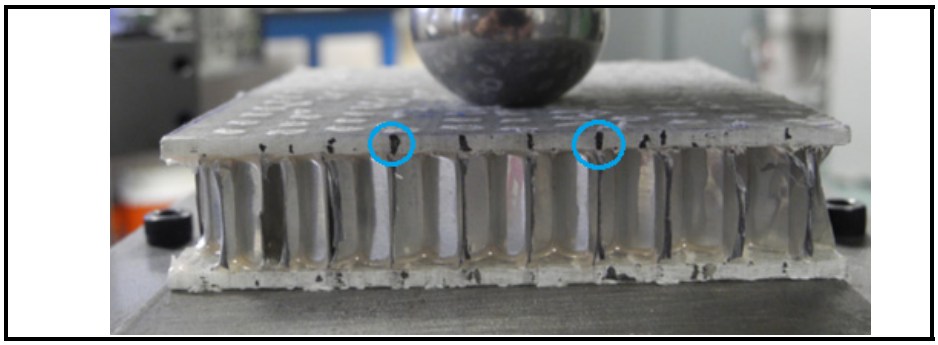

Figure 4.14. Experimental setup of quasi-static local compression test
(note: the circled regions are not void, but appeared by diamond saw in cutting process)

Bending test

Three point bending test was conducted to investigate the influence of through-thickness tufting reinforcements on the flexural strength. This test was carried out in accordance with ASTM standard C393. The specimen sizes were 200 mm x 20 mm x 25 mm. The length of loading span length was 125 mm. The sample was bent at a speed of 2 mm/min. Figure 4.15 shows the experimental test setup for bending test.

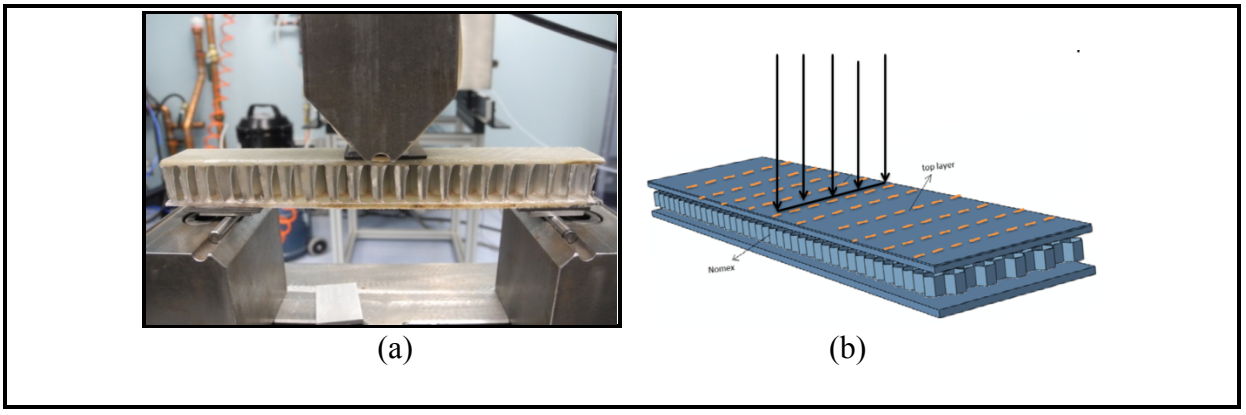

(a) (b)

Figure 4.15. Experiment setup of bending testing
for honeycomb composites (a) Untufted (b) Tufted

4.3 Results and discussion

4.3.1 Tufted composite

Static test

Composite tensile coupons were tested to failure. Typical stress–strain curves of tufted composites with longitudinal (tufting direction is parallel to tensile loading direction) and transverse tufting are shown in Fig. 4.16. Results of the static tension tests are summarized in Tables 4.3 & 4.4. It should be noted that to remove the effects of varying fiber volume from the experimental data, the nominal thickness was used to calculate the specimen stress.

Tensile strengths were measured using specimens cut from Panel K. The average static tension strengths of the 0^o (KL1-KL3) and 90° (KT1-KT3) tufted samples were 278 and 276 MPa, respectively.

The stress-strain response of all samples was nearly linear to failure and did not have distinct yield points. All tufted composites exhibited formation of transverse cracks in matrices and interfaces of fabrics, in particular around tufting region.

It appeared that composite samples with transverse tufting had lower strengths than longitudinal tufted samples. However, the difference between them was around 1%. As a whole, neither the ultimate strain nor the strength differed considerably for the longitudinal and transverse tufting.

Results of the static tension tests for untufted samples are summarized in Tables 4.5. According to Fig. 4.16, it is evident that untufted composite specimens exhibit nearly linear curves up to failure, which is what is observed for tufted composites. Tensile strengths were measured using specimens cut from Panel K. Although the data are limited, they indicate that the tufting had little effect on the tension response.

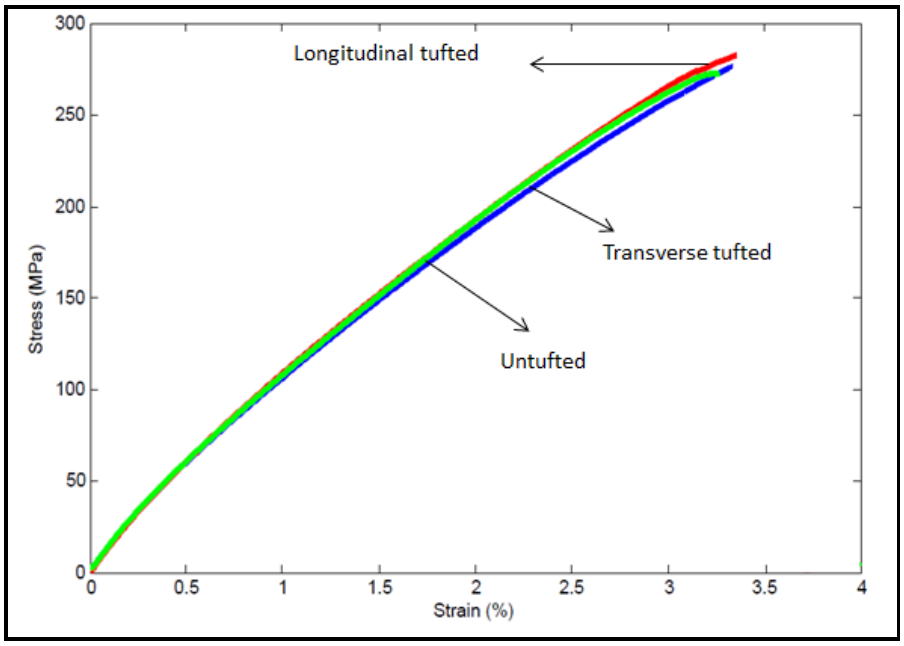

Figure 4.16. Stress-strain curves of tufted and untufted specimens under tensile loading

Table 4.3. Quasi-static tension test results of longitudinal tufted specimens

Specimen	**4) Stitch orientation**	**5) Strength (MPa)**	**6) Ultimate strain (%)**
7) KL-1	0^o	275.4	3.33
KL-2	0^o	290.2	3.45
KL-3	0^o	267.4	3.25
	Mean	277.7	3.34
	Standard deviation	11.7	0.1
	Coefficient of variation	0.04	0.03

Table 4.4. Quasi-static tension test results of transverse tufted specimens

Specimen	Stitch orientation	Strength (MPa)	Ultimate strain (%)
KT-1	90^o	254.8,	2.85
KT-2	90^o	282.3	3.35
KT-3	90^o	290.7	3.21
	Mean	275.9	3.14
	Standard deviation	18.7	0.25
	Coefficient of variation	0.06	0.08

Table 4.5. Quasi-static tension test results of untufted specimens

Specimen	8) Stitch orientation	9) Strength (MPa)	10) Ultimate strain (%)
11) NT-1	0^o	273.1	3.24
NT-2	0^o	277.7	3.15
NT-3	0^o	262.2	2.96
	Mean	271.04	3.12
	Standard deviation	7.9	0.13
	Coefficient of variation	0.02	.04

Open hole tension

Figure 4.17 depicts the quasi-static tension tests results related to tufted specimens with open hole. During tensile testing, the stress strain graph of open hole samples was approximately linear and samples was ruptured from hole region due to high stress concentration on this area. In comparison, the failure strength of open-hole untufted composite was below the strength of tufted sample. It seems that stress concentration due to hole in tufted composites is less than untufted composite such that the tufting process has arrested the major damage such as delamination adjacent to the hole. However more research is needed to explicitly verify this phenomenon to investigate the improving of tensile strength in open-hole tufted composite.

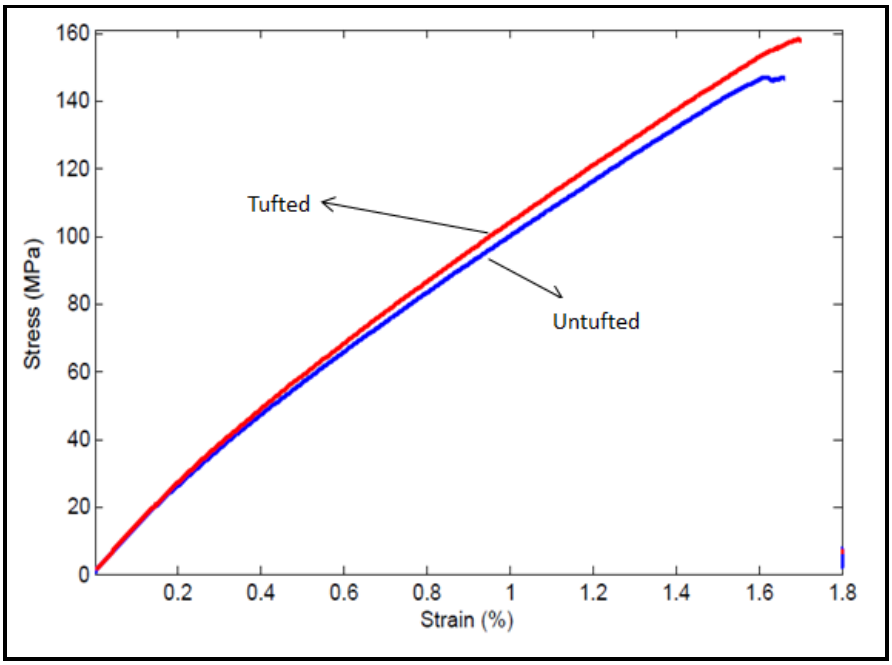

Figure 4.17. Stress-stain curves of specimens with open hole

High strain rate tensile

In addition to tensile test at low speed, tension tests at high strain rate around 0.1 s^{-1} was done to investigate the influecne of strain rate on stress strain curves of tufted and untufted composite. The results of high strain tensile test are shown in Fig. 4.18 and results of the tension strength of tufted and untufted specimens are summarized in Table 4.6. Only one test was conducted on each type of open-hole specimen because of the limited number of samples.

At low strain, the tension properties of the tufted specimen were about 10% higher than the untufted sample. This reveals that tufting did not degrade the tension properties. However, high strain rate could cause specific increase in mechanical performance of tufted sample such that tensile strength of tufted composite samples was improved around 18% while untufted composite did not have such increase in tensile strength. This phenomenon can be explained with the asumption that small damage at the interface of fiber and matrix and resin rich regions does not find sufficient time to develop at high strain rate loading (see chapter 5)

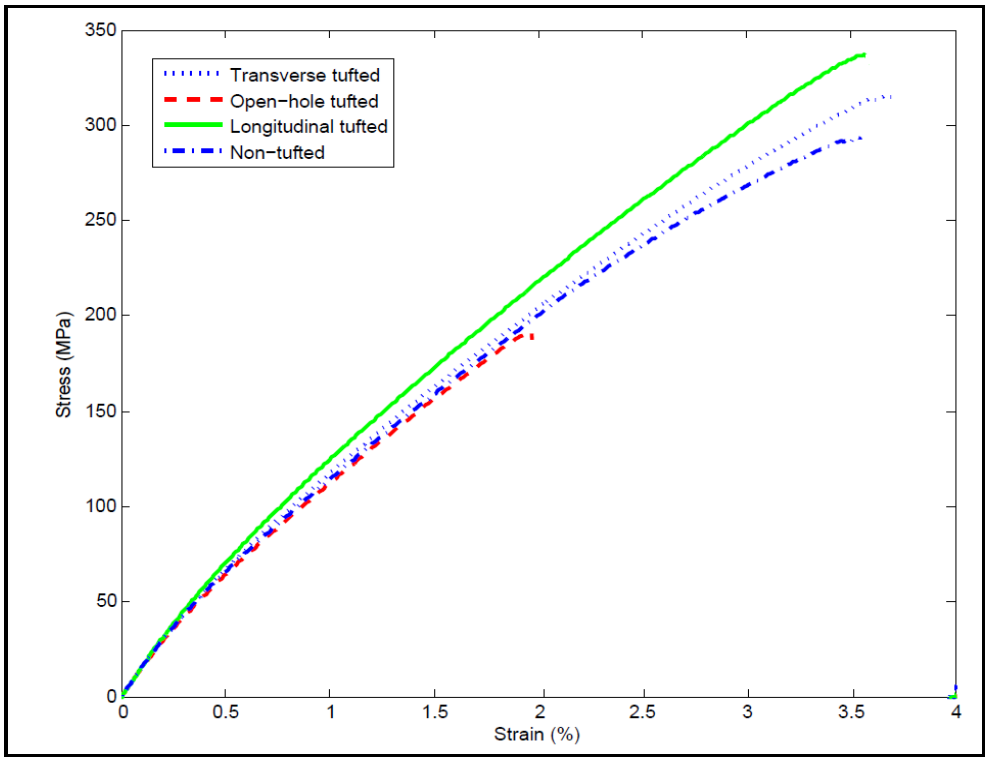

Figure 4.18. High strain rate tensile test of composite samples

Table 4.6. Test results of high strain tension test

Specimen	Tufting orientation	Strength (MPa)		Ultimate strain (%)
		Low strain rate	High strain rate	
KL-1	0^o	277.7	315.4	277.7
KLH-1	0^o	158.1	189.7	158.1
KT-1	90^o	275.6	336.3	275.6
NT-1	0^o	275.4	292.6	275.4

Compression

Figure 4.19 indicates the composite samples strength plot under compression loading. The tufted composite sample was loaded in at tufting direction (0^o). The failure behaviour of tufted sample is generally the same with untufted composite while the tufting process increasing the compression strength. Therefore, it could be said that the tufting has positive impact on composite performance and improved the damage resistance of sample. Based on

our observation, for all sample, the compression failure happened in transverse shear mode and details is explained in next chapter.

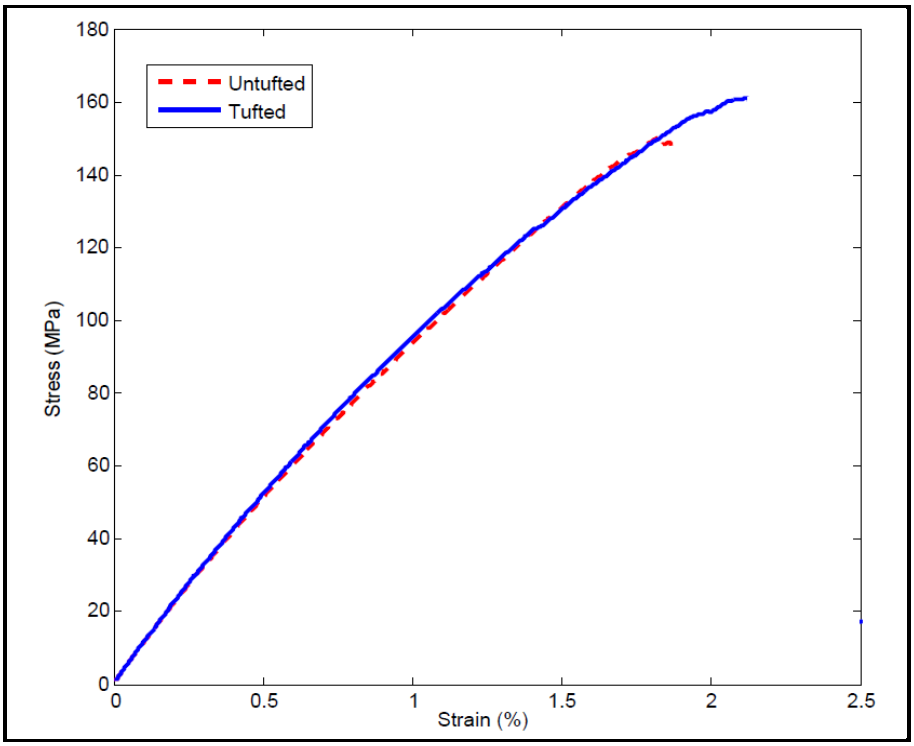

Figure 4.19. Stress-strain curves of samples subjected to compressive loading

Table 4.7. Compression test results of untufted specimens

Specimen	Tufting orientation	Strength (MPa)	Ultimate strain (%)
NC-1	0^o	151.4	1.81
NC-2	0^o	150.1	1.81
NC-3	0^o	143.3	1.68
	Mean	148.23	1.77
	Standard deviation	4.38	0.07
	Coefficient of variation	0.02	0.04

Table 4.8. Compression test results of transverse tufted specimens

Specimen	Tufting orientation	Strength (MPa)	Ultimate strain (%)
MC-1	0^o	160.7	2.07
MC-2	0^o	137.8	1.89
MC-2	0^o	157.4	2.10
	Mean	152	2.02
	Standard deviation	12.3	0.11
	Coefficient of variation	0.08	0.05

Fatigue testing

The Figure 4.20 displays the stress level versus the number of fatigue cycles to failure of tufted composite samples under six different stress levels including 65%, 55%, 50%, 45%, 35 % and 30%. Each experimental data point in this Figure represents one tension fatigue test. Mostly, delamination damage and matrix crack in tufting regions happened during the early steps of fatigue loading. At low fatigue load, these damage types were arrested between tufting thread and propagated with increasing fatigue cycles. At high fatigue load for instance around 65% stress level, tufting threads were broken at some regions at the beginning stages of fatigue cycles.

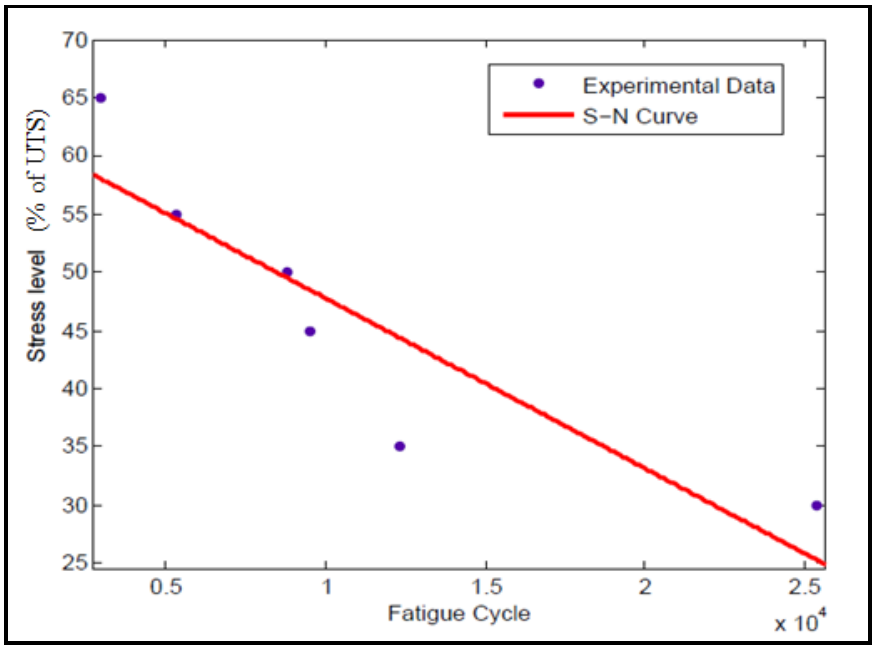

Figure 4.20. S–N curve for the tufted composite sample
under different stress levels

The curve of stress versus displacement for tufted composite samples subjected to a stress level of 50% of static ultimate stress is shown in Figure 4.21. An extensometer was used on the specimens to measure displacement in the loading direction.

It was observed that two specific regions, labled A and B, appear. These regions are between 300 to 800 cycles, and 8740 to 8770, respectively. Significant changes in displacement are seen for both regions. Before cycle 300, the minimum stress and maximum stress in each fatigue cycle were constant. No significant degradation was seen in region A. In region B, progressive damage due to cyclic loading appears. Finally, a sudden increase in displacement results in specimen rupture.

.

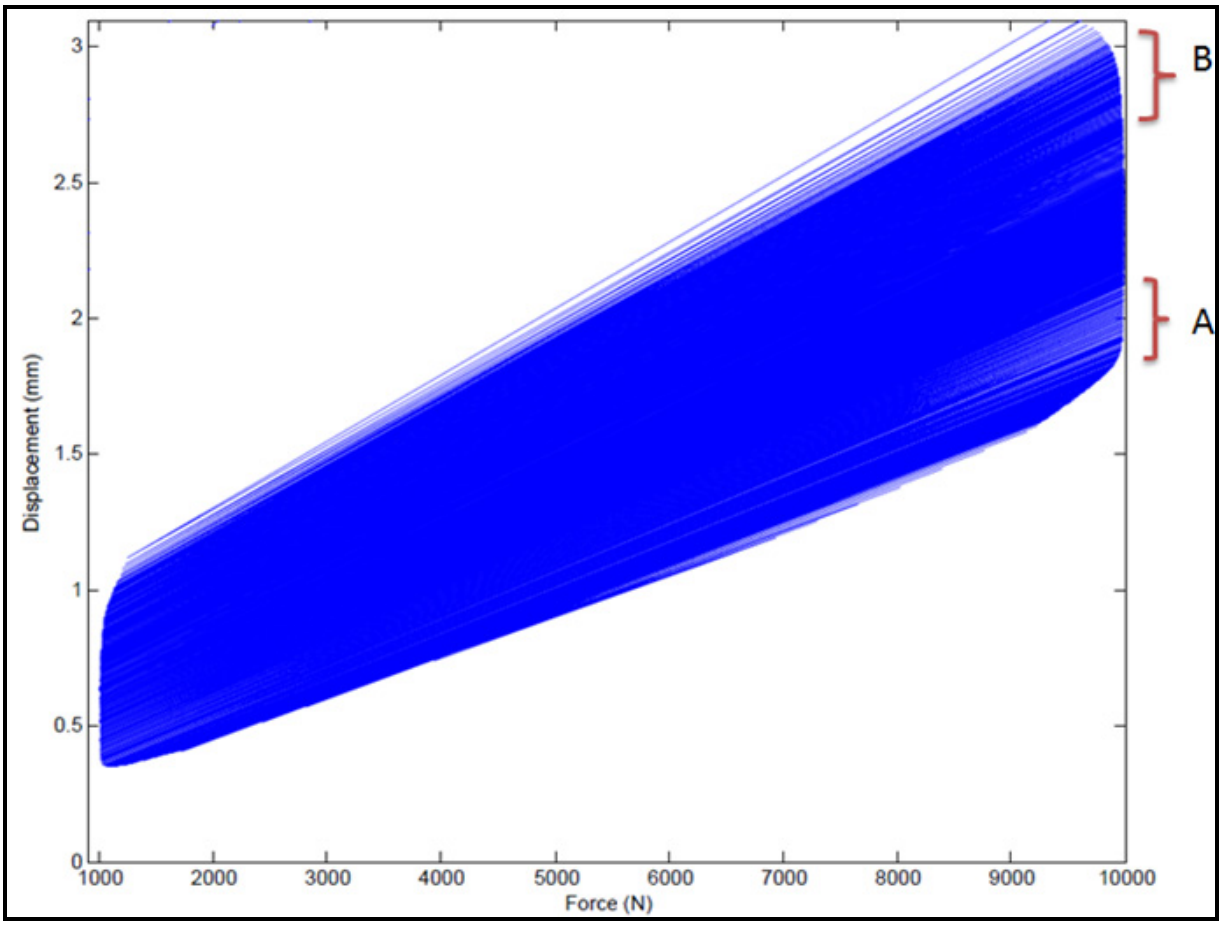

Figure 4.21. A plot of displacement vs. fatigue loading of tufted composite depicts two regions, A and B, occurring between the 300 to 800 cycles, and 8740 to 8770 cycles, respectively

Stiffness degradation

In order to better understand the variation of the tufted composite performance under cyclic fatigue loading, a research was conducted to observe the stiffness degradation. The result is shown in Fig. 4.22. The stiffness of tufted composite sample decreased as the numbers of loading cycles increase. It can be said that the specimen performance degrades progressively under cyclic loading. Plot of stiffness vs. fatigue cycles and its degradation may be divided into three regions: the first region displays a preliminary decay usually for 200-1000 cycles fatigue life. The second region that covers a large part of fatigue life displays a slow decay. A sudden decay is observed in third region with slight increase in the fatigue life.

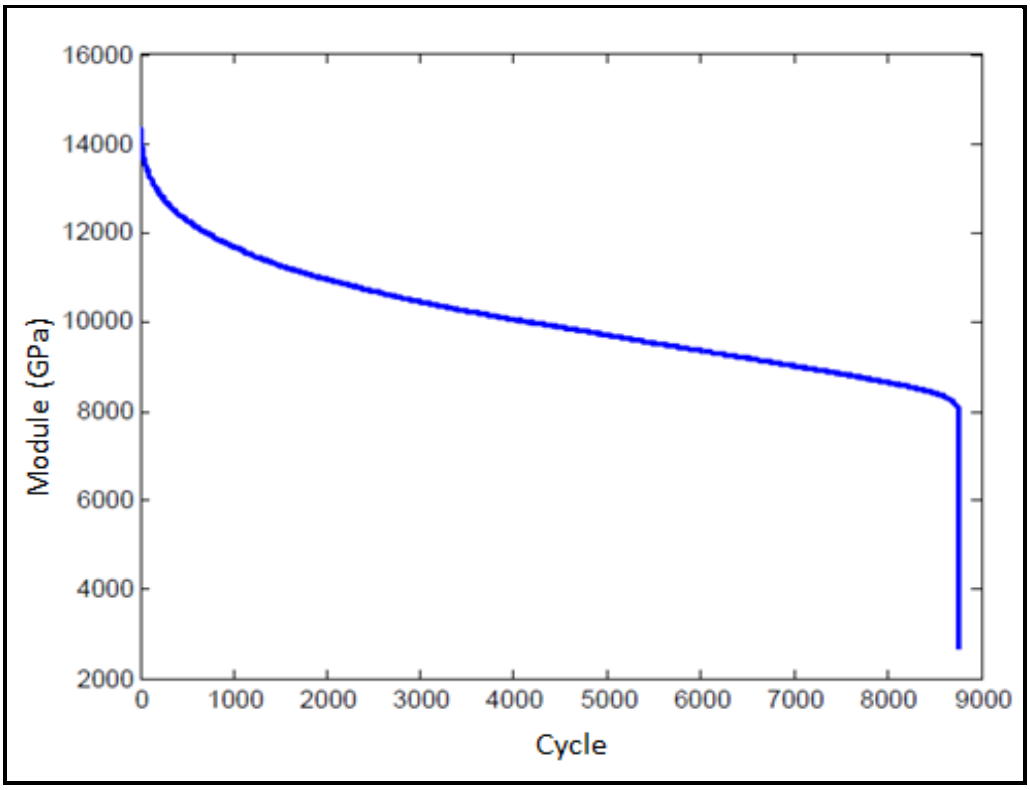

Figure 4.22. Stiffness degradation of tufted composite under fatigue loading

The Figure 4.23 depicts the displacement versus fatigue loading of an untufted sample. These specimens exhibited two stiffness loss stages that were like the pattern observed in tufted composites. At the first 10% of life, no sharp stiffness loss was observed, which is same as the case for tufted laminates. Then, a gradual stiffness decline was seen in the first 90% of life. Lastly, a knee in the stiffness curve was observed in the final 10% of fatigue life.

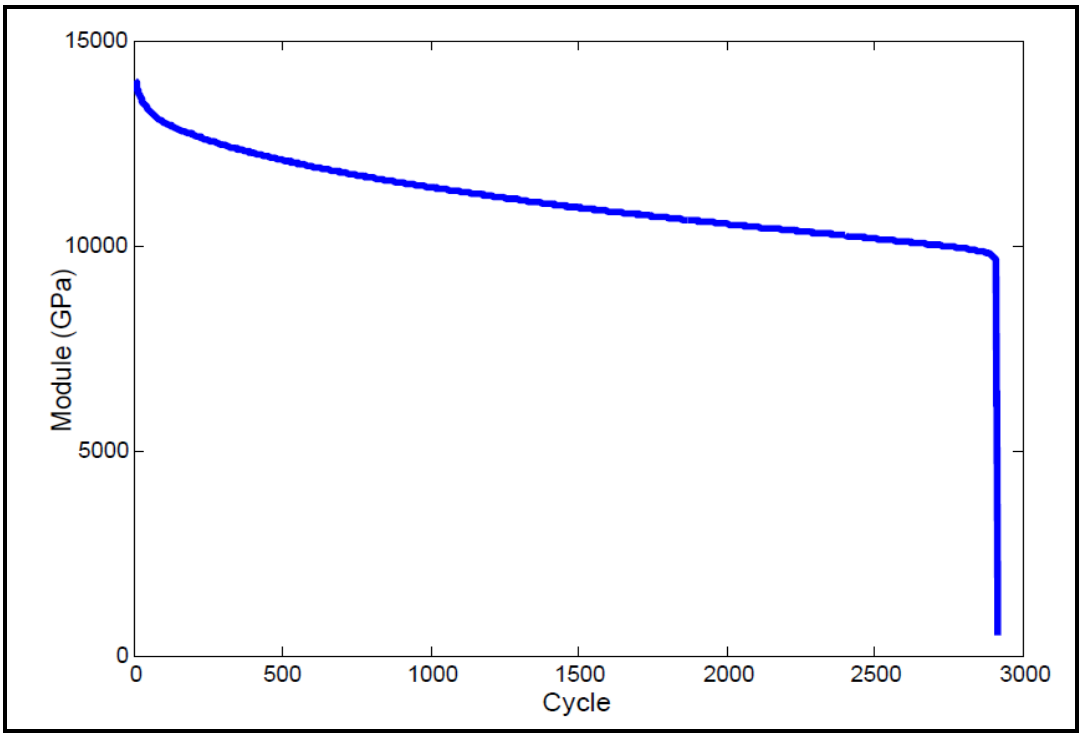

Figure 4.23. Stiffness degradation of untufted composite under fatigue loading

The Figure 4.24 depicts the displacement versus fatigue cycle and specific regions appeared during damage progression for tufted composite. The rapid increase in the deflection between cycles of 200 and 500, and after cycles of 8740 can be observed. At first range, the damage of the tufted composites becomes more important because of the fatigue damage initiation. In the locations where damage begin to occur, the stiffness is reduced as shown in previous Figure and the remaining material including fibers and matrix has to carry the cyclic loading during fatigue test. After cycles of 8740 cycles, the sample rupture occur, since the fibers and tufting threads as load bearing material within a composite are completely ruptured.

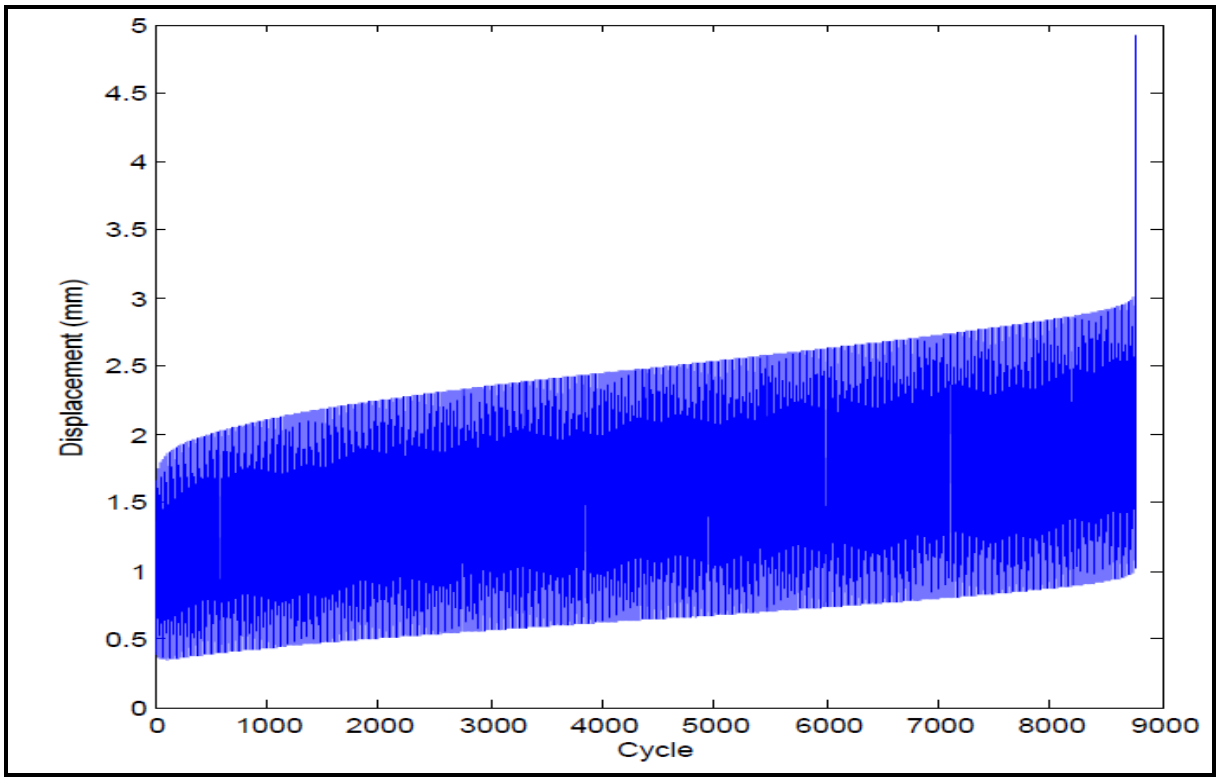

Figure 4.24. The displacement vs. fatigue cycle of tufted composite

Because of the limited quantity of samples, two tests were conducted on open-hole specimens. At 60% of the static failure strength of untufted specimens, the tufted specimens easily survived 2500 cycles whereas the untufted specimens can last only about 2000 cycles. More research is needed to explicitly verify this phenomenon.

Post fatigue tension test

In this section, three composite samples have experienced the tension loading after 1000 fatigue cycle. Figure 4.25 displays the stress- strain curves of these specimens and test results summarized in the table 4.9 in term of residual tensile strength. On comparing the average failure strain of untufted sample with that of the tufted sample, it was found that the tufting improved the static tensile strength of samples after 1000 fatigue cycles. It should be noticed that the comparison of the obtained mechanical properties exhibit only the influence of

fatigue on the residual strength, but no exhaustive results could be extracted from this research due to the limited number of samples.

Table 4.9. Test results of post fatigue tension tests

Specimen Number	12) Tufting direction	13) Fatigue cycle	14) Residual stress (MPa)	15) Failure strain (%)
16) NR-1	0^o	1000	245.7	2.87
KRL-1	0^o	1000	270.8	3.22
KRLH-1	0^o	1000	115.4	1.24

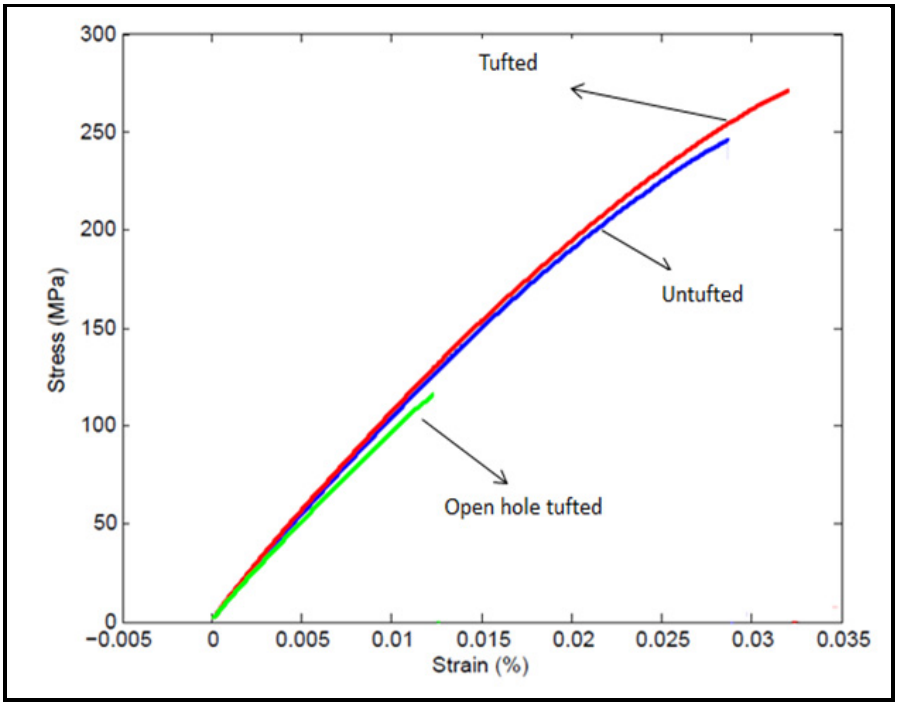

Figure 4.25. Post-fatigue tension test results

4.3.2 Honeycomb composites

Local compression

The impact responses of tufted honeycomb composite were simulated with quasi-static compression and characterized in terms of failure behaviour and peak force. Only one test was conducted on each type of specimen because of the limited quantity of specimen,

therefore, no statistical analysis was provided. It was observed that the loading peak is dependent on the facesheet type. The sandwich panels with tufted facesheets experienced higher peak forces compared to untufted honeycomb composite.

The behaviour of both tufted and untufted honeycomb composite under loading was approximately identical before force peak, but dissimilar after failure point. As shown in Figure 4.26, at the first stage of perforation at tufted honeycomb composite, as the spherical plunger moved down the load gradually increased until reaching point A. The point A corresponds to first failure and damage appearance in top facesheets along with core crush. With increasing the displacement, loading increased and damage propagated inside top face sheet. It caused a sudden small drop in loading displacement curve appeared in point B. This point corresponds to the penetration of specimen by plunger. Finally the core and upper face sheets completely fail with some load fluctuations after point C due to friction force as the spherical plunger penetrate the sandwich panel. In detail, both tufted and untufted panel specimens reveal same behaviour before point C, but because of crushing tufted sample in resin rich region around thread, a sudden load drop is seen after point C for tufted facesheet. The higher strain ability of the untufted honeycomb composite after point C could be discussed to obtain high damage tolerance accompanied with low core crushing.

Based on visual inspection, the resin rich region surrounding the tufting reinforcement was the damage initiation region. Of the defects observed using microscopic and X-ray computed tomography techniques, the most deleterious to local compression could be related to fiber breakage, since the fracture initiated from the back surface of upper facesheet that experiences tension loading. The broken fibers cause microcracks at the tension surface of upper facesheet that ultimately cause the tufted composite to rupture along a single row of tufting reinforcements. In untufted composites, there are little local variations in the preform architecture, fiber breakage and fiber distortion. Therefore, specimen rupture was due to fiber fracture and multiple delamination damage.

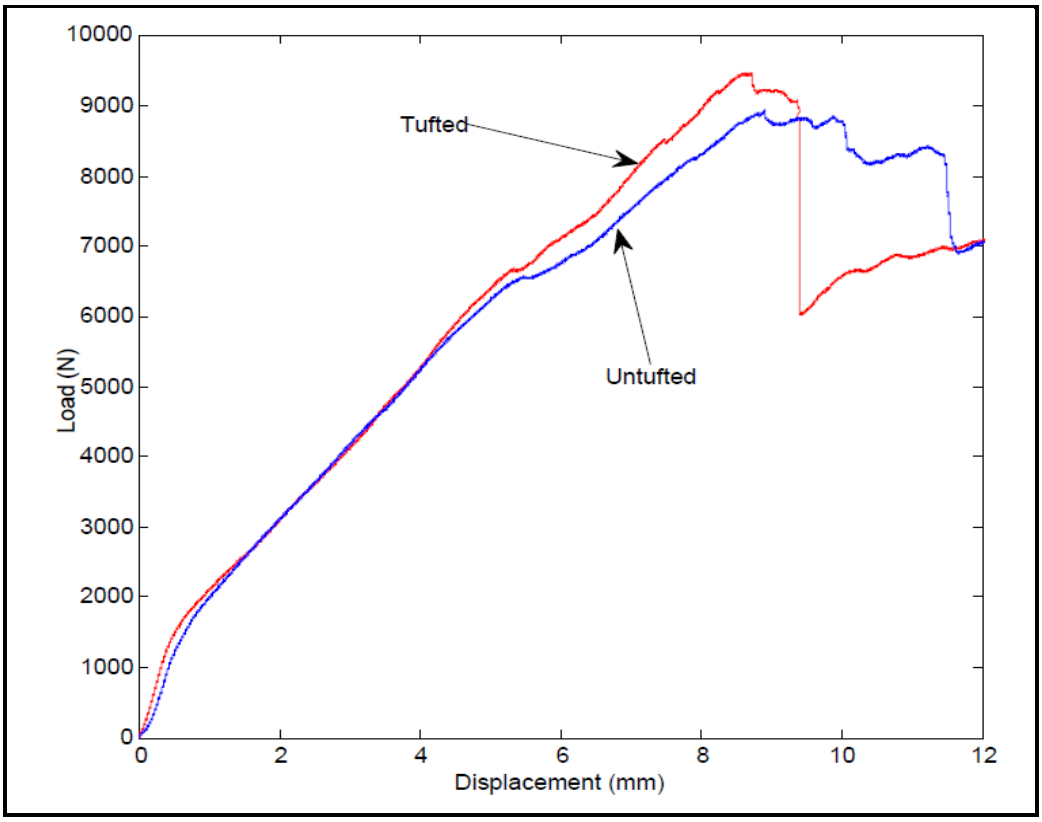

Figure 4.26. Load-displacement curves of sandwich composites under local compression

Bending test

Figure 4.27 depicts the load-displacement responses and failure behaviour of two sandwich composites. Only one test was conducted on each type of specimen because of the limited quantity of material, therefore, no statistical analyzed was provided. There are three load drops for each loading curve. The letters A, B, C, in the plot of tufted honeycomb composite indicate critical stages of loading before failure, at failure point, and after failure, respectively. In this plot, the linear elastic behavior is evident until the load approaches about 800 N at point A. Following this point, with loading increase, plastic failure occurs at the honeycomb core corresponding to region between A and B. At the first drop indicated in the point A, one shearing crack initiated at one upper loading point just below the face sheet and propagated across the core at 45^{o} reaching the bottom face sheet. Point B indicates the shear crack in core reached the bottom face sheet. It gradually continued to grow at the interface

between the facesheet and the core until failure (load drop indicated with point C). After this point, the load started to increase until the sample rapture. Damage observed in facesheets and honeycomb core for two tested sandwich specimens will be discussed in the next chapter.

The mode of damage initiation in untufted composites depends on the support conditions. In our case, same as for the local compression test, the untufted sample failed under bending loading and the main cause of failure was fiber fracture and multiple delaminations in the upper facesheet. Tufted composited rupture was influenced by fiber breakage around tufting reinforcement.

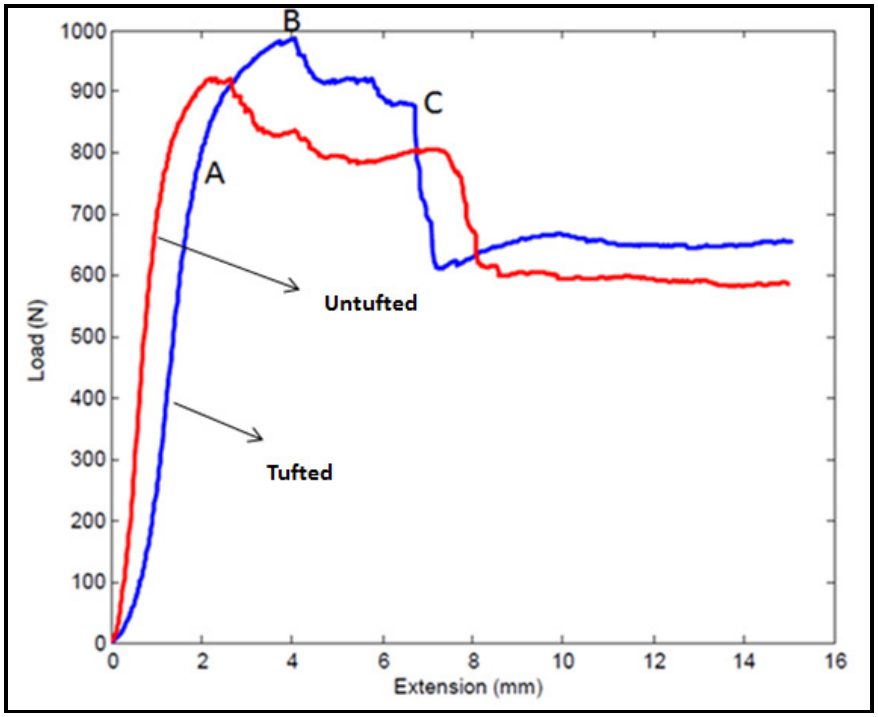

Figure 4.27. Load-displacement curves of honeycomb composites under bending load

4.4 Conclusion

Quality control of 3D tufted preform and composite panels was performed using laser scanning and X-ray computed tomography techniques. The thickness variation of a preform was measured using the laser scanning technique and the parameters that affect the measurement by laser scanner, without contact, were examined. X-ray computed tomography images provided the possibility to detect manufacturing defects such porosity, fabric orientation and also characterization of the location of the damages.

Experimental investigation of the effect of through-thickness tufting on the static tension, compression and fatigue performance was performed. Open-hole tension tests at low and high velocity were performed on the tufted and untufted samples. The following conclusions may be made on the effect of tufting reinforcements on the mechanical performance:

- Longitudinal tufted composite revealed higher strengths than for transverse tufting;
- Tufted composite specimens exhibit nearly linear curves up to failure, the same as for untufted composites;
- Tufting did not degrade static compression properties;
- Under high velocity tension loading, tufted composites showed higher strengths and greater damage resistance that untufted composites and transverse tufted samples;
- Untufted specimens were superior to tufted specimens in fatigue;
- Post-fatigue performance of tufted samples was greater than for untufted specimens. Tufted composites showed an increase in residual tensile strength in tension fatigue.

Quasi-static local compression, bending tests were carried out to investigate the mechanical response of sandwich composite panels composed of aluminum core and 3D tufted composite skins. Based on the limited number of samples tested, the strength of the sandwich composites was strongly influenced by the reinforcing of facesheets, and the beams with tufted skins ruptured at a higher load compare to composites without tufting.

CHAPTER 5

DAMAGE CHARACTERIZATION OF 3D COMPOSITES

5.1 Introduction

This chapter presents the characterisation of tufted composite using microscopic and NDT techniques. As stated in chapter two, X-ray computed tomography could provide more details about damage in 3D composites than other techniques. Therefore, in the present research, X-ray technique along with optical and Scanning Electron Microscopy (SEM) technique are applied to characterize the microstructure and the damage in tufted composites and recognizing the failure modes.

5.2 Materials and experimental equipment

Table 5.1 list all sample were characterized to detect damage and the fracture mode occurred during mechanical tests. Micro structural analysis of composites using optical microscopy and SEM at different magnifications was carried out by preparing small cross sectional samples. X-ray Micro CT scanning was conducted using a commercial scanner at Jesse Garant & Associates Company in Canada. The machine consisted of a micro focus x-ray tube at 36KV within spot size of 0.005 mm and 2376 projections. The sample size of 20 mm X 20 mm was prepared from each composite plate to provide high resolution scanning around 0.045mm. The scanner created two dimensional X-ray images of composite sample, and then a specific software program constructed 3D X-ray images. The 3D CT data were analysed using the volume graphic software toward damage characterization purposes.

Table 5.1. List of the composite samples characterized using microscopy and X-ray computed tomography techniques

Test / Specimen	Tension	Compression	Fatigue	Local compression	Bending
2D textile	• Intact • Damaged				
Untufted	• Stopped at 21KN, • Fractured	Fractured	Stopped at 1000 cycle	-	
Tufted	• Intact • Stopped at 21KN • Fractured	Fractured	• Stopped at 1000 fatigue cycle • Fractured	-	-
Open hole tufted	Stopped at 21KN	-	-	-	-
Honeycomb	-	-	-	Fractured	Fractured

5.3 Results and discussion

5.3.1 2D textile composite

2D woven composites were studied to examine the capabilities and limitations of X-ray computed tomography for the characterization of those defects localized artificially. Those defects were two different types of breakage in fiber bundles. The results demonstrate that X-ray computed tomography with current resolution cannot detect that small internal damage including microcracking in fibers. The sample size should be decreased by 1.5 mm that detection of microcracks would be possible.

5.3.2 Tufted composite characterization

Tensile test

The specimens with transverse tufting usually break along the tufting lines while the specimen with longitudinal tufting breaks in angular direction to the tensile loading direction. At the initial stage of loading, when the tensile loading exceeds a threshold value of 3kN, damage (darker areas) appears in surface of composite in the proximity of tufting thread

region shown in Fig. 5.1. Damage initiation for the tufted specimens was audible at load levels between 7 and 9 kN, whereas, the damage initiation for untufted composites was audible between 4 and 6 kN

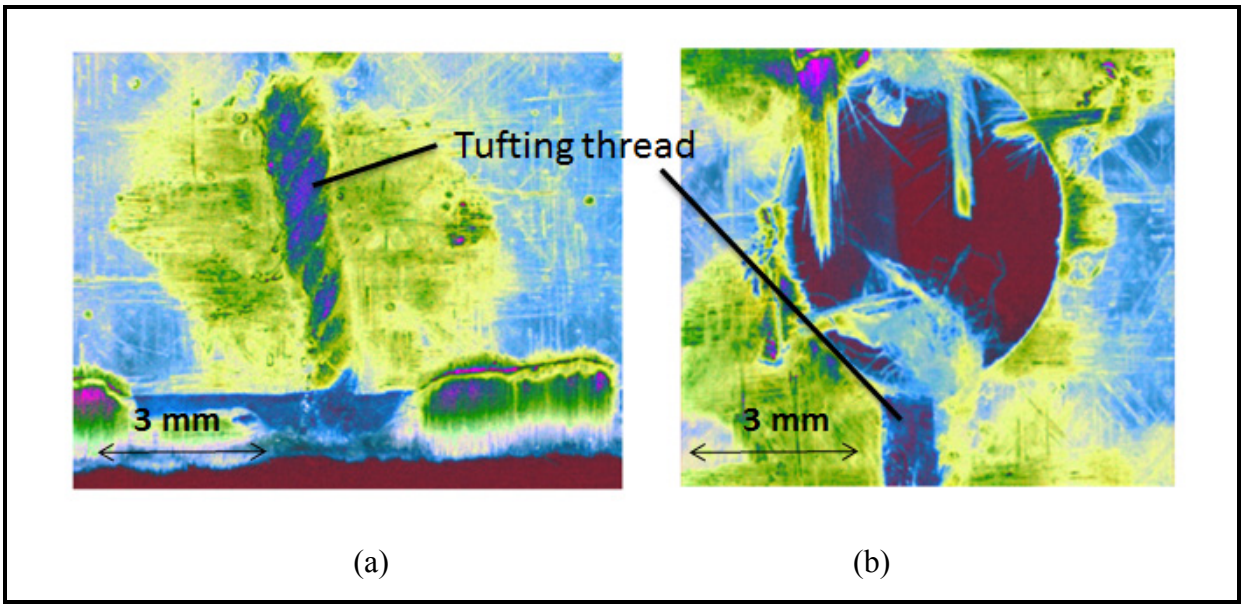

Figure 5.1. Microscopic images of delamination crack in tufted composite during fatigue (a) Tufted sample (b) Open-hole tufted sample

Figure 5.2 present X-ray CT images of ruptured tufted specimen. Figure 5.2a represents cross sectional X-ray images correspond to moving the cutting plane in thickness direction, while 5.2b depicts the sectioning of open-hole composite sample stopped at 80% of failure strength. White area indicates fibers and dark region indicates matrix and cracks. The distributions of major damage in through-the-thickness direction of tufted composites were dissimilar at different regions. In the fractured tufted specimen, largest damage including delamination and fiber fractures are seen at the center of the composite coupon. In open hole sample, the damage were initiated from the tufting thread region, and the largest damage prior to complete rupture is seen at the top and bottom surfaces. The appearance of these damage including delamination and transverse crack on near the surface of the samples decreased the stiffness as explained in the previous chapter.

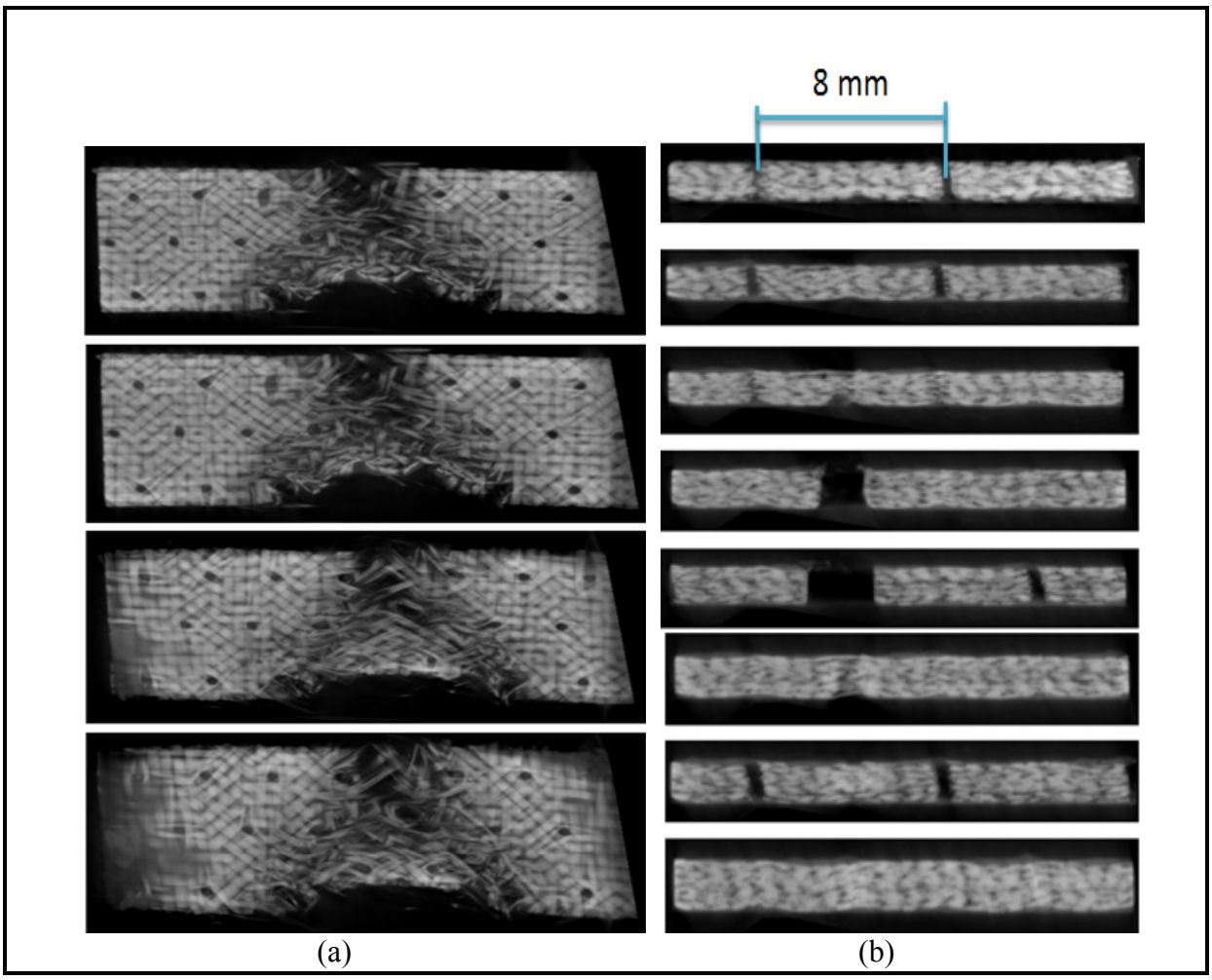

Figure 5.2. Reconstructed 2D images of fractured specimen in static tension test (a) Top surface (b) Side view of open-hole sample with dimensions of 20 mm x 25 mm

To observe damage using destructive technique, several samples including tufted and untufted samples were stopped before rupture and then post-mortem examination was conducted based on micrographs and SEM images. Figure 5.3 shows the photograph of the failure modes of composites under tension. At the beginning of loading, for untufted specimens, failure occurred at the interface between the layers while for the tufted specimens, the tufting threads were observed to prevent the complete separation of layers. Upon continued loading, some tufting threads ruptured at the interface and were

subsequently pulled out. As the delamination damage propagates ultimately sample failed in the form of fiber and thread breakage.

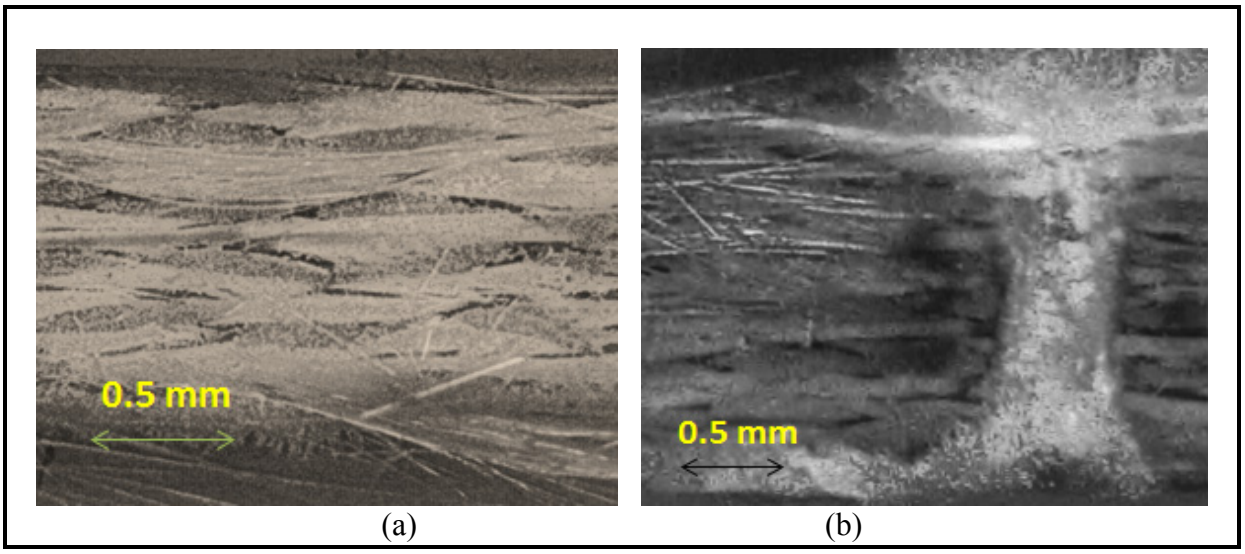

Figure 5.3. SEM micrograph of fractured tufted composite in tensile test (a) Delamination between tufting thread (b) Delamination arrested in tufted region

The tensile damage progress in the form of micro cracks could be seen in SEM microscopic images shown in Figure 5.4 & 5.5. In these Figures, transverse crack in fiber and initial stages of damage progression as well as micro damage occurring in resin rich are clearly observed.

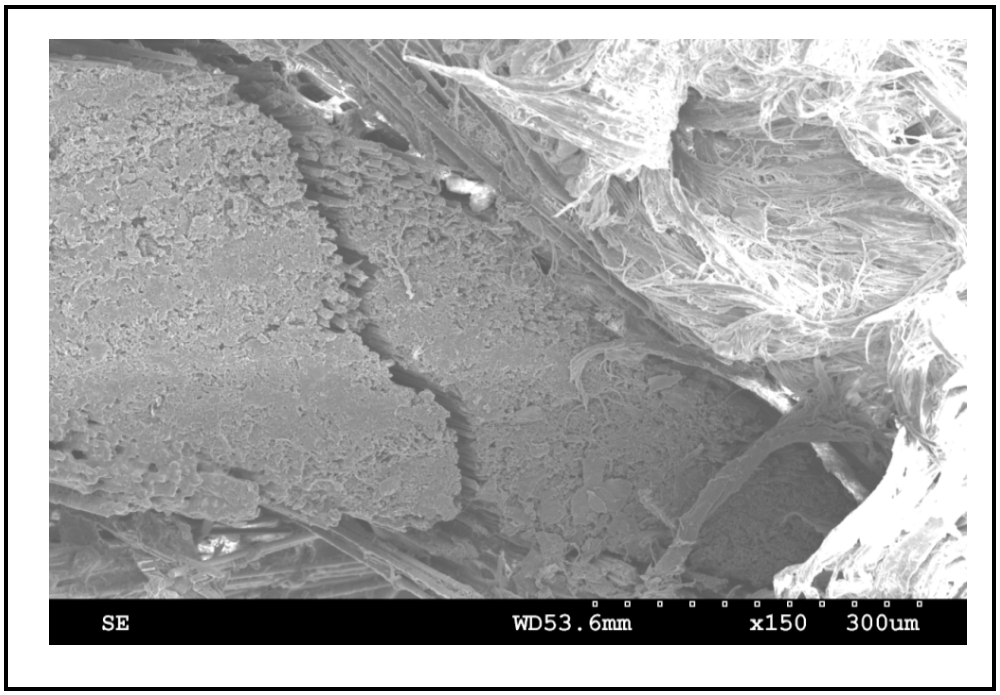

Figure 5.4. Transverse matrix crack in tufted composite in tension test

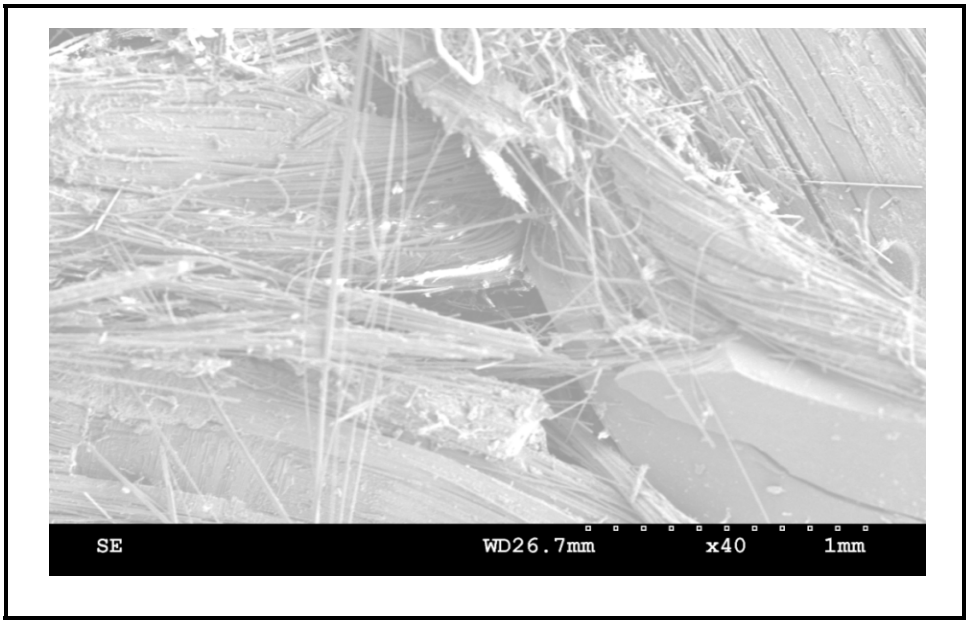

Figure 5.5. Crack originated from resin rich region

Fatigue test

From X-ray images with high resolution, it was found that the fatigue damage progress in the form of micro crack through the composite between tufting threads. Microcracks are another frequently observed occurrence in the tufted composite. They are mostly found in the vicinity of the tuft fiber, often at the dome created by the stitch fibers. Examples of microcracks can be seen in Fig. 5.6. Microdamage weakened the stiffness of tufted composite and increased the displacement over the fatigue life.

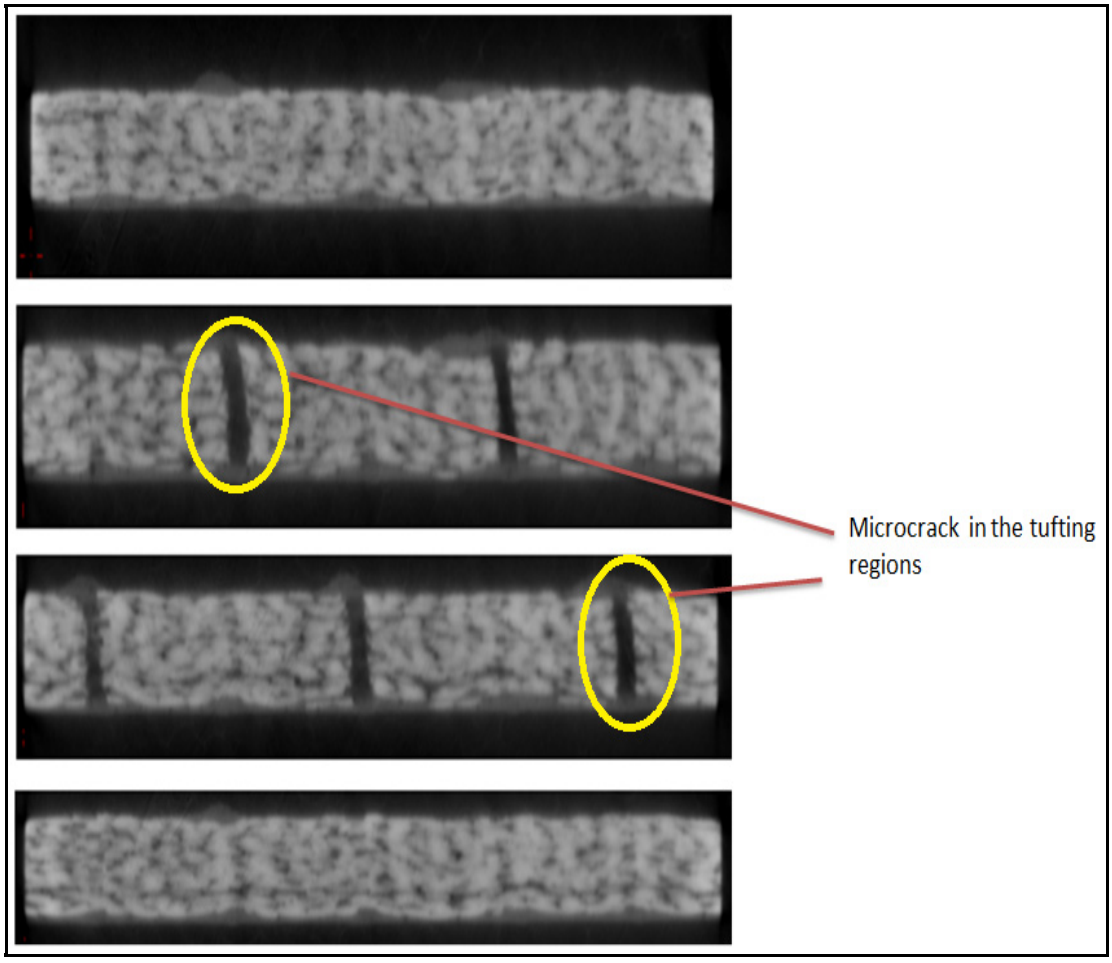

Figure 5.6. X-ray side images of sample with dimentions of 20 mm x 25 mm subjected to fatigue loading

Using microscopic imaging various forms of damage were evident as the fatigue cycling progressed. Figure 5.7 shows the side surface of tufted sample damaged at the stress level of 50% at two different magnifications. It is found that the matrix cracking, transverse cracks within fiber boundles, delaminations and thread breakages as well as the debonding of fiber matrix interface are the major damage modes for tufted composite experienced tensile fatigue loading. This damage progress can be interpreted based on changes of displacement of composite over the fatigue life as described in previous sections. Furthermore, the delamination and transverse crack growth were arrested temporarily by tufting thread and prevented from extending further; only delamination grow was observed after some tufting threads were broken. Fig. 5.8 show microscopic image of tufted specimens taken before sample failure in fatigue test. We can observe that delaminations originate along the edge.

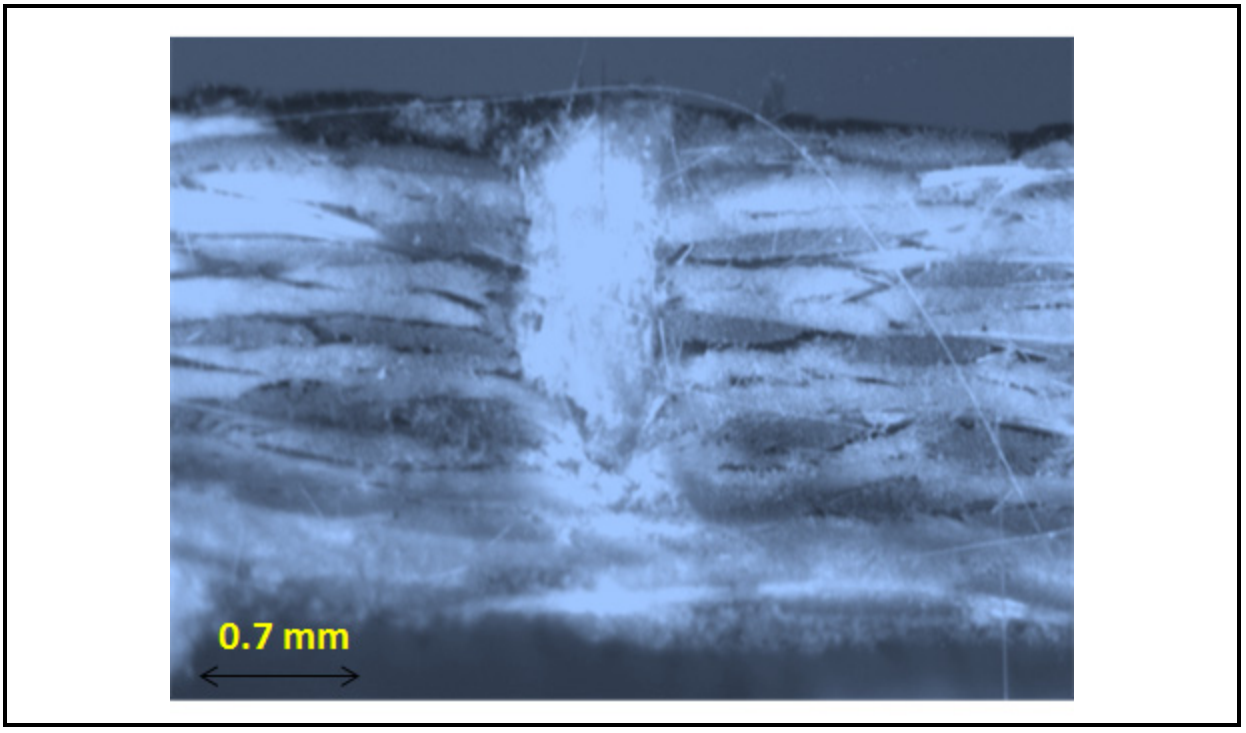

Figure 5.7. Optical microscopic image of micro crack inside of tufted composite under fatigue test

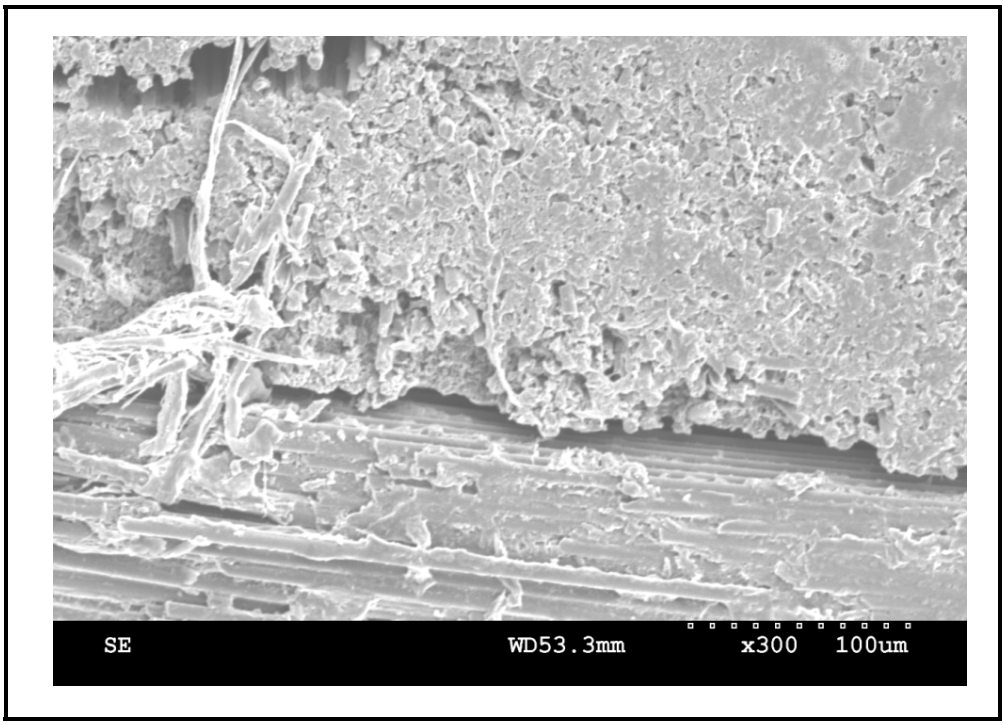

Figure 5.8. Delamination crack in tufted composite

The fatigue damage progressed in the form of micro crack through the composite is shown in SEM images in Fig. 5.9. The delamination cracks shown in this Figure were seen in all fatigue specimens at the first inspection interval stopped at cycle 1000. The number and extent of such delamination cracks increased as the tests progressed.

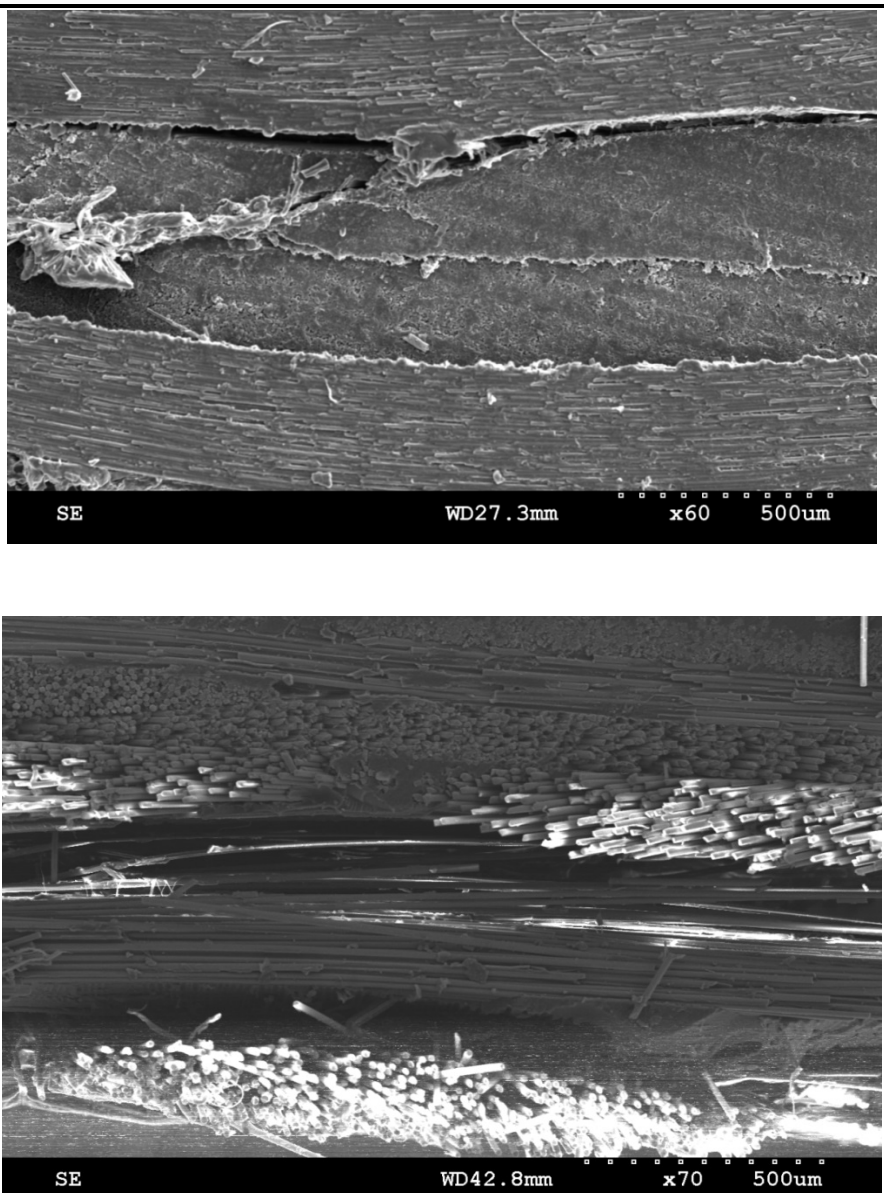

Figure 5.9. SEM Images of delamination in tufted composite in fatigue test

Compression

Examination of cross-sectional X-ray computer tomography images shown in Fig. 5.10 clearly present the shear failure happened and fabrics moved from their original direction near the tufting thread. With respect to the obtained X-ray images, the specimen failure

tended to occur as a combination of the most significant damage including fibre breakage and transverse shear. Tufting thread decreased delamination but increased the kink banding and fiber misalignment and out of plane waviness. While shear failure and kink bands damage have commenced in the vicinity to the tufting thread, no precise correlation could be proved between them.

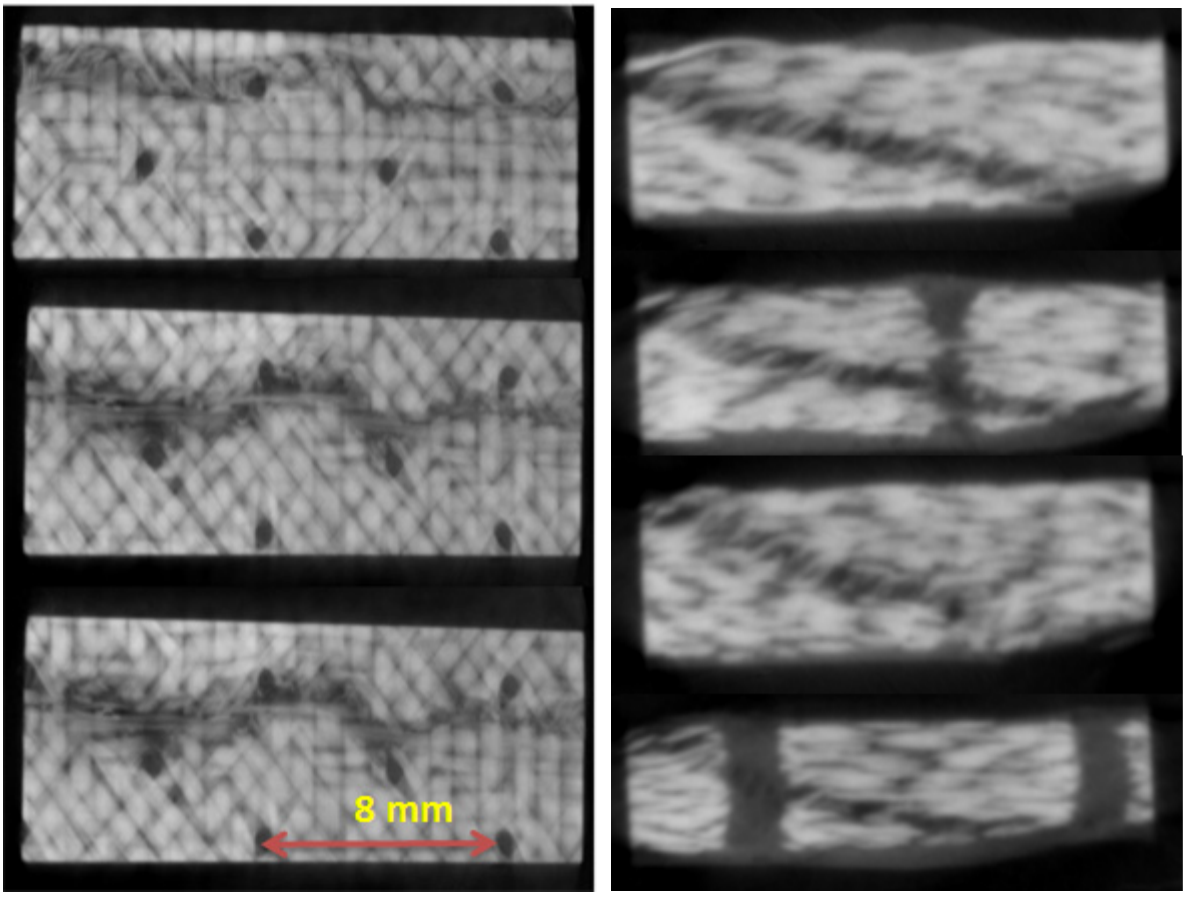

Figure 5.10. (a) Top and (b) Side X-ray images of tufted sample ruptured in compression test with dimensions of 20mm x 10mm

Based on microscopic images shown in Fig. 5.11, it could be said that surface fabrics of coupon specimens are not effective lamina for carrying compression loading in compare to

interior fabric of sample. Furthermore, it was observed that the rupture mostly commenced as fibre micro buckling around the tufting thread and misaligned fiber which will extend through the whole sample. Therefore, the reduction of compressive strength could be seen in tufted composite including preforms with high tufting density.

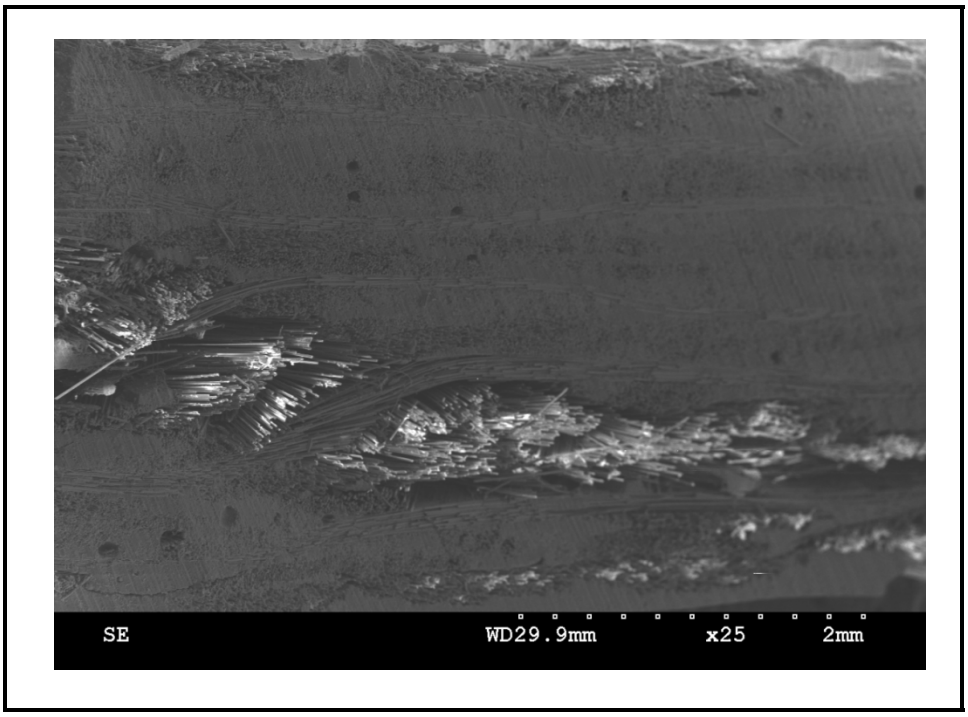

Figure 5.11. SEM image of tufted sample ruptured in compression test

Honeycomb composite

Based on the observations done on honeycomb composite discussed in previous chapter, the reinforcing of facesheets could influence on loading threshold and failure behaviour. From aspect of damage state in Quasi-static local compression, major damage in honeycomb composites consisted of skin ruptures, and core failure. The destructive sectioning toward microscopic investigation shown in Figure 5.12, demonstrates that the extent of damage in facesheet region exceed the core damage except in the region under the plunger. Extensive damage in the skin was fiber breakage, and debonding of aluminum core from skin.

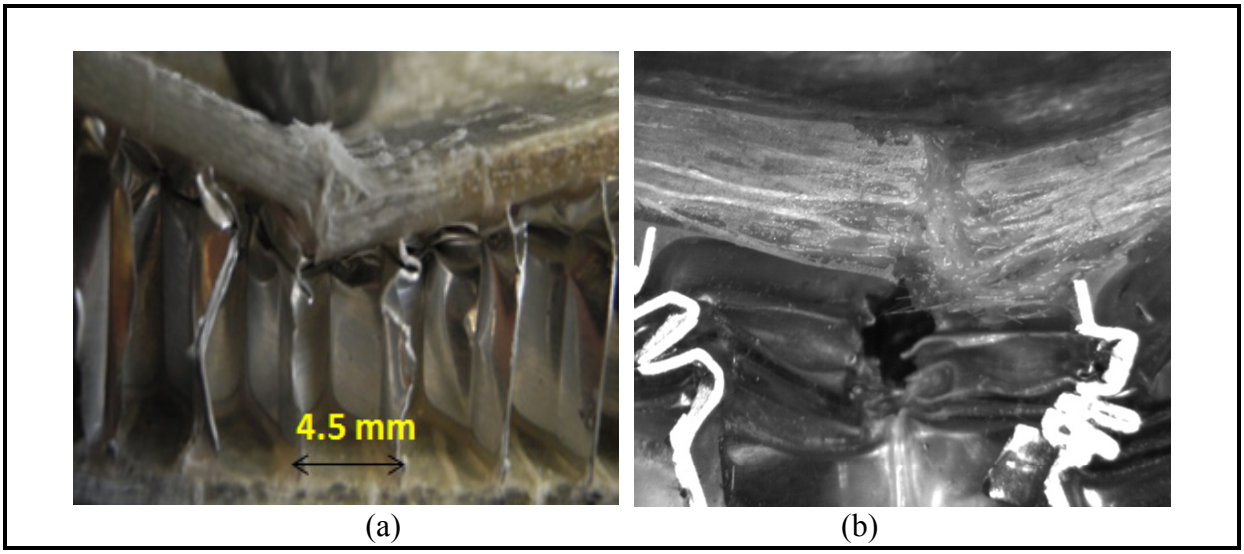

Figure 5.12. Images of honycomb composites ruptured in quasi-static compression
(a) Side image (b) Sample cutted from the point under plunger

Fig 5.13 depicts microscopic images of samples ruptured in static bending test. Major damage observed in loaded sample was: debonding in skins in the vicinity of resin rich region and core in shear mode.

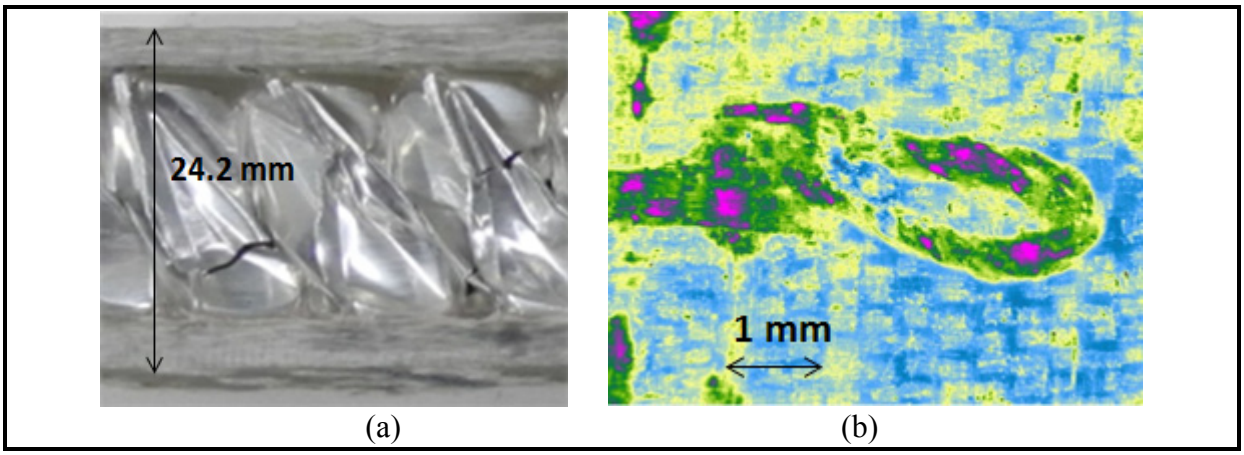

Figure 5.13. Damage occurring on tufted composite subjected to three point bending test (a) Core shear (b) Damage intiation observed in resin rich region

Based on experimental observation during compression test, a core shear failure accompanied with debonding of skin from aluminum core was the main failure reason of tufted honeycomb composite (see Figure 5.18). While, the primary modes of failure for honeycomb composite with laminated skin comprised of debonding of skin from aluminum core, delamination and core shearing.

5.4 Conclusion

Microscopic examination at different magnifications was utilized to investigate the intrinsic damage in tufted composites after loading. X-ray images provided the possibility to realize the manufacturing defects such as void and porosity, and also the characterization of the location of the damage. The major damage in composites during mechanical loading consisted of transverse crack, debonding, and delamination. It was found that to detect localized micro damage in two dimensional composites, the sample size should be decreased. It was observed that the delamination damage was arrested by tufting thread during static and fatigue test. The resin rich regions were first locations for damage initiation during compression and bending loading of honeycomb composites.

CONCLUSION

This thesis investigated the manufacturing process and inspection of textile composites, as well as correlation between defects and mechanical performance. A few non-destructive techniques were used to detect major process-induced defects in textile composites. The behaviour of preform and textile composites under static and fatigue loading were investigated. Damage states and progression was studied toward characterization purposes. The main finding and outcomes of this thesis are summarized in present section.

VARTM techniques were used to manufacture all composite samples. As observed, voids were likely to be present in all samples impregnated with vacuum process. The voids weren't directly dependent on the presence of the tufting thread, but had more with the impregnation process itself and, more specifically, with the resin flow front. Good quality composite panels are obtained if the degassing processing is performed and the vacuum line and resin distribution media are placed in an appropriate way.

Ultrasonic C-scanning of the textile composite samples suffered from a high attenuation of the ultrasonic waves which prevented detecting small damage and orientation of middle layers.

Mid-layer orientation of samples appeared to influence their dynamic behavior including FRF and natural frequencies. FEM modeling was used to investigate the experimental results.

X-ray computed tomography is the best NDE technique for studying layers orientations in textile. Thanks to high resolution computed tomography, local fiber misalignment caused by tufting thread appeared in the X-ray images. However, small size of sample was a limiting factor to see whole sample.

Along with NDT studies, mechanical testing and fractographic characterization was also used to determine the influence of artificial manufacturing defects on the performance of 2D textile composite. Decreased strength was observed due to existence of damage.

The tufted preform characterisation was carried out by different mechanical test. Deformation mode of tufted textile fabrics and their specification was identified using microscopic technique.

The static tension at different strain rates and fatigue mechanism in tufted composites were observed much more complex than that of untufted composites. The tufting process did not influence the quasi tensile strength at low strain rate. The tensile strength was approximately identical for both tufting directions. The tufting process decreased the fatigue life of samples under high stress levels. The tufting process improved both compression and tensile strengths at high strain rate.

Through testing of tufted honeycomb composite, it was observed that tufted skin had the significance effect on the damage resistance of the composite panel. The results indicated various differences in damage initiation and propagation during bending and compression. This difference was highly attributed to the mechanical behaviour of the tufted facesheets.

The damage states were characterised using the microscopic and X-ray tomography. Various damage modes were observed in tufted composites including matrix crack around tufting thread, fiber breakage, delamination and failure in a fiber/matrix interface. Tufting arrested delamination damage during the fatigue test and transverse shear failure mode happened during compressive loading.

There is an impediment to the acceptance of tufted textile fabrics for primary aerospace composite structures due to uncertainty and conflicting research results concerning their degradation and in plane properties.

Although, this research work concentrated on experimental investigation of textile composites, some finite element study was also conducted to evaluate the structural integrity of textile composite with artificial defects. Good correlation was obtained between the experimental and modeling results. The modeling methodology used in this thesis could be adapted to other type of textile composites.

RECOMMENDATIONS

Based on the results and findings of this thesis, recommendations and guidelines for further research work are delivered in present section.

Conventional and polar pulse echo C-scanning of the textile composite samples suffered from a high attenuation of the ultrasonic wave by the fabric layers, which prevented detection of defects. One potentially promising approach to overcome this issue could be implementation of Lamb waves and a focused transducer.

Composite surface's roughness could affect polar scanning results. Therefore it is recommended to measure the surface roughness to determine the upper limits of detectability of fiber misalignment in textile composite. It should be necessary to smooth the surface of composite before testing and evaluate its effect on the C-scan results.

Attenuation of the signal in textile composites is extremely high due to scattering by the fibers. Ultrasonic inspection in low frequency range using advanced transducer called "Gas matrix transducer (GMP)" is suggested. The most attractive feature of GMP transducer is their less sensitivity to scattering from fibers.

Placing optical fiber inside tufted preform is proposed for monitoring the structural integrity of composite samples.

Using of shaker, which applies continuous excitation on specimen, could reduce the amount of noise. It may allow a better sensitivity of the technique. This method is especially efficient at the higher natural frequencies, where the effect of misalignment appears to be more significant.

Artificial defects introduced in composite specimens may display unrelated failure modes. Additional characterization tests are proposed to simulate with real conditions.

It is normal for the loops of tufted laminates to be 'squashed' on the backside of the composite panels. Further research should be conducted to find out if loops have detrimental effect on the composite performance.

Because of not disclosing the key parameters such as thread tension, needle size etc., future experiments is proposed to understand the optimum tufting parameters such as needle size, tufting pattern, shape of the needle tip, etc.

The damage tolerance analysis and durability characteristics of tufted composite materials still need to be addressed.

The optical techniques are suggested to investigate efficiently local failure occurring in 3D textile composites. This technique could provide further information from a single mechanical test rather than several tests.

We did not correlate the depth of dent occurring during the local compression to core damage region, and critical span size to core failure. Therefore, more research is needed to characterize the correlation between dent depth and real extent of damage in aluminum core.

Further examinations in the intermediate and high strain rate regime are proposed to conduct to understand the behaviour of tufted preforms and 3D tufted composites.

Finite element modeling of 3D dry preform forming process is recommended to investigate the damage initiation and propagation in meso and micro scale levels. Modeling could help for recognizing the shear locking angle with consideration of friction between fiber bundles and tufting thread.

BIBLIOGRAPHY

Adams D., and Cawley P. 1988. « A review of defect types and nondestructive testing techniques for composites and bonded joints ». *NDT International,* vol. 21, n° 4, p. 208-222.

Ajay K. 2008. *Non Destructive Testing of Composite Materials*. < http://www.twi.co.uk/ >.

Ali R. 2008. « Probing System Characteristics In Coordinate Metrology ». In., sous la dir. de Review, Measurement Science.

Alten F., and Grandt J. 2004. *Fundamentals of Structural Integrity: Damage Tolerant Design and Nondestructive Evaluation*. John Wiley and Sons.

Andrea M. 2009. « Looking Right into the Texture ». *Materials Research,* vol. 5, p. 42-45.

Andreas E. 2003. « Investigation of the Influence of Local Inhomogeneities in the Textile Permeability on the Resin Flow in Liquid Composites Moulding Processes ».

Antonio M. 1999. *3-D Textile Reinforcements in Composite Materials*. Woodhead

Arkadiusz J. Ż. 2005. « Non-linear vibration of a delaminated composite beam ». *Key Engineering Materials*, p. 607–614.

Aroush D. 2006. « A study of fracture of unidirectional composites using in situ high-resolution synchrotron X-ray microtomography ». *Composites Science and Technology* p. 1348–1353.

Bachnak R., and Scott K. 2007. « Non-destructive evaluation and flaw visualization sing an eddy current probe ». In *ICONS*. p. 134-139.

Baoxing C., and Tsu-Wei C. 1999. « Compaction of woven-fabric preforms in liquid composite molding processes: single-layer deformation ». *Composites Science and Technology,* vol. 59, n° 10, p. 1519-1526.

Bar-C. Y. 1993. « Nondestructive characterization of defects using ultrasonic backscattering ». In *Ultrasonics International* Vol. 26, p. 345–352.

Bekir Y., Murat S. and Murat S. 2009. « Variation of part thickness and compaction pressure in vacuum infusion ». *Composites Science and Technology,* vol. 69, n° 11, p. 1710-1719.

Bogdanovich A.E., and Mohamed M.H. 2009. « Three-Dimensional Reinforcements for Composites ». p. SAMPE Nov/Dec 2009.

Buckley M. 2007. « http://www.adcom.org.uk/ ».

Carosena M., and Giovanni C. 2004. « Recent advances in the use of infrared thermography ». *Measurement Science and Technology,* vol. 15, p. 27-58.

Carvelli V., Tomaselli V. N., Lomov S. V., Verpoest I., Witzel V. and Broucke B. V. d. 2010. « Fatigue and post-fatigue tensile behaviour of non-crimp stitched and unstitched carbon/epoxy composites ». *Composites Science and Technology,* vol. 70, n° 15, p. 2216-2224.

Cawley P., and Adams R. 1979. « The localisation of defects in structures from measurements of natural frequencies ». *Strain Analysis*, n° 14, p. 49-57.

Chandra R., Singh S. P. and Gupta K. 1999. « Damping studies in fiber-reinforced composites – a review ». *Composite Structures,* vol. 46, n° 1, p. 41-51.

Chao Z. X., Ong S. S. and Tan S. L. 2011. « Improvement of measuring accuracy of an optical CMM ». *Physics Procedia,* vol. 19, n° 0, p. 122-128.

Chen B., and Chou T. 2000. « Compaction of woven-fabric preforms: nesting and multi-layer deformation ». *Composites Science and Technology,* vol. 60, n° 12–13, p. 2223-2231.

Choi S.W., Hahn H. T. and Shyprykevich P. . 2002. « Damage development in notched composite laminates under compression-dominated fatigue ». *Composites Science and Technology,* vol. 62, n° 6, p. 851-860. .

Claudia H. 2003. « Load-adapted 3D-reinforcement by means of function-adjusted ready-making process ». *Clothing Science and Technology* p. 189 - 197.

Datta S. K., and Shah A. H. 2009. *Elastic Waves in Composite Media and Structures with Applications to Ultrasonic Nondestructive Evaluation*. CRC Press.

Declercq N. F., Degrieck J. and Leroy O. 2006. « Ultrasonic polar scans: Numerical simulation on generally anisotropic media ». *Ultrasonics,* vol. 45, n° 1–4, p. 32-39.

Declercq N. F., Teklu A. and Breazeale M. 2005. « Detection of fiber direction in composites by means of a high-frequency wide-bounded ultrasonic beam and schlieren photography ». *Research in nondestructive evaluation,* vol. 16, n° 2, p. 55-64.

Dell'Anno G., Cartié D. D., Partridge I. K. and Rezai A. 2007. « Exploring mechanical property balance in tufted carbon fabric/epoxy composites ». *Composites Part A: Applied Science and Manufacturing,* vol. 38, n° 11, p. 2366-2373.

Dennis R., Kirk R. and Randy D. 2010. *Detection of Hail Impact Damage in Composite Structures at the Failure Threshold Energy*. < http://www.airlines.org >.

Dong C. 2003. *Dimension Variation Prediction And Control For Composites*.

Dow M., and Benso H. 1997. *Development of Stitched, Braided and Woven Composite Structures*.

E1441-00. 2002. « Standard Guide for Computed Tomography Imaging ». *ASTM,* vol. E1441-00.

Endruweit A., and Ermanni P. 2004. « The in-plane permeability of sheared textiles. Experimental observations and a predictive conversion model ». *Composites Part A: Applied Science and Manufacturing,* vol. 35, n° 4, p. 439-451.

Esmeralda C., Miquel L. and Mónica G. 2012. « Ultrasonic Techniques and Industrial Robots: Natural Evolution of Inspection Systems ». In *NDT in Aerospace 2012*.

Francis D., Tatam R. P. and Groves R. M. 2010. « Shearography technology and applications: a review ». *Materials Science and Engineering,* vol. 21, p. 102001.

Francois R., and Raymond G. 1998. « Compaction of textile reinforcements for composites manufacturing. I: Review of experimental results ». *Polymer Composites,* vol. 19, n° 2, p. 198-216.

Friedrich K., Fakirov S. and Zhong Z. 2005. *Polymer-Composites : From Nano- to Macro-Scale*. Springer

Hamidi Y.K., Aktas L. and Altan M. C. . 2009. « Effect of Fiber Content on Void Morphology in Resin Transfer Molded E-Glass/Epoxy Composites ». *Engineering Materials and Technology,* vol. 131, n° 2.

Hashin Z. 1980. « Failure criteria for unidirectional fiber composites ». *Applied Mechanics,* vol. 47, n° 2, p. 329-334.

Herszberg B. 1997. « Research in textile composites at the Cooperative Research Centre for aerospace structure ». *Textile Institute*

Hexcel Composites Ltd. 2000. *Honeycomb sandwich design technology*. Hexcel Co. Ltd.

Hong H., and Yong X. 2002. « Vibration-based Damage Detection of Structures by Genetic Algorithm ». vol. 133, n° 3, p. 449-461.

Hosur M. V., Vaidya U. K., Ulven C. and Jeelani S. 2004. « Performance of stitched/unstitched woven carbon/epoxy composites under high velocity impact loading ». *Composite Structures,* vol. 64, n° 3–4, p. 455-466.

http://www.aeronautics.nasa.gov.

Veuillez sélectionner un type de document autre que « Generic » afin de faire afficher la référence bibliographique.

http://www.avantgardetechnologie.de/.

http://www.industrial-lasers.com.

http://www.interempresas.net.

http://www.qinetiq.com.

Hufenbach W., Ritschel T., Böhm R. and Langkamp A. 2004. « Ultrasonic determination of anisotropic damage in fibre and textile reinforced composite materials ». *Mechanics of Composite Materials,* vol. 40, n° 6.

Huiwen H., and Jieming H. 2009. « Damage detection of a woven fabric composite laminate using a modal strain energy method ». *Engineering Structures,* vol. 31, n° 5, p. 1042-1055.

Hung Y.Y. 2009. « Review and comparison of shearography and active thermography for nondestructive evaluation ». *Materials Science and Engineering,* vol. 64, p. 73–112.

Hunga Y., and Hob P. 2005. « Shearography: an optical measurement technique and applications ». *Materials Science & Engineering,* vol. 49, p. 61-87.

Hussain M. A. Q., and Subhendu K. D. 2008. « laser-generated thermoelastic waves in an anisotropic infinite plate: exact analysis ». *Thermal Stresses,* vol. 31, p. 569–583.

Veuillez sélectionner un type de document autre que « Generic » afin de faire afficher la référence bibliographique.

James H. S., Benson H. and Norman J. J. 2003. *Composite Structures and Materials Research at NASA Langley*.

Jin L., Jin B C., Kar N., Nutt S., Sun B. and Gu B. 2013. « Tension–tension fatigue behavior of layer-to-layer 3-D angle-interlock woven composites ». *Materials Chemistry and Physics,* vol. 140, n° 1, p. 183-190.

Jing L. 2003. « Development of integrated process design environment and statistical analysis of RTM process ».

Jinlian H. 2008. *3-D fibrous assemblies: Properties, applications and modelling of three-dimensional textile structures*. Woodhead Publishing.

Kang K., Lee H. and Hahn T. 2000. « Formation of microvoids during resin-transfer molding process ». *Compos. Part A,* vol. 12, n° 1, p. 2427–2434.

Karal M. 2005. *AST composite wing program - Executive summary*. Coll. « NASA Report ».

Kimberley D., Caroline B. and Yiu-Wing M. 1994. « Improving the delamination resistance of CFRP by stitching—a review ». *Composites Science and Technology,* vol. 50, n° 3, p. 305-317.

Koissin V., Kustermans J., Lomov S. and Verpoest I. 2008. « structurally stitched preforms: experimental characterization, geometrical modelling, and FE analysis ». In *European Conference on Composite Materials (ECCM-13)*. (location:Stockholm).

Kundu T. 2004. *Ultrasonic Nondestructive Evaluation: Engineering and Biological Material Characterization* CRC Press.

Kundu T. 1999. « A Lamb wave scanning approach for the mapping of defects in [O/90] titanium matrix composites ». *Ultrasonics* p. 43-49.

Kyriazoglou C. 2004. « Vibration Damping For Crack Detection In Composite Laminates ». *Composites: Part A*, n° 24, p. 945–953.

Lapczyk I., and Hurtado J. 2007. « Progressive damage modeling in fiber-reinforced materials ». *omposites Part A Applied Science and Manufacturing,* vol. 38, n° 11, p. 2333-2341.

Lawrence J., Fried P. and Advani S. 2005. « Automated manufacturing environment to address bulk permeability variations and race-tracking in resin transfer molding by redirecting flow with auxiliary gates ». *Compos Part A,* vol. 36, p. 1128–114.

LayStitch LTD. < http://www.laystitch.com/Index.html >.

Leopold J., Günther H. and Leopold R.m. 2003. « New developments in fast 3D-surface quality control ». *Measurement,* vol. 33, n° 2, p. 179-187.

Lomov S. V., Boisse P. and Morestin E. 2008. « Full-field strain measurements in textile deformability studies ». *Composites Part A: Applied Science and Manufacturing,* vol. 39, n° 8, p. 1232-1244.

Long A. 2006. *Design and manufacture of textile composites*. CRC Press.

Louis M., and Huber U. 2003. « Investigation of shearing effects on the permeability of woven fabrics and implementation into LCM simulation ». *Composites Science and Technology,* vol. 63, n° 14, p. 2081-2088.

Luycker E., Morestin F., Boisse P. and Marsal D. 2009. « Simulation of 3D interlock composite preforming ». *Composite Structures,* vol. 88, n° 4, p. 615-623.

Mabrouki F., Thomas M., Genest M. and Fahr A. 2009. « Frictional heating model for efficient use of vibrothermography ». *NDT & E International,* vol. 42, n° 5, p. 345-352.

Mal A.K., Bar-C. and Lih S. Y. 1992. « Wave attenuation in fiber-reinforced composites ». In *Proceedings of M 3 D, Kinra, V.K. (editor), ASTM STP,*. (Philadelphia), p. 245-261.

Maldague X.P.V. 2001. *Theory and practice of infrared technology for nondestructive testing*. Coll. « Wiley series in microwave and optical engineering ». : John Wiley & Sons.

Mark O., and David K. 2008. « Application of Laser Ultrasonics for the Non-Destructive Inspection of Complex Composite Aerospace Structures ». In *1st International Symposium on Laser Ultrasonics*. Montreal, Canada

Maslova K. 1997. « Selection of Lamb modes for detecting internal defects in composite laminates ». *Ultrasonics,* vol. 2, n° 35, p. 141–150.

Matzenmiller A., Lubliner J. and Taylor R. 1995. « A constitutive model for anisotropic damage in fiber-composites ». *Mechanics of Materials,* vol. 20, n° 2, p. 125-152.

Mazumdar S. K. 2002. *Composites Manufacturing: Materials, Product and Process Engineering*. CRC Press LLC, Boca. Raton FL.

Meola C., and Carlomagno G. 2009. « Infrared thermography of impact-driven thermal effects ». *Applied Physics A,* vol. 96, n° 3, p. 759-762.

Merotte J., Simacek P. and Advani S. G. 2010. « Resin flow analysis with fiber preform deformation in through thickness direction during Compression Resin Transfer Molding ». *Composites Part A: Applied Science and Manufacturing,* vol. 41, n° 7, p. 881-887.

Michulitz C. 2007. « Prozessgestaltung zur Herstellung von Textilen Preforms ». In *RWTH Aachen: Institut für Unternehmenskybernetik*.

Mitschang P. , and Ogale A. 2009. « quality aspects of and thread selection for stitched preforms ». In *ICCM17*.

Mook G., and Koeser R. 2001. « Non-destructive characterisation of carbon-fibre-reinforced plastics by means of eddy-currents ». *Composites Science and Technology,,* vol. 61, p. 865-873.

Moser F., Jacobs L. J. and Qu J. 1999. « Modeling elastic wave propagation in waveguides with the finite element method ». *NDT & E International,* vol. 32, n° 4, p. 225-234.

Mouritz A. 1997. « Review of Applications for Advanced Three-Dimensional Fibre Textile Composites ». *Compsoite,* vol. 30(12) p. 1445- 1461

Mouritz A. P., and Cox B. N. 2000. « A mechanistic approach to the properties of stitched laminates ». *Composites Part A: Applied Science and Manufacturing,* vol. 31, n° 1, p. 1-27.

Mouritz A. P., and Cox B. N. 2010. « A mechanistic interpretation of the comparative in-plane mechanical properties of 3D woven, stitched and pinned composites ». *Composites Part A: Applied Science and Manufacturing,* vol. 41, n° 6, p. 709-728.

Mouritz A.P., and Cox B. N. 2000. « A Mechanistic Approach to the Properties of Stitched Laminates ». *Composites: Part A,* vol. 31, n° 1, p. 1–27.

Nayfeh A.H. 1995. *Wave Propagation in Layered Anisotropic Media with Applications to Composites*. Elsevier Publishing Company.

Neitzel M., and Mitschang P. 2004. *Handbuch Verbundwerkstoffe.*: Carl Hanser Verlag.

Ogale A., and Mitschang P. 2004. « Tailoring of Textile Preforms for Fibre Reinforced Polymer Composites ». vol. 34, n° 2, p. 77-96.

Osterkamp M. 2006. « Analysis of Commercial Aeronautics Applications of
Laser Ultrasonics for Composite Manufacturing ». In *ECNDT Berlin*.

Paolo E. 2009. *textile halbzeuge*. Zentrum für Strukturtechnologien, ETH Zürich.

Poe C.C., and Dexter H.B. 1997. *A review of the nasa textile composites research*.

Potluri P., Sharif T. and Jetavat D. 2008. « Robotic approach to textile preforming for composites ». *Indian Journal of Fibre & Textile Research,* vol. 31, p. 333-338.

Potluri P., and Atkinson J. 2003. « Automated manufacture of composites: handling, measurement of properties and lay-up simulations ». *Composites Part A: Applied Science and Manufacturing,* vol. 34, n° 6, p. 493-501.

Randolf H., Theobald F. and Norman U. 2008. « X-ray based methods for non-destructive testing and material characterization ». *Nuclear Instruments and Methods in Physics Research*, p. 14-18.

Renshaw J., Chen J. C., Holland S. D. and Bruce T. R. 2011. « The sources of heat generation in vibrothermography ». *NDT & E International,* vol. 44, n° 8, p. 736-739.

Richard H. A. 2000. *Handbook of technical textiles* Manchester, Cambridge Woodhead Publishing Ltd.

Rudov-C. S. 2007. « Experimental investigation of the tensile properties and failure mechanisms of three-dimensional woven composites ». RMIT University.

Safran Group Ltd. 2011. < http://www.safran-group.com/ >.

Schmitt R. 2007. « A method for edge detection of textile preforms using a light-section sensor for the automated manufacturing of fibre-reinforced plastics ». In *Proceedings of SPIE Optical Measurement Systems for Industrial Inspection V at the World of Photonics Congress*. (Munich).

Sickinger C., Wilmes H. and Herbeck L. 2000. « Eine Maßnahme zur Realisierung von Hochleistungsfaserverbundstrukturen ». *Textile Technologien*.

Sickinger C., and Herrmann A. 2001. *Structural stitching as a method to design high-performance composites in future*. < http://www.dlr.de/ >.

Simacek P., Advani S.G. and Iobst S.A. 2008. « Modeling flow in compression resin transfer molding for manufacturing of complex lightweight high-performance automotive parts ». *Compos Mater 42*, p. 2523–2545.

Solaimurugan S., and Velmurugan R. 2008. « Influence of in-plane fibre orientation on mode I interlaminar fracture toughness of stitched glass/polyester composites ». *Composites Science and Technology,* vol. 68, n° 7–8, p. 1742-1752.

Sozer E.M., Chen B., Graham P. J., Chou T.W. and Advani S. G. 1999. « Characterization and Prediction of Compaction Force and Preform Permeability of Woven Fabrics During the Resin Transfer Molding Process ». In *Flow Processes in Composite Materials* (Plymouth), p. 25-36.

Stanislav R., Dale C. and Peter N. 2011. *Physical Ultrasonics of Composites*. Oxford University Press.

Stein J. 2008. « Porosity measurement service using X-ray tomography ».

Veuillez sélectionner un type de document autre que « Generic » afin de faire afficher la référence bibliographique.

Suarez S. A., Gibson R. F., Sun C. T. and Chaturvedi S. K. 1986. « The influence of fiber length and fiber orientation on damping and stiffness of polymer composite materials ». *Experimental Mechanics,* vol. 26, n° 2, p. 175-184.

Swiderski W., Szabra D. and Szudrowicz M. 2008. « Nondestructive testing of composite armours by using IR thermographic method ». In *9th International Conference on Quantitative InfraRed Thermography*. (Krakow - Polan).

Thuis H. 2004. *Composite landing gear components made with Resin Transfer Moulding. National Aerospace Laboratory NLR, Amsterdam*. The Netherlands.

Tomek R. 2004. « Mixed mode fracture toughness of stitched laminated composites ». university of florida.

Tong L., Mouritz A.P. and Bannister M.K. 2002. *3D fibre reinforced polymer composites*. London: Elsevier Science Ltd.

Tong L. M. 2002. « 3D Fibre Reinforced Polymer Composites ». *Elsevier Science*.

Ulf H. 2008. « Carbon Fibre Preform Inspection by Circular X-ray Tomosynthesis ». In *IEEE Nuclear Science Symposium Conference*. (Dresden, Germany), p. 590 - 592.

Ulf H., Stephan S. and Randolf H. 2007. « Computed tomography for analysis of fiber distribution in carbon fiber preforms ». In - *International Symposium on Digital industrial Radiology and Computed Tomography*. (Paric, france).

Unnþórsson R. 2004. « NDT methods for Evaluating Carbon Fiber Composites ». In *Composites Testing and Model Identification*.

Uozumi T., Kito A. and Yamamoto T. 2005. « CFRP using braided preforms/RTM process for aircraft applications ». *Advanced Composite Materials,* vol. 14, n° 4, p. 365-383.

Van D., and Speijer W. 1981. « Nondestructive composite laminate characterisation by means of ultrasonic polar-scan ». *Materials evaluation,* vol. 39, n° 10, p. 922-925.

Varada R. A., and Blouin A. « Void Content, Density and Weight Reduction Studies on Short Bamboo Fiber–Epoxy Composites ». *Reinforced Plastics and Composites,* vol. 23, n° 2, p. 127-130.

Vorgelegt V. 2007. « Induktions-Lockin-Thermograein neues Verfahren zerst orungsfreien Prufun». Stuttgat Uni.

Wael B. L., Ibarra-C. C. and Xavier M. 2009. « London, Ontario, Canada ». In *Sixth International Workshop, Advances in Signal Processing for Non Destructive Evaluation of Materials (IWASPNDE)*. (London, Ontario, Canada).

Warren J. 1994. *Real-time Fabric Defect Detection & Control In Weaving Processes*.

Weimer C. 2003. « Preform-engineering: applied sewing technologies to incorporate part and process functions into dry textile reinforcements ». *Composite science and technology* p. 2089-2098

www.compositesworld.com. « Integrated, optimized aircraft door - High Performance Composites ».

Yam C. 2005. « Damage detection of composite structures using dynamic analysis ». *Key Engineering Materials*, p. 33-39.

Yashiro S., and Takatsubo J. 2007. « An NDT technique for composite structures using visualized Lamb-wave propagation ». *Composites Science and Technology,* vol. 67, n° 16, p. 3202-3208.

Yim J., and Gillespie J. 2000. « Damping characteristics of 0° and 90° AS4/3501-6 unidirectional laminates including the transverse shear effect ». *Composite Structures,* vol. 50, n° 3, p. 217-225.

Yoseph B.-C., and Shyh-Sh. L. 2001. « NDE of Composites Using Leaky Lamb Waves (LLW) ». *NDT&E J.*

Yu J. Z., Cai Z. and Ko F. K. 1994. « Formability of textile preforms for composite applications. Part 1: Characterization experiments ». *Composites Manufacturing,* vol. 5, n° 2, p. 113-122.